Near-Far Resistant Detection for CDMA Personal Communication Systems

by

Pantelis Nikolaos Monogioudis

Thesis submitted to the University of Surrey
for
the degree of Doctor of Philosophy

Dept. of Electronic and Electrical Engineering
University of Surrey
Guildford, Surrey
U.K.

Summary

The growth of Personal Communications, the keyword of the 90s, has already the signs of a technological revolution. The foundations of this revolution are currently set through the standardization of the Universal Mobile Telecommunication System (UMTS), a communication system with synergistic terrestrial and satellite segments. The main characteristic of the UMTS radio interface, is the provision of ISDN services. Services with higher than voice data rates require more spectrum, thus techniques that utilize spectrum as efficiently as possible are currently at the forefront of the research community interests. Two of the most spectrally efficient multiple access technologies, namely, Code Division Multiple Access (CDMA) and Time Division Multiple Access (TDMA) concentrate the efforts of the European telecommunity.

This thesis addresses problems and proposes solutions for CDMA systems that must comply with the UMTS requirements. Prompted by Viterbi's call for further extending the potential of CDMA through signal processing at the receiving end, we propose new Minimum Mean Square Error receiver architectures. MMSE detection schemes offer significant advantages compared to the conventional correlation based receivers as they are NEar FAr Resistant (NEFAR) over a wide range of interfering power levels. The NEFAR characteristic of these detectors reduces considerably the requirements of the power control loops currently found in commercial CDMA systems. MMSE detectors are also found to have significant performance gains over other well established interference cancellation techniques like the decorrelating detector, especially in heavily loaded system conditions. The implementation architecture of MMSE receivers can be either Multiple-Input Multiple Output (MIMO) or Single-Input Single-Output. The later offers not only complexity that is comparable to the conventional detector, but also has the inherent advantage of employing adaptive algorithms which can be used to provide both the despreading and the interference cancellation function, *without* the knowledge of the codes of interfering users. Furthermore, in multipath fading channels, adaptive MMSE detectors can exploit the multipath diversity acting as RAKE combiners. The later ability is distinctive to MMSE based receivers, and it is achieved in an autonomous fashion, without the knowledge of the multipath intensity profile.

The communicator achieves its performance objectives by the synergy of the signal processor and the channel decoder. According to the propositions of this thesis, the form of the signal processor needs to be changed in order to exploit the horizons of spread spectrum signaling. However, maximum likelihood channel decoding algorithms need not

change. It is the way that these algorithms are utilized that needs to be revis ed. In this respect, we identify three major utilization scenarios and an attempt is made to quantify which of the three best matches the requirements of a UMTS oriented CDMA radio interface. Based on our findings, channel coding can be used as a mapping technique from the information bit to a more "intelligent" chip, matching the "intelligence" of the signal processor.

Acknowledgement

I would like to express my graditude to Rahim Tafazolli and Barry Evans, whose support, guidance and patience throughout my stay at Surrey, were an invaluable motivating force to conclude this work. I am also grateful to Mark Edmonds and Rodney Gibson for their motivation, trust and patience they have shown during my stay at Philips Research Laboratories. I am also thankful to Peter Sweeney for his constructive and helpful comments during the preparation of my thesis.

I dedicate this thesis to the memory of my father and to my lovely mother whose countless hard working days will come soon to an end. I would also like to thank Greta whose love and patience during these long years kept me running in full speed till the very end.

Contents

List of Figures

List of Tables

Chapter 1

INTRODUCTION

1.1 BACKGROUND

The abbreviation PC has been, and still is, one of the most widely known technological abbreviations of the last decade or so. During the 80s the revolution of Personal Computers (PC) and their introduction to almost every level of information processing procedure led to an unprecedented technological breakthrough. For the 90s the idea that another technological revolution will be witnessed is gaining widespread acceptance as the first Personal Communications (PC) services are lunched. The need for high performance flexible mobile computing and global communications will lead inevitably to the integration of the Personal Computer and Personal Communicator into one device.

The idea behind Personal Communications started during the late 80s when the epilogue of the European research effort towards 2nd generation digital cellular systems was the standardization of a Pan-European digital cellular system known as GSM (Global System for Mobile communications). During the 90s, research towards 3rd generation digital cellular systems was already peaking. In Europe, the third generation system known as Universal Mobile Telecommunication System (UMTS) was formed through research projects the majority of which ran under the umbrella of RACE Mobile. The first phase of this program was completed in 1992. During this phase the user requirements and services for the next generation cellular systems have been studied in depth and hundreds of reports have been written regarding the suitability of the various multiple access techniques to provide these services. The second phase of the program started in 1992 and is currently reaching a mature stage. During this most critical phase, the two stronger candidate multiple access techniques, namely Time Division Multiple Access (TDMA) and Code Division Multiple Access (CDMA), have been extensively researched. The outcome of this research will be two testbeds, namely CODIT for the CDMA technique and ATDMA for the TDMA technique, which realise in hardware the two candidate technologies. The two testbeds will be used in extensive field trials where each technology will be validated against commonly agreed criteria. Two of the most important criteria are spectral efficiency and system flexibility. The importance of these two projects for the future of the European cellular industry is obvious. The European telecommunication industry giants, partially supported by European Commission funds have created two opposite camps each having as a coretask the production of a system which will outperform the system of the contending technology.

1.1.1 The Philosophy of CDMA

Code Division Multiple Access technology originates from spread-spectrum communication systems which have been, and still are, used extensively in providing Anti-Jam (AJ), Low Probability of Intercept (LPI), secure military communications. Spread spectrum signals occupy a much wider bandwidth compared to the one required for the reliable transmission of the information signal. This can be achieved with two methods: The first, called Frequency Hopping, involves the switching of the information-modulated carrier frequency in deterministic steps over the available frequency band. The second, called Direct Sequence (DS), achieves the spreading, by multiplying the modulated information-rate signal with a deterministic signal (of not necessarily similar modulation format) having higher data rate, called the spreading code. The resulting signal has a bandwidth which is determined by the data rate of the spreading code. This work considers only DS-CDMA systems since, under the assumption of equally received signal power from all the users, they have been found to offer capacity advantages compared to FH systems, being at the same time a fully implementable architecture [9]. In DS-CDMA, the symbols comprising the deterministic spreading code are usually called chips and the ratio of the rate of chip-signal to the rate of the information-bearing signal is called spreading factor or processing gain (in dB). Due to the spectral spreading, the level of the power spectral density is reduced according to the ratio of the spreading factor, thus spread spectrum signals have noise-like power spectral densities.

In every multiple-access technology, the main goal is to use the available bandwidth as efficiently as possible among the users. The classic Frequency Division Multiple Access (FDMA) approach where every user has a distinct frequency chunk has been used extensively in the first-generation analog mobile radio systems. However, FDMA is considered to be a low spectral efficient multiple access method unless it it is combined with a Time

Division component. The latter, currently employed in the second-generation digital cellular system (GSM), through a careful synchronization strategy, permits the time-sharing of the available frequency chunk in a transparent to the end user way. The concept that underlines the combination of TDMA/FDMA system is easier to comprehend compared to the CDMA concept.

Considering a single cell system, signals recorded in a given carrier frequency, will belong to only one user. Thus, the detection of TDMA signals incorporate a single user detector tuned to the carrier frequency of interest. In CDMA systems however, all users transmit spread-spectrum signals concurrently and completely un-co-ordinated. Thus, the inherent orthogonality of TDMA systems is not present in CDMA. The signal which is recorded at a given carrier frequency is the *sum* of the spread spectrum signals of all the active users in the cell. The discrimination ability at the receiver end relies on the accurate knowledge of the deterministic spreading sequences. The receiver performs the two functions that have been performed at the transmitter in reverse order, ie. despread the signal of interest and detect the resulting narrowband signal.

The successful despreading of the signal of interest, in the presence of interfering signals is unique to CDMA systems and makes the detection problematic under specific interference patterns. In a cell with K users, there will be K-1 interfering spread-spectrum signals the sum of which is called multiple access interference. Constraining ourselves to a single-cell case, in TDMA there is no such meaning of multiple access interference due to the time and frequency orthogonality of the user transmissions. In the direction from the mobile station to the base station, called the uplink, the multiple access interference is more problematic since in a multi-point to single point transmission system it is impossible to apply orthogonalization of the simultaneous transmissions. The reverse direction however, called the downlink, is a point to multi-point transmission system, where orthogonalization of the K simultaneous transmissions can be applied. As the road of spectral efficiency passes through the successful multiple access interference mitigation strategies, addressing techniques that reduce the effects of interference is of particular importance to CDMA technology's future.

1.2 APPROACHES AND MOTIVATION

The author's work forms part of the radio interface and radio transceivers coretasks of the RACE CODIT project. Although it had been realized from the early stages of the project that CODIT will be an advanced technology testbed it did not follow innovative routes as far as the physical layer design was concerned. Thus, CODIT employs conventional technology at the receiver side which to the author's opinion can not exploit fully the potential of CDMA. What was really needed was a revision of the receiver architecture under the prism of UMTS. It seems that one of the most influential of Viterbi's publications also points to this direction. In [61], Viterbi discussed the present and the future of wireless digital communications based on three lessons that unfortunately engineers have never completely learned. These lessons were the driving force behind this research and are worth summarising.

- **Lesson 1:** Never discard information prematurely that may be useful in making a decision until after all decisions related to that information have been completed.
- **Lesson 2:** Completely separate techniques for digital source compression from those for channel transmission, even though the first removes redundancy and the second inserts it.
- **Lesson 3:** In the presence of interference, the communicator, through signal processing at both transmitter and receiver, can ensure that performance degradation due to interference will be no worse than that caused by Gaussian noise at equivalent power levels. This implies that a jammer's optimal strategy is to produce Gaussian noise interference. Against such interference the communicator's best waveform should statistically appear as Gaussian noise. Thus the "minimax" solution to the contest is that signals and interference should all appear as noise which should be as wideband as possible.

It is the third lesson that is not widely accepted in the wireless telecommunity. The third lesson simply states that spread spectrum signalling is the best way to overcome interference. TDMA systems are prone to co-channel interference and it is only through careful and expensive frequency and cellular planning that the performance of TDMA systems is preserved at acceptable levels. On the other hand, Code Division Multiple Access systems are prone to co-channel interference not in the spatial domain but in the time and frequency domain. As Viterbi suggests, it is only through signal processing that the optimality of CDMA can be realized. What kind of signal processing is Viterbi talking about ? Are there better receiver architectures of reasonable complexity that can replace the well known correlation-type receiver and offer even greater spectral efficiency?

Attempts to answer these questions by various researchers in this field were based on the understanding that the advanced signal processing of the optimal CDMA receiver is a receiver based on the Viterbi algorithm [58]. Since this detector is too complex to implement, with complexity that increases exponentially with the number of users in the system, researchers looked at suboptimal solutions. Two of the fundamental research outcomes towards sub-optimum CDMA receivers is the work of Lupas [31], [32], who proposed the decorrelating receiver and Varanasi who proposed the the multistage receiver [57].

1.3 OUTLINE OF THE THESIS

From the start of the project it was realised that the proposed solutions should comply with the Universal Mobile Telecommunication System (UMTS) working assumptions. Thus, all the problems that we address are realistic problems that must be solved if CDMA is ever to be used as the UMTS multiple access technique. The role of Chapter 2 is twofold. First, it reviews the UMTS concept and what are its implications for the radio interface design. Second, it summarises what CDMA offers but also the points where CDMA is challenged by competing technologies such as TDMA. Three main points were identified, namely, the provision of high rate data, the associated processing gain limitations and the near-far effect due to power control errors.

We start our investigations with Chapter 3 which addresses the various forms of the conventional receiver architecture for both single path and multipath fading channels. Emphasis is given on multipath diversity (RAKE) receiver architectures. A comparison of coherent and non-coherent RAKE receivers reveals that the multipath diversity gain of the latter is not present for moderate signal to noise ratios. Our efforts are then directed in finding the limits of conventional multipath diversity receivers in the uplink direction which can only be achieved by coherent RAKE reception. Contrary to the downlink direction where coherent detection is feasible due to the existence of a pilot channel, in the uplink, up to now, only differential phase coherency could be achieved. In this respect we research techniques that permit RAKE receivers to perform coherent combining of the tracked multipaths in the uplink. The proposed channel estimation technique is employed in the Channel Adapted RAKE (CARAKE) receiver whose performance is compared against the ideal maximal ratio combining receiver and the differentially coherent equal gain combining receiver. Although with the CARAKE receiver the benefits of multipath diversity in the uplink direction can be fully exploited its operational concept is rather simplified. RAKE-type receivers are in effect a bank of correlators each of them synchronised to a path both in time and in frequency/phase. In this respect it is no surprise that this simple receiver architecture is inadequate to handle severe interference of a near-far nature. As will be shown in the final sections of Chapter 3, the solution to the near-far effects through power control are inadequate and cause severe performance loss under certain conditions.

Based on the disappointing results of conventional detection under near-far interference conditions, Chapter 4 aims to set the foundations of advanced CDMA receivers that, although originating from the conventional detectors, do not inherit their limitations. The aim of this chapter is twofold: First, to present Multiple Input Multiple Output Output (MIMO) Minimum Mean Square Error detection schemes for CDMA systems. In this respect, we establish the connection between CDMA and MIMO representation of interference, introducing the equivalent CDMA channel model which is of fundamental importance to interference equalization. Second, to demonstrate the NEar FAr Resistance (NEFAR) of the MIMO MMSE detectors for both synchronous and asynchronous CDMA systems. In this respect, we prove the NEFAR ability by demonstrating the invariance of the Mean Squared Error over a wide range of interfering power levels. Due to the UMTS requirements to provide high bit rate services, CDMA faces a challenge because of its processing gain limitations. Thus, it is important to research effects of reduced processing gain ie. increased system loading. A comprehensive comparison of MIMO MMSE receivers as opposed to other MIMO receiver architectures, under heavily loaded conditions, reveals the significant performance gains of the former. Finally, we address the complexity issue which prompts for downsizing to simpler detector structures.

In Chapter 5 we propose a downsized version, namely, SISO MMSE detectors that can adaptively, without the knowledge of the interfering spreading codes, provide interference rejection. The despreading operation by adaptive transversal filtering is first investigated, emphasizing the effects of factors related to the implementation of the adaption algorithm. Based on this symbol spaced MSE minimising despreader, two receivers are presented: (1) the Linear Fractionally Spaced Equalizer (LFSE) and (2) The Fractionally Spaced Decision Feedback Equalizer (FS-DFE). Their interference rejection ability is demonstrated for both static and time-varying channels. As a direct consequence of the *implicit* despreading as compared to the explicit despreading of the conventional receiver, MMSE based receivers do not need the estimation of the Delay Power Spectrum in multipath channels. LFSE and FS-DFE receivers can act as RAKE combiners without any need to explicitly estimate the delay of every path.

In Chapters 3,4 and 5 we concentrate on the signal processing aspects of advanced CDMA receiver architectures. The hostility of the mobile radio channel makes channel coding mandatory. However, the role of channel coding in CDMA systems has caused considerable confusion in the research community. Although it is widely acknowledged that channel coding is beneficial, it is the tradeoff between channel coding and PN spreading that is questioned. In Chapter 6 we provide a thorough investigation in this subject, trying to identify the factors, not necessarily related to information theory, that influence the coded system performance.

The conclusions and our suggestions for further research in this area are outlined in Chapter 7.

1.4 ORIGINAL ACHIEVEMENTS

In summary, we contend that the original work covered in this thesis is as follows:

1. Thorough evaluation of RAKE-type receivers in various single path and multipath channels. The multipath diversity gain is dependent on the ability to provide phase coherency especially for moderate values of SNR/bit.

2. A new channel estimation algorithm which provides the means to perform coherent demodulation in the uplink.

3. New advanced CDMA receiver architectures based on Multiple Input Multiple Output (MIMO) equalization theory.

4. Linear and Non-Linear MIMO MMSE receivers are proved to be NEar-FAr Resistant (NEFAR) over a wide range of near-far interference scenarios. A thorough investigation on the effect of system loading to the performance of MIMO MMSE receivers as compared to Zero-Forcing MIMO receiver architectures (decorrelator).

5. New Single Input Single Output (SISO) Linear and Non-Linear MMSE detectors and extensive simulations of their performance under realistic single path and multipath channels.

6. A thorough investigation into the abilities of SISO MMSE detectors to replace the RAKE receivers exploiting the multipath diversity with no need for explicit delay estimation of each path.

7. A new concept concerning the role of channel coding in CDMA systems. The myth that spreading the information signal through channel coding has detrimental effects in receiver performance is dispelled through analytical and simulation results.

8. A novel technique of physical layer mapping to support multimedia services in a CDMA radio interface.

Chapter 2

3rd GENERATION PERSONAL COMMUNICATION SYSTEMS

2.1 INTRODUCTION

Every research effort towards the design of a new communications infrastructure always has as its starting point a list of working assumptions. For the design of third generation personal communication systems the definition of these working assumptions has been a major component in the standardization of the Universal Mobile Telecommunication System. In section 2.2, we review the constitution of UMTS and its key objectives. We then review the major working assumptions regarding the type of services that are to be supported in the UMTS radio interface.

Since the pioneering work of Neppleton [41] at the end of the 70s, the spread of CDMA technology has been dramatic. After the first field trials in the late 80s of the first commercial CDMA cellular system, the interest of the research community boomed. Today, CDMA is considered to be one of the two major mobile radio multiple access technologies. In the United States CDMA technology has been standardised and it is known as the IS-95 standard. Claims of increased capacity offerings compared to Time Division Multiple Access (TDMA) were loud enough to initiate a plethora of publications regarding capacity estimation of both TDMA and CDMA based cellular systems [14],[63].

In Europe these claims initiated research towards a CDMA based implementation of UMTS radio interface. The main motivating factors towards CDMA research are outlined in section 2.3. CDMA's spread spectrum signaling format makes it ideal for interference limited wireless applications. However, CDMA has to face the challenges imposed by the provision of higher bit rate services. These design challenges are outlined in section 2.4.

2.2 THE UNIVERSAL MOBILE TELECOMMUNICATION SYSTEM (UMTS)

This section addresses the various aspects of the 3rd generation personal communication system, which for the European standardization body ETSI (European Telecommunications Standards Institute) is also known as UMTS. The responsibility for the standardization of UMTS within ETSI has been given to the technical committee SMG (Special Mobile Group) which has been very successful in developing, during the 80s, the GSM and DCS1800 standards.

As Fig.2.1 illustrates, although the effort towards UMTS standardisation is driven by *European* research effort, such as the RACE and COST projects, ETSI itself is committed to worldwide standards bodies such as the International Telecommunication Union (ITU) with the objective of establishing a common set of standards for 3rd generation systems. This commitment would enable worldwide interoperability and roaming for mobile terminals. The ITU through the Technical Group TG 8/1, is producing the standards for the International Mobile Telecommunications system IMT-2000, formerly known as Future Public Land Mobile Telecommunication System (FLMTS). ETSI in effect influences the standardization of IMT-2000 by feeding Europe's developed standards into the ITU TG 8/1, taking full advantage of the European lead over the US and Japan on the digital mobile/personal communications arena.

2.2.1 Key Objectives of UMTS

UMTS will integrate various markets and applications into one system solution in order to support a wide range of services with universal availability. This 3rd generation system, the standardization of which will be finalised by the end of this decade, will offer Universal Personal Telecommunications (UPT). UPT is a service concept and provides personal mobility, ie. mobility of the users between terminals. UMTS although providing terminal mobility ie. mobility of terminals between networks, will have the capability of providing the most user friendly and flexible support for UPT.

UMTS is designed with an open architecture in mind in order to accommodate emerging applications that cannot be fully defined during the design stage. This openness

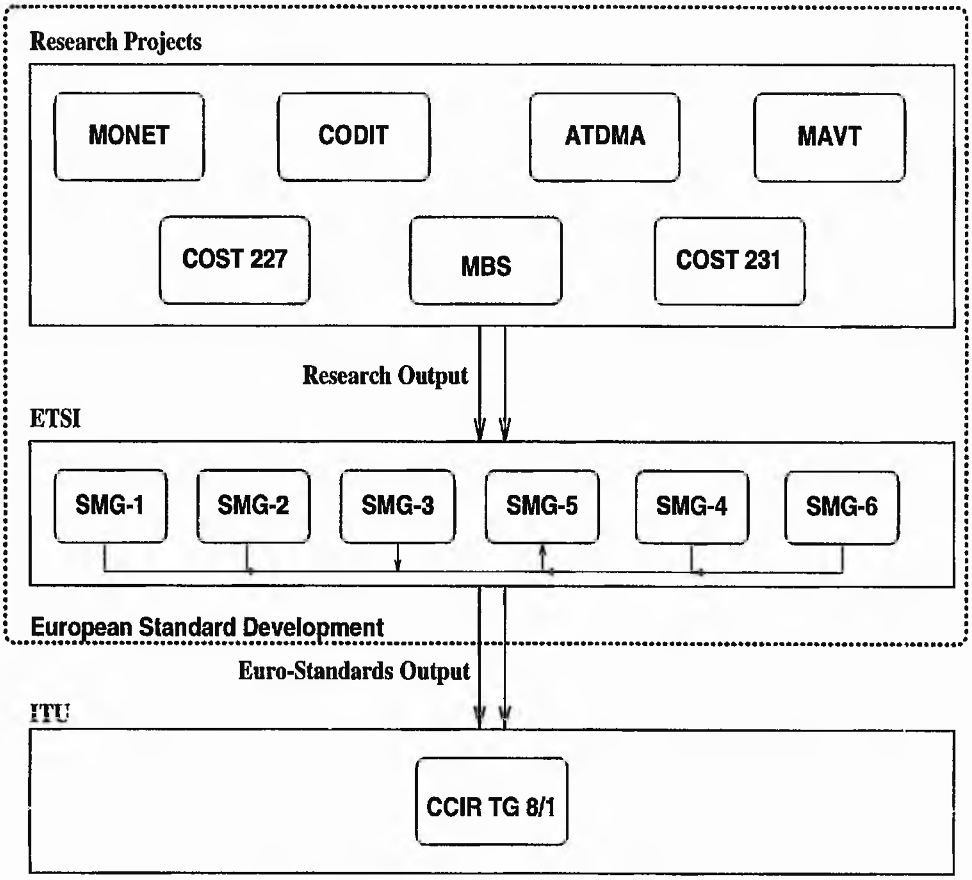

Figure 2.1: Relation Between UMTS and IMT-2000 Standards

dictates that, apart from capacity, system flexibility is another important variable. System flexibility can be achieved only by co-design of the radio interface and network interface. The intelligent network (IN) concept is an integral part of the services that the radio interface will offer. Since UMTS will operate in a wide variety of environments flexibility of the supporting network has to co-exist with the flexibility of the radio interface. It is the aim of this thesis to demonstrate that the radio interface based on CDMA technology is able to provide this with the services listed in the next section.

2.2.2 UMTS Services

The provision of the services listed in Table 2.1 is considered mandatory.

Where MPEG 4 is the emerging Low Bit Rate (LBR) video transmission standard while the H.261 is a p x 64 kbps standard of ITU-T (previously known as CCITT).

The ability to provide the services relies on the radio access network which includes

Service	Average Data Rate (kbps)	Post-decoder BER	Delay (ms)
Voice Telephony	9.6	10^{-3}	< 30
Data (Low Delay)	9.6 - 128	10^{-6}	< 30
Data (High Delay)	9.6 - 2048	10^{-6}	< 300
Video Telephony (MPEG 4, H.261)	64 - 384	10^{-5}	< 40

Table 2.1: Major UMTS Services

the radio interface. The choice of multiple access technique is a critical decision. The two major contending technologies for UMTS are TDMA/FDMA and CDMA/FDMA. The importance of the radio interface technology is highlighted in Fig. 2.1, where the two major RACE projects namely CODIT for CDMA and ATDMA for TDMA have attracted in two opposite camps the European telecommunication industry. The potential of each technology will be realized in 1995 when the results from the field trials of the two testbeds will be compared. In the next section, the advantages and disadvantages of CDMA/FDMA over TDMA/FDMA are highlighted under the prism of UMTS radio interface requirements.

2.3 TOWARDS CDMA BASED UMTS

Each of the two contending technologies has some inherent advantages over the other. Although the advantages of CDMA technology over TDMA have been widely advertised and shown both analytically and in practice, some of its disadvantages have lead to doubt about its true potential. This doubt is exaggerated by those who have invested heavily in TDMA technology over the last 10 years. An unbiased (in the author's opinion) outline of the advantages of CDMA follows:

- **Increased Order of Diversity:** CDMA offers greater diversity order. On top of time diversity (channel coding), common to both technologies, CDMA offers frequency diversity and multipath diversity. The frequency diversity is due to the wideband ($\geq 1MHz$) nature of spread spectrum signals whilst the multipath diversity is due to the time discrimination ability of the spread spectrum receiver. The receiver which exploits the multipath diversity is fundamental to mitigating multipath induced fading and is widely known as the RAKE receiver. With the RAKE receiver the detrimental effects of multipath propagation can be translated into gain. This is in contrast to TDMA systems, where a channel equalizer has to be employed in order to handle multipath induced ISI.

- **Power Efficiency:** The required E_b/N_0 to achieve the same performance is much smaller in CDMA compared to TDMA systems. For voice services the Pan-European TDMA digital cellular standard (GSM) needs without frequency hopping an average SNR/bit of 12.5 dB whilst, the IS-95 CDMA standard needs an average of 7 dB.

- **Frequency Reuse:** The deployment of CDMA networks is very much simplified compared to TDMA. This is due to the ability of CDMA to provide orthogonal down links with proper PN coding and due to its ability for inherent interference cancellation of other signals by an amount equal to the processing gain. Thus, the frequency planning is minimized since the same frequency band can be reused in neighbouring cells. As a comparison, TDMA offers only orthogonality in time and careful frequency planning has to be performed for successful deployment.

- **Interference:** CDMA can operate in the same frequency band with other fixed narrowband services. Research is now under way to verify this ability with mobile narrowband services. Although the WARC-92 has already allocated spectrum for emerging technologies, the capability to co-exist with other services is still important due to the integrated satellite/terrestrial UMTS scenario, which requires band co-sharing of the satellite and the terrestrial segment.

- **Synchronization:** The requirement of TDMA for frequent slot synchronization increases dramatically the signalling overhead in TDMA systems. The only synchronization requirement of CDMA is during call set-up and handover. The delay power spectrum estimation circuitry can work during the whole duration of the conversation adaptively estimating the multipath intensity profile with no signalling overheads.

- **Voice Activity Detection:** CDMA transceivers can be designed to transmit and receive in various duty cycles according to the voice activity at each end. During a conversation it has been found that the voice activity is around 40%. This means that with voice activity detection 40% of the time the user is active ie. 40% of the time the user is causing interference to the rest of the users. The capacity increase is not though proportional to the voice activity detection since during silent periods the transmitter still transmits very low bit rate frames. In TDMA systems voice activity detection is used for the benefits of capacity and for battery life savings.

- **Sectorization:** In CDMA systems cells can be sectorized in order to decrease the amount of co-cell interference. If 3 sectors per cell are used then the interference is otherwise

33% of that otherwise which would have been experienced. The capacity increase is again not proportional to the interference decrease since the antennas used in sectorizing the cells are not perfectly directional.

- **Soft Handover:** During handover the mobile terminal is able to track both the originating and the target Base Stations. The mobile terminal receiver is then able to optimally combine these two signals to the advantage of link quality. Moreover, the ability to track the target Base Station before leaving the originating Base Station improves the grade of service by minimizing the probability of call drop due to modem unavailability in the target cell.

- **Macrodiversity:** With macrodiversity the mobile terminal is able to optimally combine the downlink signals from surrounding cells. This is particularly useful feature when the link quality of the currently serving cell temporarily degrades. The combining of one degrading and two possibly non-degrading links improves the decision statistic to the benefit of performance. However, the macrodiversity mode is associated with signalling transactions between the mobile, the base and the network controller for all the functions of the co-operating base stations to be performed.

- **Soft Capacity:** In TDMA systems the number of time slots that are available in a given cell is equal to the number of time slots (N_T) per carrier times the number of carriers per cell (N_C). If the number of users that are currently active in a cell service area is $N_C \times N_T$ then each service request from other subscribers in that cell will be rejected. In CDMA though, provided that the base station site has sufficient number of modems, additional service requests can be accommodated with the understanding that the additional transmissions will increase the error floor of the customers already in service. This softness of CDMA capacity is particularly useful in overloaded system conditions. For example, if the traffic distribution peaks in a number of cells, ie. across a motorway, and the surrounding cells are lightly loaded, the system is able to accommodate more users along the motorway by taking advantage of the reduced inter-cell interference.

The aforementioned advantages of CDMA have been theoretically proved and partially demonstrated in practical field trials. However, the only practical implementation of a CDMA system is the U.S. IS-95 standard which is heavily oriented towards voice only services. CDMA systems for UMTS must accommodate the services tabulated in

Table 2.1. The design of the radio interface which is able to provide, apart from voice, ISDN oriented services gives rise to the design challenges outlined in the next section.

- **Multirate Radio Interface:** As mentioned previously the requirement to provide multiple bit rates over radio is associated with novel design of the radio interface. There are two implementation methods to provide multiple bit rates as shown in Fig.2.2.

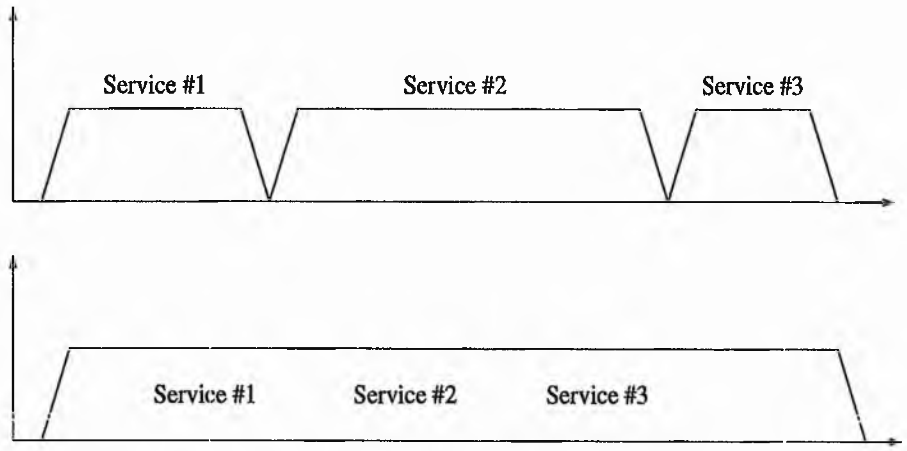

Figure 2.2: Implementation of the Radio Interface For Multiple Bit Rate Provision

The main difference between the first and the second radio interface implementation scenarios lies in the provision of multiple chip rates. According to the first scenario there must be different frequency bands for each of the services since each service requires different spreading factors. However, lower rate services can be accommodated in wider frequency bands. This is the architecture followed in the RACE CODIT project. In order to demonstrate how the provision of multiple bit rates is achieved we have tabulated in Table 2.2 the CODIT services and the respective required chip rates.

Service	Data Rate (kbps)	Chip Rate (Mcps)
Voice Telephony	16	1.023
Data (Low Delay)	128	5.115
Data (High Delay)	2048	20.0

Table 2.2: CODIT Services and Required Chip Rates

Each of the services will be allocated a nominal chip rate. The allocation of chip rates is shown in Fig.2.3.

Assuming BPSK modulation, voice services are provided by narrowband chunks of spectrum of typical bandwidth 1 MHz. They can also be provided by medium

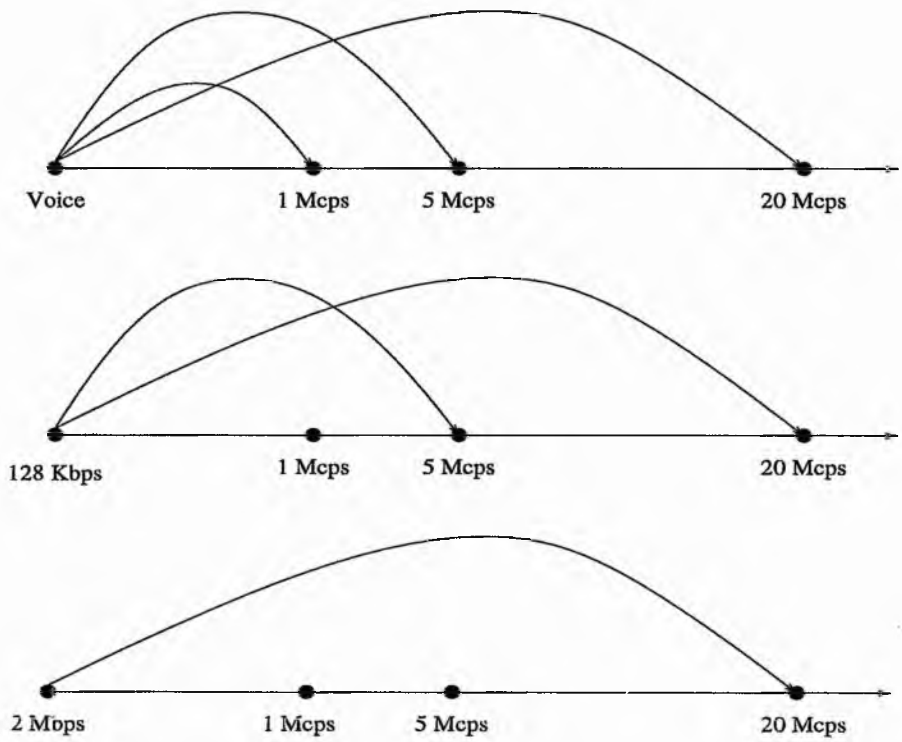

Figure 2.3: Mapping of Multiple Bit Rate Services to Corresponding Chip Rates

band and wideband carriers of typical bandwidth 5 and 20 MHz respectively. ISDN type of services (up to 128 kbps) can only be accommodated by medium band and wideband carriers. High data rate services (2 Mbps) can be accommodated by wideband indoor carriers only.

The second scenario, provides a single chip rate for all services. The common chip rate concept has the following advantage. Since the common chip rate is provided by a single carrier, there is no need for inter-frequency handover from one carrier to the next as is required in the first scenario. The inter-frequency handover requirement is important since means have to be provided for soft handover between different carrier frequencies without the need to incorporate into the handset different Radio Frequency (RF) front-ends. In CODIT, the soft-handover procedure between different carriers is called *seamless handover* and is performed in time-division between the target and the originating carrier [8].

- **Processing Gain Limitations:** The provision of ISDN types of service in the radio link is associated with a reduction in the processing gain, ie. a reduction in capacity compared to the voice only services. For example the transmission of 128 kbps in 5 MHz of bandwidth is associated with a processing gain of 16 dB. A 9.6 kbps voice service in the same bandwidth would have a processing gain of 27 dB. In addition the transmission of data/video services becomes problematic since: (1) These services require much lower BER compared to voice communications. (2) Data users are more vulnerable to multiple access interference compared to the voice users. (3) The advantageous voice activity detection feature cannot be provided with services other than voice. The requirements to transmit only when it is needed can also be partially applied to video services by transmitting only the difference between successive picture frames, thus compressing the required bandwidth. However, the degradation in quality has not yet been evaluated for transmissions over radio.

- **Power Control:** One of the inherent disadvantages of the classic CDMA receiver, with or without multipath diversity, is the strict requirement for continuous power control of the mobile station transmitter. Without power control the receiver becomes near-far limited and its performance starts degrading. The degradation is severe when the standard deviation of the power control error is greater than 2-3 dB. The inability of the receiver to withstand near-far interference is a disadvantage of the particular receiver structure and not an inherent disadvantage of CDMA.

In this thesis we will look at all of the aforementioned problems and attempt to demonstrate the benefits of advanced signal processing receivers as presented in Chapters 4 and 5. However, the understanding of the behaviour of current CDMA receiver technology under non-favorable interference patterns is very significant. In this respect, we have tried to provide a quantitative evaluation of the simplistic correlation based CDMA receiver in a variety of channel conditions. This is the subject of the next chapter.

Chapter 3

CONVENTIONAL CDMA DETECTION

3.1 INTRODUCTION

In this chapter, we address the problem of conventional detection in a multiple access interference limited system. The conventional detection is based on correlation and constitutes the simplest detection technique available. Its optimality for the single user Additive White Gaussian Noise (AWGN) channel has lead to an unprecedented popularity and advanced implementations of this detector can be found in receivers complying to both IS-95 and CODIT specifications. The emphasis is not on providing an exhaustive treatment of multipath diversity reception, but to search for the limits of the multipath diversity receiver both in the downlink and more important in the uplink. For the later the limit is approached through coherent demodulation, and its performance has been demonstrated through various channel estimation techniques.

In section 3.2 a comprehensive description of a general CDMA transmission model is given. In section 3.3 we describe the concept of correlation and the equivalence between the two main implementation architectures of conventional detectors in single path fading and non-fading channels. The performance is evaluated for both AWGN and Rayleigh fading channels, numerically and by Monte-Carlo simulation. In section 3.4 we present the concept of multipath diversity reception. In section 3.5 we investigate methods to provide coherent demodulation in the uplink direction. One of these methods, based on the CODIT radio interface scenario, is of particular importance to any third generation system that employs outbound control channels. The coherent demodulation in the uplink direction is achieved through the combination of a maximal ratio combining RAKE and the equal gain combining RAKE into a single device called Channel Adapted RAKE (CARAKE). The discussion in section 3.6 identifies the performance gains of CARAKE over the Differential RAKE receivers. However, all the gains of CARAKE can be diminished under near-far interference. This is discussed in section 3.7 where we identify the near-far problem and the associated performance degradation of conventional receivers. The power control solution which is subsequently discussed, has a number of inherent characteristics which makes impossible the tracking of rapid power variations.

3.2 NOTATION AND SYSTEM MODEL

For the description of the various system variables, the following notation will be used throughout this thesis.

- N, the spreading factor.
- K, the number of users in the system.
- l, the loading of the system.
- $A(t)$ the Rayleigh faded amplitude of a signal.
- $L(t)$, the Log-normal faded amplitude of the signal.
- $s_k(t)$, the transmitted spread spectrum signal of the kth user.
- $c_k(t)$, the code sequence used by the kth user.
- a_i^k, the ith chip of the kth code sequence.
- $\psi(t)$, the chip waveform.
- R_b^k, the bit rate of the kth user.
- R_c^k, the chip rate of the kth user.
- r, the code rate of the channel encoder.
- N_0, the thermal (or background) noise variance.
- N_I, the noise density of interference.
- D, the diversity order at the receiver.

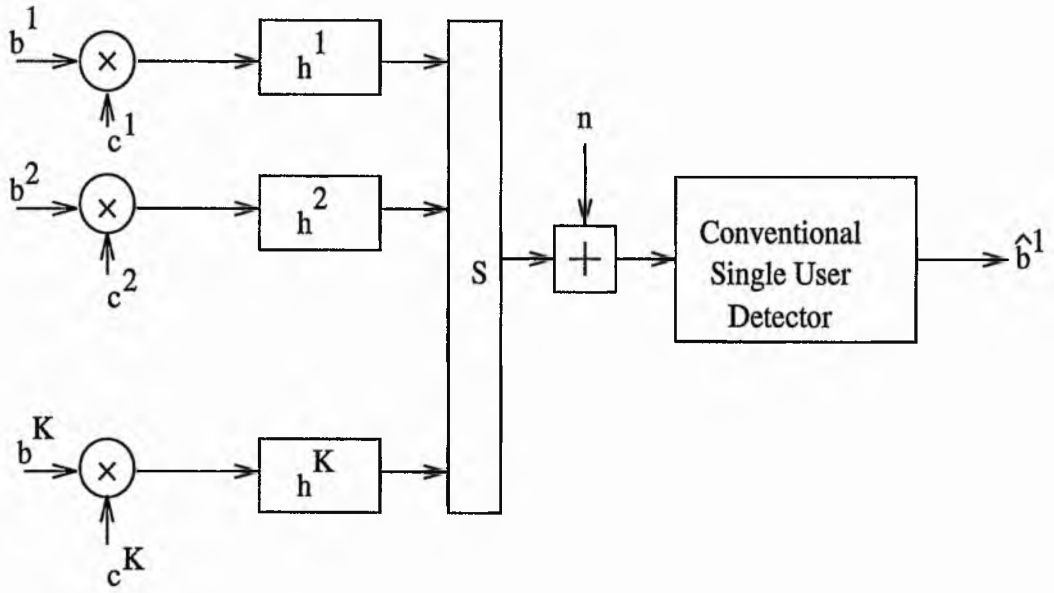

Figure 3.1: System Model of Asynchronous DS-CDMA System

- L, the number of paths of the channel.
- E_b, the energy per bit.
- T_b, the bit duration.
- T_c, the chip duration.
- T_s, the encoded symbol duration.
- b_i^k, the ith information bit of th kth user.
- h_k, the channel impulse response of the kth transmission link.
- ω_c, the carrier frequency
- θ_k, the phase of the carrier of the kth user.

The general CDMA system model is shown in Fig. 3.1.

The model consists of K transmitters each assigned a code sequence of length N,

$$c_k(t) = \sum_{i=0}^{N-1} a_i^k \psi(t - iT_c) \tag{3.1}$$

The transmitted signal can then be written as,

$$s_k(t) = \sqrt{2P_k}\, b_k(t) c_k(t) cos(\omega_c t + \theta_k) \tag{3.2}$$

where P_k is the power of the kth user. The received signal is the sum of the K transmitted signals each convolved with the corresponding channel impulse response plus white Gaussian background noise $n(t)$ of variance $N_0/2$.

$$r(t) = \sum_{i=1}^{K}(s_k(t) * h_k(t)) + n(t) \tag{3.3}$$

Important Parameters of the CDMA System Model: The system model has been left intentionally very general since in DS-CDMA there are a great number of interrelated variables that influence to a great extend the performance of the conventional detector. Concentrating on uncoded transmission, the crucial parameters are,

- **System Load:** Defined as the ratio of the number of users in system over their spreading factor. It is usually expressed as a percentage,ie.

  $$l = \frac{K}{N}100 \tag{3.4}$$

  For example consider a CDMA system with 20 users each employing a spreading factor of 128. If the system is operating in a single path fading channel then the system load will be 15.6%,

  It is customary to express the system load without taking into account the number of propagation paths and this will be followed throughout this thesis.

- **Spreading Factor:** The spreading factor determines the vulnerability to multiple access interference as well as the ability of the receiver to co-exist with narrowband systems (eg. fixed microwave radio, analog and digital mobile services etc). The spreading factor is the number of times that the energy of the transmitted symbol (chip) is reduced compared to the information symbol (bit). In multipath channels, the spreading factor determines also the multipath diversity gain.

- **Spreading Sequences:** For the CDMA uplink transmissions through time-varying multipath channels, the choice of the spreading sequences is not critical since each user's sequence is convolved with the channel impulse response, increasing the cross-correlation interference among the resultant transmissions. Usually, long maximal-length sequences are employed in order to avoid finite family size limitations. On the CDMA downlink on the other hand we can achieve perfect isolation among the user signals by orthogonal (Walsh) spreading. This technique is employed in the IS-95 CDMA standard and benefits the coherent mobile station receiver which observes a downlink signal free of intra-cell interference. As a conclusion, exhaustive research into finding low cross-correlation spreading sequences is unnecessary for the uplink, while it is very important for the synchronous downlink.

- **Demodulation Technique:** Although the modulation format is not crucial to the performance of the detector, the capability to provide coherency at the receiver end is of vital importance. As it will be shown later, the DPSK RAKE is associated with several dB loss in performance as compared to the coherent RAKE for the Bit Error Rates (BER) of interest. Furthermore, as will be also shown, the multipath diversity gain becomes insignificant for DPSK demodulation at low values of E_b/N_0.

In the following section we examine more closely the different implementations of the single path conventional receiver, demonstrating the ability to despread.

3.3 CORRELATION BASED RECEPTION

3.3.1 Correlator vs Matched Filter Detector

The conventional detector has two implementation forms. The first is the matched filter type and consists of a complex Finite Impulse Response (FIR) filter cascaded with a bit-rate sampling device. The second is the correlation type and consists of a complex multiplier cascaded by an integrate and dump filter. The matched filter and correlator detector types are shown in Fig. 3.2 and Fig. 3.5 respectively.

The function of a conventional detector is to despread the signal at its input. The two types of conventional detectors act differently but they yield the same result.

Code Matched Filter The code matched filer performs, in the time domain, the convolution of the input signal with the impulse response of the filter. For a proper operation, the impulse response must be equal to the, reversed in time,complex conjugate of the code sequence. The frequency of a filter matched to an m-sequence of period 31 is shown in Fig.3.3.

If without loss of generality assume that we have real only signals (BPSK modulation) and chips with rectangular pulse shape p_{Tc}, the impulse response of the filter is then as follows:

$$g_k(t) = \sum_{i=0}^{N-1} a^k_{N-i} p_{Tc}(t - (N-i)T_c) \tag{3.5}$$

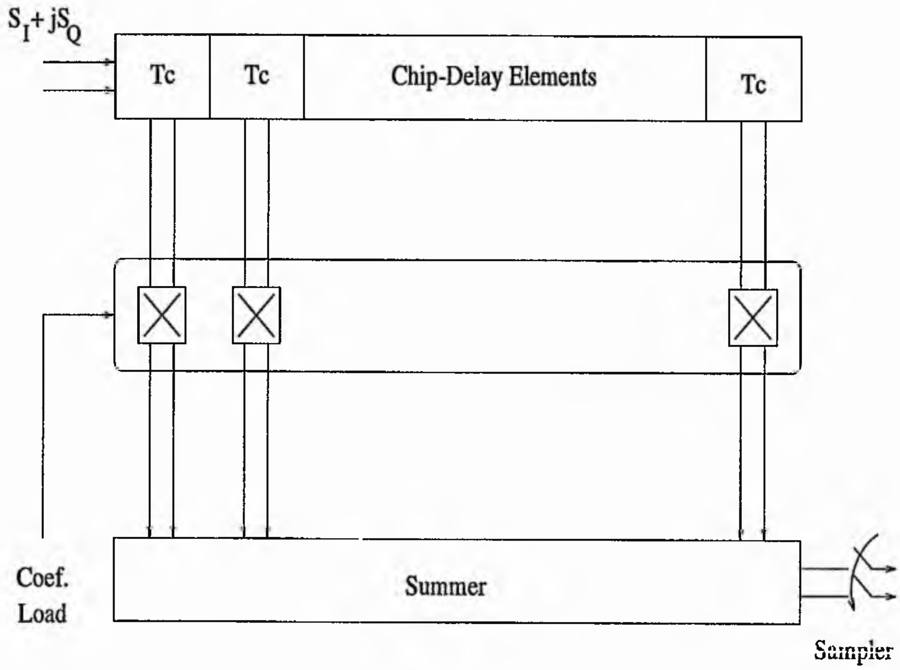

Figure 3.2: Matched Filter Type

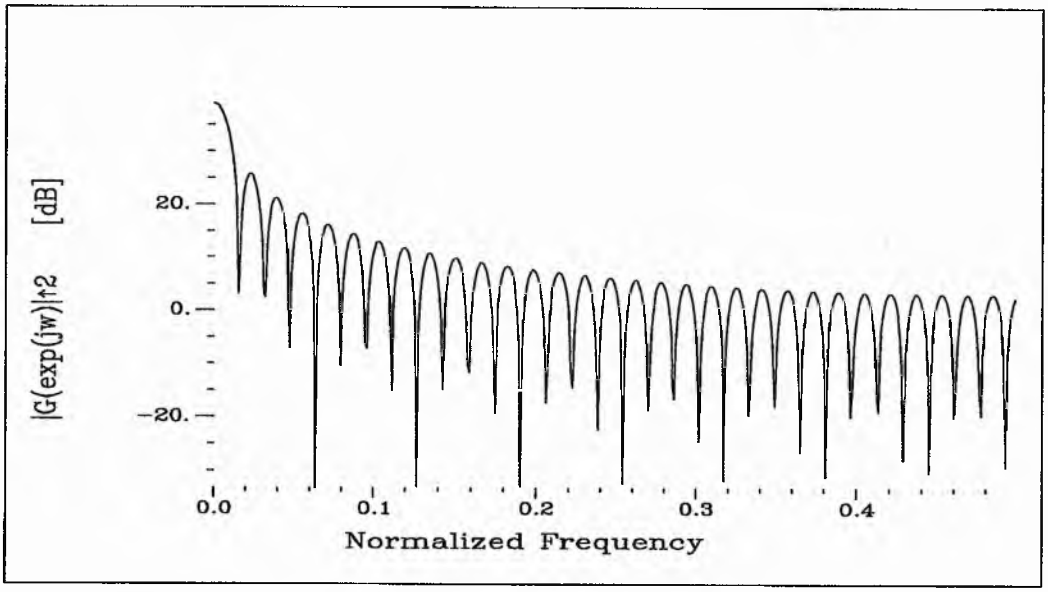

Figure 3.3: Frequency Response of a Filter Matched to an M-Sequence of Period N=31

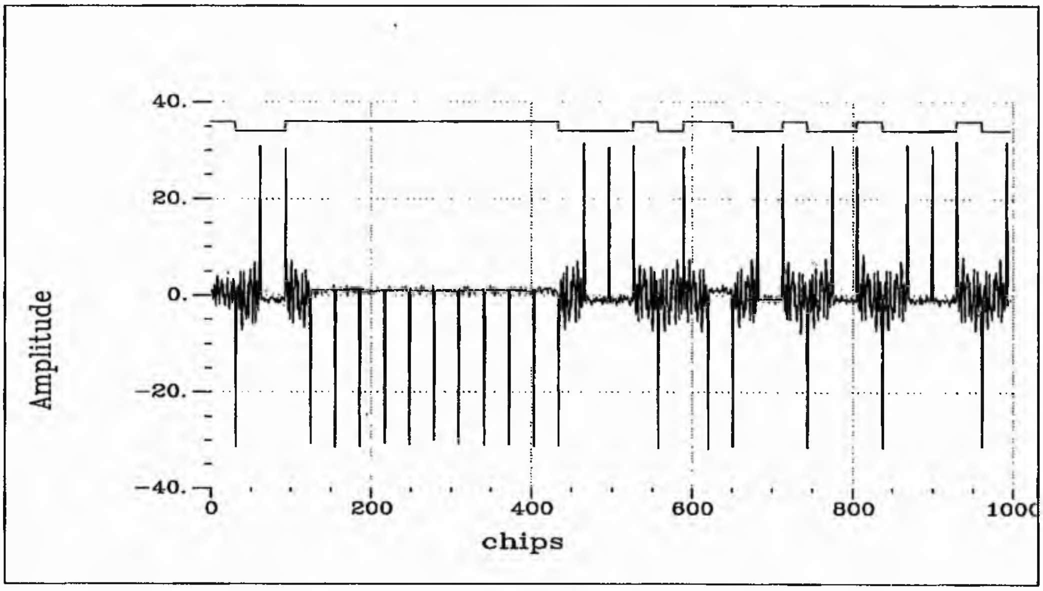

Figure 3.4: Output of a Filter Matched to an M-Sequence of Period N=31, $E_b/N_0 = 10$ dB

For successful despreading the tap delay line should be of length equal to that of the spreading sequence. In addition if oversampling took place at the transmitter, downsampling should be performed before the matched filter, in order to keep the length of the filter equal to the spreading code period. With the response $g_k(t)$ as given in (3.5), the despreading operation can be described as follows:

The kth user baseband spread spectrum signal during the transmission of the jth bit can be written as,

$$s_k(t) = \sqrt{2P_k} b_j^k \left(\sum_{i=0}^{N-1} a_i^k p_{T_c}(t - iT_c) \right) \tag{3.6}$$

By sampling the matched filter output every N chips the decision statistic produced by the the convolution of $s_k(t)$ and $g_k(t)$ will be $N\ b_j^k$. This is illustrated in Fig. 3.4 where the output signal of a filter matched to an m-sequence of period 31 has been produced. The polarity of the data bits is also shown . Notice that the correlation peaks appear every 31 chips while between these peaks the signal is significantly suppressed owing to the good autocorrelation properties of m-sequences.

Correlator The correlator performs in the time domain a complex multiplication on a sample by sample basis and subsequently an N chip accumulation. The accumulator is

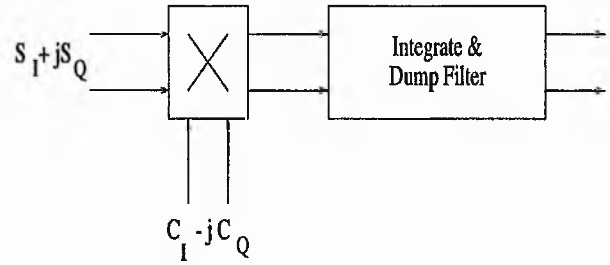

Figure 3.5: Correlator Type

usually implemented by an integrate and dump filter. For the general case of complex input signal, the incoming signal is multiplied by the complex conjugate of the spreading sequence. The decision statistic, in the absence of any channel noise, is the same as in the matched filter case and can be written as,

$$y_k^j = \int_0^T s_k(t)\ c_k^*(t)dt = \int_0^T \sqrt{P_k} b_j^k (c_k(t) c_k^*(t))dt = \sqrt{P_k} b_k(t) \tag{3.7}$$

The correlator type is popular in systems that employ very long spreading sequences because its complexity does not increase linearly with the spreading factor. The code matched filter, on the other hand, is popular in systems that employ short spreading sequences. In addition, for the moderate Doppler frequencies met in terrestrial mobile communication systems, code matched filters are widely used as delay estimation devices, especially in the downlink where a pilot channel is provided [7].

3.3.2 Performance in AWGN

In depth analysis of the conventional detectors in the AWGN environment has been reported by various researchers [49], [19]. The multiuser AWGN channel performance analysis is mostly based on the approximation of multiple access interference as Gaussian noise. This approximation has been found that is quite tight when the number of users in the system is greater than 10 *and* when the signals arriving at the receiver have equal average power. With no doubt, the Gaussian approximation has been of great value from the simulation point of view, since it involves a simple adjustment of the noise variance as the number of users changes.

Let us consider the general model of section 3.2. The complex impulse response of each user's channel in the AWGN case can be written as,

$$h^k(t) = \delta(t - t_0^k) \tag{3.8}$$

where t_0^k is the modulo-T relative delay of the kth user with respect to the user of interest. Notice that the weight of the Dirac delta function is $\alpha = 1.0$. It might be the case that the single path of each user is attenuated, which in this case, $\alpha < 1.0$ and the performance will be inferior to the one considered here. When $\alpha < 1.0$, a static AWGN channel arises and in the general case with many paths this channel have been used to model fixed satellite communication systems.

If we assume that the received signal $r(t)$ is correlated with the time-aligned replica of the code of the user of interest (user #1), the output of the correlator is given by,

$$y_1 = \int_0^{T_b} r(t)a_1(t - \tau_1)cos(\omega_c(t - \tau_1) + \phi_1)dt \tag{3.9}$$

The decision statistic y_1 is not straightforward to describe since it depends on:

- The relative time delays between the user of interest and each interfering user ie. on the channel impulse responses of all the users in the system.
- The family of the codes used for spreading the K-user signals.

However, for the simple AWGN channel case considered here, it is possible to analytically treat these dependences by using special functions, known as crosscorrelation functions. The more important cross-correlation functions are,

Aperiodic Crosscorrelation Function: The aperiodic crosscorrelation function between two binary codes c^k and c^i each one with period $N = 2^n - 1$ is defined as,

$$C_{k,i}(l) = \begin{cases} \sum_{j=0}^{N-1-l} a_j^k a_{j+l}^i & 0 \leq l \leq N-1 \\ \sum_{j=0}^{N-1-l} a_{j-l}^k a_j^i & -(N-1) \leq l < 0 \\ 0 & |l| \geq N-1 \end{cases} \tag{3.10}$$

Periodic Crosscorrelation Function: The periodic crosscorrelation function has two definitions depending on the relationship between the current and the preceding bit. If

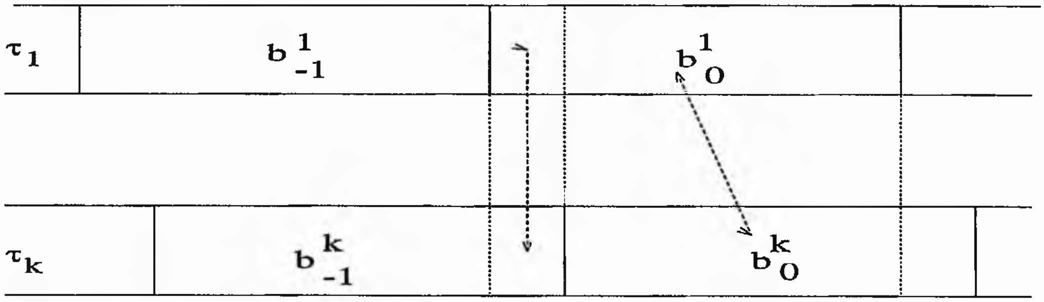

Figure 3.6: Graphical Representation of Crosscorrelation Functions

these bits have the same polarity then we can define the *even* periodic crosscorrelation function as,

$$\theta_{k,i}(l) = \sum_{j=0}^{N-1} a_j^k a_{j+l}^i = C_{k,i}(l) + C_{k,i}(l-N) \tag{3.11}$$

If the bits have opposite polarity then we define the *odd* periodic crosscorrelation function as,

$$\hat{\theta}_{k,i}(l) = C_{k,i}(l) - C_{k,i}(l-N) \tag{3.12}$$

In Fig. 3.6 the relative position of the underlying bits stream in a two user system has been drawn.

The user of interest is represented with index 1 while the interfering user, with index k. Assuming that we are interested in detecting the 0th bit of user 1, it can easily be observed that this bit overlaps with two other bits, namely b_0^k, b_{-1}^k, of the interfering user. Thus, the interference depends on two variables:

- The value of the crosscorrelation function between the codes of the two users.
- The polarity of the two interfering bits.

Now that the definition of the crosscorrelation functions is well in place, we proceed with writing the output of the correlation detector of user 1 as,

$$y_1 = \sqrt{P_1} b_0^1 + \sqrt{P_1} \sum_{k=2}^{K} [b_{-1}^k R_{k,1}(t_k) + b_0^k \hat{R}_{k,1}(t_k)] cos(\phi_k - \phi_1) + z(t) \tag{3.13}$$

where b_0^1 is the bit of the 1st user, $z(t)$ is Gaussian noise of variance N_0 and the functions $R_{k,m}$ and $\hat{R}_{k,m}$ are defined as follows,

$$R_{k,m}(\tau) = \int_0^{T_b} c_k(t-\tau)c_m(t)dt \tag{3.14}$$

$$\hat{R}_{k,m}(\tau) = \int_\tau^{T_b} c_k(t-\tau)c_m(t)dt \tag{3.15}$$

$R_{k,m}$ and $\hat{R}_{k,m}$ are called continuous-time partial crosscorrelation functions of the kth and the mth spreading waveforms. These are related to the discrete aperiodic cross-correlation function with the relations,

$$R_k, m(\tau) = C_{k,m}(l)\hat{\mathcal{R}}_\psi(\tau - lTc) + C_{k,i}(l+1)\mathcal{R}_\psi(\tau - lT_c) \tag{3.16}$$

$$\hat{R}_k, m(\tau) = C_{k,m}(l-N)\hat{\mathcal{R}}_\psi(\tau - lTc) + C_{k,i}(l+1-N)\mathcal{R}_\psi(\tau - lT_c) \tag{3.17}$$

where $\mathcal{R}_\psi(x) = \int_0^x \psi(t)\psi(t+T_c-x)dt$ and $\hat{\mathcal{R}}_\psi(x) = \int_x^{Tc} \psi(t)\psi(t-x)dt$.

Regarding the nature of the decision statistic, it is evident that,

- The decision statistic can be written as the sum of the detected bit corrupted by a K-1 term sum which represents the multiple access interference and a *colored* noise component z(t).
- For K sufficiently large, ($K > 10$), the K-1 term sum of the previous equation can be approximated by additive Gaussian noise. This is a fundamental observation that led Pursley ([49]) to his famous treatment of DS-CDMA performance analysis.
- The additive result of the noise and the interference is not white but colored. Thus we can argue that with conventional detector we use a detection structure which is optimum for white noise environments, to detect signals in colored noise environment. This observation is fundamental and lead us to propose new detector structures in Chapter 4 and Chapter 5.

The performance of the conventional detector with coherent antipodal demodulation in the AWGN channel is given by [49],

$$P_b = \frac{1}{2} erfc\left[\sqrt{\frac{E_b/N_0}{1+\frac{2}{3}\frac{K-1}{N}E_b/N_0}}\right] \tag{3.18}$$

In the above equation, for a single user system ($K = 1$) we get the well known equation for the bit error probability,

$$P_b = \frac{1}{2} erfc\left[\sqrt{E_b/N_0}\right] \tag{3.19}$$

This means that for the uncoded system the variance of the white Gaussian noise source must be adjusted by a factor F in order to account for the $K-1$ asynchronous interfering users. This factor is,

$$F = 1 + \frac{2}{3}\frac{K-1}{N}E_b/N_0 \tag{3.20}$$

The variance of the additive noise channel which takes into account the multiple access interference is then given by,

$$\sigma^2 = P_1\ 10^{-\frac{E_b/N_0}{10}}\ \frac{1}{log_2 M}\ N\ F \tag{3.21}$$

where N is the spreading factor, M is the order of modulation (eg. $M = 4$ for QPSK, $M = 2$ for BPSK) and P_1 is the power of the user of interest. The performance of a multiuser system in the AWGN channel is shown in Fig. 3.7 and Fig. 3.8 for 31 and 255 chips/bit respectively. The graphs have been plotted based on equation (3.18).

The performance of a multiuser system in the AWGN channel has also been evaluated using Monte-Carlo simulation. These results are shown in the Fig. 3.9 and Fig. 3.10 for 31 and 255 chips/bit respectively.

3.3.3 Performance in Rayleigh Fading

The performance of the conventional detector in a single path Rayleigh fading channel will now be evaluated starting again from the general system model introduced in section 3.2.

For the Rayleigh fading case the complex channel impulse response for each user is time-varying. The probability density function (PDF) of the real and imaginary components of the channel variations is Gaussian. The envelope of the kth user signal has amplitude A_k given by,

$$A_k = \sqrt{h_{Ik}^2 + h_{Qk}^2} \tag{3.22}$$

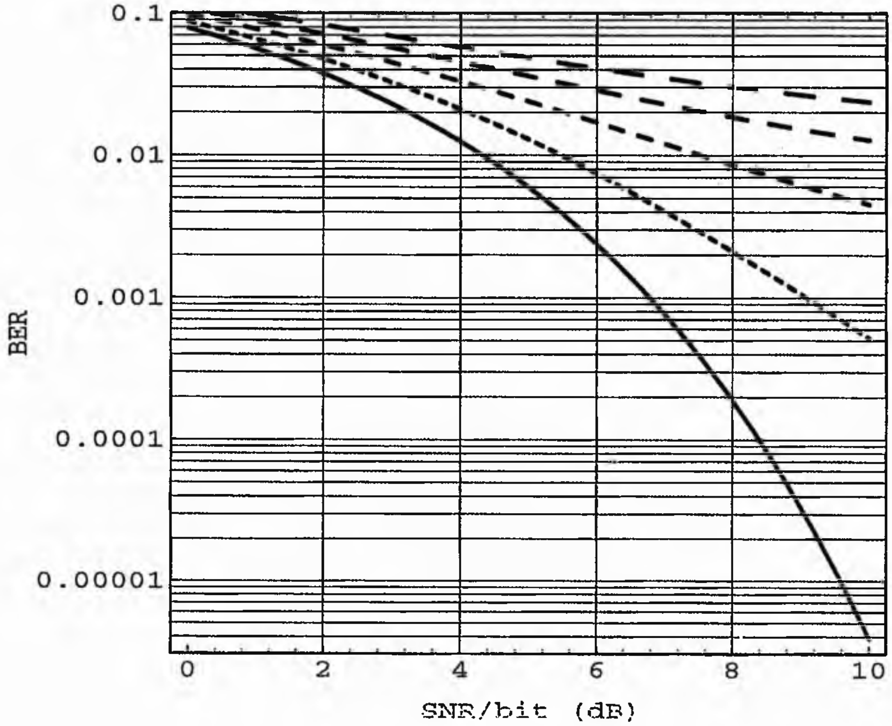

Figure 3.7: Performance of Conventional Detector in Multiuser AWGN Channel, N=31, —- 1 User, - - 5 Users, – – 10 Users, — — 15 Users, —— —— 20 Users

If h_{Ik} and h_{Qk} are Gaussian random variables then A_k follows the Rayleigh distribution. The PDF of A_k is given by,

$$p(A_k) = \frac{1}{2\sigma_{Ak}^2} exp\left[-\frac{A_k}{2\sigma_{Ak}^2}\right] \tag{3.23}$$

From basic probability theory it is known that if A_k is Rayleigh distributed then A_k^2 is chi-square distributed. Since A_k^2 is the sum of two Gaussian distributed random variables,namely h_{Ik} and h_{Qk}, then A_k^2 will be chi-square distributed with two degrees of freedom. This leads us to determining the distribution of the $(E_b/N_0)_k$ ratio of the kth user. This ratio will be a random variable as it is given by the product $A_k^2(E_b/N_0)_k$. Since A_k^2 is chi-square distributed the product $\gamma_b^k = A_k^2(E_b/N_0)_k$ will be also chi-square distributed, consequently, the PDF of γ_b^k will be given by,

$$p(\gamma_b^k) = \frac{1}{E(\gamma_b^k)} exp\left[-\frac{\gamma_b^k}{E(\gamma_b^k)}\right] \tag{3.24}$$

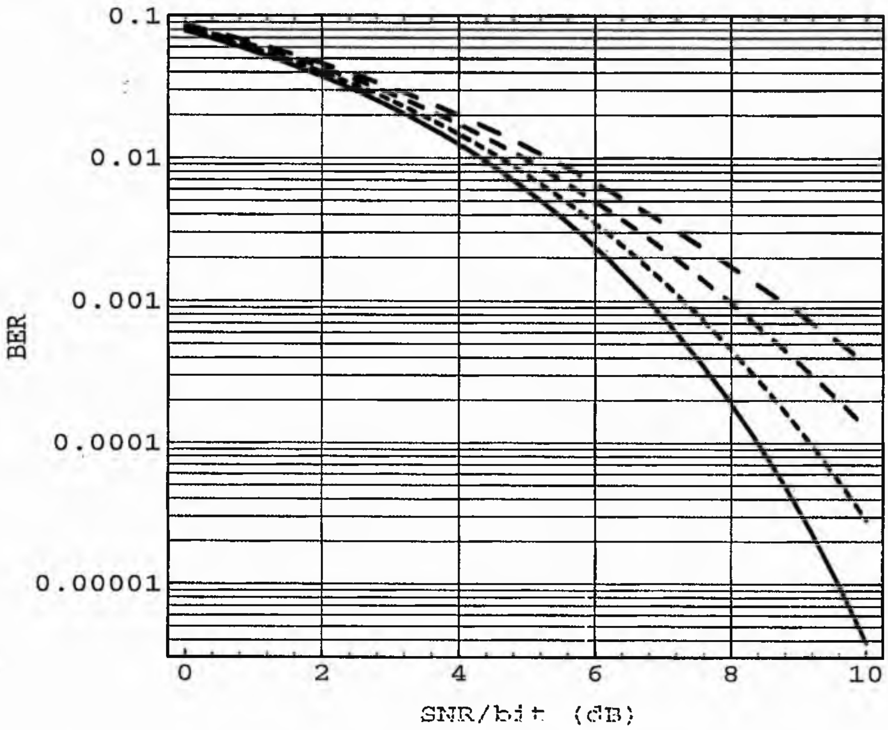

Figure 3.8: Performance of Conventional Detector in Multiuser AWGN Channel, N=255, — 1 User, - - 10 Users, – – 20 Users, — — 30 Users

Single User System: In the single user case we drop the superscript k from the SNR/bit expression. The probability of error can be obtained by the following formula:

$$P_b = \int_0^{\infty} \frac{1}{2} erfc[\ \sqrt{\gamma_b}\ ]\ p(\gamma_b)\ d\gamma_b \tag{3.25}$$

After substitution of (3.24) into (3.25) and carrying out the integration we come to the well known result [47],

$$P_b = \frac{1}{2}\left[\ 1 - \sqrt{\frac{E(\gamma_b)}{1 + E(\gamma_b)}}\ \right] \tag{3.26}$$

where$E(\gamma_b)$ is the expected value of the γ_b. All performance curves for Rayleigh fading channels in this thesis are plotted against the average SNR/bit.

Multiuser System: In a multiuser system the computation of the bit error probability involves again the assumption concerning the statistics of the multiple access interference. It has been found [20] that the Gaussian approximation is still valid for fading

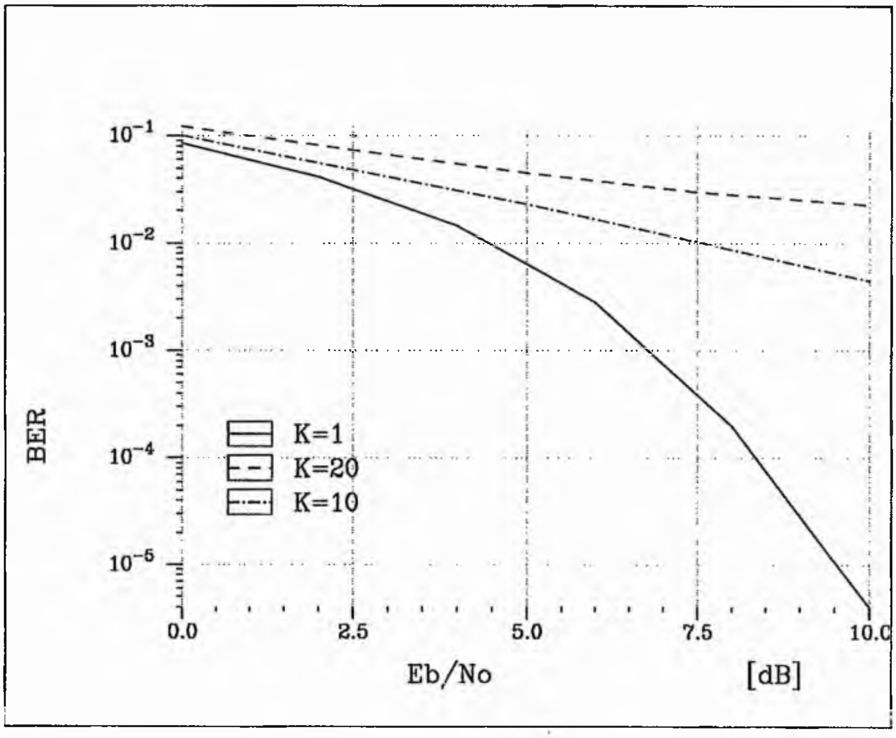

Figure 3.9: Simulated Performance of Conventional Detector in Multiuser AWGN Channel, N=31

channels. The evaluation of the bit-error rate with the assumption of Gaussian interference is straightforward. The starting point is to find the expression of the equivalent SNR/bit in the presence of K-1 interfering users. This is given by,

$$\gamma_b^K = \frac{\gamma_b^k}{1 + \frac{2}{3}\frac{K-1}{N}\gamma_b^k} \tag{3.27}$$

If we now replace (3.27) into (3.26) we come up with,

$$P_b = \frac{1}{2}\left[1 - \sqrt{\frac{E(\gamma_b^K)}{1 + E(\gamma_b^K)}}\right] \tag{3.28}$$

The last equation has been plotted in Fig. 3.11 and Fig. 3.11 for 31 and 255 chips per bit respectively.

The performance of the conventional detector has been also evaluated through Monte-Carlo simulation. Of interest is again the measurement of the E_b/N_0 degradation caused by multiple access interference. The Rayleigh fading is assumed to be constant over one bit duration. The results of the simulation can be seen in Fig. 3.13 and Fig. 3.14

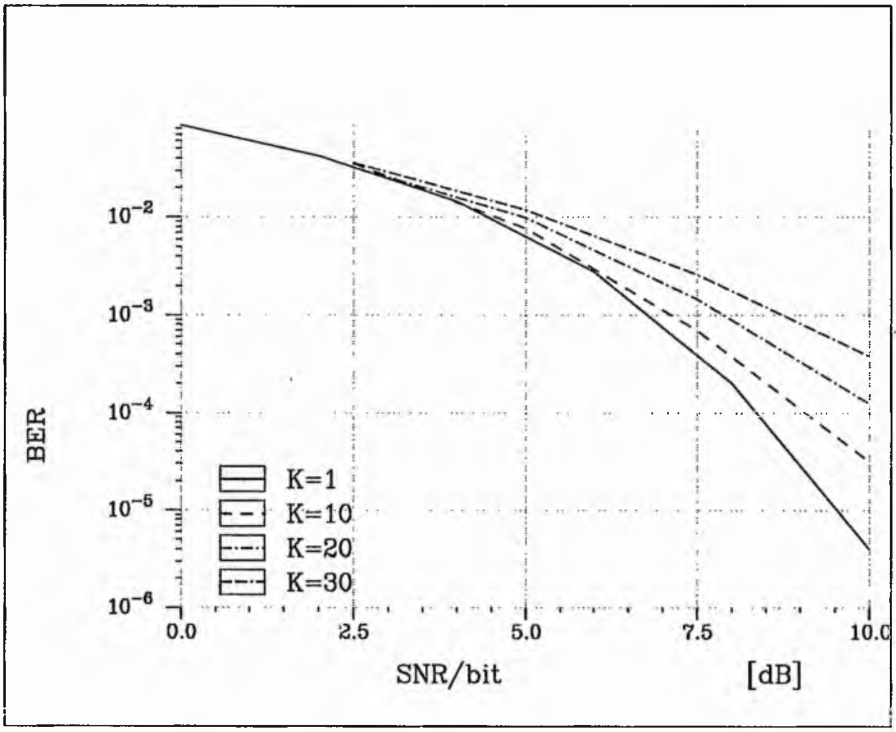

Figure 3.10: Simulated Performance of Conventional Detector in Multiuser AWGN Channel, N=255

for 31 and 255 chips per bit respectively.

3.3.4 Discussion I

An inspection at the performance results of the conventional detector in AWGN and Rayleigh fading channels, leads us to make the following observations:

- In AWGN channel and for 1% BER and 31 chips/bit, 10 users can be supported each transmitting with an E_b/N_0 ratio of 7.5 dB. In Rayleigh fading channel a 5 user system appears to have an irreducible BER of 2%.

- The conventional detector is more sensitive to multiple access interference in Rayleigh fading channels than in the AWGN case. This is clearly shown in Fig.3.15 where the BER has been plotted against the system loading l.

  The curve for Rayleigh fading channel reaches the irreducible BER levels for much lower loading conditions compared to AWGN. The conventional detector in Rayleigh

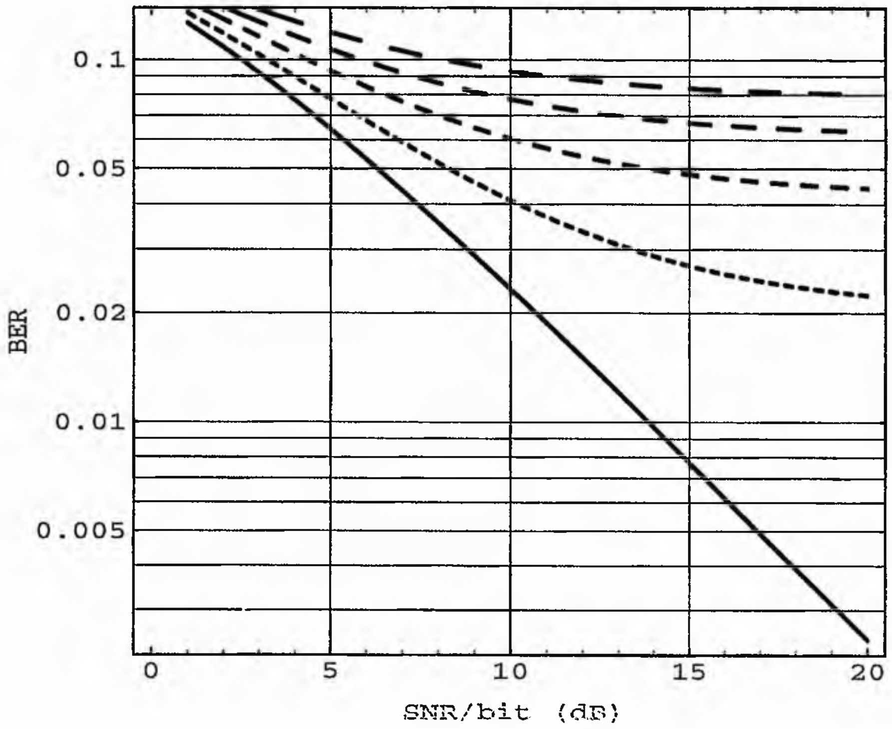

Figure 3.11: Performance of Conventional Detector in Multiuser Rayleigh Fading Channel, N=31

fading will not cross the 1% BER floor loading is kept below 5% while in the AWGN the same BER target will be achieved if the system loading is below 40%.

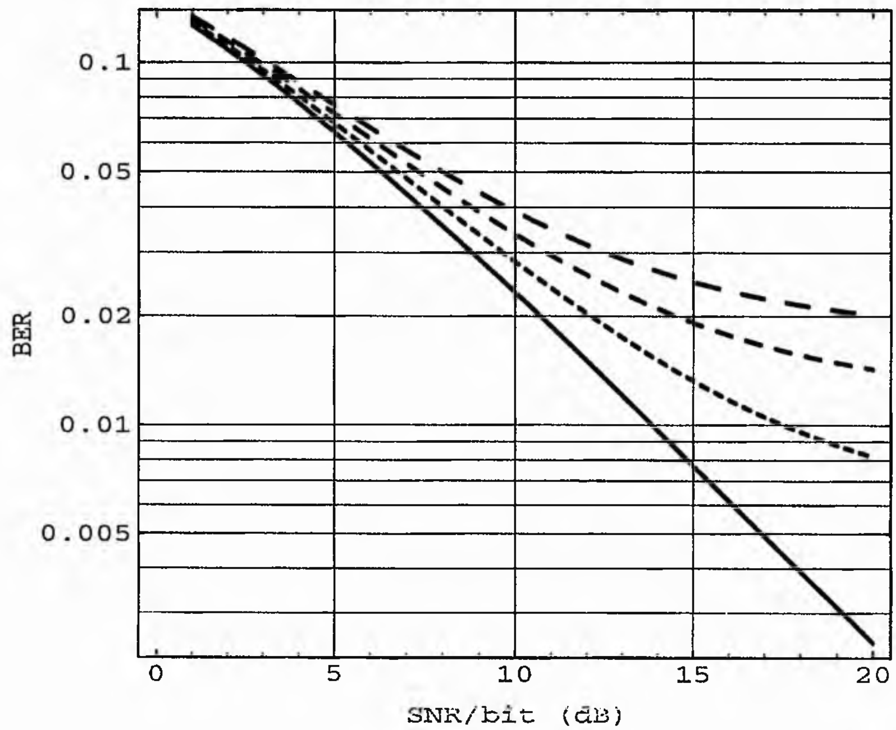

Figure 3.12: Performance of Conventional Detector in Multiuser Rayleigh Fading Channel, N=255

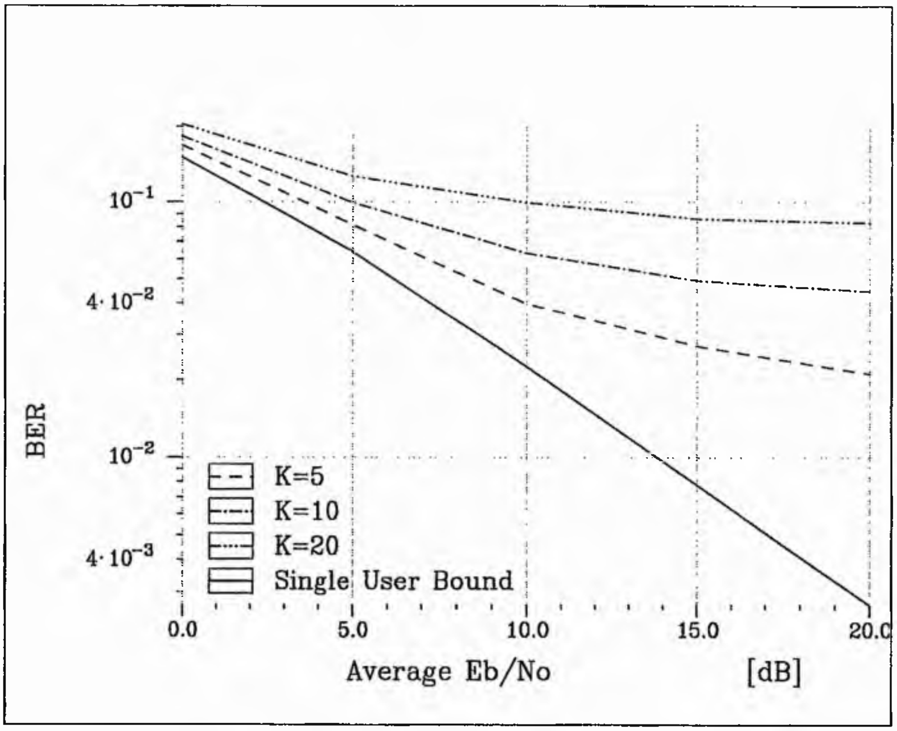

Figure 3.13: Simulated Performance in Multiuser Rayleigh Fading Channel, N=31

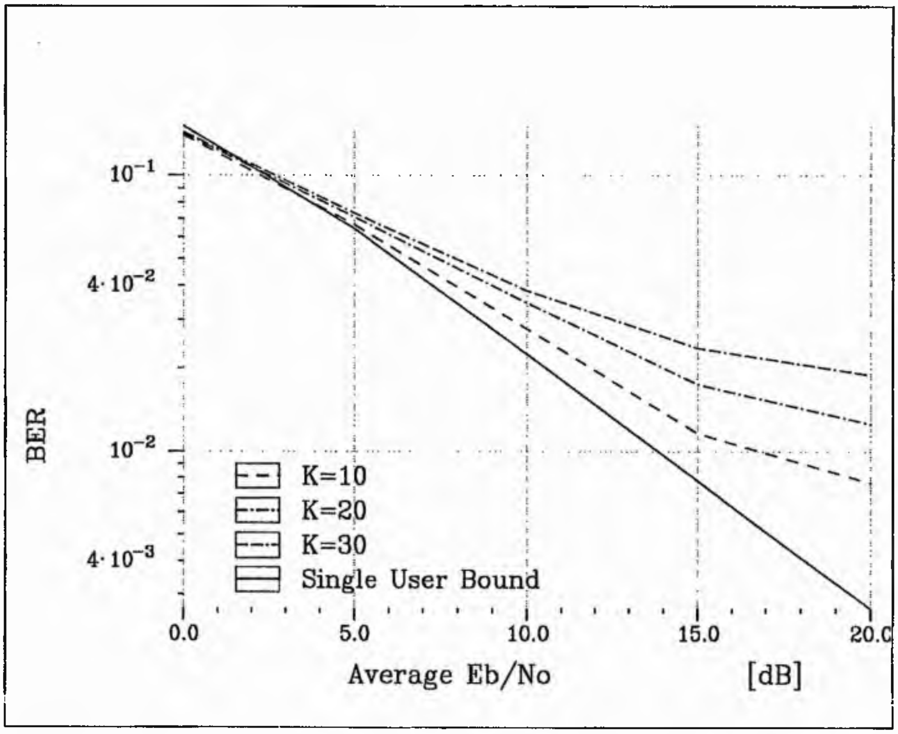

Figure 3.14: Simulated Performance in Multiuser Rayleigh Fading Channel, N=255

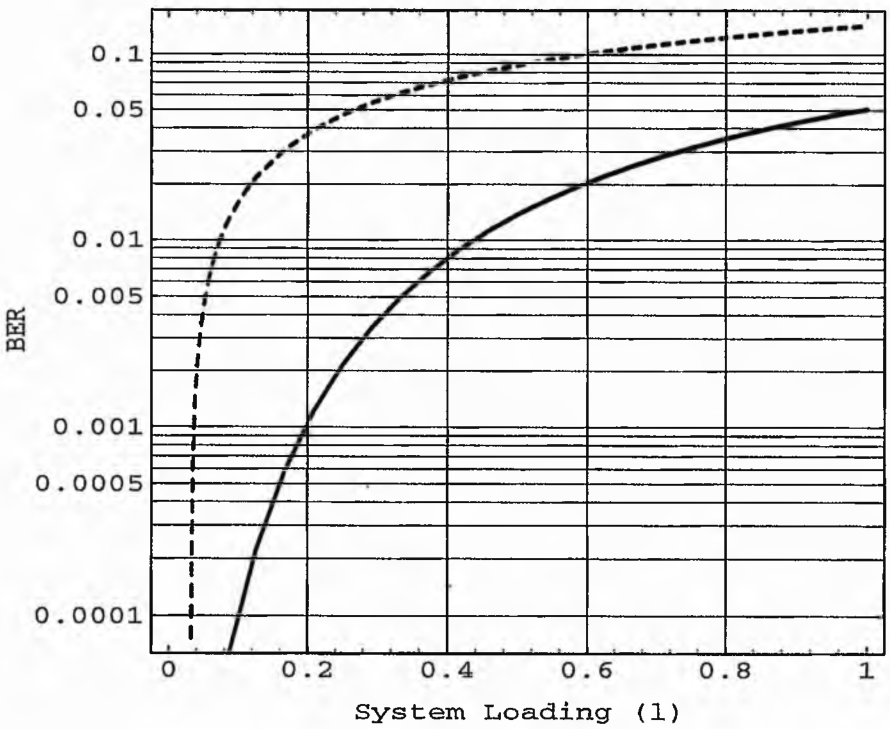

Figure 3.15: Effect of System Load in (—) AWGN and (- -) Rayleigh Fading Channels

3.4 MULTIPATH DIVERSITY RECEPTION

One of the inherent and most useful attributes of CDMA is known as multipath diversity reception. It is this technique that allows CDMA to overcome the detrimental effects of multipath fading and in the majority of the cases, convert the loss due to multipath fading into gain.

3.4.1 Multipath Diversity

Multipath diversity is the technique which provides the means to: (1) jointly detect the information bearing signal the energy of which has been spread into different paths and (2) combine the detector outputs to form the final decision variable. The concept of multipath diversity is based on the observation that the probability that the information bearing signal will fade is greatly reduced if several replica of this signal are transmitted over independent fading paths and processed by the receiver in parallel. The real world transmission medium can be modelled as a tapped delay line whose taps are time varying and follow specific probability distributions. A typical multipath channel model is shown in Fig. 3.16.

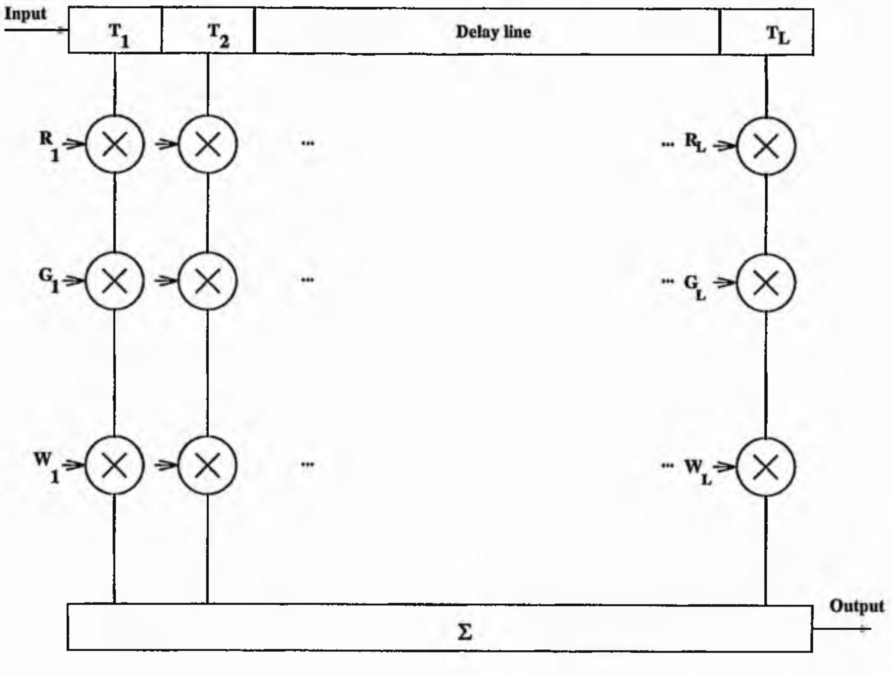

Figure 3.16: The Multipath Propagation Channel Model

The model consists of L paths. The ith path is characterised by a path delay

T_i, a constant path weight W_i and a set of time-varying weights which represents the multiplicative distortion of the signal. The two main time-varying distortions are the Rayleigh fading R_i and the Log-normal fading G_i. The later is caused by propagation shadowing and is relatively slower than the Rayleigh fading. In real-world of relatively wideband channels there is inter-path correlation [43] but it is customary to assume that each path fadesindependently of the others. In computer modeling this is achieved easily by feeding the Rayleigh/Log-normal generators of each path with different starting values.

With this channel model in mind, the diversity can be exploited if there is some way of distinguishing the individual paths from their sum. This can only be possible if the transmitted signal occupies a bandwidth W such that:

$$W >> B_c \tag{3.29}$$

where B_c is the coherence bandwidth of the channel which is related to the delay spread with,

$$T_m \approx \frac{1}{B_c} \tag{3.30}$$

In CDMA mobile systems because the signal is spread the previous inequality is always true even for moderate spreading factors. The CDMA receiver is able to distinguish paths that their inter-arrival time is longer than T_c ie. the duration of one chip. In other words the time resolution of CDMA is $1/W$ and consequently for a multipath delay spread of T_m there are T_m/T_c resolvable paths. These paths can be detected and optimally combined with structures known as RAKE receivers, the subject of the next section.

3.4.2 The RAKE Receiver

The RAKE receiver was named for its ability to act as a garden rake and gather the energy of the signal that has been spread over multiple paths. A typical 4-finger RAKE receiver can be seen in Fig. 3.17.

Starting point to the description of the functions of the RAKE receiver is the RAKE fingers which are individual single path conventional detectors. Their architecture depends on the bit-level modulation format.

The bit-level modulation can be one of the following forms:

- BPSK, where the same bit is fed to both in-phase and quadrature chip-level channels as depicted in Fig. 3.18(A).

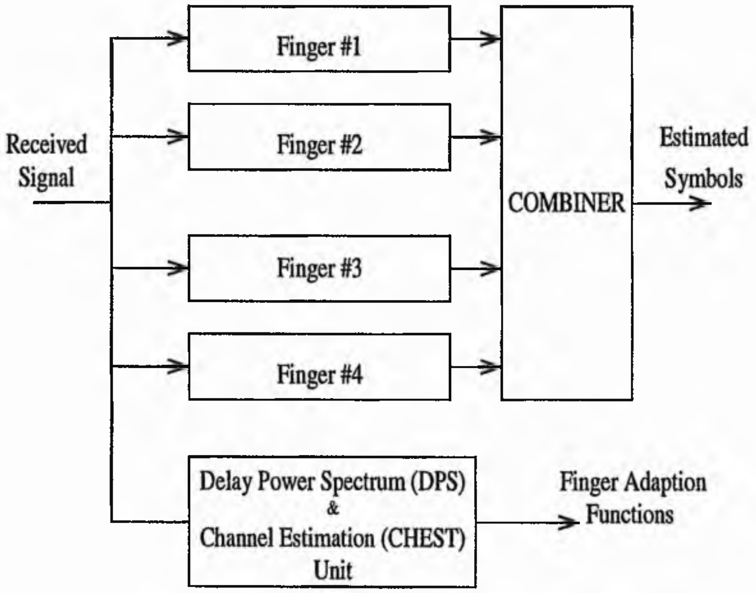

Figure 3.17: Typical 4-Finger RAKE Receiver Architecture

- QPSK, where the chip-level in-phase and quadrature channels carry different information bits (Fig. 3.19A).
- Differential BPSK, which is a BPSK bit-level modulation with differentially encoded information bits (Fig. 3.18B).
- Differential QPSK, which is a QPSK bit-level modulation with differentially encoded information bits (Fig. 3.19B).

Notice that that the Balanced QPSK (BQPSK) modulation is BPSK at the bit-level and QPSK when viewed at the chip level. Variants of the above modulation formats can be obtained by offsetting the quadrature chip-level channel by a chip duration. For the purposes of this thesis, QPSK and DQPSK modulations are sufficient to illustrate the two major combining techniques used in RAKE receivers,namely, Maximal Ratio Combining (MRC) and Equal Gain Combining (EGC).

Because of the existence of a pilot channel in the downlink, phase coherency is easily obtained at the mobile station receiver. Thus, MRC RAKE combining can be easily implemented in the downlink. On the other hand, differentially coherent demodulation is used in the uplink due to the inability to provide a phase reference. [1] Thus, EGC RAKE combing is employed in the uplink.

[1]Recent developments of CDMA uplink channel estimation will inevitably lead to coherent demodulation in both downlink and uplink as will be demonstrated in section 3.5.

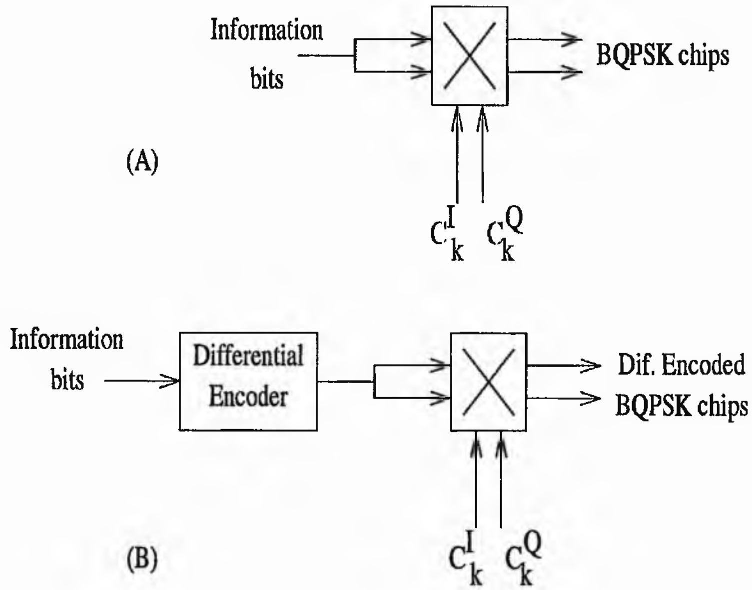

Figure 3.18: Balanced QPSK (A) and Differentially Encoded Balanced QPSK (B) Modulation

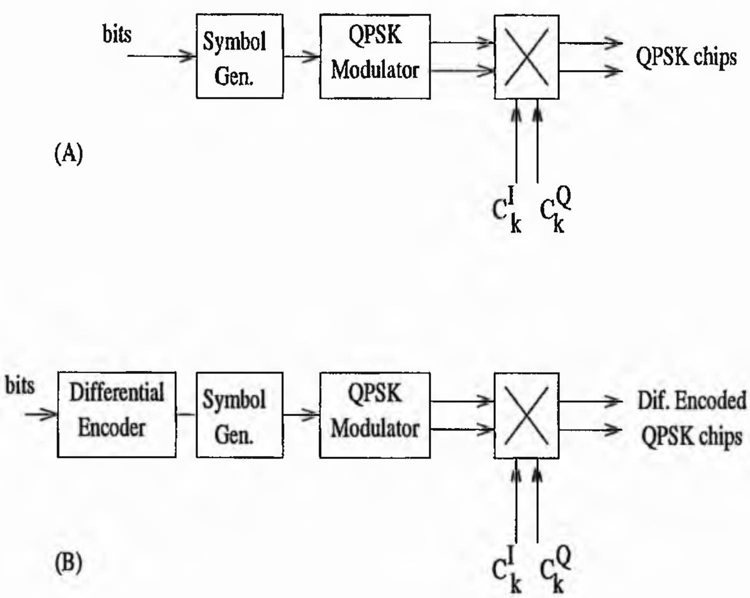

Figure 3.19: QPSK (A) and Differentially Encoded QPSK (B) Modulation

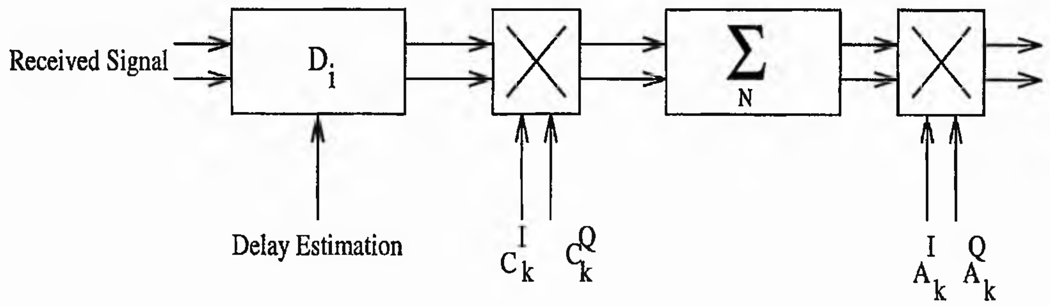

Figure 3.20: Finger Detail for PSK Modulated Signals

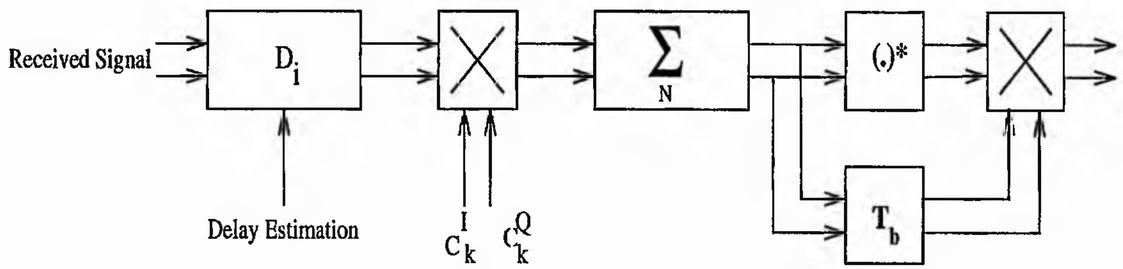

Figure 3.21: Finger Detail for DPSK Modulated Signals

In Fig. 3.20 and Fig. 3.21 the standard finger configuration, for coherent and non-coherent demodulation options, is depicted.

The first element of the signal processing chain is a delay (buffer) with variable size. The size is determined from the delay estimation unit. The function of the unit is to estimate the delay of each path. We have two major methods for estimating the delay, one for the downlink and one for the uplink. The delay estimation is based in conventional code acquisition techniques [25] as far as the delay of the strongest path is concerned. The delay power spectrum estimator then provides the delays of the multipath components by cross-correlating the received signal over a finite window around the delay of the strongest path. The second signal processing step is the despreading operation, achieved by a correlator and integrate and dump filter. For coherent combining, the despread signal is multiplied by the complex conjugate of the channel impulse response, while for the non-coherent case it is conjugated and multiplied by the unit bit-delayed replica of the integrate and dump filter output.

3.4.3 Performance of RAKE in the Multipath Fading Channel

The analytical evaluation of the performance of the D-finger RAKE receiver over an L-path multipath fading channel is based again on the general model introduced in section 3.2. In the multipath fading case, each the K channel impulse responses can be written as,

$$h_k(t) = \sum_{l=1}^{L} A_l(t) exp(-j2\pi f_c \tau_l(t))\delta(t - \tau_l(t)) \tag{3.31}$$

where L is the number of paths, τ_l is the lth path delay and $A_l(t)$ is the time-varying attenuation of each path.

Given that the user of interest is the user #1, the output of the the first correlator during the ith bit interval, assuming that the fading process can be regarded almost constant over the bit duration, is given by,

$$y_i = A_i^1 \sqrt{E_b} b_0^1 + \sum_{l=2}^{L} A_l^1 cos(\phi_1^l - \phi^1)[b_{-1}^1 R_{1,1}(t_1^l) + b_0^1 \hat{R}_{1,1}(t_1^l)] \tag{3.32}$$

$$+ \sum_{l=1}^{L} \sum_{k=2}^{K} A_l^k cos(\phi_k^l - \phi^1)[b_{-1}^k R_{k,1}(t_k) + b_0^k \hat{R}_{k,1}(t_k)] + n(t) \tag{3.33}$$

We can now make the following observations:

- The correlator output consists of 4 terms. The first is the bit of interest attenuated by the fading term A_i^1. The second is the self-noise created from the cross-correlation between the first and each of the $L-1$ multipath components. The third is the multiple access interference, created by the cross-correlations between the first path of the user of interest and each of the L multipath components of the $K-1$ interfering users.

- The second term dictates for channel equalization, since its effects on the receiver performance will be severe. By assuming that the delay spread does not exceed the bit duration, the received signal is corrupted by interchip interference (ICI) instead of intersymbol interference (ISI) commonly found in narrowband systems. The assumption is valid for the typical urban environment and for moderate spreading factors ie. for chip rates greater than 1 Mcps.

- By exploiting the multipath diversity the self-noise is treated to the advantage of the receiver performance as will be shown shortly.

If D denotes the order of diversity that is exploited at the receiver (ie. the number of RAKE fingers) then we can distinguish two cases:

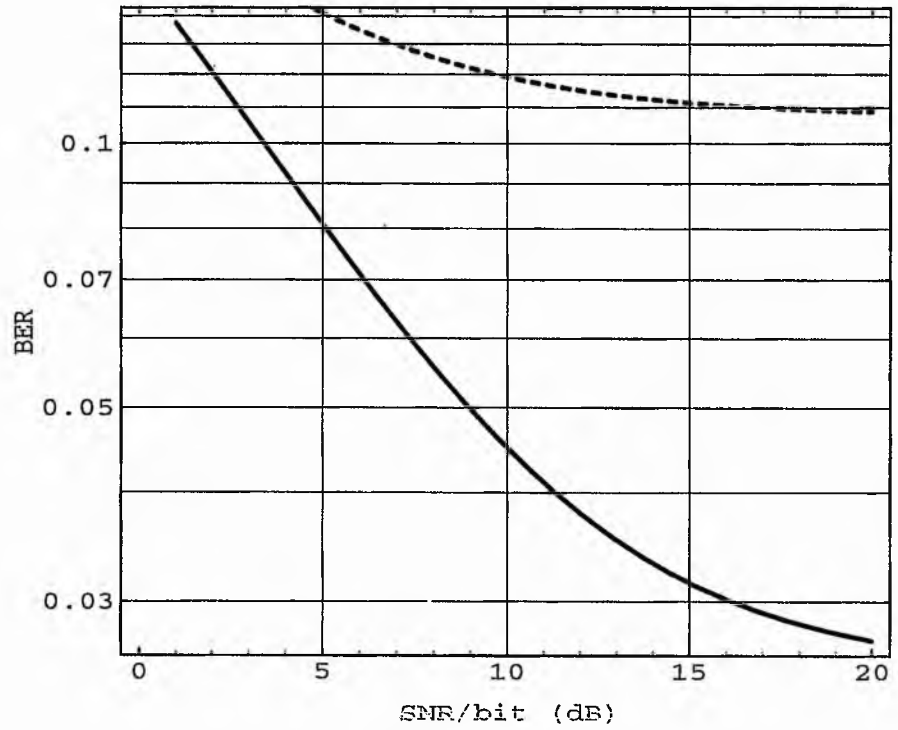

Figure 3.22: Performance of Conventional Detection in Multipath Rayleigh Fading Channel,(—) K=1, (- -) K=5, L=6, D=1, N=31

Single RAKE Finger (D=1)

In multipath channels we have an additional source of degradation termed self-noise. Self-noise in an L-path channel is the noise generated from the cross-interference of one path with the L-1 echoes of the signal of interest. Since the interfering signals propagate through multipath channels, in a K-user system, there will be $LK-1$ interfering signals. Thus, unless multipath diversity is not applied, the performance expected from a K-user system in an L-path fading channel is close to the performance of a KL system in a single path channel. This makes the Gaussian assumption of multiple access interference to be even stronger in a multipath channel. Thus, the bit error probability of a RAKE receiver with only one finger is given by,

$$P_b = \frac{1}{2}\left[1 - \sqrt{\frac{E_b/N_0 E(A_k^2)}{1 + \frac{1}{E_b/N_0 E(A_k^2)} + \frac{2}{3}\frac{LK-1}{N}}}\right] \tag{3.34}$$

In Fig. 3.22 and 3.23, the equation (3.34) has been plotted for N=31 and N=255 respectively. A channel with L=6 equally strong multipath components has been assumed.

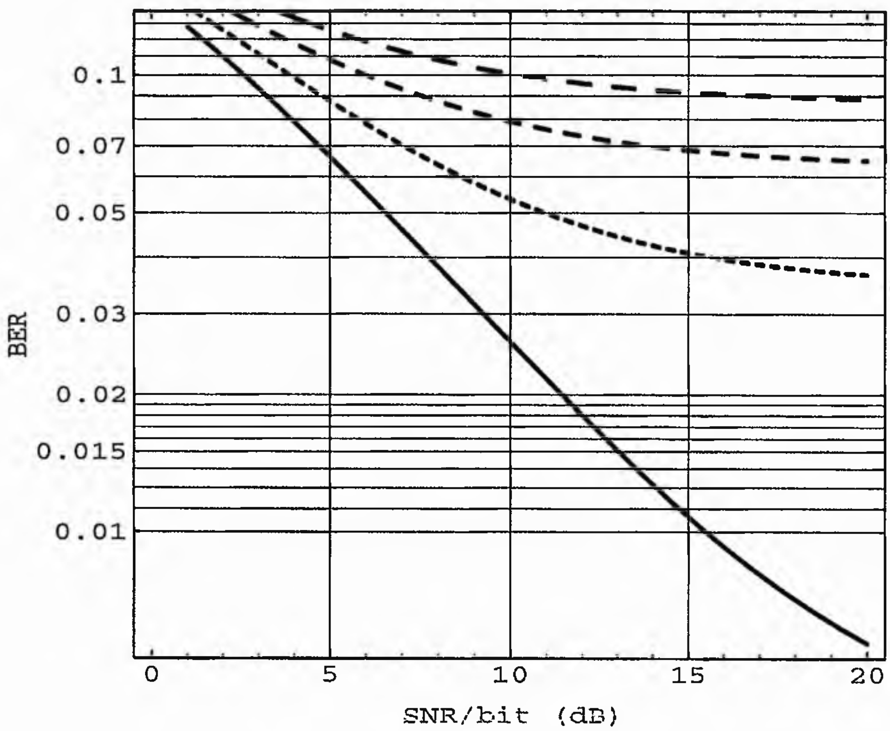

Figure 3.23: Performance of Conventional Detection in Multipath Rayleigh Fading Channel, (—) K=1, (- -) K=10, (– –) K=20, (— —) K=30, L=6, D=1, N=255

The performance degradation due to multipath fading when the receiver does not employ diversity is severe. The self-noise has increased the BER so much that even with E_b/N_0 ratio of 20 dB, the BER hardly approaches the 1% limit.

Multi-Finger RAKE ($D \neq 1$)

In a multi-finger RAKE receiver the multipath diversity is exploited and this is translated into an SNR/bit gain that depends on the following parameters:

- The modulation format with the coherent demodulation offering significant better multipath diversity over the non-coherent one.
- The ratio between the number of multipath components L and the diversity order exploited at the receiver D. The number of fingers is limited because of the receiver complexity. Also, their effectiveness depends on the delay power spectrum (DPS) of the channel.

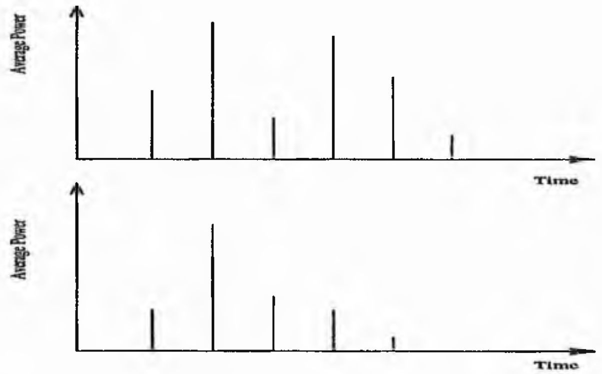

Figure 3.24: Effect of Delay Power Spectrum on Multipath Diversity Gain

- The shape of the DPS is very important. In Fig.3.24, two DPS profiles have been plotted. For the same number of channel induced multipath components, the receiver facing the first DPS (A) will have increased diversity gain compared to the second DPS (B).

- The combining technique is usually related to the modulation format. For coherent demodulation MRC is usually employed, for non-coherent demodulation Equal Gain Combining is used.

We assume that the DPS estimation unit adjusts the RAKE fingers always to the strongest paths. This function of the DPS unit is critical to the operation of the RAKE receiver because inclusion of noise-only paths to the combiner leads to severe degradation in performance. However, the aim in this part of the thesis is not to highlight the disadvantages of conventional RAKE receivers but to provide the environment that RAKE receivers need to perform best. Consequently, it is also assumed that all the paths are of equal strength, an assumption that maximises the multipath diversity gain from RAKE reception. The latest assumption removes also the dependence of our results from the shape of the Delay Power Spectrum (DPS).

For the two combining techniques under consideration, the following formulas derived in [47] apply:

Full Equal Gain Combining (EGC) The bit error probability for a Dth order EGC diversity receiver is given by,

$$P_b = \left(\frac{1 - \frac{\frac{E_b}{D\,N_0}}{1+\frac{E_b}{D\,N_0}}}{2} \right)^L \sum_{i=0}^{D-1} \begin{pmatrix} D-1+i \\ i \end{pmatrix} \left(\frac{1 + \frac{\frac{E_b}{D\,N_0}}{1+\frac{E_b}{D\,N_0}}}{2} \right)^i \tag{3.35}$$

Full Maximal Ratio Combining (MRC) The bit error probability for Dth order MRC diversity receiver is given by,

$$P_b = \left(\frac{1 - \sqrt{\frac{\frac{E_b}{D\,N_0}}{1+\frac{E_b}{D\,N_0}}}}{2} \right)^L \sum_{i=0}^{D-1} \begin{pmatrix} D-1+i \\ i \end{pmatrix} \left(\frac{1 + \sqrt{\frac{\frac{E_b}{D\,N_0}}{1+\frac{E_b}{D\,N_0}}}}{2} \right)^i \tag{3.36}$$

In the numerical evaluation of (3.35) and ((3.36), the value of D equal to 4 has been used. Notice that the formulas refer to full RAKE receivers, ie. all the multipath components have been acquired and combined. Fig.3.25 and Fig.3.26 depict the effect of multiple access interference on the performance of Differential RAKE receiver for N=31 and 255 respectively. Fig.3.27 and Fig.3.28 refer to the performance of RAKE receiver for N=31 and 255 respectively.

The effect of diversity order on the performance of full RAKE and DRAKE receivers can be seen in Fig. 3.29 and Fig. 3.30 respectively.

Although the results presented so far give a first insight into the gains of multipath diversity reception, in realistic conditions the number of fingers (order of diversity) will be smaller than the number of multipath components introduced by the channel. The formulas of [47] can be altered to take into consideration the difference between L and D, as follows:

Equal Gain Combining (EGC) The bit error probability for a Dth order EGC diversity receiver in an L-path Rayleigh Fading channel is given by,

$$P_b = \left(\frac{1 - \frac{\frac{E_b}{L\,N_0}}{1+\frac{E_b}{L\,N_0}}}{2} \right)^L \sum_{i=0}^{D-1} \begin{pmatrix} D-1+i \\ i \end{pmatrix} \left(\frac{1 + \frac{\frac{E_b}{L\,N_0}}{1+\frac{E_b}{L\,N_0}}}{2} \right)^i \tag{3.37}$$

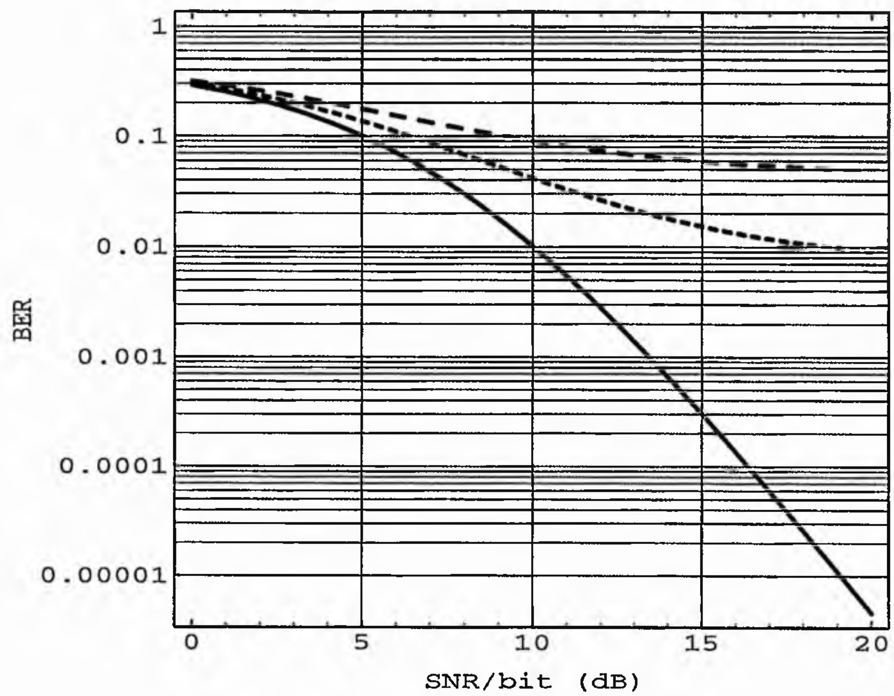

Figure 3.25: Performance of DRAKE Receiver in Multipath Rayleigh Fading Channel, N=31, D=L=4, — 1 User, - - 5 Users, – – 10 Users

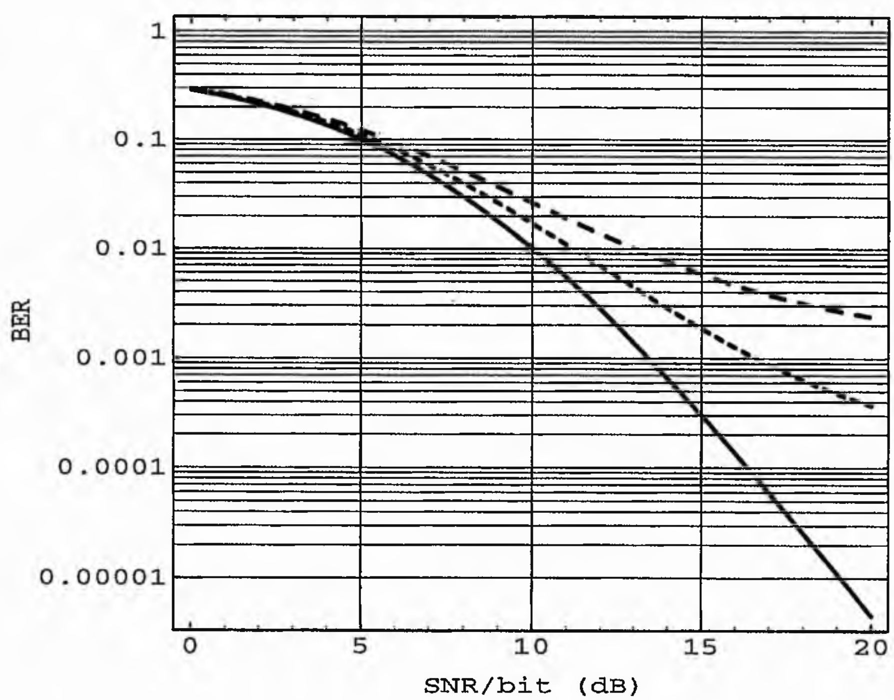

Figure 3.26: Performance of DRAKE Receiver in Multipath Rayleigh Fading Channel, N=255, D=L=4, — 1 User, - - 10 Users, – – 20 Users

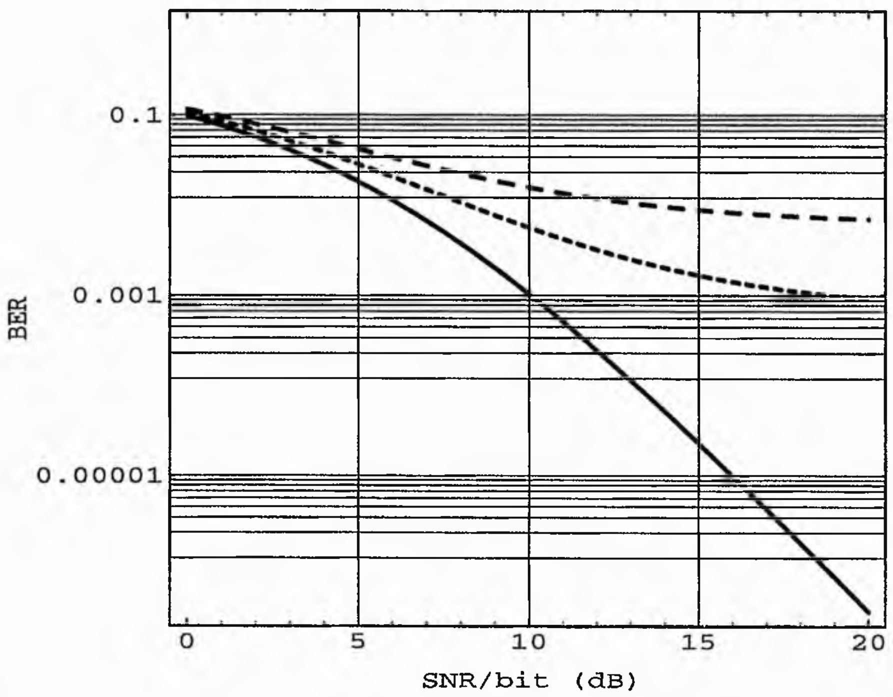

Figure 3.27: Performance of RAKE Receiver in Multipath Rayleigh Fading Channel, N=31, D=L=4, — 1 User, - - 5 Users, – – 10 Users

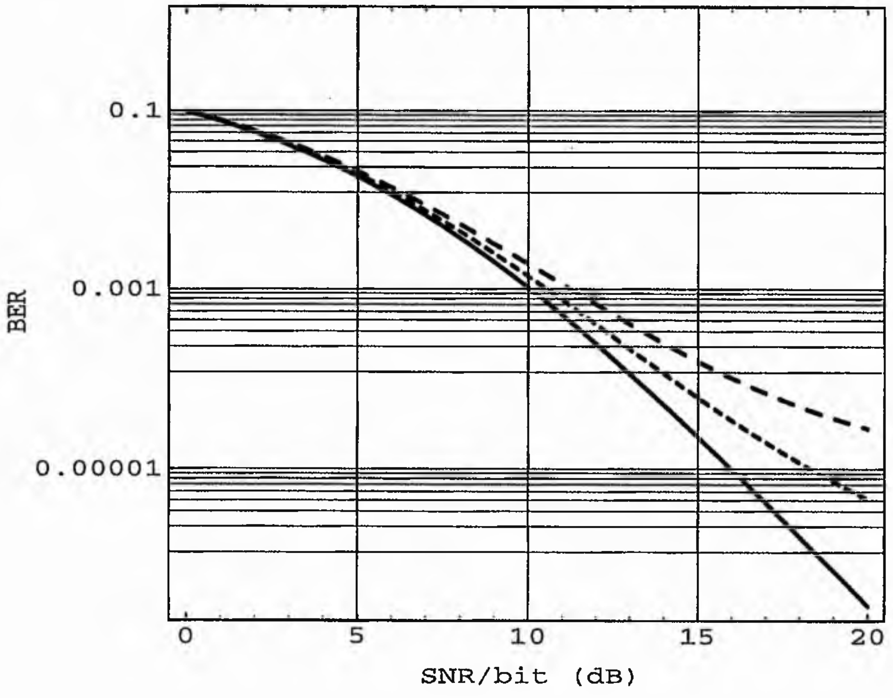

Figure 3.28: Performance of RAKE Receiver in Multipath Rayleigh Fading Channel, N=255, D=L=4, — 1 User, - - 10 Users, – – 20 Users

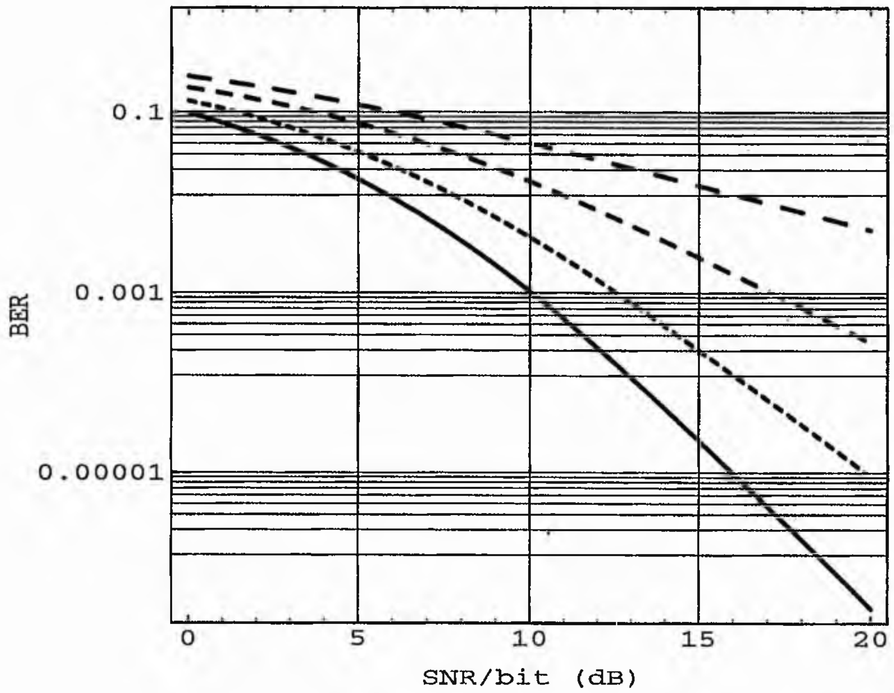

Figure 3.29: Effect of Diversity Order on RAKE Receiver Performance,D=L, L= — — 1, – – 2, - -3, —— 4

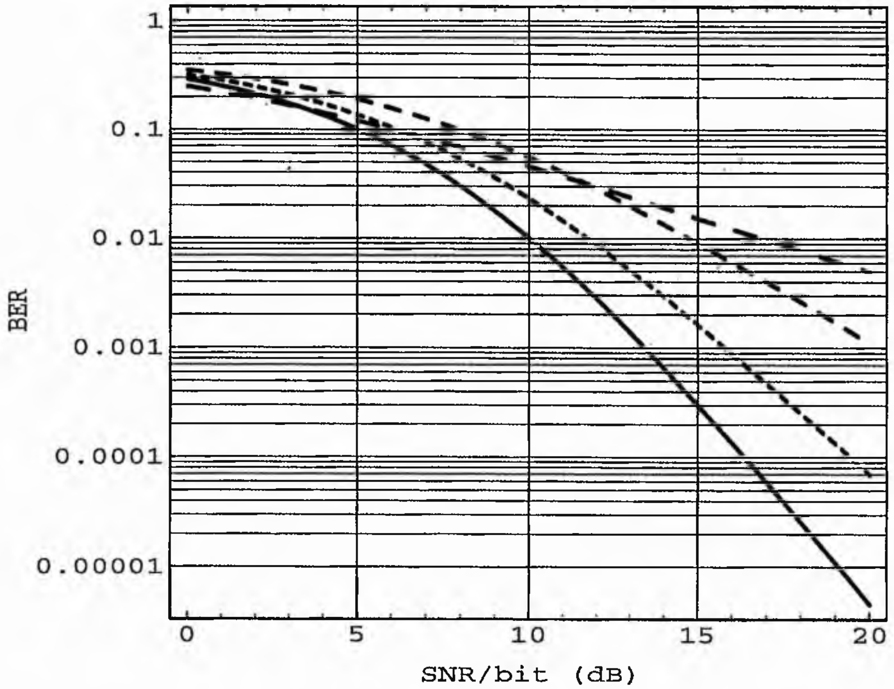

Figure 3.30: Effect of Diversity Order on DRAKE Receiver Performance, D=L, L= — — 1,– – 2,- -3,—— 4.

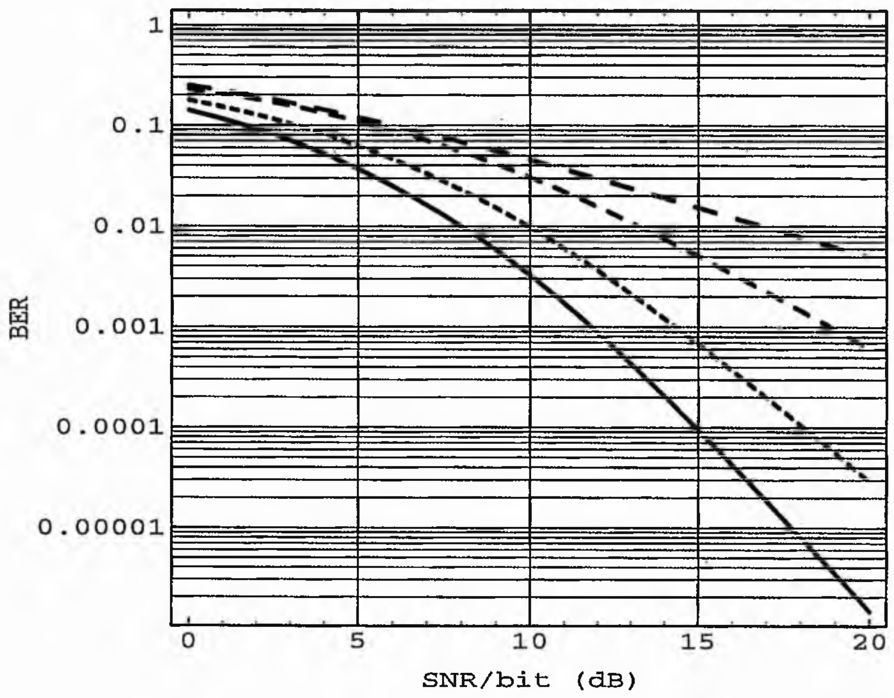

Figure 3.31: Performance of RAKE Receiver with D= – – 2,- - 3, — 4 in a L=6 Path Rayleigh Fading Channel. The — — Curve Represents the Performance of L=D=1 Case.

Maximal Ratio Combining (MRC) The bit error probability for Dth order MRC diversity receiver in an L-path Rayleigh Fading channel is given by,

$$P_b = \left(\frac{1 - \sqrt{\frac{\frac{E_b}{L\ N_0}}{1+\frac{E_b}{L\ N_0}}}}{2} \right)^L \sum_{i=0}^{D-1} \binom{D-1+i}{i} \left(\frac{1 + \sqrt{\frac{\frac{E_b}{L\ N_0}}{1+\frac{E_b}{L\ N_0}}}}{2} \right)^i \qquad (3.38)$$

Fig.3.31 and Fig.3.33 depict the effect of diversity order on the performance of RAKE and DRAKE receivers respectively. The effect of the number of equal strength multipath components on the performance of RAKE and DRAKE receivers with 4th order multipath diversity is shown in Fig.3.32 and Fig.3.34 respectively.

Due to the simplifications involved in the derivation of (3.37) and (3.38) the results obtained from the numerical evaluation of these formulas may lead sightly optimistic conclusions. Thus, we developed Monte-Carlo simulation models to investigate the correlation between the analytical and the simulated system performances.

The model uses AO/LSE Gold Sequences of period 31. The multiple access interference has been modelled as Gaussian noise. The multipath channel consists of 6 paths

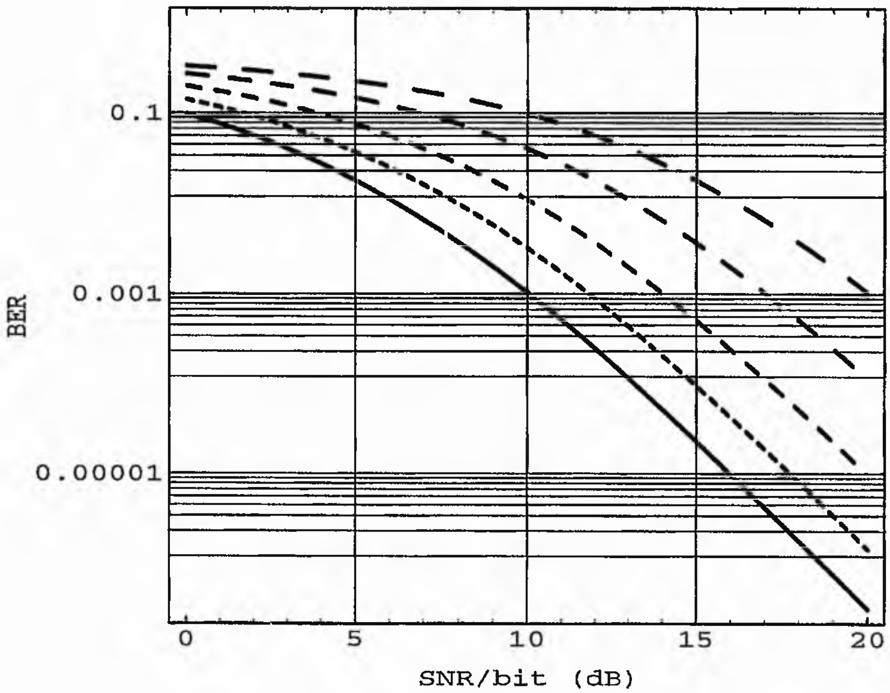

Figure 3.32: Performance of RAKE Receiver with D=4 in a L= — 4, - - 6, – – 10, — — 20, —- — 40 Path Rayleigh Fading Channel.

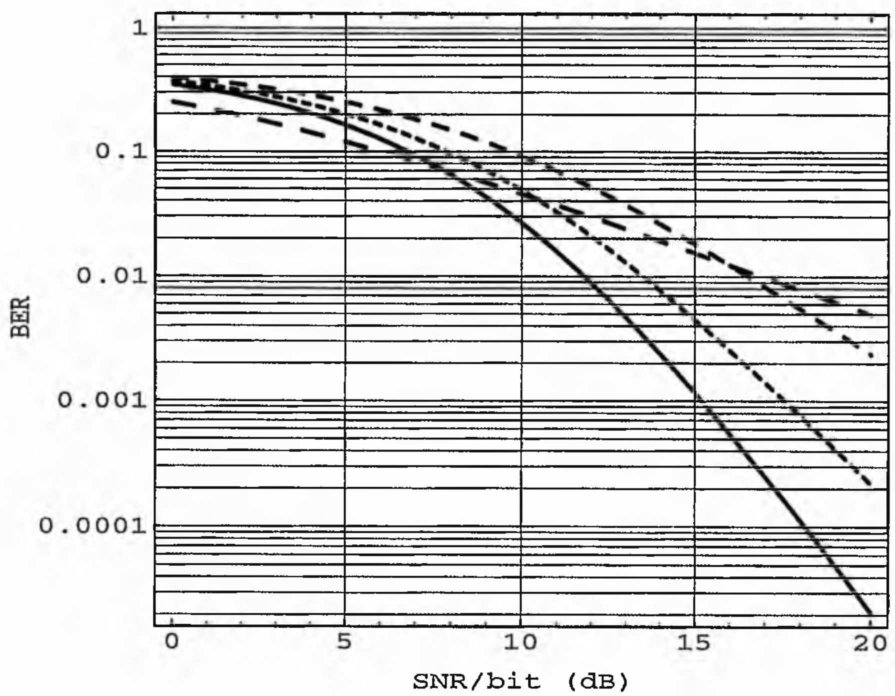

Figure 3.33: Performance of DRAKE Receiver with D= – – 2, - - 3, — 4 in a L=6 Path Rayleigh Fading Channel. The — — Curve Represents the Performance of L=D=1 Case.

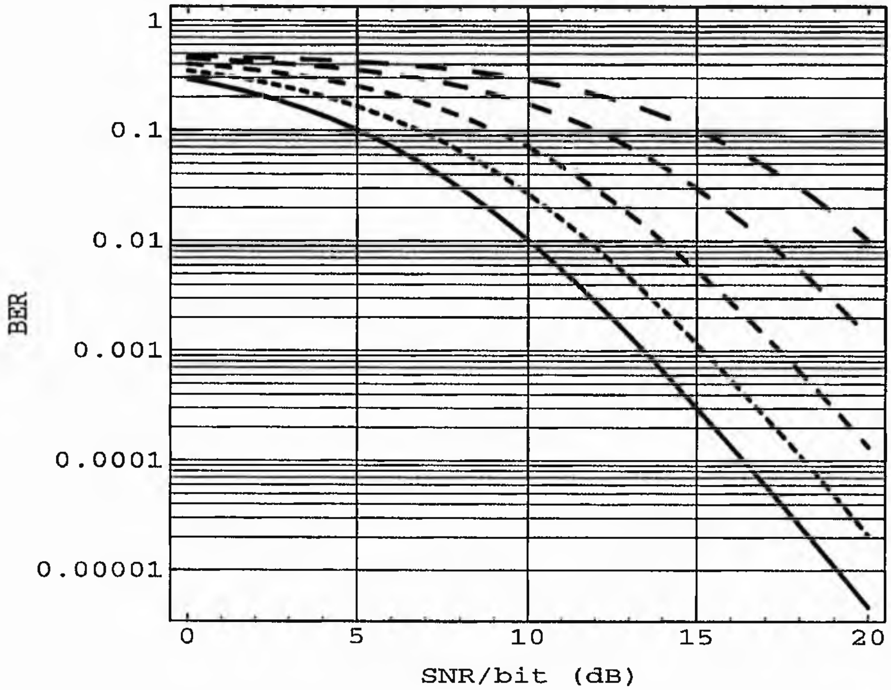

Figure 3.34: Performance of DRAKE Receiver with D=4 in a L= — 4, - - 6, – – 10, — — 20, —- —- 40 Path Rayleigh Fading Channel

of equal strength whose delays have been chosen as 0,2,4,6,8 and 10 chips. The choice of Gold sequences was based on their low level of auto-correlation values which minimises the self-noise in multipath channels with any delay spread. Thus the choice of the relative delays among the paths is not a critical parameter for Gold sequences. Fig.3.35 and Fig.3.36 depict the simulation results of the Differential RAKE and RAKE receiver respectively.

It would also be of interest to investigate the 127 chips/bit case for two reasons: (1) This spreading factor is used in the IS-95 CDMA standard. (2) The uncoded 127 chips/bit results will be of use in Chapter 6 to compare the coding gain of trellis coded CDMA systems. Additionally, the choice of 127 chips/bit is dictated from the non-existence of Gold codes of period 255.

Fig. 3.37 and Fig. 3.38 depict the simulation results for the RAKE and DRAKE receiver respectively.

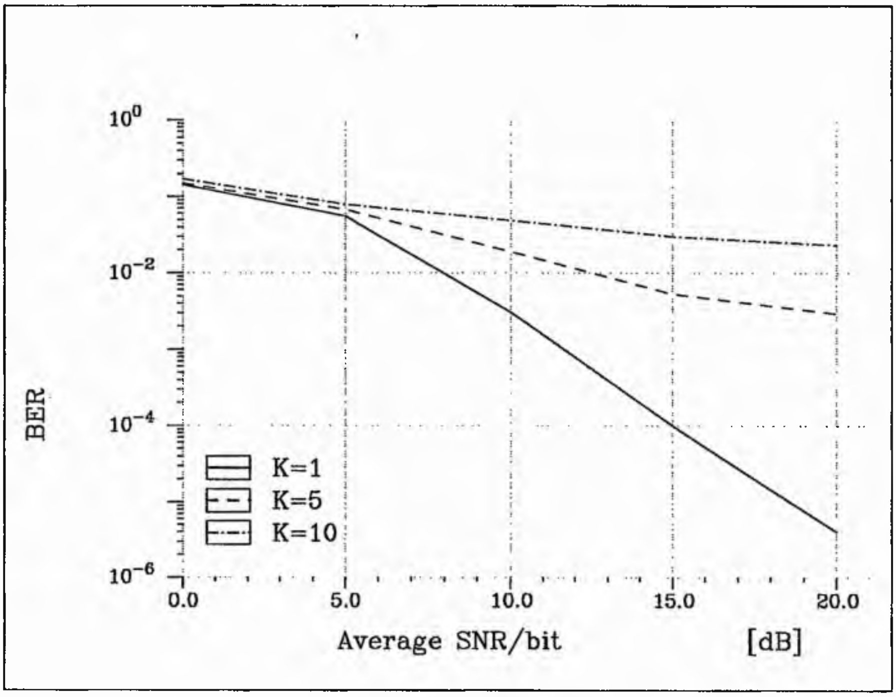

Figure 3.35: Simulated Performance of 4-Finger RAKE Receiver in L=6 Path Rayleigh Fading Channel, N=31

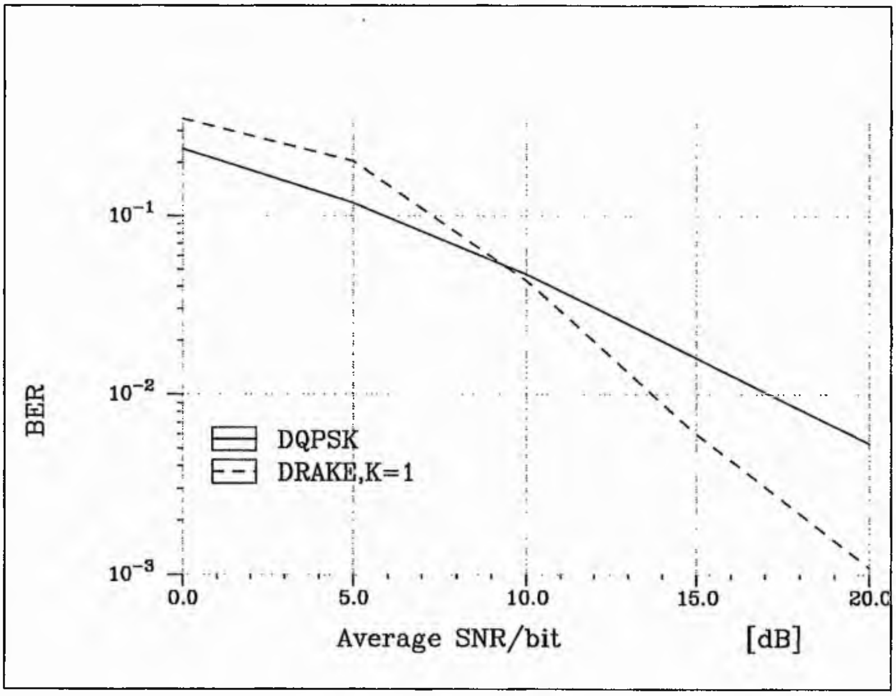

Figure 3.36: Simulated Performance of a 4-Finger DRAKE Receiver in L=6 Path Rayleigh Fading Channel, N=31

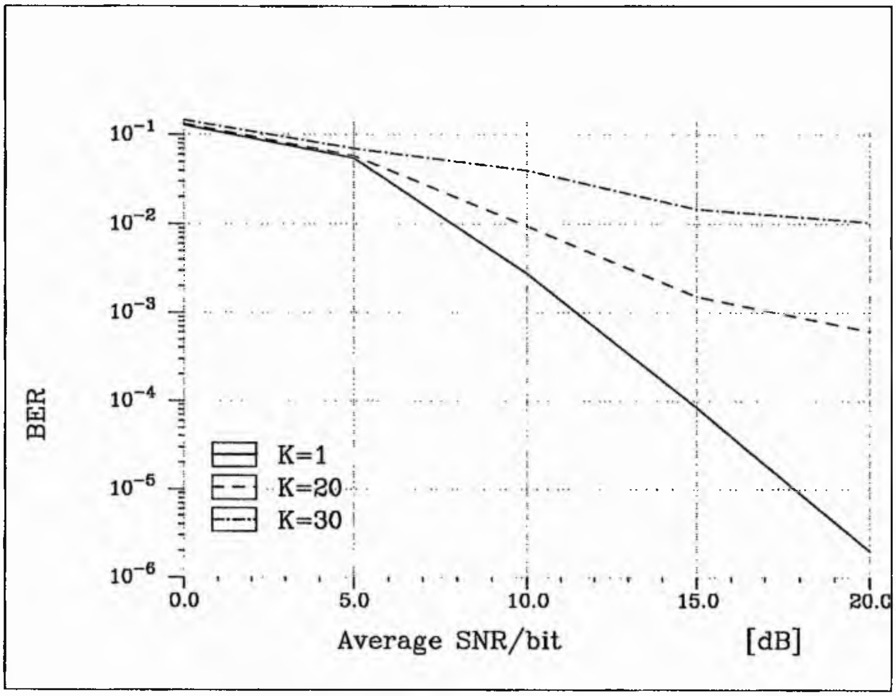

Figure 3.37: Simulated Performance of 4-Finger RAKE Receiver in L=6 Path Rayleigh Fading Channel, N=127

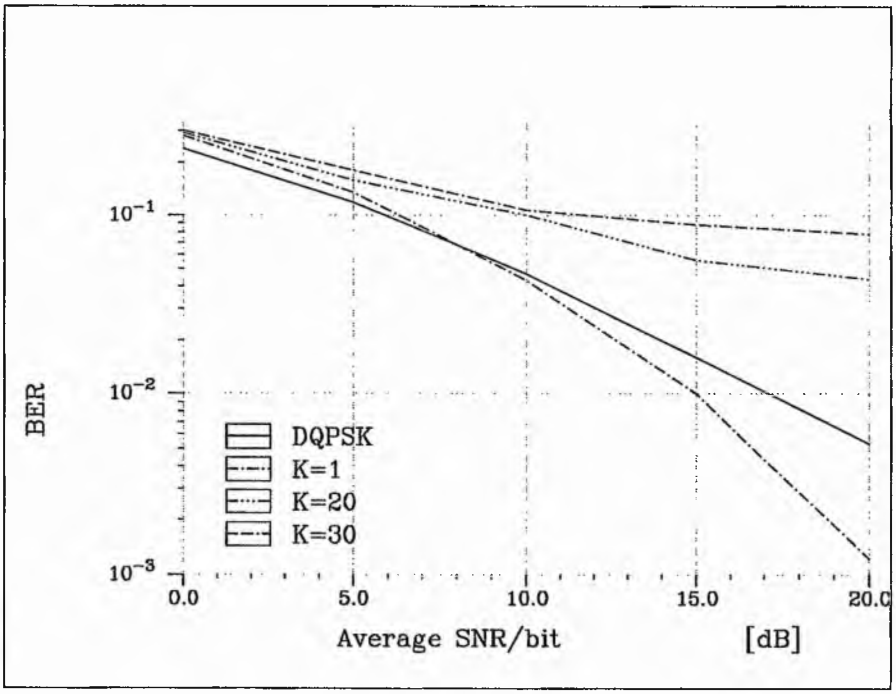

Figure 3.38: Simulated Performance of 4-Finger DRAKE Receiver in L=6 Path Rayleigh Fading Channel, N=127

3.4.4 Discussion II

From the results reported in section 3.4.3 we can obtain a comprehensive view for the performance enhancements that multipath diversity offers. The multipath diversity receiver performance should be compared against the multipath rejecting receiver ie. a receiver with the capability to despread only one of the multipath components. If all the multipath components are of equal strength, then this comparison would have been fare. However in all the practical applications this is not very realistic.

Thus, the multipath diversity receiver performance will be compared against the receiver that operates in a single-path channel ie. the ideal performance of coherent PSK and DPSK detection. For a single user channel, the non-diversity receiver needs an E_b/N_0 ratio of 27 dB in Rayleigh fading to achieve a BER of 10^{-3}. With a 4-finger RAKE receiver in a 6-path Rayleigh fading channel this figure is reduced to 11.8 dB while with a similar DRAKE receiver it is reduced to 20.1 dB. In Fig.3.39 the SNR/bit which required for DRAKE receivers to start producing a multipath diversity gain is shown. As can be also be observed in this figure RAKE receivers start producing multipath diversity gain from 0 dB SNR/bit. In Fig.3.40 the irreducible bit error rate is plotted for the single-path and multipath diversity receiver, against the number of users. RAKE receivers approach the performance of the single path receiver as the number of users increase. This is just a verification of the well known fact that multiple access interference is the main limiting factor even when optimum multipath diversity reception has been achieved.

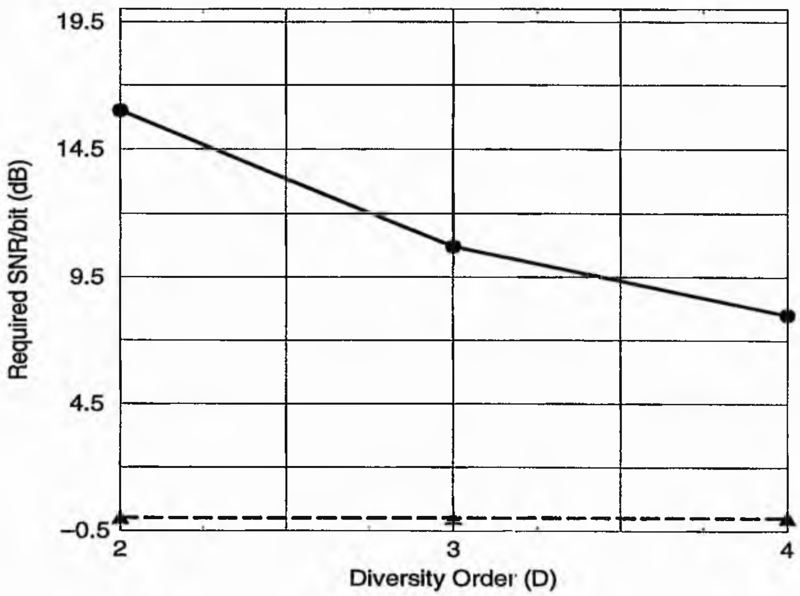

Figure 3.39: Minimum Required SNR/bit To Achieve Multipath Diversity Gain for RAKE (- -) and DRAKE (—) Receivers with D=4 in a L=6 Path Rayleigh Fading Channel

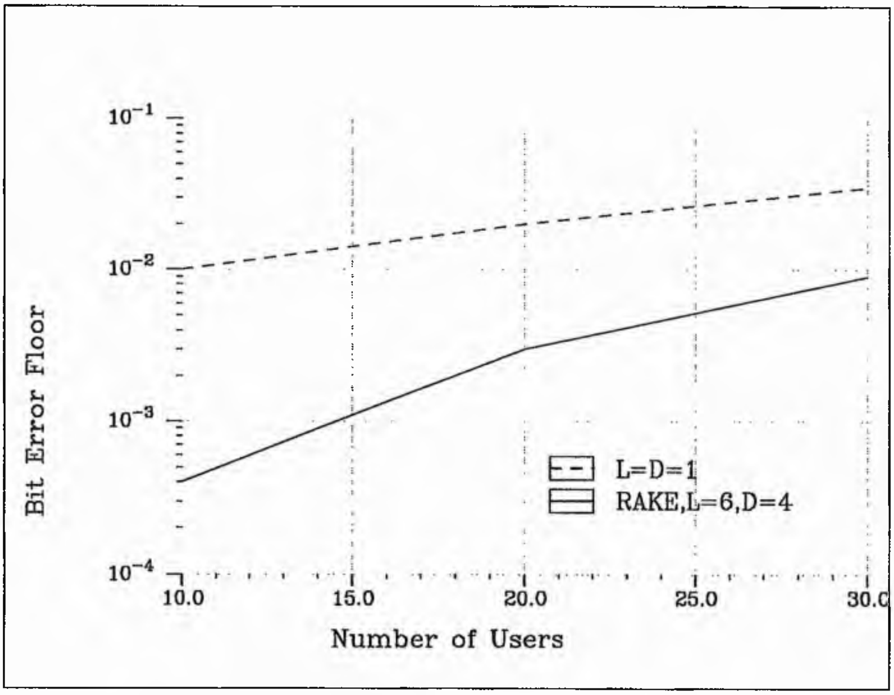

Figure 3.40: Comparison Between the Bit Error Floors Caused by Multiple Access Interference for the L=D=1 Receiver (- -) and the L=6, D=4 RAKE (—) Receiver

3.5 CHANNEL ESTIMATION

In this section, the problem of estimating the downlink/uplink mobile radio propagation channel will be addressed. The downlink channel estimation methods are all reference based due to existence of the pilot channel. The provision of the pilot channel in the downlink makes possible the coherent demodulation at the mobile station receiver. On the other hand, for the uplink direction there is no pilot channel and the channel estimation process is based on either decision directed or non-decision directed methods. We have chosen to address a particular decision directed method in which the decisions are not traffic channel data, but control channel data. The aim is to provide quantitative measures of performance degradation due to imperfect channel estimation for the uplink direction. Such research is important for a variety of reasons:

- The performance of the RAKE receiver is strongly influenced from the performance of the delay power spectrum *and* the channel estimator. With the exception of [28] who quantified the performance degradation due to imperfect delay power spectrum estimation and of [42] who evaluated the effect of measurement noises on the performance of a single-path spread spectrum receiver, the performance loss from the channel estimation imperfections is not widely available in the open literature.

- There are mainly two ways one could overcome the penalty associated with the lack of phase coherency in the uplink. The first, already employed in the IS-95 CDMA standard involves a 64-ary orthogonal modulation format [26]. The detection of M-ary orthogonal modulated signals does not require phase coherency. The second, is to find the means to perform channel estimation in the uplink through the exploitation of side-information. The classic way of estimating the channel through side-information is to devote a portion of the frame to a training sequence. Although this technique has been shown to offer some advantage compared to the maximum-likelihood demodulation strategy of the IS-95, is inherently power inefficient [30]. Side-information can however be provided by the control channel which is associated with a traffic channel. Given a CDMA system with *outbound* control channels, channel estimation can be easily applied as will be shown shortly. This particular technique has been extensively researched during the development of the CODIT testbed, and the aim here is to highlight the factors that affect its performance in realistic mobile radio channel conditions.

3.5.1 Downlink Channel Estimation

The downlink channel estimation function is performed on the pilot channel which is an information-free channel transmitted by each base station. Let the power level (weight) of this pilot channel be a_P which is higher than the weight of the traffic channel a_T. The downlink channel estimation concept can be seen in Fig. 3.41.

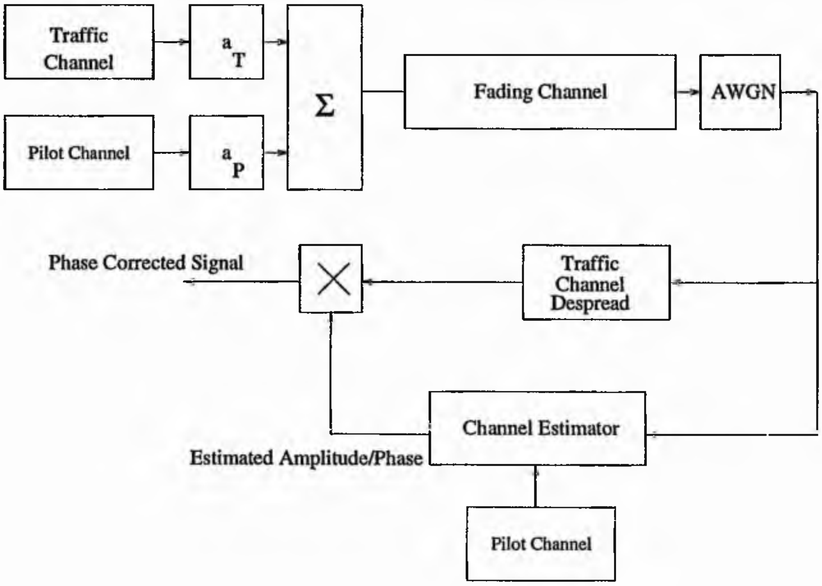

Figure 3.41: Downlink Channel Estimation

The mobile station channel estimator has the knowledge of the spreading sequence used to spread the pilot channel. The function it performs is based on the correlation concept. It correlates the distorted by the channel pilot signal with the perfectly aligned pilot sequence which acts as continuous training sequence. The outcome of this correlation is the channel estimate, the complex conjugate of which rotates the despread constellation according to the phase/frequency estimate.

In CDMA cellular systems we can distinguish two cases as far as the pilot channel spreading sequence is concerned:

1. Synchronized Base Stations: In this case, the base stations share a common clock distributed by a suitable mechanism (eg. through Global Positioning System receivers). The base station uses a very long code that is offset in time from the codes used in the downlink transmissions of the other base stations. The great advantage of having synchronized base stations is that code synchronization is trivial during handover.

2. Unsynchronized Base Stations: In this case, there is no common clock distribution and consequently the spreading sequence used by this channel is always periodic with typical periods of 512-1023 chips. The fact that with unsynchronized base stations we must use periodic sequences is imposed by code synchronization issues. The spreading code of the pilot channel is used to provide the synchronization functions necessary for despreading the signal of the traffic channel. The shorter the period of the code used the shorter will be the acquisition time. However, the period of the pilot channel has to be of adequate length so that one code to be available to every base station in the system. Thus, there must be some compromise between the synchronization and the family size issues.

Although the channel estimator quality is not relevant to the periodicity of the pilot channel code, the overall receiver performance is in fact determined by the quality of the code synchronization circuitry or in multipath channels by the quality of the delay power spectrum estimator. In Chapter 5, this issue is revisited but for the scope of this chapter we shall assume that the time-synchronization has been ideally achieved for all multipath components.

The following theorem has been originally stated in [42]. The proof is repeated here with slight alterations taking into account the downlink transmission layout found in CDMA mobile radio systems.

Theorem 3.1 *The Minimum Mean Square Error (MMSE) solution for estimating a time-varying equivalent channel impulse response having L elements is given by,*

$$\hat{c}_k(i) = \frac{1}{E_p} E[u_{i-k} r_i], \;\; 1 \le k \le L \tag{3.39}$$

where L is the number of propagation paths, k is an integer that indexes each propagation path, $\mathbf{u}$ is a complex vector that denotes the pilot spreading code (reference signal) of energy per symbol E_p and $\mathbf{r}$ denote the input to the channel estimator during the ith chip interval.

Proof: The received signal can be written as

$$r_i = \sum_{k=1}^{L} c_k(i) u_{i-k} + n(i) \tag{3.40}$$

The channel estimator forms the received signal based on the estimates of the channel taps. This is mathematically given by the equation,

$$\hat{r}_i = \sum_{k=1}^{L} \hat{c}_k(i) u_{i-k} \tag{3.41}$$

The MMSE criterion is given by,

$$E[|r_i - \hat{r}_i|^2] = min \tag{3.42}$$

If we choose the length of the channel estimator equal to L, then the (L,L) correlation matrix of the tap inputs denoted by $\mathbf{R}$ can be written,

$$\mathbf{R} = E[\mathbf{u}(i)\mathbf{u}^H(i)] \tag{3.43}$$

Similarly, the (L,1) cross-correlation vector between the tap-inputs of the filter and the reference signal $\mathbf{u}$ is given by,

$$p = E[\mathbf{r}(i)\mathbf{u}(i)] \tag{3.44}$$

It is now well known that the Wiener-Hopf system of equations that describe the problem can be given by,

$$\mathbf{R}\ \hat{\mathbf{c}} = \mathbf{p} \tag{3.45}$$

where $\hat{\mathbf{c}}$ is the MMSE estimate of the tap gains which is given by,

$$\hat{\mathbf{c}} = \mathbf{R}^{-1}\mathbf{p} \tag{3.46}$$

For a statistically independent reference signal, such as a PN-sequence, $\mathbf{R}$ is a diagonal matrix with diagonal elements equal to the SNR/bit. In CDMA the pilot channel is transmitted at a higher power level compared to the traffic channels. Thus, if we denote by E_p the energy per chip of the pilot channel then,

$$\hat{\mathbf{c}} = \frac{1}{E_p} E[\mathbf{u}\ \mathbf{r}] \tag{3.47}$$

From the previous theorem it is obvious that the MMSE channel estimator can be implemented in two ways. The first is called correlation-based channel estimation (CB-CHEST) and implements equation (3.47). The second is the Least Mean Squares adapted channel estimation (LMS-CHEST) and implements equation (3.46). There is though a distinct relationship between the two estimators as described subsequently.

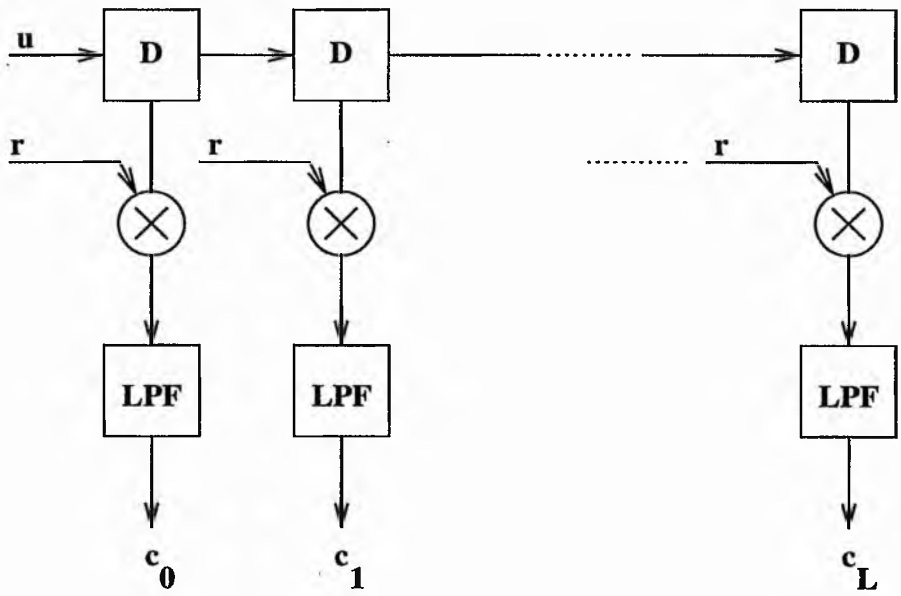

Figure 3.42: Correlation Based Channel Estimator

3.5.2 Relation Between CB-CHEST and LMS-CHEST

The block diagram of CB-CHEST is shown in Fig. 3.42.

The reference signal is passed through a tapped delay line, the tapped signals are multiplied with the received signal and then passed through a bank of low pass filters. The low pass filtering approximates the expectation of equation (3.47).

The block diagram of LMS based channel estimation is shown in Fig. 3.43.

The input signal is the reference signal which is fed into a tapped delay line filter whose taps are adapted by the adaption algorithm. The output of the estimator is subtracted from the received signal producing the error signal,

$$e_i = r_i - \hat{r}_i = r_i - \sum_{k=1}^{L} \hat{c}_k(i) u_{i-k} \tag{3.48}$$

The error signal is used to update the taps of the filter according to the well known LMS adaption equation,

$$\begin{aligned}
\hat{c}_k(i+1) &= \hat{c}_k(i) + 2\mu e_i u_{i-k} && (3.49)\\
\hat{c}_k(i+1) &= \hat{c}_k(i) + 2\mu \left[r_i - \sum_{k=1}^{L} \hat{c}_k(i) u_{i-k} \right] u_{i-k} && (3.50)\\
\hat{c}_k(i+1) &= \hat{c}_k(i) + 2\mu \left[r_i u_{i-j} - \hat{c}_j(i) u_{i-j} u_{i-j} - \sum_{k=1, k\neq j}^{L} \hat{c}_k(i) u_{i-k} u_{i-j} \right] && (3.51)
\end{aligned}$$

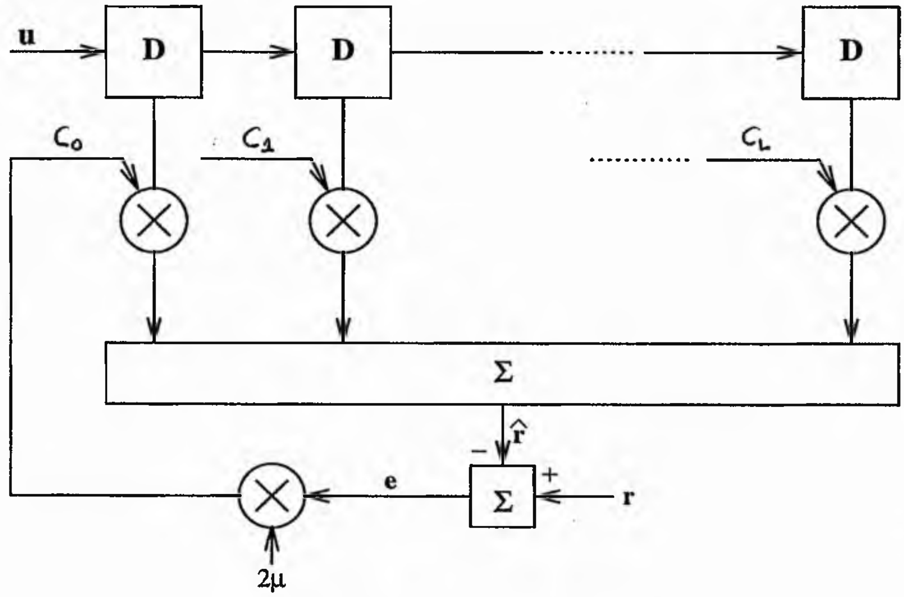

Figure 3.43: LMS Adapted Channel Estimator

$$\hat{c}_k(i+1) = \hat{c}_k(i) + 2\mu \left[r_i u_{n-j} - \hat{c}_j(i)|u_{i-j}|^2 - \sum_{k=1,k\neq j}^{L} \hat{c}_k(i) u_{i-k} u_{i-j} \right] \tag{3.52}$$

$$\hat{c}_k(i+1) = \hat{c}_k(i)[1 - 2\mu E_p] \tag{3.53}$$

The latest equation is a first-order difference equation that can be implemented by passing **r u** through a bank of first-order digital filters having transfer function,

$$H(z) = \frac{2\mu}{z - (1 - 2\mu E_p)} \tag{3.54}$$

Equation (3.53) shows the partial equivalence relationship between the LMS and the correlation based channel estimator. The LMS-CHEST is a first-order approximation of the CB-CHEST, consequently, it is expected that the CB-CHEST will outperform the LMS-CHEST. To what extent the CB-CHEST offers better MSE performance than LMS-CHEST can be evaluated through simulation. Simulation results comparing these two channel estimator can be found in the next section.

3.5.3 Uplink Channel Estimation

Uplink channel estimation techniques are necessary for the coherent demodulation of the despread signal. The technique to be addressed in this section was the subject of extensive discussions during the design of the CODIT receiver and has received extensive research due to its significance to the uplink capacity improvement. One further reason why this technique is significant is that in CODIT, because of the outbound signalling format, two physical channels need to be established per user. This is in contrast to the voice-oriented IS-95 system where inbound signalling is used and only a single physical channel is needed per user. It is not the aim of this thesis to determine the efficiency of mapping control and traffic information into two separate channels. However, a possible capacity reduction due to this particular mapping of dedicated control channel information in the radio interface, makes any attempt to reduce the required SNR/bit by coherent combining of the multipath components, important.

In the IS-95 system the optimum performance of a coherent RAKE receiver *without* channel estimation overheads is approached. This is achieved by maximum-likelihood detection which in the IS-95 receiver demands the presence of a bank of 64 correlators. However, it has been demonstrated recently that coherent demodulation methods employing training symbols insertion are 1.0 dB better off compared to the IS-95 scheme [30].

Concept: The channel estimator for the uplink extracts the necessary information from the control channel (CCH) which is associated with the given traffic channel (TCH). The mobile station transmits, the multiplexed control and the traffic channel,

$$a_T b_{TCH} + a_C b_{CCH} \tag{3.55}$$

The multiplexing has an inherent power inefficiency since not all the power is dedicated to the traffic channel. The performance degradation depends on the weight of the control channel; the optimal channel weight will be determined later on.

At the base station receiver the information that is transmitted in the control channel is first decoded and then re-encoded. With this way, the unknown information can be treated as known provided that the post-decoder error rate is zero. This is illustrated in Fig.3.44.

The dedicated control channel information (b_{CCH}) is encoded and the coded symbols (b_{CCH}) are sent through the super-channel (the terminology used in concatenated coding

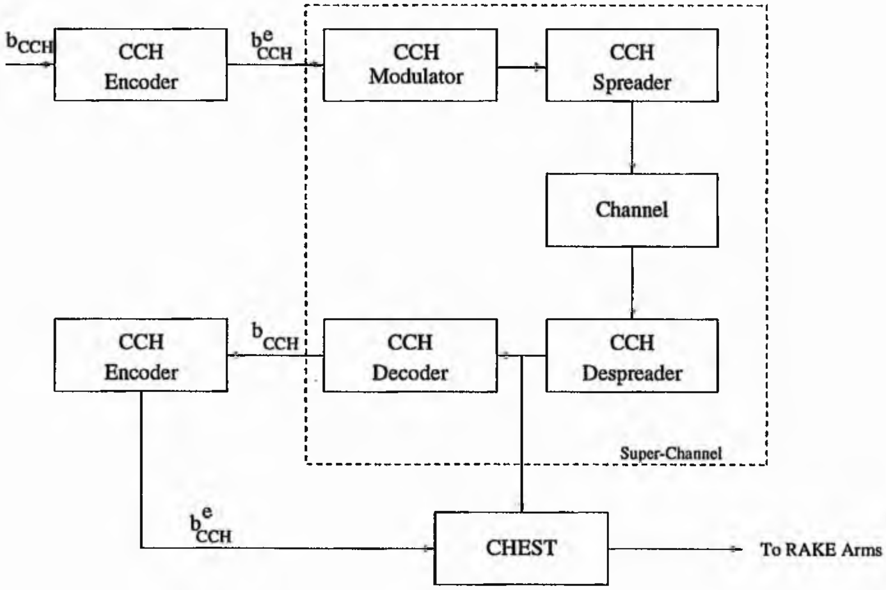

Figure 3.44: Concept of Uplink Channel Estimation

schemes has been adopted). At the output of the superchannel under ideal conditions the original control channel information (b_{CCH}) should appear. The channel estimator attempts to estimate the time-varying component of the super-channel. Since this is a system identification problem, the input to the channel estimator and the input to the super-channel has to be the same ie. the symbols sent through the channel and the symbols used by the channel estimator have to be the same. By re-encoding the control channel information this can be easily achieved.

Thus, the control channel acts as the pilot channel for the uplink. In practice, the ideal zero post-decoder error rate won't be achieved but the technique is designed to be robust if the error rate is below a certain threshold. Thus, careful consideration must be given to the coding scheme of the control channel ie. the trade-off between decoding complexity (delay) and achievable post-decoder BER under worst case scenarios.

It is well known from Wiener filter theory and the treatment in the previous section that the optimal unbiased channel estimate in the sense of maximizing the signal energy to the variance of the estimation error can be obtained by passing the output of the CCH despreader through a linear phase filter whose magnitude is equal to the square root of the quotient of the Doppler spectrum divided by the noise spectrum. Practically, it is difficult to implement such an optimal estimator because the Doppler and noise spectra are usually not known and will be also time-variant. A sub-optimum solution is to use a fixed linear-phase low pass filter whose cut-off frequency is greater than or equal to the

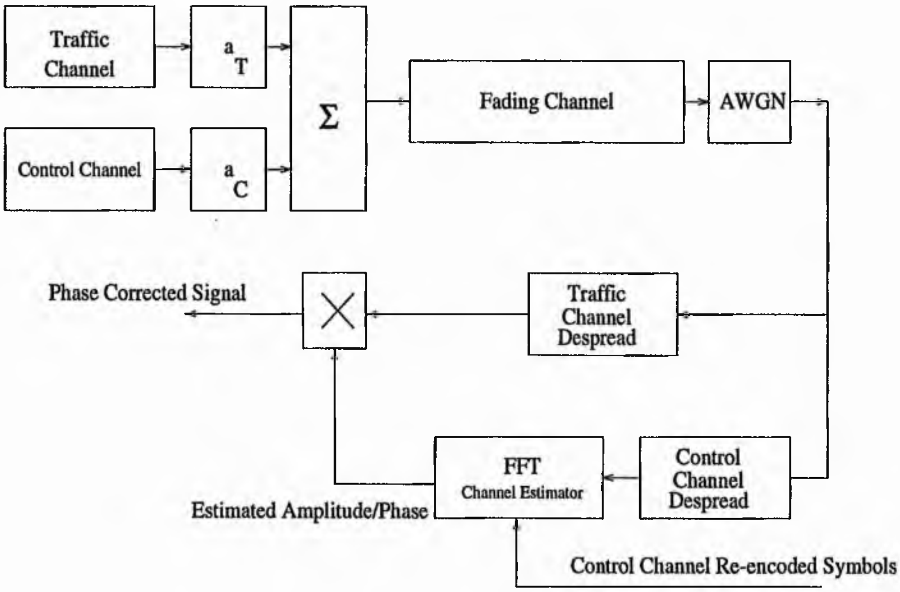

Figure 3.45: FFT Based Channel Estimation

maximum Doppler frequency. The ideal low pass filter method has been implemented on frequency domain and the Monte-Carlo simulation model is shown in Fig.3.45.

A critique of the FFT-based CHEST is that the method is too expensive to be implemented in practice requiring extensive signal processing power even for approximating a brick-wall filter. Since the filter has to be time-varying as well due to the changing velocity, more practical solutions seem attractive.

Adaptive channel estimation based on Least Mean Square algorithm can offer significant computational gains compared to the FFT approach. Prompted from the equivalence of LPF and LMS CHEST it is intuitive to compare the performances of the two schemes. The simulation model for the LMS CHEST is shown in Fig.3.46.

Before evaluating any particular channel estimation technique it is important to realise the detrimental effects of channel estimation error on the BER. The channel estimation error variance influences the performance as shown in Fig.3.47.

The power weight of the control channel a_C, with respect to the traffic channel a_T is also important. The larger the weight the better the estimation but because of equation 3.55, the associated E_b/N_0 loss in the traffic channel is also significant. This can be seen for the case of perfect channel estimation in Fig.3.48

For the FFT and LMS channel estimators considered here, the weight dedicated to the control channel has been chosen equal to 0.1 since no significant performance

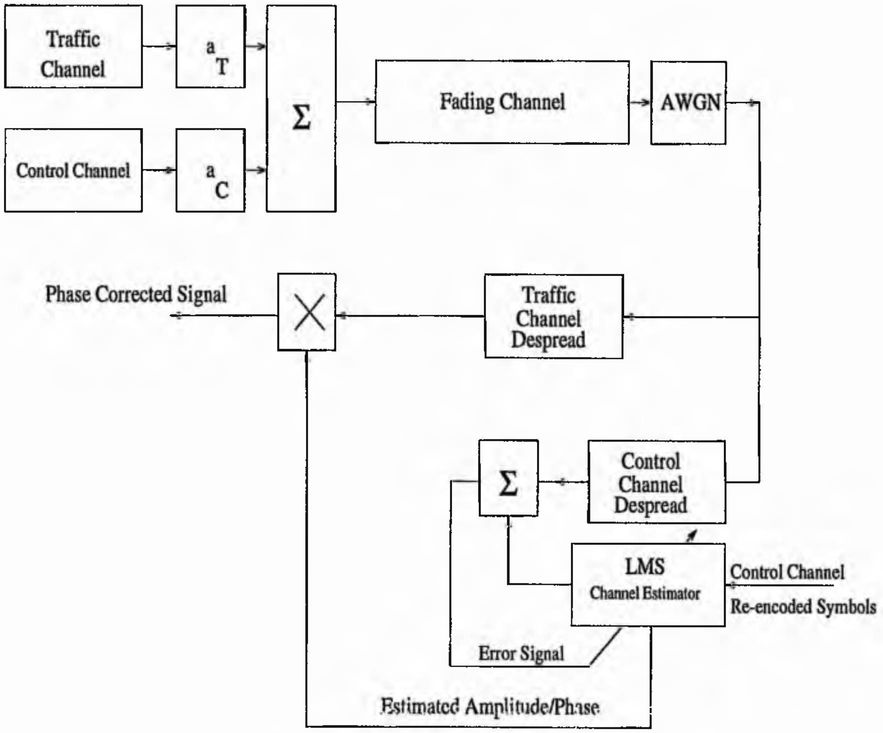

Figure 3.46: LMS Based Channel Estimation

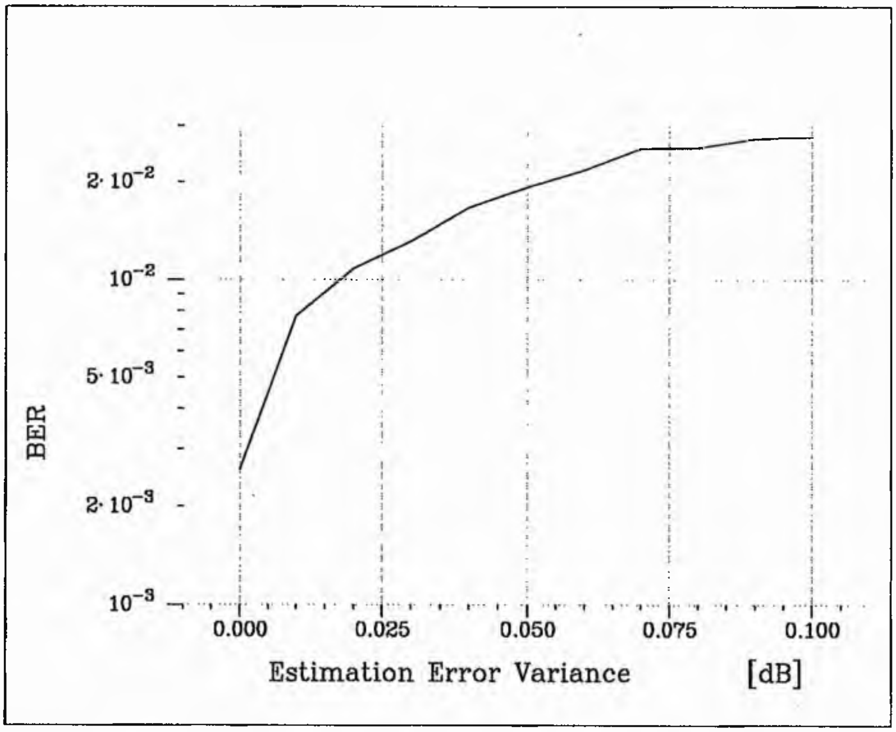

Figure 3.47: Effect of Estimation Error Variance on Performance, $E_b/N_0 = 20dB$, Single Path Rayleigh Fading Channel

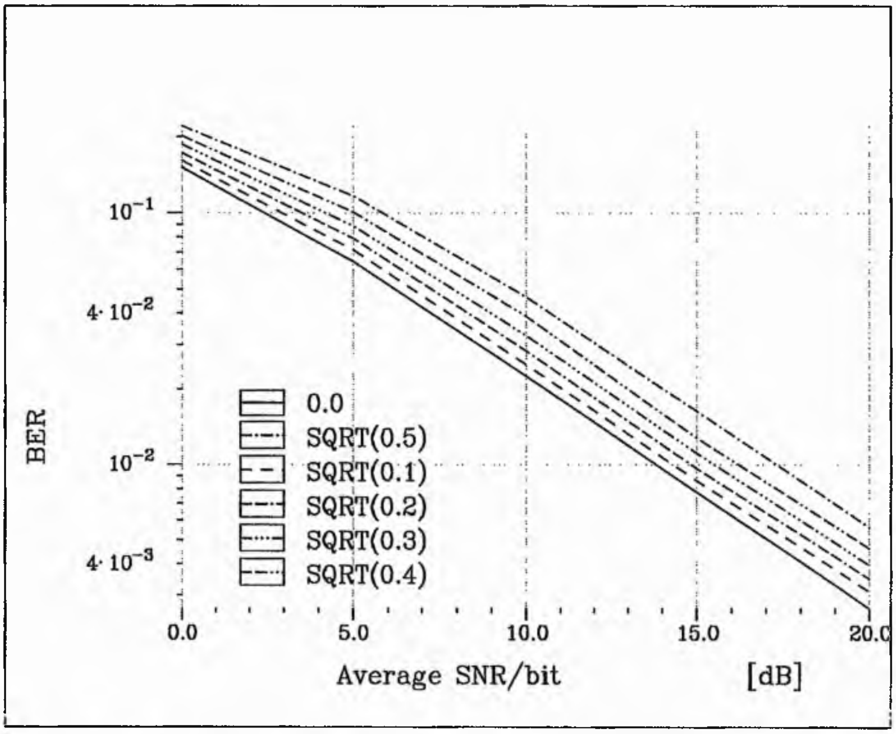

Figure 3.48: Effect of Control Channel Weight on Performance, Perfect CHEST

improvement can be observed, as it is demonstrated in Fig.3.49, with larger weights.

The results from the Monte-Carlo simulation of the two estimators are shown in Fig.3.50.

The results of Fig.3.50 were all based on the assumption that the control channel information has been decoded with zero BER. This assumption is however not realistic. It is then of interest to examine the effect of incorrect control channel decoding on the performance of the traffic channel. This is shown in Fig.3.51 for the LMS channel estimator and $E_b/N_0 = 20$ dB.

The LMS channel estimator is robust as far as the post decoding BER of the control channel is below 10^{-2}. For higher bit error rates, the channel estimator rapidly looses the ability to track the phase variations. It should be mentioned at this point that the BER of 10^{-2} refers to *random* errors. This means that the post-decoder errors of the control channel considered in the simulation are not of bursty nature. Careful consideration has to be given to the interleaving depth of the control channel which is however limited by the delay that the control information has to be delivered to the channel estimator. Alternatively, burst error correction codes could be used to encode the control information.

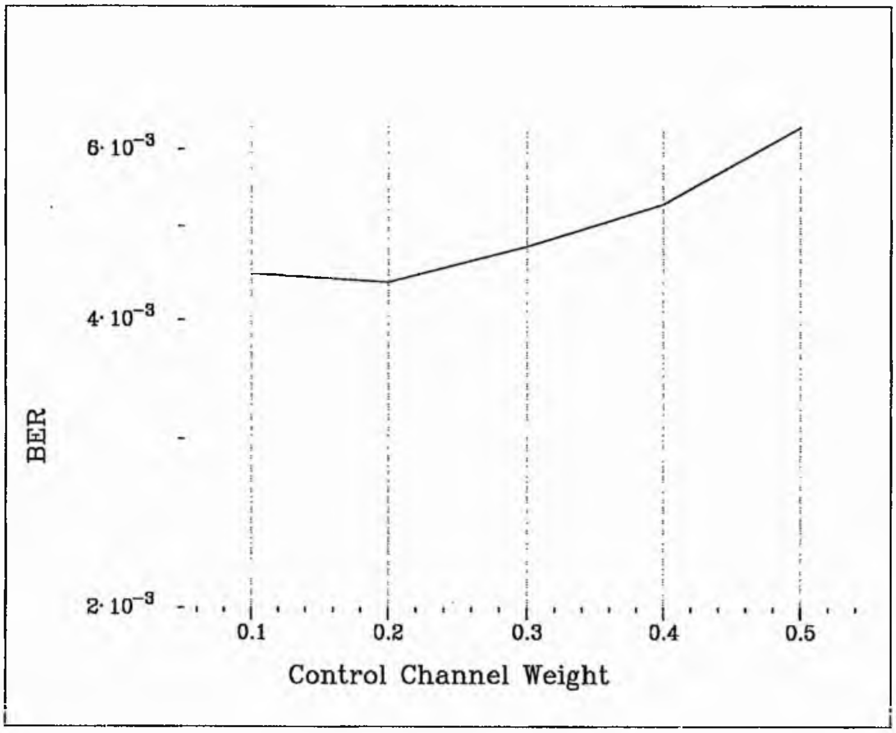

Figure 3.49: Control Channel Weight vs BER for $E_b/N_0 = 20$ dB, LMS CHEST

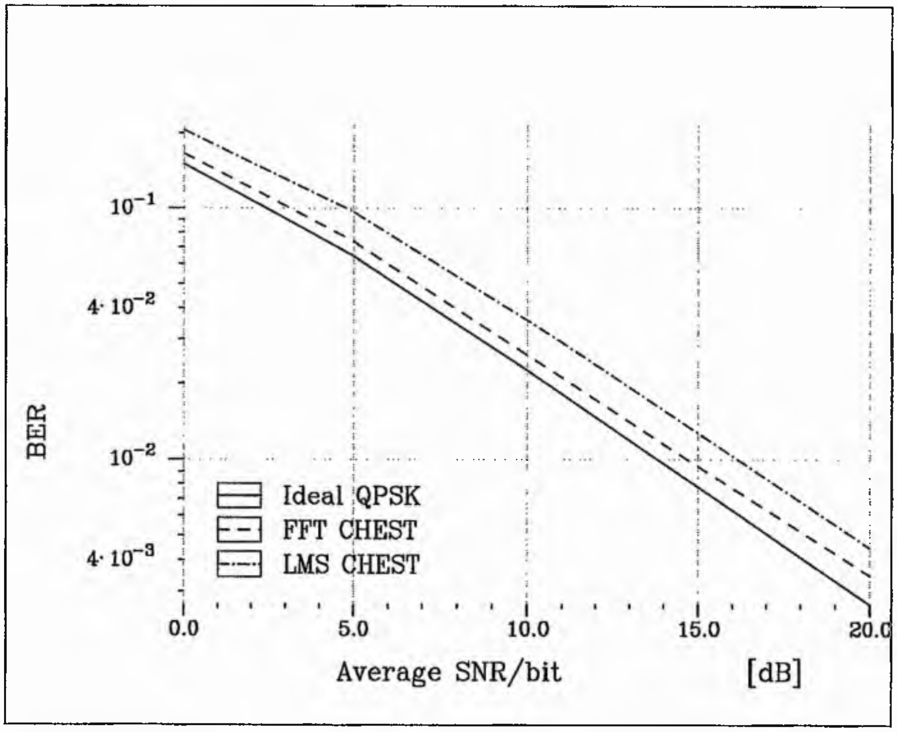

Figure 3.50: Performance Comparison for Perfect, FFT and LMS Estimated Rayleigh Fading Channel

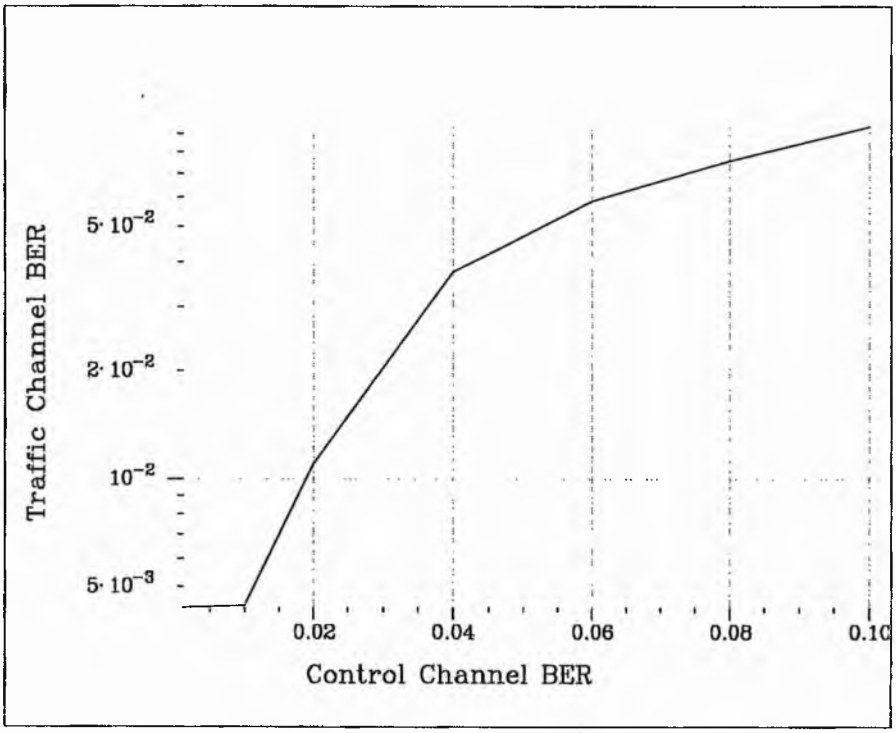

Figure 3.51: Effect of Control Channel BER on Performance of LMS CHEST, $E_b/N_0 =$ 20 dB

Remark: The channel estimators outlined in this section differ from the ones employed in the CODIT testbed on that the control channel despreader correlates the received signal with the PN sequence of the control channel over the whole duration of a bit. In the CODIT testbed this correlation is *partial* because it was felt that at high velocity the channel will change significantly over the duration of a control channel bit. If we assume that the control channel information is transmitted at 4 kbps then the duration of a bit is 250 μ s. In practice, in our delay budget we have to add the delay associated with decoding and re-encoding the control channel bits. Since in our simulation models no channel coding was implemented, the delay budget is dominated by the code matched filtering delay only.

3.6 CHANNEL ADAPTED RAKE (CARAKE)

In this section we demonstrate by Monte-Carlo simulation the benefits of coherent channel estimation in the uplink. The model that has been developed will permit to compare the performance of an ideal channel estimated RAKE receiver with the LMS channel adapted RAKE receiver. The simulation model is shown in Fig.3.52.

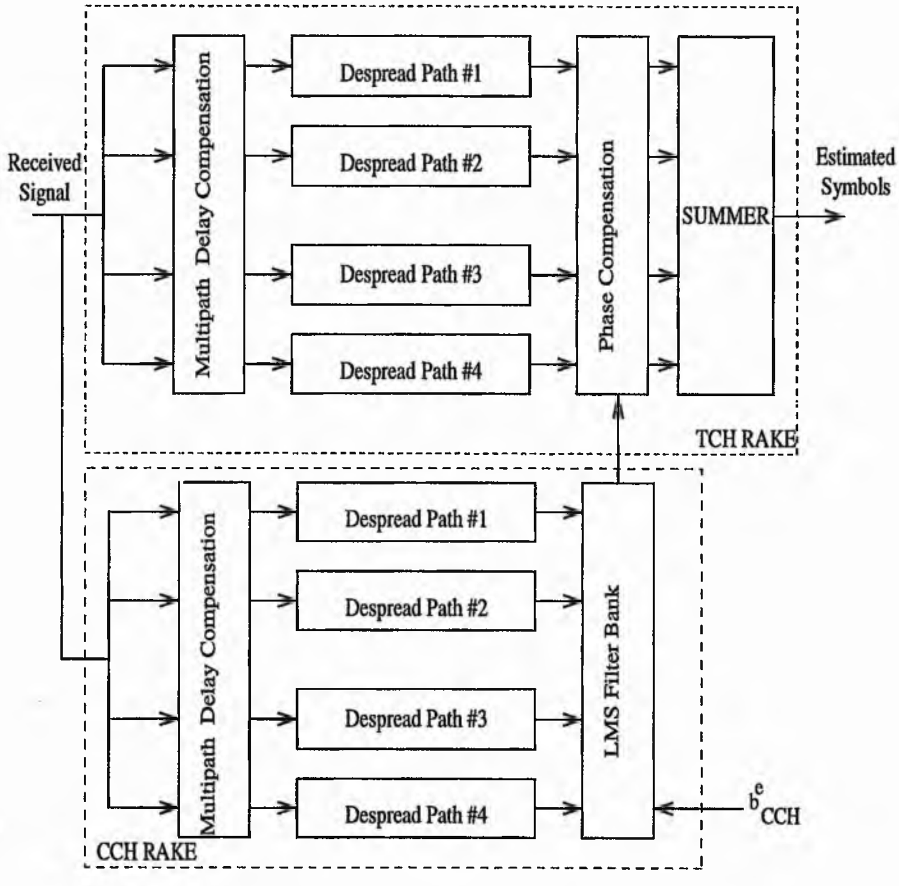

Figure 3.52: CARAKE Simulation Model

The base station receiver consists of two RAKE receivers. The traffic channel (TCH) is coherent detected while the control channel (CCH) is differentially coherent detected. Since the BER of interest is that of the traffic channel only the TCH RAKE structure is shown in full. The CCH RAKE structure is shown up to the point which is of use to the LMS filter bank. The later tracks each individual path producing complex amplitude estimates which are subsequently used in the TCH RAKE receiver to compensate for the phase variations.

Fig.3.53 compares the performances of the CARAKE and the RAKE receivers. The

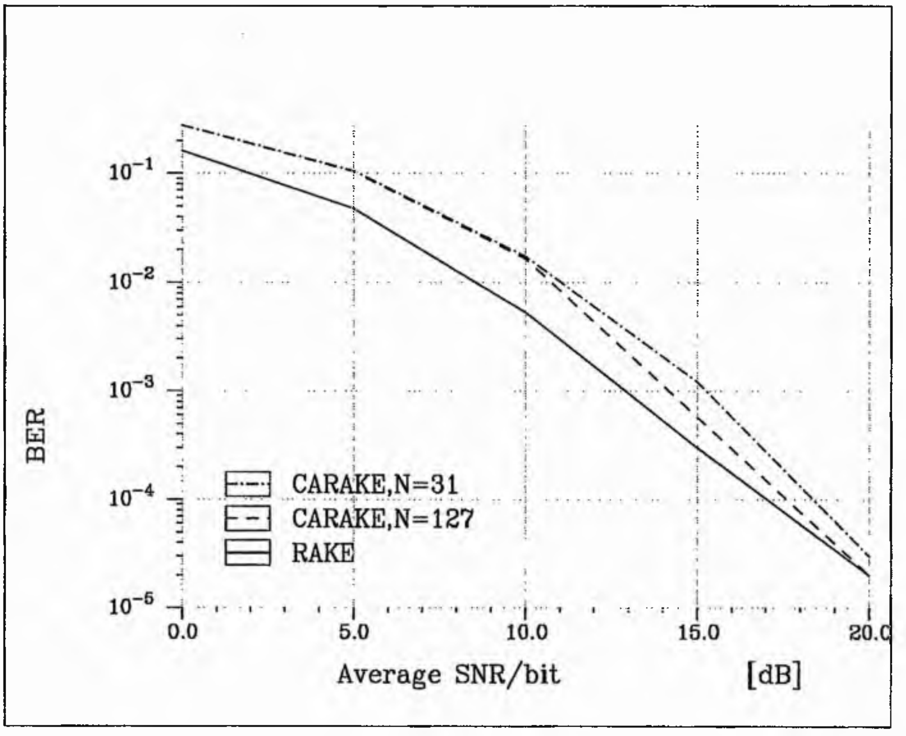

Figure 3.53: Performance Comparison Between CARAKE and RAKE Receivers, D=4,L=6

later performance deviates from the performance of Fig.3.37 since there is an E_b/N_0 penalty associated with the multiplexing of the control channel in the transmitter.

From the results of Fig.3.53 it is evident that practical RAKE receivers have performances that deviate from those predicted theoretically under the assumption of perfect phase compensation. The E_b/N_0 loss observed was 2.0 dB for a BER of 10^{-3} while there is a considerable improvement for higher values of E_b/N_o. The results of Fig.3.53 can be explained heuristically by taking into consideration the fact that the overall loss due to imperfect channel estimation is not related only to the channel estimation performance but also to the combining loss which is associated with the RAKE receiver.

3.7 NEAR-FAR EFFECT AND POWER CONTROL

In this section, the performance of the conventional detector under near-far interference will be studied. It is first necessary though to have a closer look to what exactly is the near-far interference and what factors influence its presence in CDMA personal communication systems.

3.7.1 Near-Far Effect

Near-Far interfering signal is called every signal whose either the average or instantaneous power exceeds the average or instantaneous power of the user of interest. The effects of near-far interference in the receiver performance is widely known as near-far effect. Near-far interference is present to both the uplink and the downlink. In the downlink, the cause of near-far interference is the signals from the surrounding base stations while in the uplink is due to the transmissions from intercell and intracell mobile users. Near-Far problems are commonly met in the uplink direction because of the random movement of the mobile users and the random fluctuations of their power levels.

Many studies have been conducted regarding the effects of near-far interference to the performance of the conventional detector. Before presenting the results of our own studies, it is intuitive to introduce the figure of merits that describe the ability of the receiver to overcome near-far interference.

3.7.2 Multiuser Performance Measures

The performance measures that are described in this section have been originally introduced by [59] and subsequently used by many others [31],[32].

Asymptotic Efficiency

For simplicity, consider the Gaussian multiple access channel and the multiuser model of section 3.2. Each user's efficiency is defined as the ratio

$$Efficiency = \frac{(E_b/N_0)_1}{(E_b/N_0)_K} \tag{3.56}$$

where, the values of $(E_b/N_0)_K$ and $(E_b/N_0)_1$ are shown in Fig. 3.54.

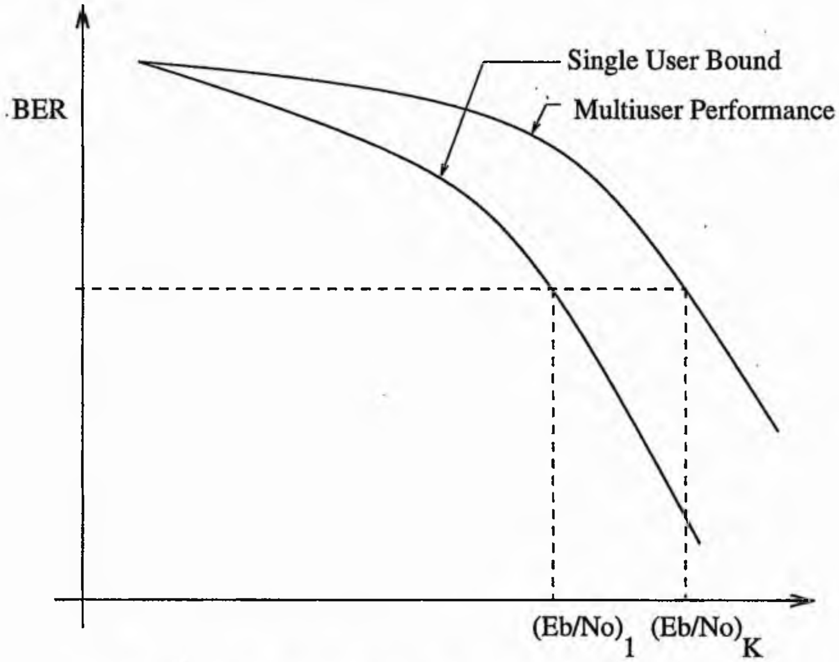

Figure 3.54: Definition of the User Efficiency

It is clear that the SNR/bit value needed to achieve a given BER without the presence of other users, bounded by the single user performance, is always lower than the SNR/bit needed to achieve the same BER in the presence of multiple access interference. Thus, the user's efficiency is always less than or equal to unity. The asymptotic efficiency is now defined as the limit of the user efficiency when the background Gaussian noise vanishes,

$$\eta_k = lim_{N_0 \to 0} \frac{(E_b/N_0)_1}{(E_b/N_0)_K} \tag{3.57}$$

Thus, the asymptotic efficiency η_k is a measure of the performance loss experienced by the kth use due to the presence of other users that share the same band. The asymptotic efficiency of zero is related to the irreducible BER phenomena experienced in the previous sections, due to the interfering users (increased system loading). Indeed, when the value to $(E_b/N_0)_K = \infty$ then $\eta_k = 0$. The conclusion which can be reached from this discussion is that receivers with asymptotic efficiency of one are optimum in a multiuser environment but not necessarily optimum in a single-user environment. This conclusion will be recalled when the receiver structures of Chapter 4 are addressed.

Near-Far Resistance

The near-far resistance is defined as the worst case asymptotic efficiency over all possible energies of the interfering users. The kth user's detector is called NEar-FAr Resistant (NEFAR) when the near-far resistance of user k is nonzero.

3.7.3 Performance Under Near-Far Interference

The simulation model that has been developed for assessing the effects of near-far interference is shown in Fig.3.55. The model refers to static AWGN channels which although not of very practical interest, they have been used extensively by many researchers [31],[56] as a baseline for comparative studies in this area.

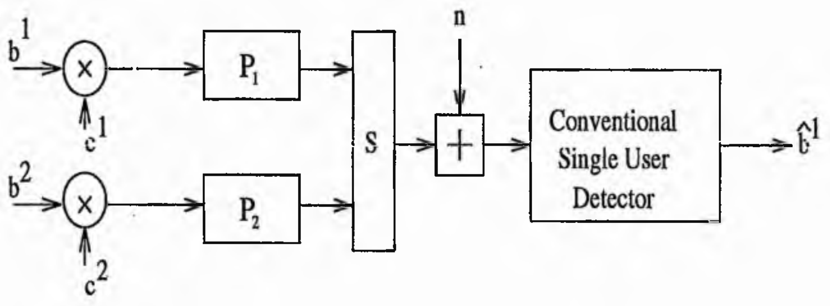

Figure 3.55: Simulation Model for Assessing the Conventional Detector Under Near-Far Interference

P_1 and P_2 are the average power levels of the user of interest and the interfering user respectively. By increasing the power level of the interfering user we create near-far interference. In Fig.3.56 the performance of the user of interest has been depicted for various values of power ratios.

As has been expected the required E_b/N_0 for achieving reliable communication (BER of 1%) increases dramatically with increasing P_2. The detector then, becomes unusable for high interfering power levels.

3.7.4 Limitations of Power Control

In this section an attempt is made to examine one of the most controversial aspects of CDMA, namely the function of the mobile's and base station's transmitter power control. Power control is broadly divided into two types, namely Open Loop Power Control (OLPC) and Closed Loop Power Control (CLPC).

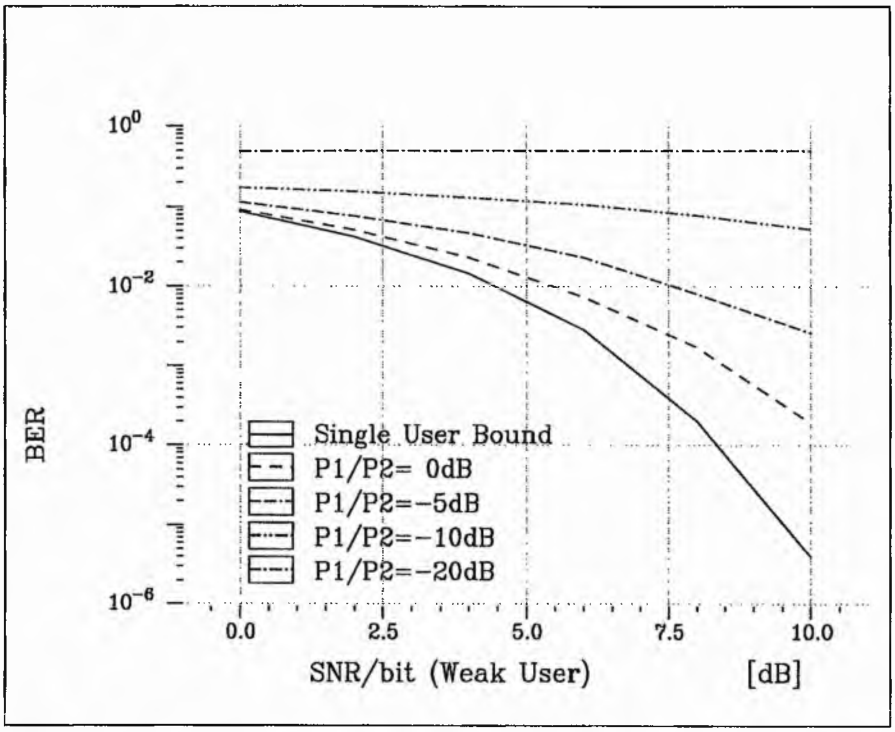

Figure 3.56: Performance of Conventional Detector Under Near-Far Interference

Open Loop Power Control

The open loop power control mechanism is depicted in Fig. 3.57 with $L(t)$ and $R(t)$ denoting the lognormal and Rayleigh fading respectively and n denoting the background noise component. b^k and c^k is the information stream and spreading code of the kth user. The open look power control estimates and cancels the power variations due to shadowing and path loss. The open loop power control acts at the mobile station receiver and during the call set-up procedure it sets the initial power of the traffic channel. The open loop control assumes that the up-link and the downlink attenuation is the same and given that there is a pilot channel in the downlink direction, it measures its power and compares this measurement with the actual power of the pilot channel transmitted from the base station. The actual power of the pilot channel can be known to the mobile station through the broadcast channel, which transmits base station specific information.

Closed Loop Power Control

The closed loop power control mechanism is depicted in Fig. 3.58. The same notation with the open loop case has been used. The closed loop power control attempts to cancel

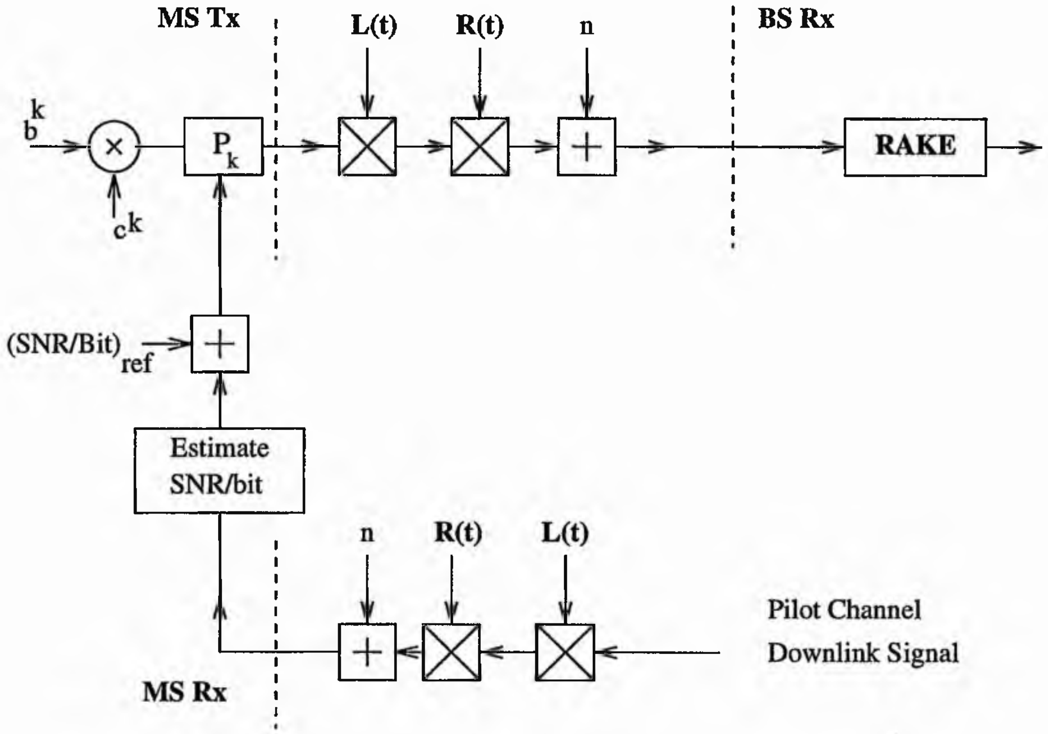

Figure 3.57: Open Loop Power Control Mechanism

the power variations due to Rayleigh fading. As illustrated in Fig.3.59 an ideal estimation of the channel envelope variations from at the BS receiver and zero delay transmission of these estimations to the MS will cause complete cancellation of the fading process.

However, Fig.3.59 is an academic example and perfect power equalization can *never* be achieved. This is because the finite accuracy of the received SNR/bit estimator and the delay constraint. The fact that there is a feedback look imposes an inherent hysteresis phenomenon. That is, by the time that the received power is measured and the actual power control commands are received by the mobile station, the fading has already changed and the command to increase of decrease the power may be irrelevant to the channel amplitude. Thus, it is very important for the success of power equalization technique to design closed power control loop with the following guidelines:

- Minimize the hysteresis of the loop.
- Provide very accurate SNR/bit estimation techniques.
- Apart from SNR/bit estimation consider any other relevant to the link quality information, such as Frame Error Rate, Post Decoder Error Rate etc.

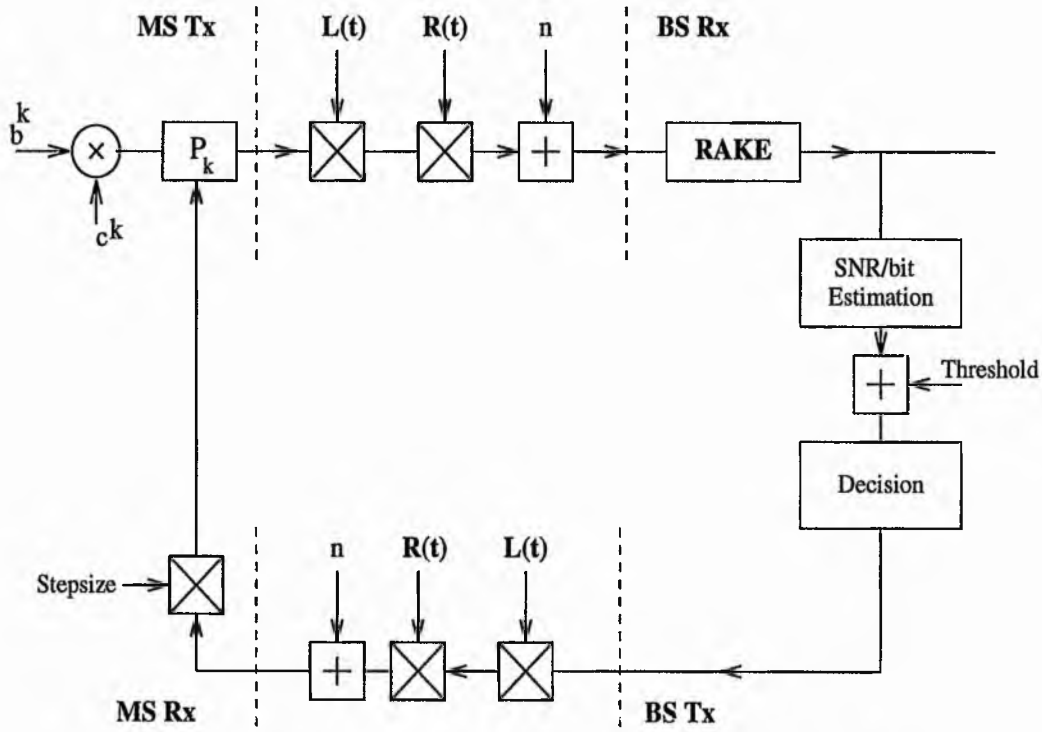

Figure 3.58: Closed Loop Power Control Mechanism

As can easily be concluded, the critical component for the operation of power equalization techniques is the E_b/N_0 estimator. The E_b/N_0 estimator which has been proposed by the author for the CODIT testbed [35],[36] operates on the despread samples $|x_j|$ in both the in-phase (I) and quadrature (Q) channels. The algorithm is as follows:

$$\frac{\hat{E}_b}{N_0} = \frac{\mu_I^2 + \mu_Q^2}{2\,(\sigma_I^2 + \sigma_Q^2)} \tag{3.58}$$

where μ and *sigma* for any of the two channels are given by,

$$\mu = \frac{1}{N}\sum_{j=1}^{N} |x_j| \tag{3.59}$$

$$\sigma^2 = \frac{1}{N}\sum_{j=1}^{N} |x_j|^2 - \mu^2 \tag{3.60}$$

In Fig.3.60 we have plotted the output of the estimated E_b/N_0 versus the variations of the Rayleigh fading channel. The number of bit samples used in the estimation is $N_{EST} = 500$ and a slow varying Rayleigh fading channel has been used.

However, in practice the number of samples used in the estimation must be much smaller due to the delay constraint. In Fig.3.61 the effect of the number of samples used

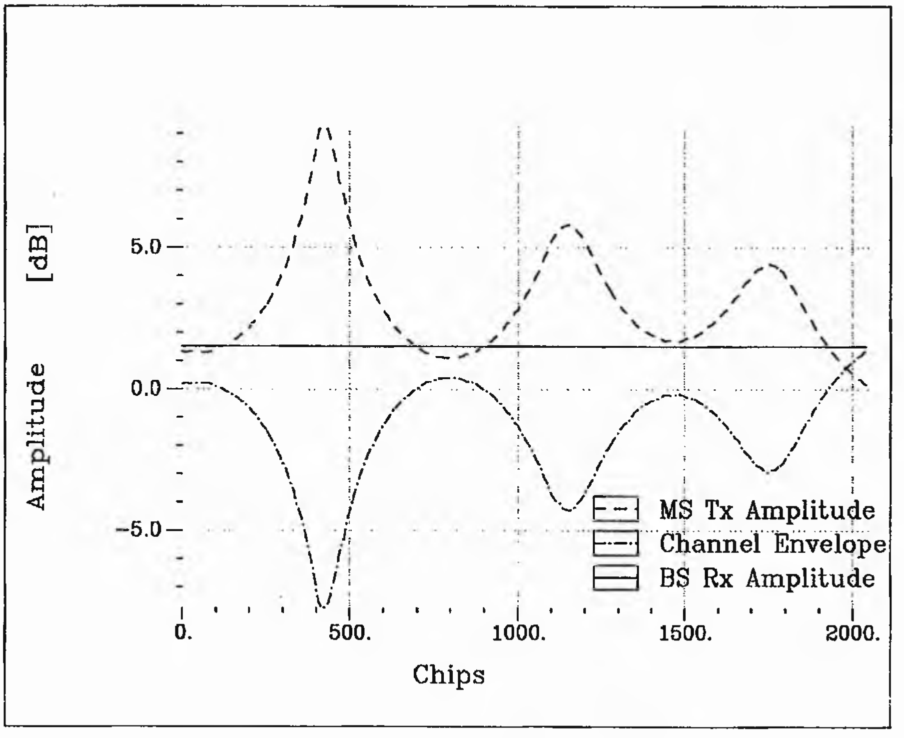

Figure 3.59: Ideal MS Transmitter Power Control

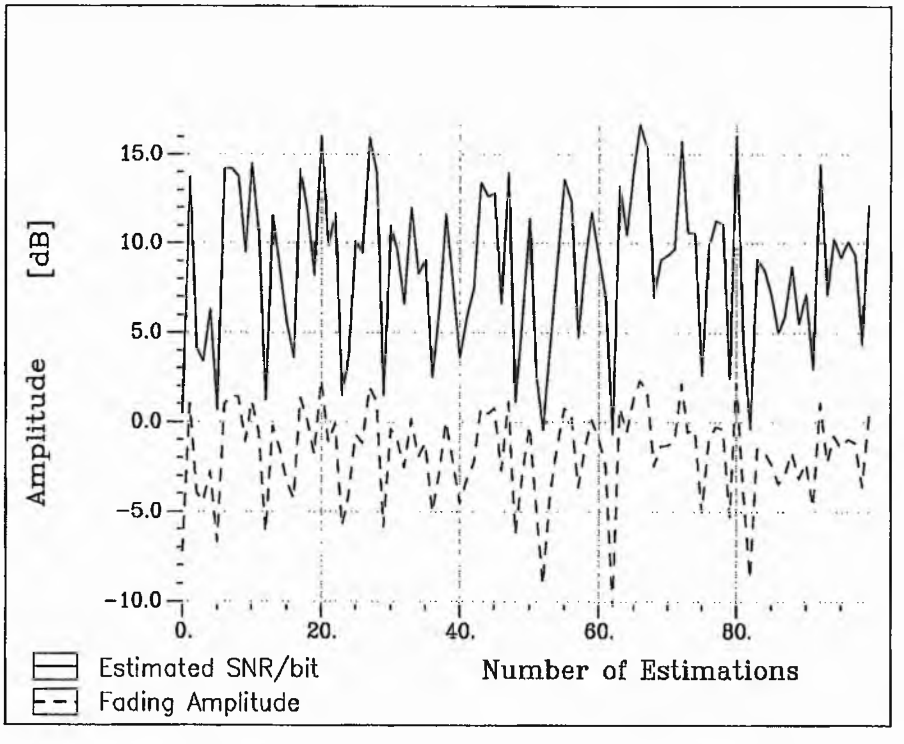

Figure 3.60: E_b/N_0 Estimation with $N_{EST} = 500$ Bits

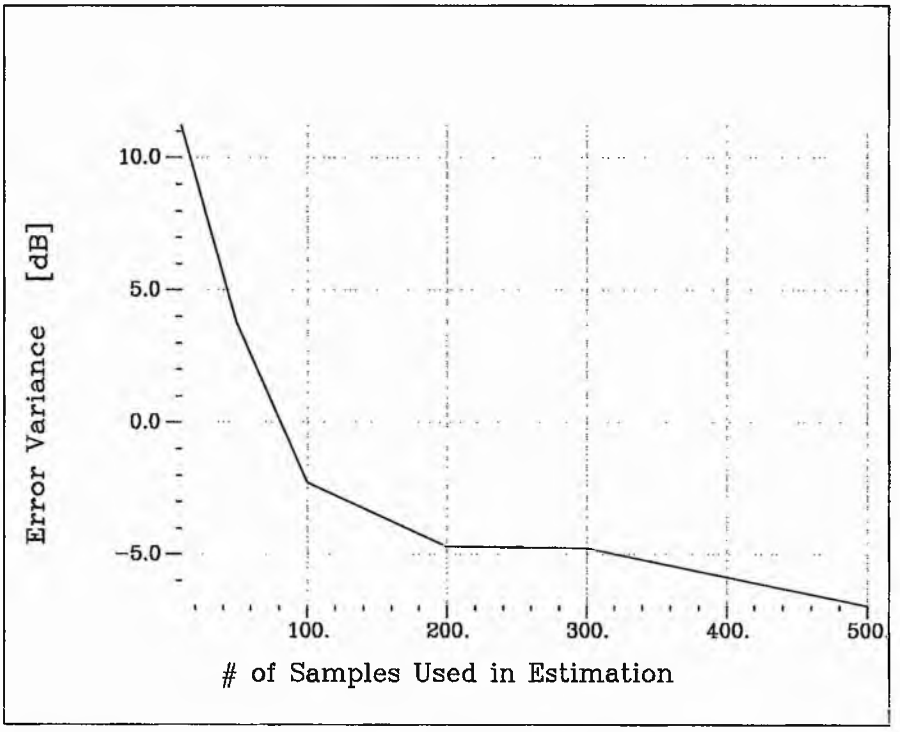

Figure 3.61: Effect of N_{EST} on Estimation Error Variance

in the estimator, on the estimation error variance can be seen. For this evaluation we are only interested to examine the inherent inaccuracy of the estimator irrespective of channel variations. Thus, an AWGN channel with a constant E_b/N_0 of 10 dB has been used, while the error statistics have been accumulated over 100 estimations.

The minimization of the hysteresis in the loop is of vital importance. Even if the estimation error variance is infinite the delay can cause the power equalization mechanism to fail as shown in Fig.3.62.

3.8 CONCLUSIONS

In this chapter an attempt was made to summarise already existing results on conventional detection and to shed some light on the effects of important system variables on the performance of RAKE receivers. On that respect the following concluding remarks can be made:

- In single path fading channels conventional detectors appear to have irreducible BER even for very lightly loading conditions.

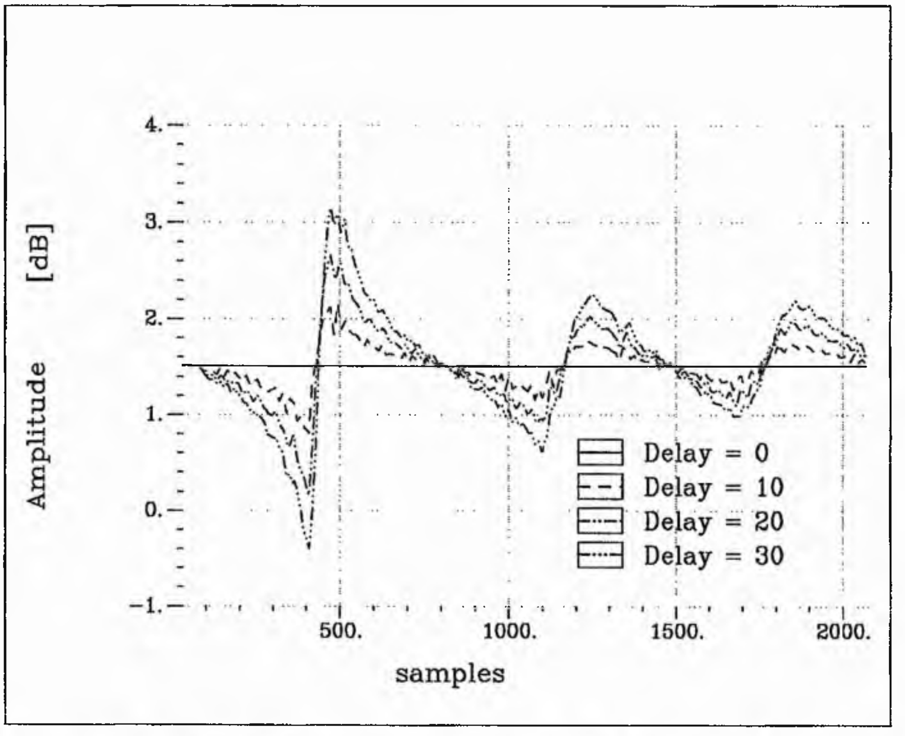

Figure 3.62: Effect of Estimation Delay on BS Received Amplitude

- In multipath fading channels the self noise increases the error floor to almost unusable levels even for a single user system. It is worth noting that for spreading factor of 31 an E_b/N_0 ratio of 20 dB is inadequate for reliable communication (BER greater than 1%) for a single user system.

- The multipath diversity receiver is able to provide adequate level of performance but its operation is not autonomous. RAKEing depends on the ability of the Delay Power Spectrum (DPS) estimator to provide the positions of the D strongest multipath components and on the capability of the channel estimator to extract the reference from these paths. On the downlink the channel estimation procedure is straightforward since the pilot channel is always available having increased power level compared to the traffic channel. Thus, coherent demodulation on the downlink is always possible.

- In the uplink the limits of the RAKE receiver can only be reached through coherently demodulating the received signal. However, since there is no pilot channel the demodulation can only be performed quasi-coherently. The technique that uses the traffic channel for coherent demodulation has given very good results and the CARAKE receiver approaches the coherent RAKE within 2 dB for $BER = 0.1\%$.

- The lack of coherency in the uplink can lead to the loss of multipath diversity gain. It was demonstrated that the DRAKE has no advantage compared to the multipath rejecting receiver when the SNR/bit is less than 9 dB.

- The performance of conventional detection under near-far interference has been found to severely deteriorate. Simulation for time-varying near-far interference indicate that the conventional detector is unusable without dynamic power control. The capability of the power control to track fast power variations has been found to be very poor due to its inherent hysteresis.

In view of the above limitations of conventional detection, Chapter 4 proposes new receiver architectures which can significantly enhance the horizons of CDMA systems.

Chapter 4

NEFAR MIMO MMSE DETECTION

4.1 INTRODUCTION

In this chapter we present Multiple Input Multiple Output (MIMO) Minimum Mean Square Error (MMSE) detection schemes for CDMA systems. The starting point is section 4.2 which addresses the general problem of cross-channel interference in MIMO channels. Section 4.3 establishes the theory of interference equalization, in systems modeled with MIMO channels, based on Mean Squared Error (MSE) minimization. Section 4.4 establishes the connection between CDMA and systems that can be modelled by MIMO channels and introduces the equivalent CDMA channel model which is of fundamental importance on interference equalization. Section 4.5 proves the NEar FAr Resistance (NEFAR) of the MIMO MMSE detectors for both synchronous and asynchronous CDMA systems. Section 4.18 provides a comprehensive description of the major rival of MIMO MMSE detection, namely the decorrelating detector. The decorrelating detector either with its linear or with its non-linear architecture is a MIMO zero forcing equalizer which is suboptimal to the presented MIMO MMSE detection schemes. However, all the MIMO receiver structures suffer from a drastically increased complexity compared to the conventional detector. In section 4.8 we summarise the drawbacks of MIMO receivers that process the code matched filter bank output and we propose downsized versions of these detector structures.

4.2 MIMO CHANNELS

Multiple Input Multiple Output channels arise in many, and sometimes diverse, fields of communication engineering. In Fig.4.1 some of the applications that incorporate MIMO channels have been depicted.

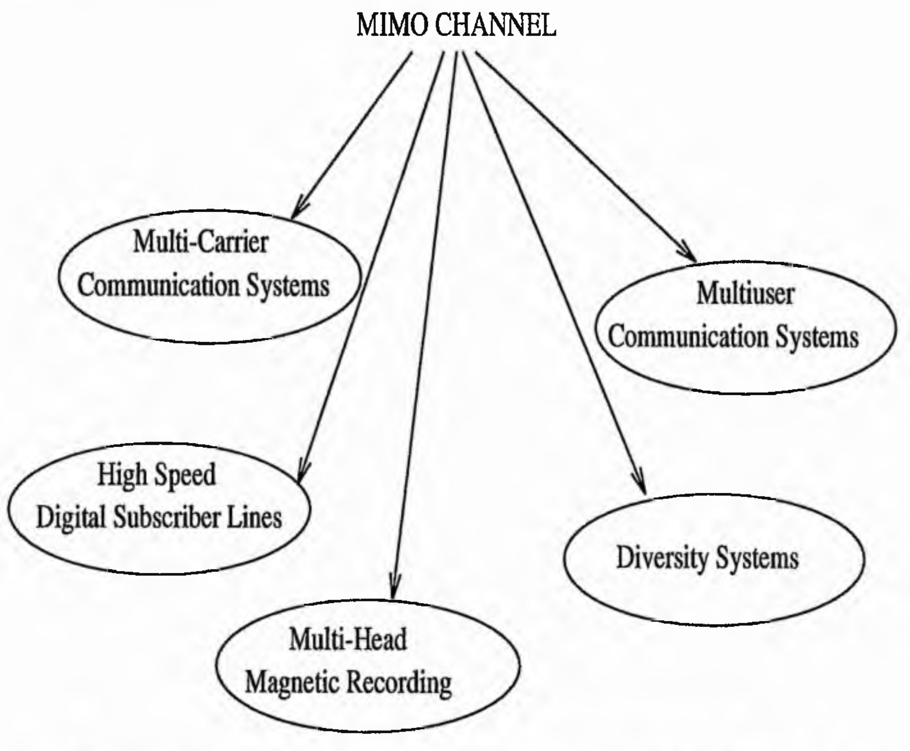

Figure 4.1: Applications Represented by MIMO Channels

Multi-head magnetic recording systems are able to increase the density of magnetic material when the inter-track interference is taken into consideration. A multiple input receiver equalizes the MIMO magnetic recording channel. Another application where MIMO channels arise is in multi-carrier systems. GSM mobile radio systems employ Frequency Division Multiplex (FDM) with carriers spaced at 200 KHz apart. By shortening the inter-carrier distance as shown in Fig.4.2, the TDMA system capacity can be increased since more carriers can be accommodated in a given bandwidth. The resulting inter-carrier interference can be mitigated through three input-three output equalization receivers [34].

Transmissions with polarization diversity can be modelled as MIMO channels if the cross-polarization interference (XPI) is considered. Again MIMO equalizers have been used to mitigate this interference. DS-CDMA systems fall in the category of multiuser

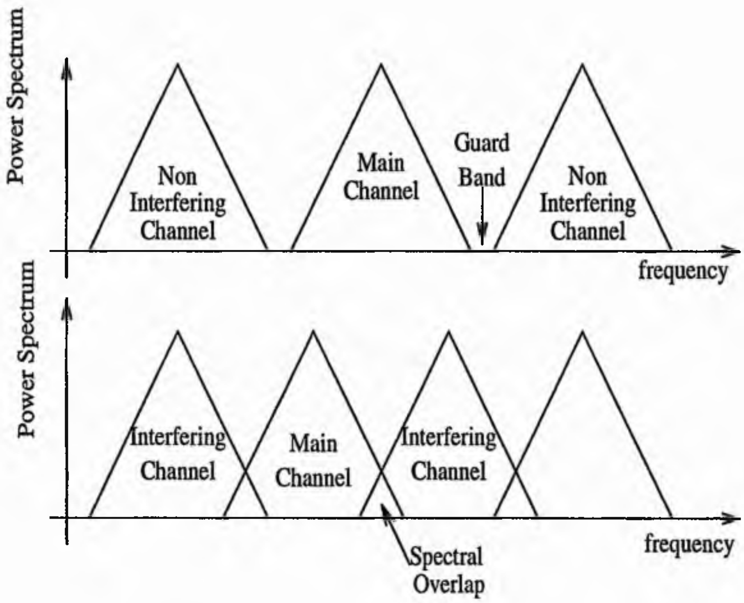

Figure 4.2: MIMO Channels and Multi-carrier Systems

systems which can be modelled as a MIMO channel if the multiple access interference is considered as will be described in 4.4. High Speed Digital Subscriber Lines (HSDL) and Asynchronous Subscriber Digital Lines (ASDL) have recently attracted research interest due to the evolving broadband wireline multimedia applications such as Video On Demand (VOD). One of the most detrimental effects in these lines is the Near End crosstalk (NEXT) that arises when many of these lines are physically located close to each other. NEXT can be equalized, again, by MIMO detection [44], [1].

4.3 MMSE DETECTION IN MIMO CHANNELS

Receiver architectures for applications where MIMO channels arise can be designed with two different philosophies. The first, Single Input Single Output (SISO) philosophy *ignores the MIMO channel induced interference.* Although this guideline may lead to catastrophic results for some of the MIMO channel applications described in section 4.2, it has been very much followed for the DS-CDMA multiuser systems. For example, consider the DS-CDMA conventional detector depicted in Fig.4.3. The conventional detection approach consists of demodulating each signal independently. This means that the received signal is demodulated by the matched filter of each user, ignoring the multiple access interference or equivalently not taking into account the crosscorrelations among the users' signals.

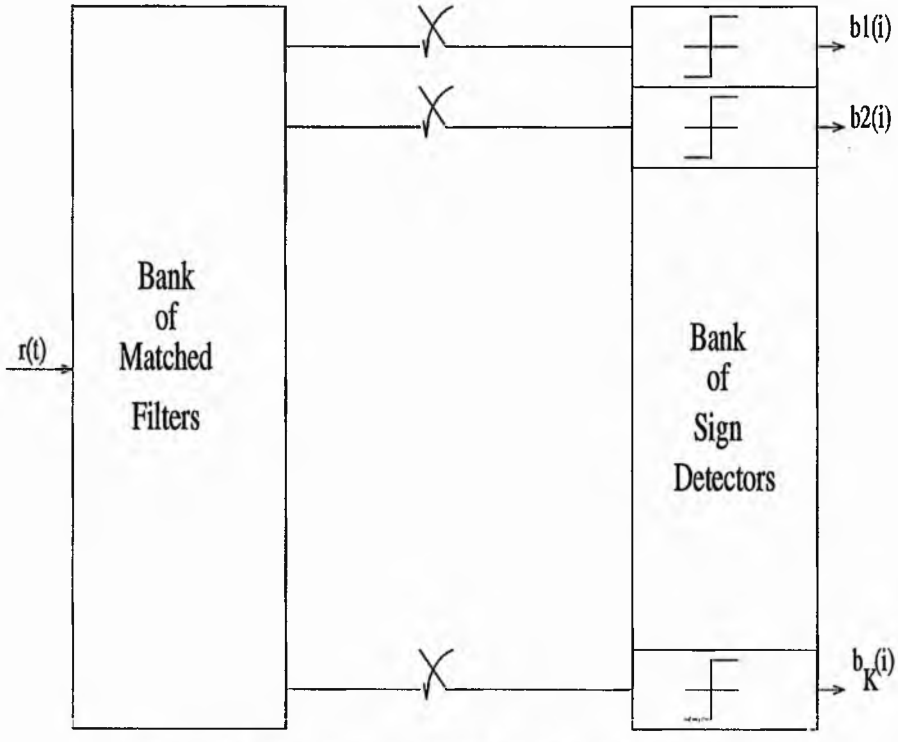

Figure 4.3: Conventional DS-CDMA Detector

It is clear that with the SISO design methology, DS-CDMA receiver design is very much simplified. However, the performance of SISO designed receivers can be severely degraded under specific interference patterns as already has been demonstrated in Chapter 3 for near-far interference.

The second, MIMO design philosophy *introduces additional signal processing and by taking into account the MIMO channel induced interference, aims to mitigate the effects of the latter.* Many researchers in this area have also used the term "multiuser receivers" to denote receivers that are optimised to work in multiuser systems. Generally, receivers built with the MIMO design methology have multiple inputs in order to exploit the information from the interfering dimensions [1], while, they have a single output to produce the estimates of the signal of interest. Although the MIMO design guideline is not specific on the type of signal processing that has to be performed, linear and non-linear signal processing techniques based on the minimization of the Mean Squared Error (MSE) have been suggested by Duel-Hallen [11]. In order to analytically formulate the linear MMSE detector for MIMO channels it is needed to present some fundamental theorems on statistical signal processing.

[1]We shall use interchangeably the term multidimensional detection and MIMO detection in future discussions.

4.3.1 Statistical Signal Processing for MIMO Channels

Consider the K-input K-output MIMO channel depicted in Fig.4.4.

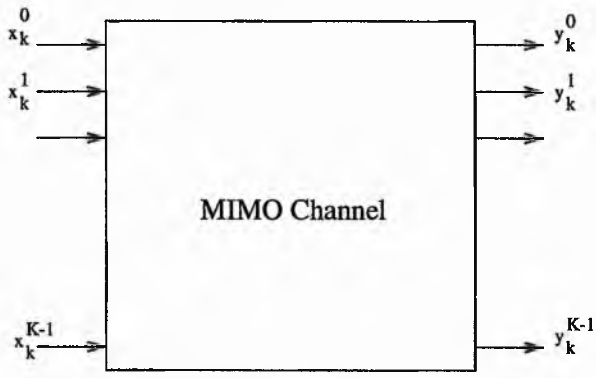

Figure 4.4: Multiple Input Multiple Output Channel

The input process is a series of vectors. The kth input vector can be written as,

$$\mathbf{x_k} = (x_k^0, x_k^1, ..., x_k^{K-1})^T \tag{4.1}$$

For the spectral representation of discrete processes we usually work on the D-transform domain. We define the D-transform of the input process as,

$$\mathbf{x_k}(D) = \sum_{i=0}^{\infty} x_k D^i \tag{4.2}$$

We assume that the input process is a zero mean, $E[\mathbf{x_k}] = 0$ and is Wide Sense Stationary (WSS) with autocorrelation matrix given by,

$$\mathbf{R_x}(i) = E[\mathbf{x_{k+i}x_k^T}] \tag{4.3}$$

The spectral matrix of the input process is given by,

$$\mathbf{S_x}(D) = \sum_{i=-\infty}^{\infty} \mathbf{R_x}(i) D^{-i} \tag{4.4}$$

We state the following fundamental theorems without proof. An extensive discussion for scalar channels can be found in [55].

Theorem 4.1 *If* $\mathbf{G}(D)$ *is the D-domain MIMO channel transfer function, and* $\mathbf{x}(D)$ *the D-domain WSS input process, the D-domain output is equal to,*

$$\mathbf{y}(D) = \mathbf{G}(D)\ \mathbf{x}(D) \tag{4.5}$$

Theorem 4.2 *If* $\mathbf{G}(D)$ *is the D-domain MIMO channel transfer function, and* $\mathbf{S}_{\mathbf{x}}(D)$ *the spectrum of the WSS input process, the spectrum of the output is equal to,*

$$\mathbf{S}_{\mathbf{y}}(D) = \mathbf{G}(D)\ \mathbf{S}_{\mathbf{x}}(D)\ \mathbf{G}^T(D^{-1}) \tag{4.6}$$

Theorem 4.3 *If* $\mathbf{G}(D)$ *is the D-domain MIMO channel transfer function, and* $\mathbf{S}_{\mathbf{x}}(D)$ *the spectrum of the WSS input process, the cross-spectrum of the input and the output is equal to,*

$$\mathbf{S}_{\mathbf{y},\mathbf{x}}(D) = \mathbf{G}(D)\ \mathbf{S}_{\mathbf{x}}(D) \tag{4.7}$$

4.3.2 MIMO Linear MMSE Detector

The MIMO MMSE detector proposed in [11] has been derived using the orthogonality principle. Since the derivation of [11] was not detailed enough we attempt a proof by recalling some of the theoretical arguments of the previous section. The notation used is shown in Fig.4.5 where the MIMO model is depicted. According to the model, the main impairment that the input signal $\mathbf{x}(D)$ experiences is the MIMO channel $\mathbf{G}(D)$ and an additive Gaussian noise component $\mathbf{z}(D)$. $\epsilon(D)$ is the D-transform of the error signal.

Theorem 4.4 *The Linear MSE minimizing MIMO detector* $\mathbf{Q}(D)$ *that processes the output of a MIMO channel denoted by* $\mathbf{G}(D)$ *whose input is* $\mathbf{x}(D)$ *is given by,*

$$\mathbf{Q}(D) = \mathbf{S}_{\mathbf{x}}(D)\,(\mathbf{G}(D)\ \mathbf{S}_{\mathbf{x}}(D) + N_0\mathbf{I})^{-1} \tag{4.8}$$

Proof: The MSE minimising linear detector attempts to minimize the mean square error. The error signal is defined as the difference of the actual and the estimated input signal.

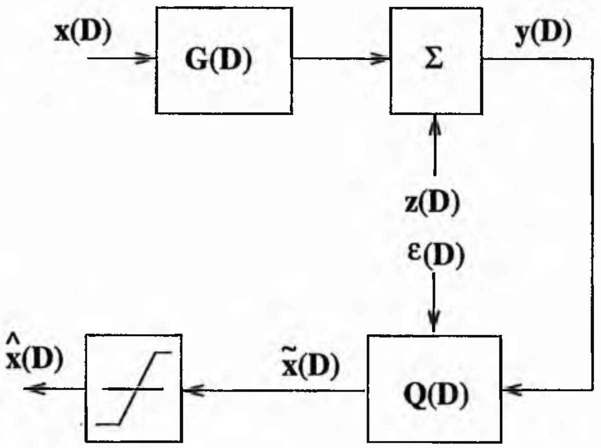

Figure 4.5: Linear MIMO Equalization System Model

$$\epsilon_k = \hat{\mathbf{x}}_k - \tilde{\mathbf{x}}_k \tag{4.9}$$

The orthogonality principle states that the error signal is orthogonal to the observation signal $\mathbf{y}_k$.

$$E[(\mathbf{x}_k - \tilde{\mathbf{x}}_k)\mathbf{y}_k^T)] = 0 \quad \forall k \tag{4.10}$$

The latest equation can be written as,

$$E[(\mathbf{x}_k \mathbf{y}_k^T)] = E[(\tilde{\mathbf{x}}_k \mathbf{y}_k^T)] \tag{4.11}$$

which, given the definition of the crosscorrelation matrix between two random vectors $\mathbf{R}_{xy}(j) = E[(\mathbf{x}_{k+j}\mathbf{y}_k^T)]$, simply states that,

$$\mathbf{R}_{\mathbf{xy}}(j) = \mathbf{R}_{\tilde{\mathbf{x}}\mathbf{y}}(j) \tag{4.12}$$

Using equation (4.4) we can now write,

$$\mathbf{S}_{\mathbf{xy}}(D) = \mathbf{S}_{\tilde{\mathbf{x}}\mathbf{y}}(D) \tag{4.13}$$

The latest equation is of great importance. It simply states that the cross- spectral matrix between the estimated input vector and the observation is equal to the cross-spectral matrix between the actual input vector and the observation. Thus, it is now straightforward to establish a connection between the matrix transfer function of the multichannel system $\mathbf{G}(D)$ and that of the MIMO filter $\mathbf{Q}(D)$ used to equalize the channel. The starting point is the following relationships,

$$\mathbf{S}_{\tilde{\mathbf{x}}\mathbf{y}}(D) = \mathbf{Q}(D)\mathbf{S}_{\mathbf{y}}(D) \tag{4.14}$$

$$\mathbf{S_{xy}}(D) = \mathbf{G}(D)\mathbf{S_x}(D) \tag{4.15}$$

Thus,

$$\mathbf{G}(D)\mathbf{S_x}(D) = \mathbf{Q}(D)\mathbf{S_y}(D) \tag{4.16}$$

Substituting $\mathbf{S_y}(D)$ with,

$$\mathbf{S_y}(D) = \mathbf{G}(D)\ \mathbf{S_x}(D)\ \mathbf{G}^T(D^{-1}) + N_0\mathbf{G}(D) \tag{4.17}$$

we conclude that

$$\mathbf{G}(D)\mathbf{S_x}(D) = \mathbf{G}(D)\left(\mathbf{S_x}(D)\ \mathbf{G}^T(D^{-1}) + N_0\mathbf{I}\right)\mathbf{Q}(D) \tag{4.18}$$

Q.E.D

4.3.3 The Non-Linear Decision Feedback MIMO MMSE Detector

The non-linear Decision Feedback (DF) MIMO MMSE detector for general multichannel systems has also been studied in [11]. The transmission system that employs a DF MIMO MMSE detector is shown in Fig.4.6.

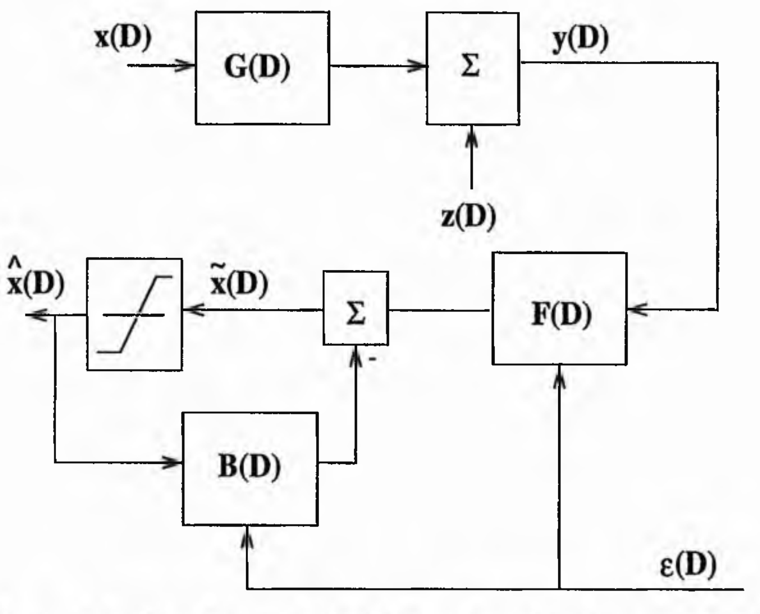

Figure 4.6: Non-Linear MIMO Equalization System Model

The non-linearity of the detector is due to the feedback filter $\mathbf{B}(D)$ that feeds back past decisions. The structure, is basically an extension of the scalar Decision Feedback Equalizer to cover multiple dimensions. The additive Gaussian noise component is $\mathbf{z}(D)$ and $\epsilon(D)$ is the error signal.

Theorem 4.5 *The Non-linear DF MSE minimizing detector that consists of a MIMO feedforward filter* $\mathbf{F}(D)$ *and a feedback filter* $\mathbf{B}(D)$*, and processes the output of a MIMO channel denoted by* $\mathbf{G}(D)$ *whose input is* $\mathbf{x}(D)$ *is given by,*

$$\mathbf{F}(D) = \mathbf{A}^d(0)(\mathbf{\Phi}^d(0))^{-1}(\mathbf{\Phi}^T(0))^{-1}\mathbf{A}^T(D^{-1}) \tag{4.19}$$

$$\mathbf{B}(D) = \mathbf{A}^d(0)(\mathbf{\Phi}^d(0))^{-1}\mathbf{\Phi}(D)\mathbf{A}^{-1}(D) - \mathbf{I} \tag{4.20}$$

where, $\mathbf{A^d}(0)$ denotes the matrix that is formed from the diagonal elements of the matrix $\mathbf{A}(D)$ which is produced by the Cholesky factorization of the input process $\mathbf{x}(D)$ ie. $\mathbf{S_x}(D) = \mathbf{A}(D)\mathbf{A}^T(D^{-1})$. $\mathbf{\Phi}^d(0))$ is also the diagonal matrix formed by the diagonal elements of $\mathbf{\Phi}(D)$ which is produced by the Cholesky factorization of $(\mathbf{S_x}(D)\ \mathbf{G}(D)\ \mathbf{S_x}(D) + N_0\mathbf{I})$.

Up to this point the theory established by the significant contributions of [11] has been presented. This theory is the starting point for our investigations in advanced CDMA receiver architectures. In fact as it will be made evident by the end of the chapter, this theory unifies previous research for advanced signal processing receivers [31],[46] and our own research under a common framework.

4.4 MMSE EQUALIZATION OF CDMA MULTIPLE ACCESS INTERFERENCE

This section addresses the application of MIMO equalization theory in CDMA systems. The starting point in our treatment will be a fundamental observation that leads to the treatment of the multiple access interference as an accumulated ISI effect. This is shown in Fig.4.7 where the signal streams of three asynchronous users are shown.

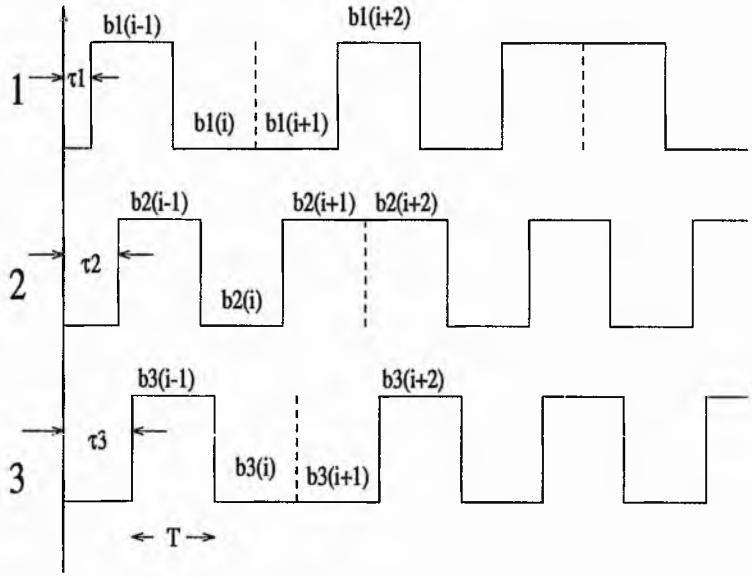

Figure 4.7: Interpretation of Multidimensional ISI in Asynchronous CDMA

The ith user delay is denoted with τ_i. The simultaneous demodulation of all active users in the multiple access channel can be regarded as a problem of periodically varying ISI. For example, symbol $b_2(i)$ interferes with $b_1(i)$ and $b_3(i-1)$ (past symbols, arriving before $b_2(i)$), and with $b_1(i+1)$ and $b_3(i)$ (future chips, arriving after $b_2(i)$).It is clear that in a K-user system, each symbol overlaps with $K-1$ previous symbols and $K-1$ future symbols. It is this partial overlap of symbols that creates what is commonly called Multidimensional InterSymbol Interference (M-ISI) and the only way that M-ISI can be removed is with multidimensional equalizers. In order though to specify the equalization process we have to quantify the mechanisms of M-ISI generation as described subsequently.

4.4.1 The Equivalent CDMA Channel

The equivalent CDMA channel is an MIMO (matrix) channel which quantifies the impairment to the signal of the user of interest (input signal) due to the simultaneous transmission from other users that share the same bandwidth. The equivalent CDMA channel is related with, mainly, three factors:

- The choice of the PN sequences used in the system.
- The relative delays among the users.
- The power level of each user.

Starting from the general asynchronous CDMA transmission model introduced in Chapter 3, we assume without loss of generality that the channel introduces white Gaussian noise and that the spreading signal is zero outside a bit duration ie. outside the interval $[0, T_b)$. The users are indexed with increasing delays $\tau_1 < \tau_2 < \dots < \tau_K < T_b$. If the ith bit of kth user information sequence is denoted as $b_k(i)$ and the energy of the kth user signal arriving at the BS antenna is denoted by w_k then the received signal $r(t)$ from all the active users in the system is given by,

$$r(t) = \sum_{i=-M}^{M} \sum_{k=1}^{K} b_k(i)\sqrt{w_k(i)}s_k(t - iT) + n(t) \tag{4.21}$$

where 2M+1 is the number of bits to be detected
and the normalized signature sequence s(t) is given by,

$$s_k(t) = \sum_{i=0}^{N-1} a_i p_{T_c}(t - iT_c) \tag{4.22}$$

If we denote the normalized signal crosscorrelation matrices with $\mathbf{R}(l)$,then,

$$R_{ik}(l) = \int_{-\infty}^{+\infty} s_i(t - \tau_i)s_k(t + lT - \tau_k)dt \tag{4.23}$$

Since the modulating signals are zero outside $[0, T]$,

$$\mathbf{R}(l) = 0, \forall |l| > 1 \tag{4.24}$$

so the crosscorrelation matrices are confined to $\mathbf{R}(0), \mathbf{R}(-1)$ and $\mathbf{R}(1)$. Fig.4.8 is a snapshot of transmissions in an asynchronous three user system and can be used as an example for the formulation of crosscorrelation matrices.

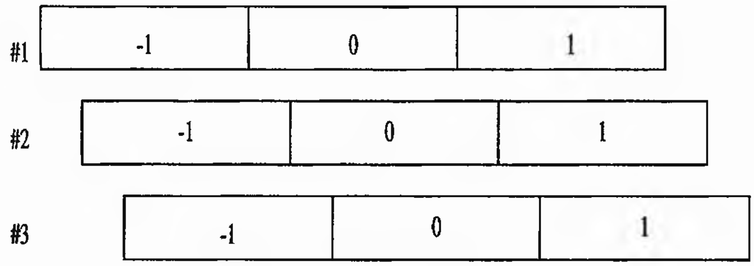

Figure 4.8: Bit Positions in an Asynchronous 3-user System

The crosscorrelation matrices $\mathbf{R}(0), \mathbf{R}(-1)$ and $\mathbf{R}(1)$, can be written as,

$$\mathbf{R}(0) = \begin{pmatrix} R_{11}(0) & R_{12}(0) & R_{13}(0) \\ R_{21}(0) & R_{22}(0) & R_{23}(0) \\ R_{31}(0) & R_{32}(0) & R_{33}(0) \end{pmatrix} \tag{4.25}$$

$$\mathbf{R}(-1) = \begin{pmatrix} R_{11}(-1) & R_{12}(-1) & R_{13}(-1) \\ R_{21}(-1) & R_{22}(-1) & R_{23}(-1) \\ R_{31}(-1) & R_{32}(-1) & R_{33}(-1) \end{pmatrix} \tag{4.26}$$

$$\mathbf{R}(1) = \begin{pmatrix} R_{11}(1) & R_{12}(1) & R_{13}(1) \\ R_{21}(1) & R_{22}(1) & R_{23}(1) \\ R_{31}(1) & R_{32}(1) & R_{33}(1) \end{pmatrix} \tag{4.27}$$

Every element of these matrices represents the cross-correlation interference among the users. Let's consider the $\mathbf{R}(0)$ matrix. Each of the elements of the main diagonal should have a value of 1.0. For example, the element $R_{22}(0)$ represents the crosscorrelation value between the 0th bit of the 2nd user and the 0th bit of the second user. The crosscorrelation between two equal code sequences is always 1, so all the elements of the main diagonal of the $\mathbf{R}(0)$ matrix are equal to 1. The element $R_{12}(0)$ represent the crosscorrelation between the 0th bit of the 1st user and the 0th bit of the 2nd user. The element $R_{21}(0)$ represent the crosscorrelation between the 0th bit of the 2nd user and the 0th bit of the 1st user. Notice that $R_{12}(0) = R_{21}(0)$ and the matrix is Toeplitz. For the formation of the $\mathbf{R}(1)$ matrix, the element $R_{23}(1)$ can be interpreted as the crosscorrelation between the 0th bit of the second with the 1st bit of the 3rd user. As can be easily concluded from Fig.4.8, there is no overlap between the concerned bits, so $R_{23}(1) = 0$. Similarly, $R_{11}(1)$ is also equal to zero since there is no overlap between the 0th bit of the 1st user and the 1st bit of the 1st user. Thus, $\mathbf{R}(1)$ is always lower-triangular. Finally, for the $\mathbf{R}(-1)$ matrix, the element $R_{23}(-1)$ is the crosscorrelation between the 0th bit of the 2nd user and the -1st bit of the 3rd user. The element $R_{32}(-1)$ is the crosscorrelation between the 0th bit of the 3nd user and the -1st bit of the 2nd user, which as can be concluded from Fig.4.8, is zero. By repeating the evaluations for the rest of the elements, we conclude that the matrix $\mathbf{R}(-1)$ is upper triangular. Also, it can be very easily shown that $\mathbf{R}(-1) = \mathbf{R}^T(1)$. Thus, for the description of the equivalent CDMA channel, only two matrices are needed, namely, $\mathbf{R}(0)$ and $\mathbf{R}(1)$.

Apart from the crosscorrelation values, the other significant parameter that influences the performance is the energy matrix. The energies of each user in a mobile radio environment are time variant due to fading but for the sake of simplicity these are assumed to be constant over the interval $[0, T)$. Under this assumption the energy matrix of all active users is a diagonal matrix given by,

$$\mathbf{W}(l) = diag([\sqrt{w_1(l)}, ..., \sqrt{w_K(l)}]) \tag{4.28}$$

The first signal processing block in the base station receiver is a bank of despreaders ie. a bank of K matched filteis whose outputs are sampled producing the samples $y_k(i)$ of the ith bit of the kth user,

$$y_k(i) = \int_{iT+\tau_k}^{iT+T+\tau_k} r(t) s_k(t - iT - \tau_k) dt \tag{4.29}$$

The samples $y_k(i)$ for $k = 0, ..., K$ and $i = -M, ..., +M$ is a sufficient statistic for the decision on the most likely transmitted information sequence $\mathbf{b}$. The matched filter outputs for $l = -M, ..., M$ can be written in a matrix form as,

$$\mathbf{y}(l) = \mathbf{R}(-1)\mathbf{W}(l+1)\mathbf{b}(l+1) + \mathbf{R}(0)\mathbf{W}(l)\mathbf{b}(l) + \mathbf{R}(1)\mathbf{W}(l-1)\mathbf{b}(l-1) + \mathbf{z}(l) \tag{4.30}$$

where, $\mathbf{z}(1)$ is the matched filter output noise vector with autocorrelation matrix given by,

$$E[\mathbf{z}(k)\mathbf{z}^T(m)] = \begin{cases} \sigma^2\mathbf{R}(0) & k = m \\ \sigma^2\mathbf{R}(1) & k = m+1 \\ \sigma^2\mathbf{R}(-1) & k = m-1 \\ 0 & otherwise \end{cases} \tag{4.31}$$

where, $\sigma^2 = N_0/2$ is the two-sided noise power spectral density.

The D-transform domain representation of the matched filter output sequence can be written as follows:

$$\mathbf{y}(D) = \mathbf{G}(D)\mathbf{W}(D)\mathbf{b}(D) + \mathbf{z}(D) \tag{4.32}$$

where $\mathbf{b}(D)$ and $\mathbf{z}(D)$ are the information sequence, and the noise sequence at the output of the matched filter. The matrix $\mathbf{G}(D)$ is the matrix which fully describes the CDMA channel in terms of multiple access interference. This is given by,

$$\mathbf{G}(D) = \mathbf{R}^T(1)D + \mathbf{R}(0) + \mathbf{R}(1)D^{-1} \tag{4.33}$$

One can regard $\mathbf{G}(D)$ as a distortion where the amplitude of this distortion is a function of the spreading sequences and the relative delays among the users. For example if the codes of the users were orthogonal (produced by Walsh function generators) then in a synchronous system the matrix $\mathbf{R}(0)$ would have been diagonal and the matrices $\mathbf{R}(1), \mathbf{R}(-1)$ would have been zero.

Based on the theoretical contributions of [11] regarding the transfer function of the Linear and the DF MMSE detectors for general MIMO channels, we can now focus on CDMA multiuser communication systems.

4.4.2 CDMA MIMO MMSE Detection

The two theorems in [11] can be restated for CDMA systems as follows:

Theorem 4.6 *The Linear MSE minimizing detector* $\mathbf{Q}(D)$ *that processes the output of the equivalent CDMA channel denoted by* $\mathbf{G}(D)$ *whose input is* $\mathbf{W}\mathrm{b}(D)$ *is given by,*

$$\mathbf{Q}(D) = \mathbf{W}^2 \left(\mathbf{G}(D)\ \mathbf{W}^2 + N_0\mathbf{I}\right)^{-1} \tag{4.34}$$

Proof: From theorem 4.4 by direct substitution of the input spectrum we have,

$$\mathbf{Q}(D) = \mathbf{S}_{\mathbf{W}\mathrm{b}} \left(\mathbf{G}(D)\ \mathbf{S}_{\mathbf{W}\mathrm{b}} + N_0\mathbf{I}\right)^{-1} \tag{4.35}$$

For the calculation of the input spectrum $\mathbf{S}_{\mathbf{W}\mathrm{b}}$ we consider the following logical steps. Since we have assumed an AWGN channel, the channel does not introduce amplitude variations. Thus, the energy matrix will be the same at both transmitter and receiver ends. We can then consider the generation of the weighted transmitted bits as the vector that is produced by passing the bits through a linear system of transfer function $\mathbf{W}$. According to theorem 4.2, the spectrum at the output of this system will be,

$$\mathbf{S}_{\mathbf{W}\mathrm{b}} = \mathbf{W}\ \mathbf{S}_{\mathrm{b}}(D)\ \mathbf{W}^{\mathbf{T}} \tag{4.36}$$

Assuming that the bits are BPSK modulated then $\mathbf{S}_{\mathrm{b}}(D) = 1$ and equation (4.36) is written as:

$$\mathbf{S}_{\mathbf{W}\mathrm{b}} = \mathbf{W}\ \mathbf{W}^{\mathbf{T}} = \mathbf{W}^2 \tag{4.37}$$

Q.E.D.

Theorem 4.7 *The Non-linear DF MSE minimizing detector, having the form of a MIMO feedforward filter* $\mathbf{F}(D)$ *and a feedback filter* $\mathbf{B}(D)$*, that processes the output of the equivalent CDMA channel denoted by* $\mathbf{G}(D)$ *whose input is* $\mathbf{Wb}(D)$ *is given by,*

$$\mathbf{F}(D) = \mathbf{W}(\mathbf{\Phi}^d(0))^{-1}(\mathbf{\Phi}^T(0))^{-1}\mathbf{W} \tag{4.38}$$

$$\mathbf{B}(D) = \mathbf{W}(\mathbf{\Phi}^d(0))^{-1}\mathbf{\Phi}(D)\mathbf{W} - \mathbf{I} \tag{4.39}$$

where, $\mathbf{W}$ is produced by the Cholesky factorization of the input process spectrum $\mathbf{S_{Wb}}(D)$ and $\mathbf{\Phi}^d(0))$ is produced by the Cholesky factorization of $(\mathbf{W^2}\ \mathbf{G}(D)\ \mathbf{W^2} + N_0\mathbf{I})$.

The benefits of applying MIMO MMSE detection in CDMA systems will now be evaluated. Of very important significance is the proof that MIMO MMSE detectors whose transfer function is given by the aforementioned theorems are NEFAR receivers. The proof can be made by demonstrating the robustness of Mean Square Error over a wide range of interfering power ratios. This proof is the subject of the next section.

4.5 NEAR FAR RESISTANCE OF THE MIMO MMSE DETECTOR

In this section, the near-far resistance of MIMO MMSE detectors is proven by evaluating the Mean Squared Error (MSE) over a wide range of interfering power ratios. The MSE evaluation is a procedure that consists of the following steps:

1. Formation of the equivalent CDMA channel.

2. Applying the formula,

   - **Linear MMSE Detector:**

$$MMSE^k_{MIMO-LINEAR} = \frac{1}{2\pi}\int_{-2\pi}^{2\pi} N_0\mathbf{W}^2(\mathbf{W}\mathbf{G}(e^{j\omega})\mathbf{W} + N_0\mathbf{I})^{-1}_{kk}d\omega \quad (4.40)$$

   - **DF MMSE Detector:**

$$MMSE^k_{MIMO-DF} = (N_0[\mathbf{A}(0)^d(\Phi^d(0))^{-1}]^2)_{kk} \quad (4.41)$$

Where the subscript 'kk' denotes the element (k,k) of the matrix.

4.5.1 Step I: Formation of the Equivalent CDMA Channel

The formation of the crosscorrelation matrix in the synchronous case is a straightforward procedure.

1. The first step is to form the code matrix **C** as follows:

$$\mathbf{C_0} = \begin{pmatrix} c_1^1 & c_2^1 & \dots & c_N^1 \\ c_1^2 & c_2^2 & \dots & c_N^2 \\ \vdots & \vdots & & \vdots \\ c_1^K & c_2^K & \dots & c_N^K \end{pmatrix} \quad (4.42)$$

2. The second and final step is to perform the operation,

$$\mathbf{R(0)} = \mathbf{C_0}\mathbf{C_0^T} \quad (4.43)$$

For the asynchronous case, we have to know the relative delays among the users. If we assume that the delays are $0, d_2, .., d_K$ for the 1st,...,Kth user respectively, then we can form the following matrices (assuming that the user with the least delay is denoted with the smaller index),

$$\mathbf{K_0} = \begin{pmatrix} c_1^1 & c_2^1 & \dots & c_N^1 \\ 0 & c_2^2 & \dots & c_N^2 \\ \vdots & \vdots & & \vdots \\ \underbrace{0 \quad 0}_{d_K \ 0s} & & \dots & c_N^K \end{pmatrix} \tag{4.44}$$

$$\mathbf{L_0} = \begin{pmatrix} 0 & 0 & \dots & 0 \\ c_N^2 & 0 & \dots & 0 \\ \vdots & \vdots & & \vdots \\ c_{N-d_K} & c_{N-d_K-1} & \dots & 0 \end{pmatrix} \tag{4.45}$$

The matrix $\mathbf{K_0}$ was formed by replacing the first elements of each row of the matrix $\mathbf{C_0}$ with 0s according to the delay of each user. The matrix $\mathbf{L_0}$ was formed by replacing the non-zero elements of $\mathbf{K_0}$ with 0s and the zero elements of $\mathbf{K_0}$ with the last elements of each row depending on the corresponding delay.

The crosscorrelation matrix $\mathbf{R(1)}$ is given by,

$$\mathbf{R(1)} = \mathbf{L_0 K_0^T} \tag{4.46}$$

For example in a three user system employing AO/LSE m-sequences of length **31**, given the user delays of $d_1 = 0, d_2 = 5, d_3 = 10$ chips, the following crosscorrelation matrices can be formed,

$$\mathbf{R}(0) = \begin{pmatrix} 1.00 & -0.03 & -0.01 \\ -0.03 & 1.00 & -0.07 \\ -0.01 & -0.07 & 1.00 \end{pmatrix} \quad \mathbf{R}(1) = \begin{pmatrix} 0.00 & 0.00 & 0.00 \\ -0.01 & 0.00 & 0.00 \\ 0.08 & 0.04 & 0.00 \end{pmatrix} \tag{4.47}$$

4.5.2 Step II: Formula Evaluation

Given the cross-correlation matrices one can evaluate (4.40) and (4.41) and plot the resulting MMSE versus the near-far power ratios determined by the matrix $\mathbf{W}$. This results to the graphs of Fig.4.9 and Fig.4.10 for the linear MMSE detector in the synchronous and asynchronous case respectively. Notice that the x-axis is the power ratio of the user of interest over the power of each of the interfering users.

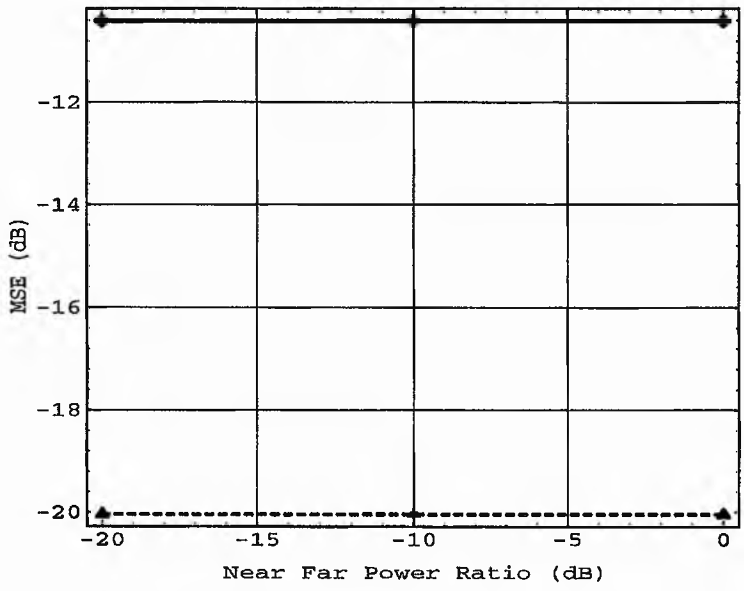

Figure 4.9: MSE Performance MIMO Linear MMSE Detector - Synchronous Transmission, — $E_b/N_0 = 10$ dB, - - $E_b/N_0 = 20$ dB

For the Decision Feedback (DF) MIMO MMSE detector we need to proceed with a Cholesky factorization of the matrix that describes the equivalent CDMA channel. The output of the Cholesky factorization of a symmetric positive definite matrix is a unique lower triangular matrix with positive diagonal entries, often called the Cholesky triangle. If **A** denotes the original matrix then after the factorization, a matrix **B** is produced so that,

$$\mathbf{A} = \mathbf{B}\ \mathbf{B}^{\mathbf{T}} \tag{4.48}$$

Several implementations of the Cholesky factorization procedure exist, a comprehensive summary of which can be found in [22]. For the matrices reported in equation (4.47), the aforementioned MSE evaluation procedure leads to the graphs of Fig.4.11 and Fig.4.12 for the synchronous and asynchronous case respectively.

4.5.3 Discussion

From the results presented so far the following observations can be made:

- MIMO MSE minimizing receivers are near-far resistant over a wide range of interfering power ratios. However the knowledge of the energy matrix is required for the calculation of the optimal equaliser's matrix transfer function.

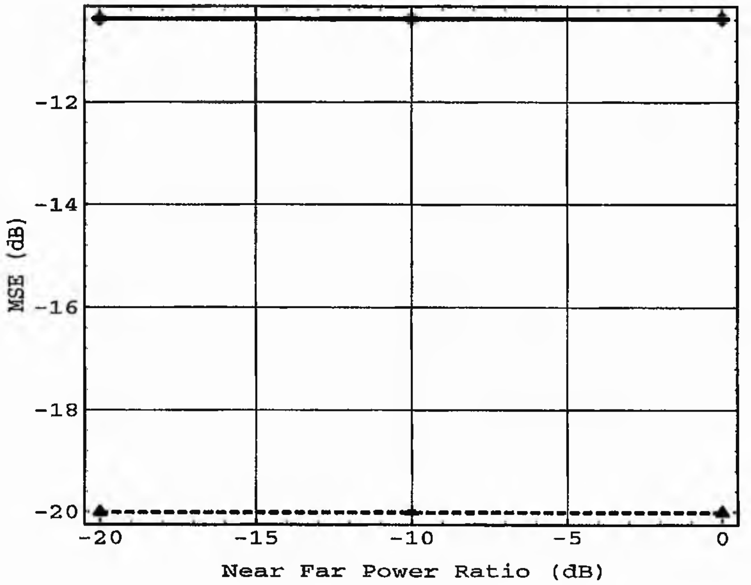

Figure 4.10: MSE Performance of MIMO Linear MMSE Detector - Asynchronous Transmission, — $E_b/N_0 = 10$ dB, - - $E_b/N_0 = 20$ dB

- The MSE performance remains insensitive to the relative delays among the users. This observation however depends on the particular spreading codes. In our case we used AO/LSE m-sequences codes which are considered to have very good cross-correlation properties.

- The results regarding the near-far resistance of MIMO MMSE detectors have been produced by examining a lightly loaded (9.6%) system ie. a system with 3 users each having a spreading factor of 31. Although we do not argue that the MIMO MMSE detectors will loose their NEFAR abilities under heavy loaded conditions, it would be of great interest to study the effects in the MSE performance as the system loading increases.

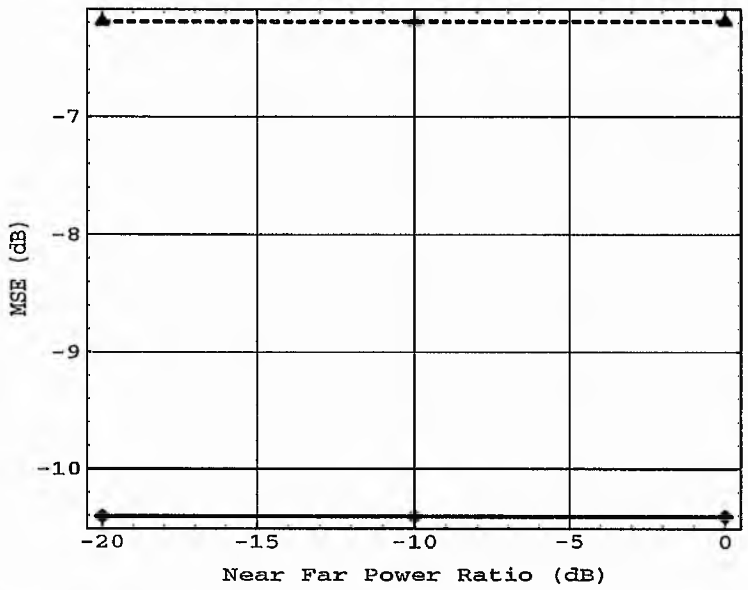

Figure 4.11: MSE Performance DF MIMO MMSE Detector - Synchronous Transmission, — $E_b/N_0 = 10$ dB, - - $E_b/N_0 = 5$ dB

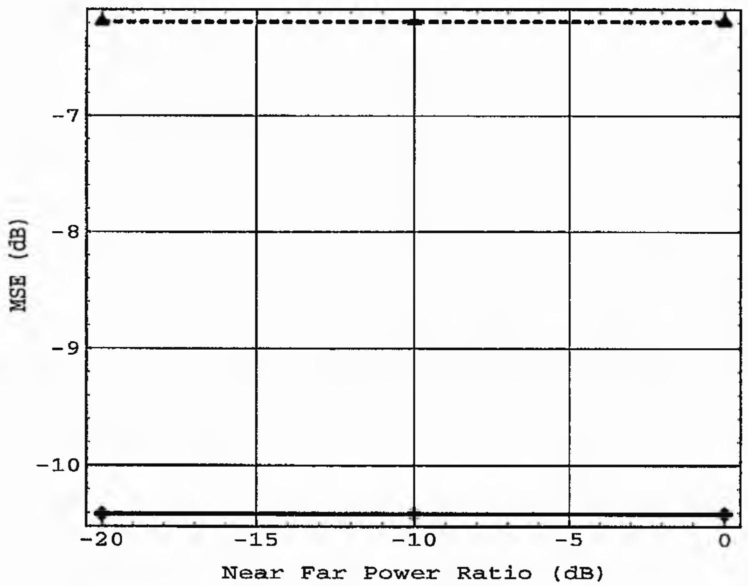

Figure 4.12: MSE Performance of DF MIMO MMSE Detector - Asynchronous Transmission, — $E_b/N_0 = 10$ dB, - - $E_b/N_0 = 5$ dB

4.6 SYSTEM LOADING EFFECTS

In this section we present new results that shed light to the behaviour of the MIMO MMSE detectors in heavily loaded systems under both near-far and power controlled scenarios. These results will inevitably lead to new conclusions regarding the optimality of the MIMO MMSE receivers to increase the capacity of CDMA systems.

For this purpose, we use as spreading codes the Gold sequences of length 7, used by Varanasi in his studies on multistage interference cancellation [57]. These spreading codes are depicted in Fig.4.13.

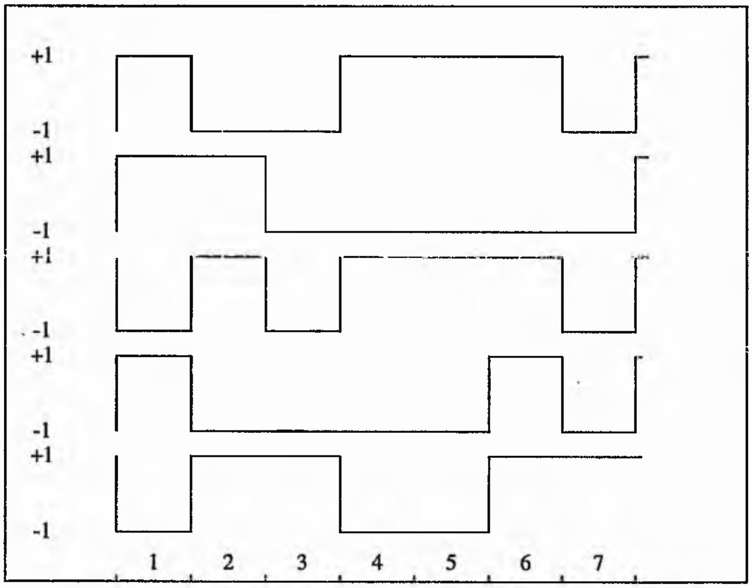

Figure 4.13: Five AO/LSE Gold Codes of Period 7

Without loss of generality we consider a synchronous transmissions. The crosscorrelation matrices for a 2,3,4 and 5 user system can easily be calculated,

$$\mathbf{R}_2(0) = \begin{pmatrix} 1.00 & -0.14 \\ -0.14 & 1.00 \end{pmatrix} \tag{4.49}$$

$$\mathbf{R}_3(0) = \begin{pmatrix} 1.00 & -0.14 & 0.42 \\ -0.14 & 1.00 & -0.14 \\ -0.42 & -0.14 & 1.00 \end{pmatrix} \tag{4.50}$$

$$\mathbf{R}_4(0) = \begin{pmatrix} 1.00 & -0.14 & 0.42 & 0.42 \\ -0.14 & 1.00 & -0.14 & 0.42 \\ 0.42 & -0.14 & 1.00 & -0.14 \\ 0.42 & 0.42 & -0.14 & 1.00 \end{pmatrix} \tag{4.51}$$

$$
\mathbf{R}_5(0) = \begin{pmatrix} 1.00 & -0.14 & 0.42 & 0.42 & -0.71 \\ -0.14 & 1.00 & -0.14 & 0.42 & -0.14 \\ 0.42 & -0.14 & 1.00 & -0.14 & -0.14 \\ 0.42 & 0.42 & -0.14 & 1.00 & -0.14 \\ -0.71 & -0.14 & -0.14 & -0.14 & 1.00 \end{pmatrix} \tag{4.52}
$$

In Fig.4.14, Fig.4.15,Fig.4.16, Fig.4.17 the MSE degradation of user #1 can easily be observed for the linear and non-linear MIMO detectors and for near-far ratios of 0 dB and -20 dB.

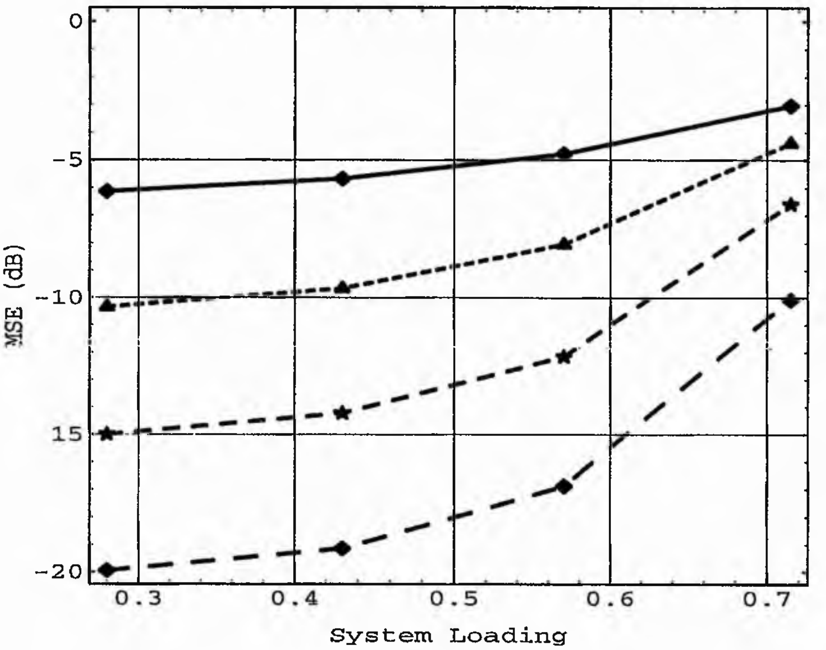

Figure 4.14: MSE Performance of MIMO Linear MMSE Detector, Near-Far Ratio = 0 dB, User #1, (–) E_b/N_0 = 5 dB, (- -) E_b/N_0 = 10 dB, (– –) E_b/N_0 = 15 dB, (— —) E_b/N_0 = 20 dB

We can now make the following observations on the effects of the system load on performance.

- The performance of the MIMO Linear MMSE detector degrades significantly as the system load increases.
- The performance of the MIMO DF MMSE detector remains constant as the system load becomes higher. This result is of fundamental importance in interference cancellation studies in general. It has been demonstrated that the multiuser channel can be made single user one *if* a number of assumptions are met. These assumptions are:

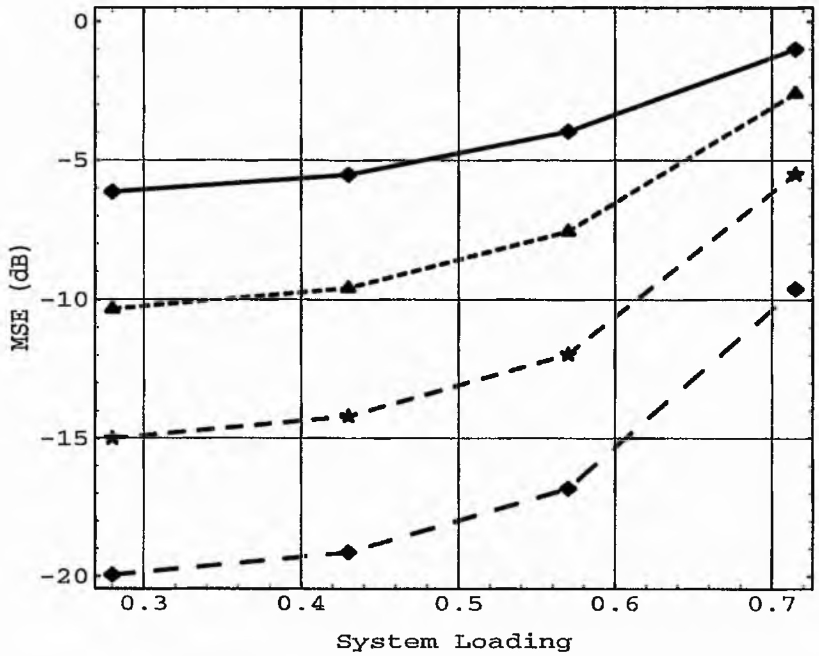

Figure 4.15: MSE Performance of MIMO Linear MMSE Detector, Near-Far Ratio = -20 dB, User #1, (–) E_b/N_0 = 5 dB, (- -) E_b/N_0 = 10 dB, (– –) E_b/N_0 = 15 dB, (— —) E_b/N_0 = 20 dB

1. There is a feedback mechanism (non-linear operation) which cancels the residual interference present in the output of linear cancellation systems.
2. There a is zero error propagation which guarantees the joint subtraction of the interfering symbols.

However, it has to be pointed out at this point that the aforementioned assumption of zero-error propagation can never be met in practice. In Chapter 5 we shall verify that although there is error propagation this propagation is not catastrophic and significant gains can be expected from non-linear cancellation techniques employing decision-feedback.

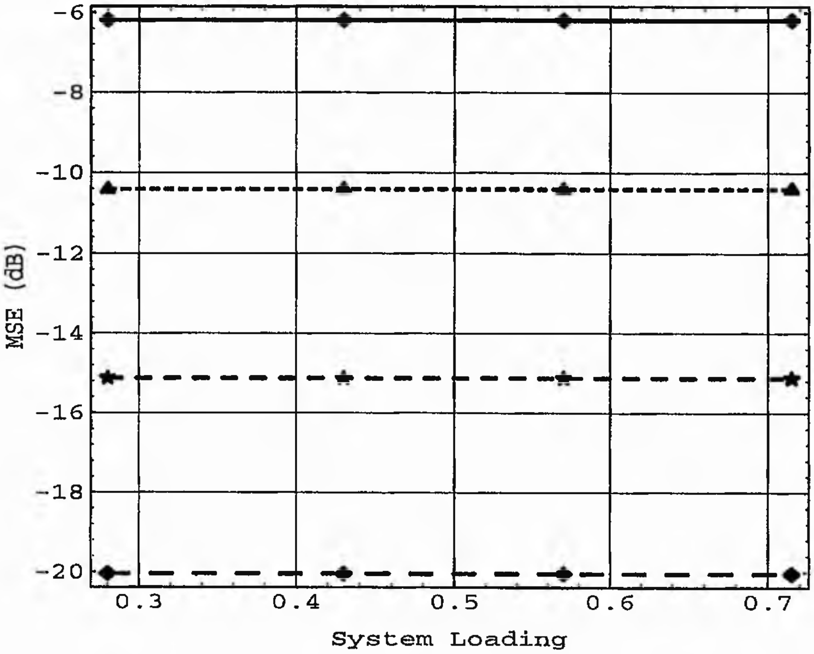

Figure 4.16: MSE Performance of MIMO DF MMSE Detector, Near-Far Ratio = 0 dB, User #1, (–) E_b/N_0 = 5 dB, (- -) E_b/N_0 = 10 dB, (– –) E_b/N_0 = 15 dB, (— —) E_b/N_0 = 20 dB

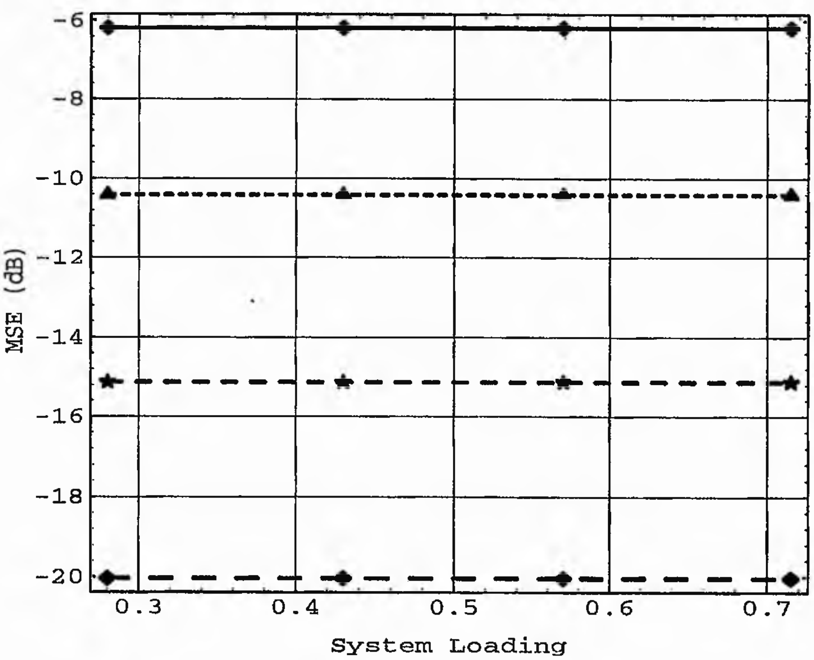

Figure 4.17: MSE Performance of MIMO DF MMSE Detector, Near-Far Ratio = -20 dB, User #1, (–) E_b/N_0 = 5 dB, (- -) E_b/N_0 = 10 dB, (– –) E_b/N_0 = 15 dB, (— —) E_b/N_0 = 20 dB

4.7 DECORRELATION VERSUS MIMO MMSE DETECTION

In this section, the true merits of MIMO MMSE detection will be made apparent, by comparing its performance with the performance of decorrelating detectors invented by Lupas for synchronous [31] and asynchronous [32] transmission systems. In [12] the decorrelator has been extended to a non-linear decision feedback architecture. This non-linear decorrelator is named, for the rest of this thesis, MIMO Decision Feedback Zero Forcing Equalizer. The original decorrelating detector is termed for the rest of this thesis either as linear decorrelator or MIMO Linear Zero Forcing Equalizer.

4.7.1 The Linear Decorrelator

The function of the decorrelating detector is a vector by a matrix multiplication. The K-dimensional vector consists of the outputs of the code matched filters or equivalently, the K-dimensional vector is the output of the equivalent CDMA channel defined in the previous section. The decorrelating detector acts as a MIMO Zero-Forcing equalizer and attempts to invert the matrix transfer function of the equivalent CDMA channel without taking into account the background noise. For the general asynchronous case, we define a $MK \times MK$ symmetric block-Toeplitz matrix $\mathcal{R}$ as follows,

$$\mathcal{R} = \begin{pmatrix} \mathbf{R}(0) & \mathbf{R}(-1) & 0 & \ldots & 0 \\ \mathbf{R}(1) & \mathbf{R}(0) & \mathbf{R}(-1) & \ldots & 0 \\ 0 & \mathbf{R}(1) & \mathbf{R}(0) & \ldots & 0 \\ \ldots & \ldots & \ldots & \ldots & \ldots \\ 0 & \ldots & 0 & \mathbf{R}(0) & \mathbf{R}(-1) \\ 0 & \ldots & 0 & \mathbf{R}(1) & \mathbf{R}(0) \end{pmatrix} \tag{4.53}$$

the matched filter output can be written as,

$$\mathbf{y} = \mathcal{R}\mathbf{W}\mathbf{b} + \mathbf{z} \tag{4.54}$$

The decorrelating detector for the ith bit of the kth user is the $(k, i)th$ row of the $\mathcal{R}^{-1}$ matrix. For the value of N encountered in practical applications inverting an $MK \times MK$ matrix is not possible. As the length of the transmitted sequence increases ($M \to \infty$), Lupas in [32] has shown that the decorrelating detector approaches the K-input K-output linear filter with transfer function

$$\mathbf{C}(D) = [\mathbf{R}^T(\mathbf{1})D + \mathbf{R}(0) + \mathbf{R}(1)D^{-1}]^{-1} \tag{4.55}$$

Fig.4.18 depicts the CDMA transmission system and the functional block diagram of the decorrelating detector. The input data vector is weighted according to the user energy matrix **W** and distorted according to the equivalent CDMA channel matrix **G**. Noise is added according to the SNR/bit of the user of interest and the decorrelation process is performed by the equivalent CDMA channel matrix (generally complex) inversion, according to:

$$\mathbf{G}^{-1}(D) = \frac{adj[\mathbf{G}(\mathbf{D})]}{Det[\mathbf{G}(D)]} \tag{4.56}$$

where $adj[\mathbf{G}(D)]$ denotes the adjoint matrix of $\mathbf{G}(D)$.

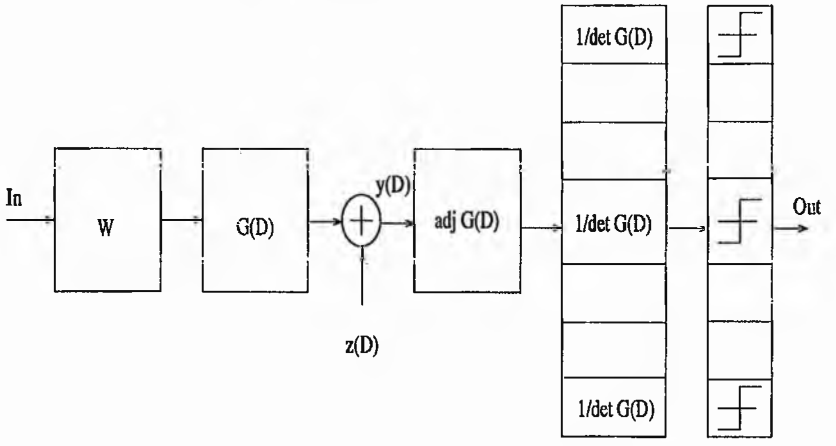

Figure 4.18: Interpretation of the Linear Decorrelating Detector

It is apparent that since the decorrelator inverts the equivalent CDMA channel transfer function without taking into account the channel noise, it is equivalent to a Zero Forcing Equalizer. In fact, Lupas has invented a MIMO device that equalizes the Multidimensional ISI, created by the simultaneous user transmissions, according to the Zero Forcing criterion. It is also apparent that the performance of the decorrelator will be dependent on the quality of the equivalent CDMA channel. This is reflected on the relationship that gives the probability of bit error for the kth user equals,

$$BER_k = P(n'_k > \sqrt{w_k}) = Q\left(\frac{\sqrt{w_k}}{\sigma\sqrt{D_{kk}(0)}}\right) \tag{4.57}$$

where,

$$D_{kk}(0) = \frac{1}{2\pi}\int_0^{2\pi}[\mathbf{R}^T(1)e^{j\omega} + \mathbf{R}(0) + \mathbf{R}(1)\bar{e}^{j\omega}]_{kk}^{-1}d\omega \tag{4.58}$$

The near-far resistance of the decorrelating concept is apparent from the MSE performance of the detector in various near-far conditions. The MSE remains unchanged irrespective of the power level of the interfering user. Although near-far resistance is important, it would be of great interest to investigate heavily loaded conditions.

The effect of system loading on the performance of decorrelating detectors can be seen in Fig.4.19.

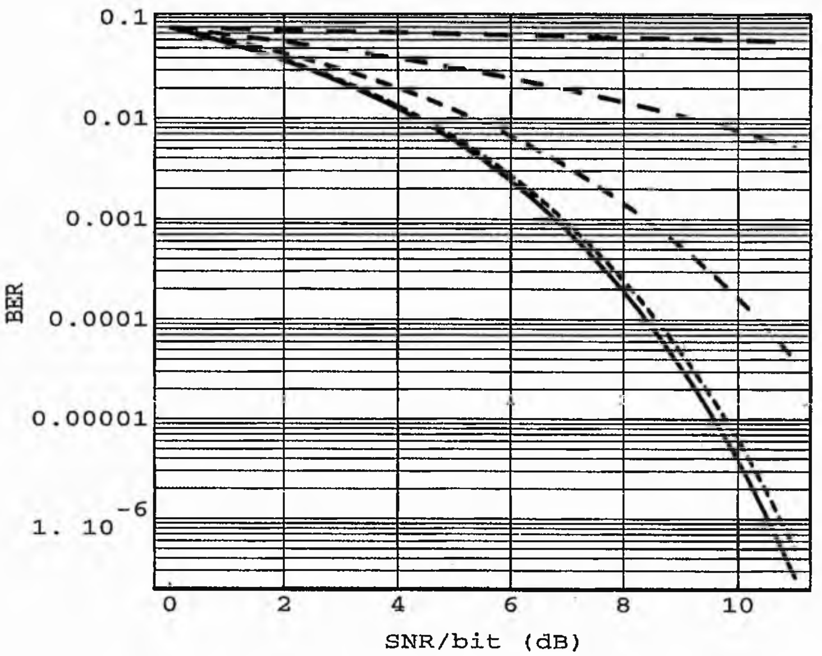

Figure 4.19: Effect of System Loading on the BER of Linear Decorrelating Detector in AWGN Channel, (—) Single User Bound, (- -) 28% Loading, (– –) 43% Loading,(— —) 57% Loading,(— —) 71% Loading

In Rayleigh fading channels, the performance of the decorrelator is also drastically affected when the system loading is increased. Fig.4.20 depicts the performance of the decorrelating detector in Rayleigh fading channels.

The question that now arises is how the MIMO linear MMSE detector compares against the linear decorrelator. It would be very interesting to examine the benefits of replacing the Zero Forcing with the MMSE criterion and to quantify the net gain.

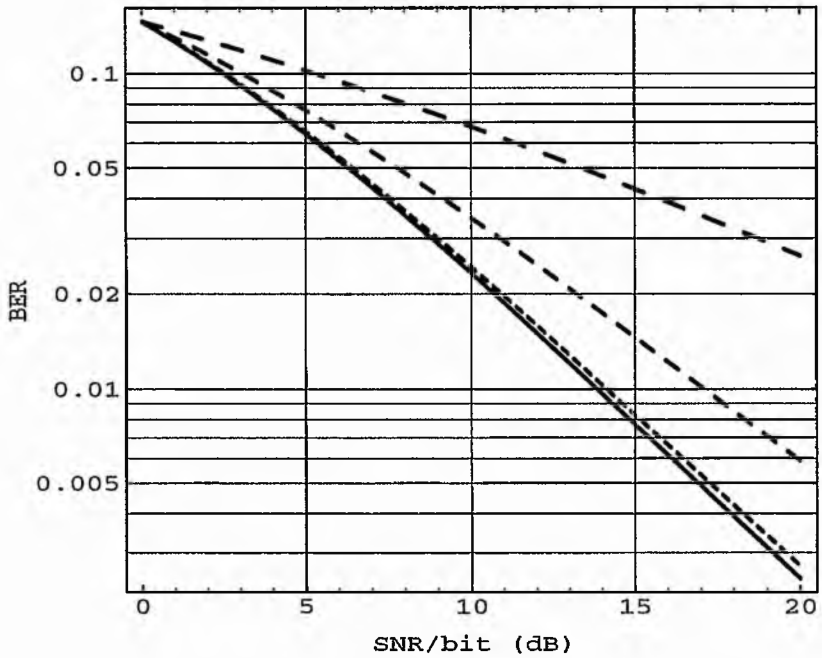

Figure 4.20: Effect of System Loading on the BER of Linear Decorrelating Detector in Rayleigh Fading Channel, (—) Single User Bound, (- -) 28% Loading, (– –) 43% Loading,(— —) 57% Loading,(— —) 71% Loading

4.7.2 Comparison of MIMO Linear MMSE Detector and Linear Decorrelator

The comparison was made using the Gold sequences of period 7 that have been used previously. The figure of merit is again the MSE which is now plotted versus the channel E_b/N_0 ratio. The results are shown in Fig.4.21 and Fig.4.23 for 28% load and for near-far ratios of 0 dB and 20 dB. Fig.4.22 and Fig.4.24 depict the 71% system loading case.

4.7.3 Discussion

The results presented so far are quite revealing about the behaviour of the linear ZF and MMSE detectors in light and heavy loaded systems. In summary we can make the following observations:

- For lightly loaded systems and high SNR/bit values the ZF and MMSE criteria appear to have the same performance.
- For low SNR/bit regions the MMSE solution which takes into consideration the channel noise performs much better compared to the decorrelating receiver.

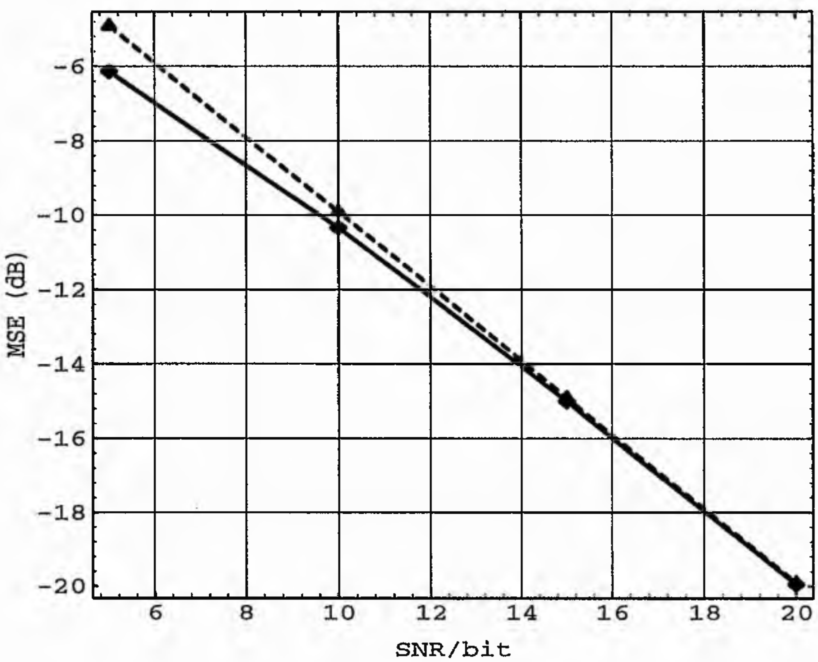

Figure 4.21: MSE Performance of MIMO Linear MMSE Detector (—) vs Linear Decorrelating Detector (- -), Loading 28%, Near-Far Ratio = 0 dB, User #1

- For heavy loaded systems the decorrelating receiver is unusable, irrespectively of the near-far power ratio. The MMSE detector on the other hand, manages to present a decent MSE performance and in fact for the near-far ratio of 0 dB with SNR/bit = 5 dB, presents a 7 dB gain over the decorrelator.

- Contrary to previous beliefs, the linear MMSE detector is *not* strictly near-far resistance in heavy loaded conditions. It appears that the energy matrix in equation (4.40) is significant contributor to the MSE under heavily loaded conditions while its significance is unimportant in moderate loaded conditions.

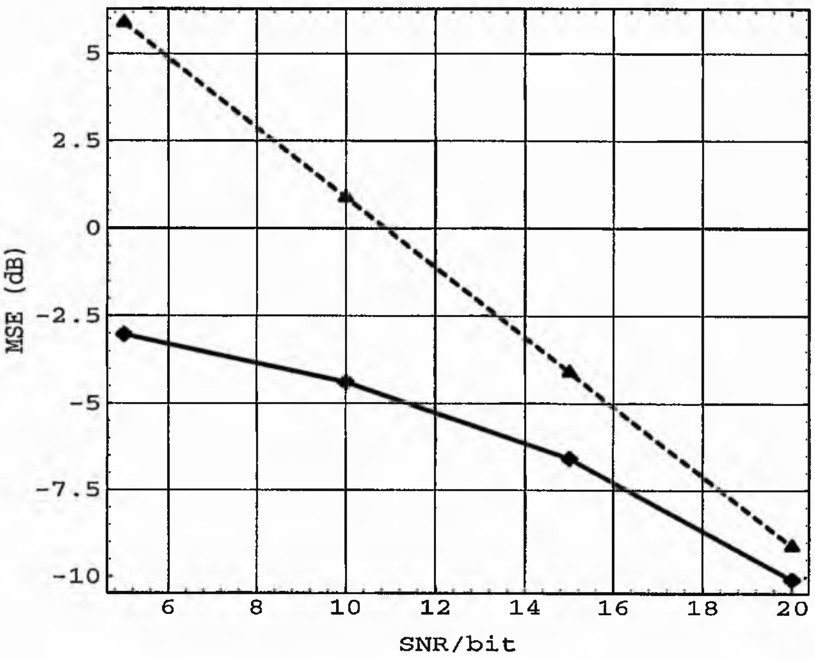

Figure 4.22: MSE Performance of MIMO Linear MMSE Detector (—) vs Linear Decorrelating Detector (- -), Loading 71%,Near-Far Ratio = 0 dB, User #1

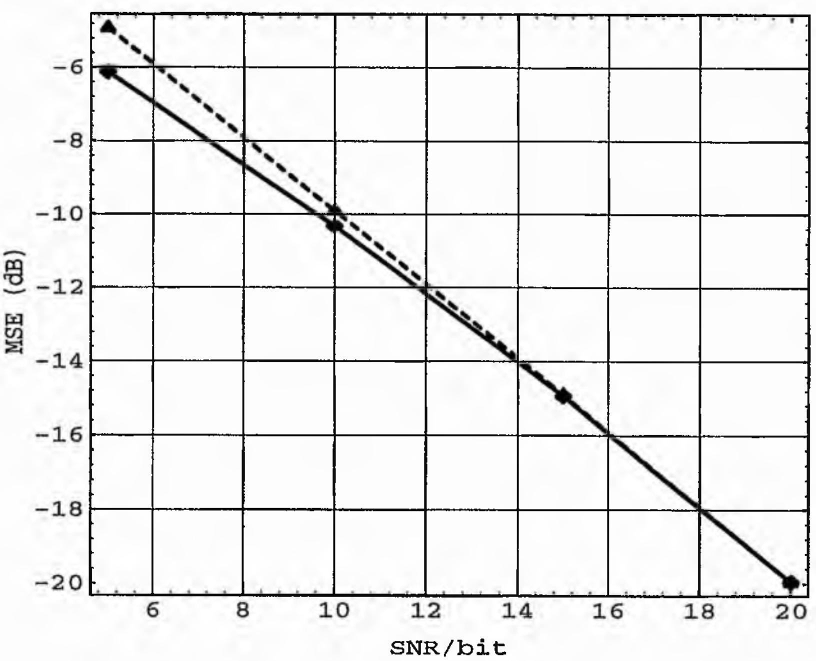

Figure 4.23: MSE Performance of MIMO Linear MMSE Detector (—) vs Linear Decorrelating Detector (- -), Loading 28%, Near-Far Ratio = -20 dB, User #1

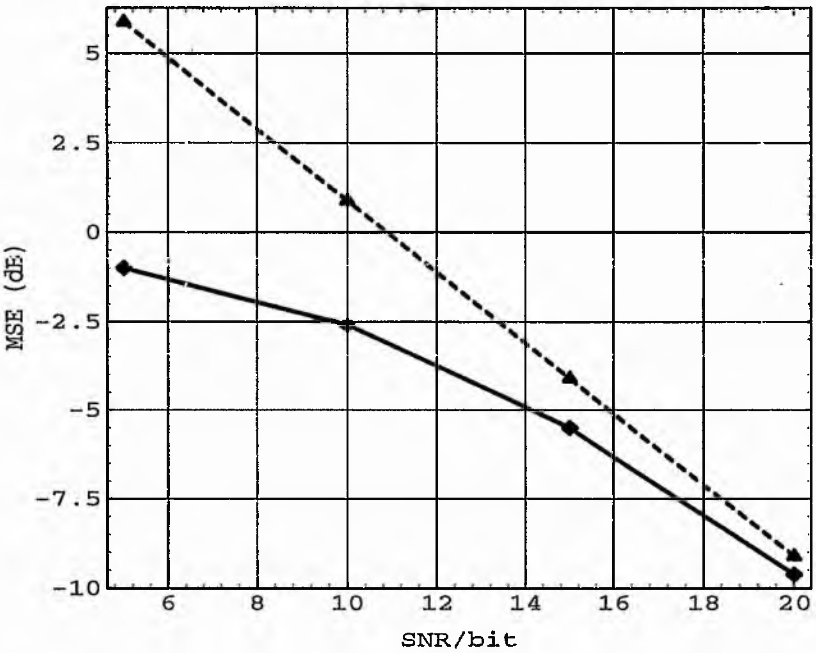

Figure 4.24: MSE Performance of MIMO Linear MMSE Detector (—) vs Linear Decorrelating Detector (- -), Loading 71%,Near-Far Ratio = -20 dB, User #1

4.7.4 The Non-Linear Decorrelating Detector

This section investigates the performance gain of the non-linear decorrelator over the linear and formulates the correspondence between the non-linear decorrelator and the non-linear MIMO MMSE equalizer with decision feedback. For simplicity consider the synchronous CDMA transmission model. The receiver architecture employing the non-linear (decision-feedback) decorrelating detector is shown in Fig.4.25.

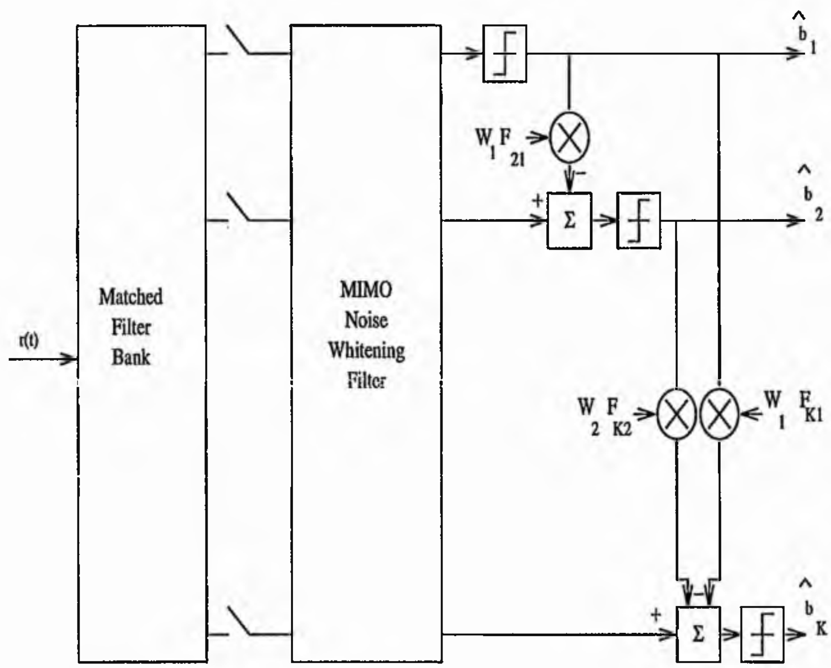

Figure 4.25: CDMA Receiver With Nonlinear Decorrelation in a Synchronous AWGN Channel

The matched filter bank output can be written, similarly to the linear decorrelator manner, as,

$$\mathbf{y} = \mathbf{R}\ \mathbf{W}\ \mathbf{b} + \mathbf{z} \tag{4.59}$$

The noise component can be whitened in a number of steps.

1. Factoring the positive definite crosscorrelation matrix **R**. Applying the Cholesky decomposition algorithm [22] on the crosscorrelation matrix **R** the Cholesky triangle **F** is produced so that,

$$\mathbf{R} = \mathbf{F}^{\mathbf{T}}\mathbf{F} \tag{4.60}$$

where F is a lower triangular matrix.

2. Inverting the matrix $\mathbf{F^T}$.

3. Multiplying the (Kx1) code matched filter vector by the matrix produced in the second step.

The signal after the MIMO noise whitening device can be written as,

$$\mathbf{y_W} = \mathbf{F}\ \mathbf{W}\ \mathbf{b} + \mathbf{n} \tag{4.61}$$

where $\mathbf{n}$ is the produced white Gaussian noise vector.

The non-linear part of the decorrelating detector is an MIMO feedback filter whose matrix transfer function is given by,

$$\mathbf{B} = (\mathbf{F} - \mathbf{F^d})\ \mathbf{W} \tag{4.62}$$

where $\mathbf{F^d}$ is the diagonal matrix produced by $\mathbf{F}$ by setting all off-diagonal elements to zero. The input of this filter is the bit decisions $\hat{\mathbf{b}}$.

Under the assumption of correct previous decisions, the probability of bit error for the kth user can be approximated by,

$$P_b = \frac{1}{2} erfc\left(F_{k,k}\sqrt{\frac{E_b}{N_0}}\right) \tag{4.63}$$

where $F_{k,k}$ is the (k,k) element of the matrix $\mathbf{F}$.

In order to evaluate the performance gains of non-linear decorrelation over the linear one, we consider a synchronous two user system whose cross-correlation matrix is given by,

$$\mathbf{R}(0) = \begin{pmatrix} 1.0 & 0.7 \\ 0.7 & 1.0 \end{pmatrix} \tag{4.64}$$

The same system has been considered in [57] for the demonstration of the capabilities of multistage interference cancellation techniques. The calculation of the probability of bit error for the kth user, as given by equation (4.63), involves averaging the conditional probability of bit error for a particular error pattern of the users 1,...,k-1, over all such error patterns. This simply means one can not determine the bit error rate of the user of interest (taken by default as the weaker user) unless the error pattern (the bit errors) of the stronger users are known. This is because the detector involves a feedback stage which has as input the bit decisions of the k-1 stronger users. Some of these bits will be in error, thus, the bit error rate of the user of interest depends on these error patterns.

However, for the two user system under consideration, there are two possibilities ie. the bit decision of the stronger user is either in error or not. Averaging over all possible values of this error pattern, we obtain the following formula for the bit error rate of the user of interest,

$$P_b = \left[1 - \frac{1}{2}erfc\left(\sqrt{\frac{E_b}{N_0}R_{2,2}(0)^{-1}}\right)\right] \frac{1}{2}erfc\left(\sqrt{\frac{E_b}{N_0}F_{2,2}W_2}\right) + \frac{1}{4}erfc\left(\sqrt{\frac{E_b}{N_0}R_{2,2}^{-1}(0)}\right)$$
$$\left[\frac{1}{2}erfc\left(\sqrt{\frac{E_b}{N_0}(F_{2,2}W_2 - 2F_{2,1}W_1)}\right) + \frac{1}{2}erfc\left(\sqrt{\frac{E_b}{N_0}(F_{2,2}W_2 + 2F_{2,1}W_1)}\right)\right] \quad (4.65)$$

Evaluation of the last equation leads to the graph of Fig.4.26 where the performance improvement compared to the linear decorrelator can be seen.

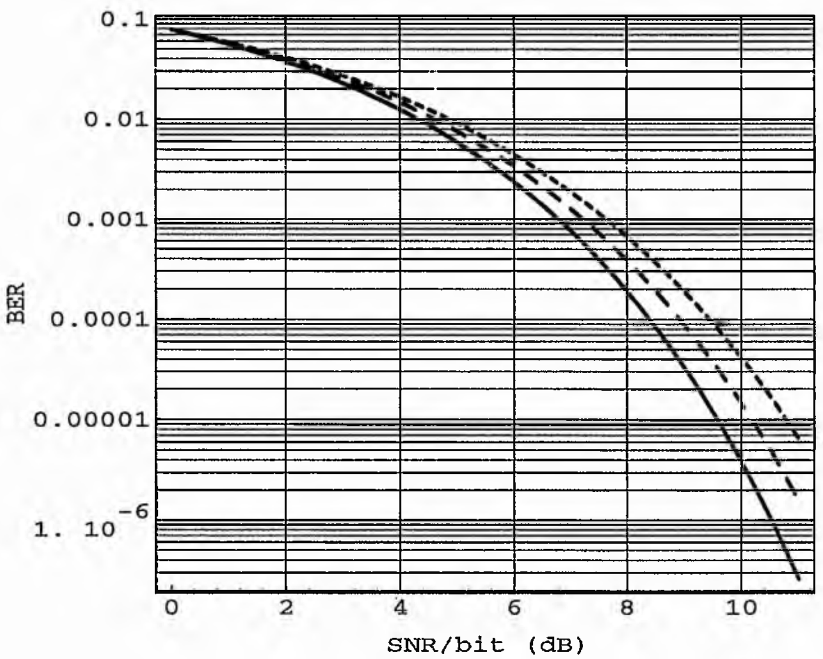

Figure 4.26: Performance Improvement with Nonlinear Decorrelation (– –) as Compared to Linear Decorrelation (- -) in the AWGN Channel. (—) Single User Bound

Again, it is required to examine how the non-linear MIMO MMSE detector compares against the non linear decorrelator. This is discussed next.

4.7.5 Comparison Between MIMO DF MMSE and MIMO ZF DF Receivers

The comparison was made using the same Gold sequences of period 7 that have been used for the comparison of the linear MIMO MMSE detector and the linear decorrelator. The effect of system load on the performance of the non-linear decorrelator, is shown in Fig.4.27.

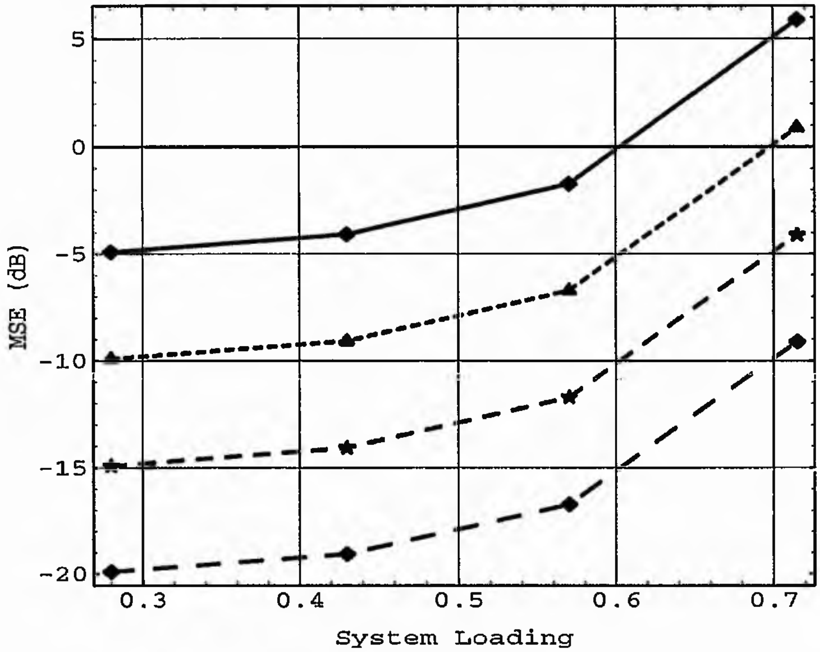

Figure 4.27: MSE Performance of MIMO DF ZF Detector,Near-Far Ratio = 0 dB, User #1, (–) E_b/N_0 = 5 dB, (- -) E_b/N_0 = 10 dB, (– –) E_b/N_0 = 15 dB, (— —) E_b/N_0 = 20 dB

The MSE performance versus the channel SNR/bit is also of interest. The results are shown in Fig.4.28 and Fig.4.29 for the 28% and 71% loading respectively. Only the power controlled case is shown.

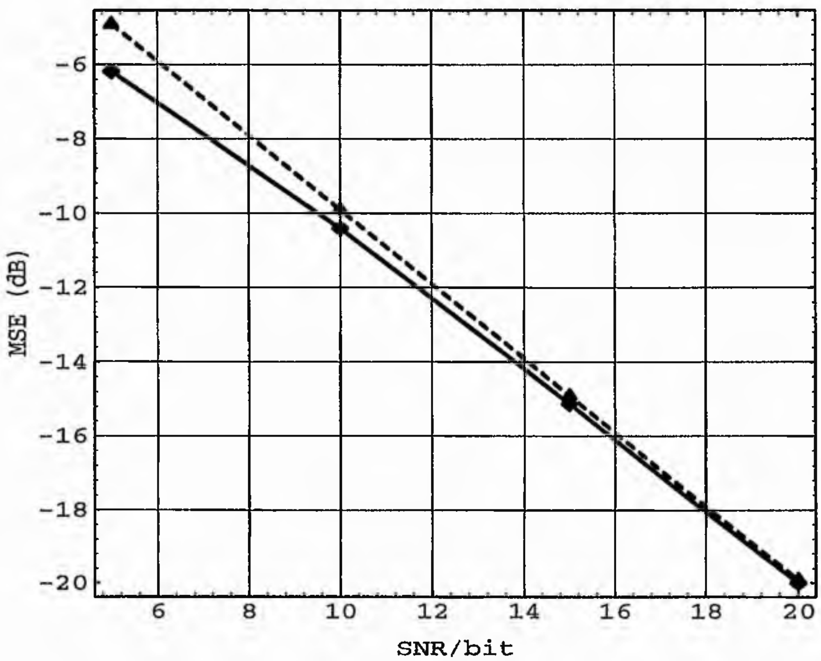

Figure 4.28: MSE Performance of MIMO DF MMSE Detector (—) vs MIMO ZF DF Detector (- -) - Loading 28%,Near-Far Ratio = 0 dB, User #1

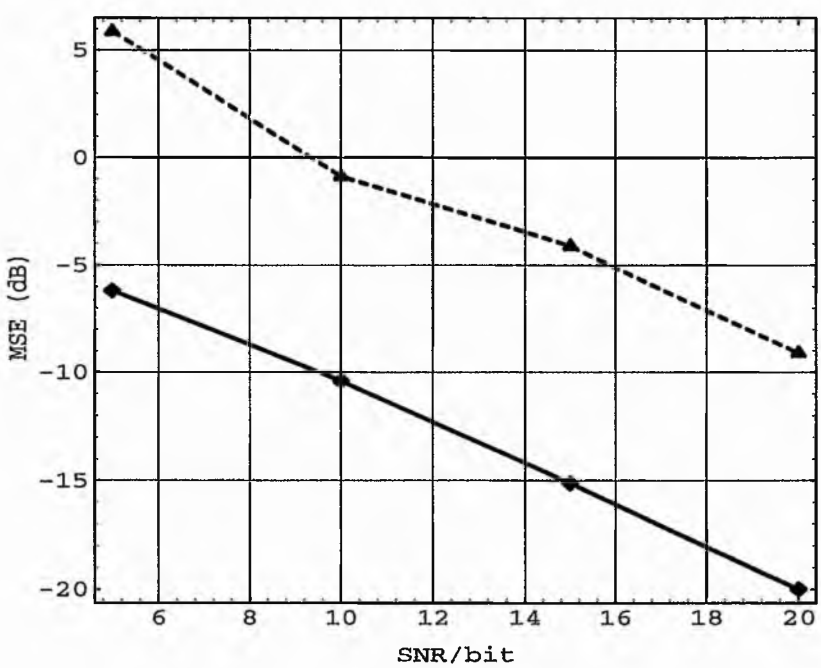

Figure 4.29: MSE Performance of MIMO DF MMSE Detector (—) vs MIMO ZF DF Detector (- -) - Loading 71%,Near-Far Ratio = 0 dB, User #1

4.8 LIMITATIONS OF MIMO DETECTION AND DOWNSIZING

Many of the theoretical foundations of MIMO MMSE detectors studied in the previous paragraphs have a common denominator. They provide bit decisions of all the users in the system simultaneously. For this reason MIMO detectors are also called *joint* detectors. If K denotes the number of users in the system, the matrix transfer function of eg. the linear MIMO detector has K^2 elements. The MIMO (joint) detector can then be implemented by a matrix equalizer. However, for studying the performance of the user of interest, we only need a Multiple-Input-Single-Output (MISO) equalizer. This will have as inputs the K code matched filter outputs, producing at its output the estimated bits for the user of interest. This is better shown in the Fig.4.30 where the linear MISO MMSE detector for user #1 has been drawn.

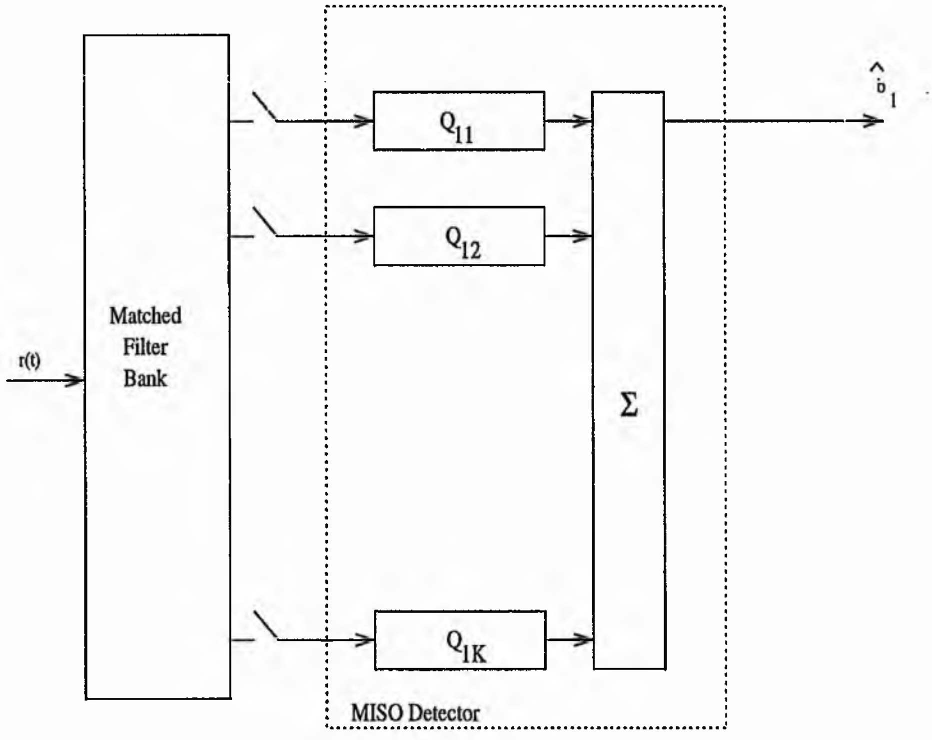

Figure 4.30: Linear MISO MMSE Detector

At this stage it is worth making the following observations:

- The MISO MMSE detector processes the vector produced by the code matched filters, which is a sufficient statistic for the estimation of the current data bit. The subsequent signal processing ie. interference equalization is performed at the bit rate.

- The fact that the operation of the MISO MMSE detector depends on code matched filtering has fundamental implications on the autonomy of the detector. Thus, the detector needs the co-operation of the delay estimation circuitry so that the signals, not only of the user of interest but also of *all interfering users*, are properly despread. It has been shown that current delay estimation methods are inadequate when operating in a near-far environment [39]. Moreover, solutions that have been proposed to overcome the delay estimation problem under near-far interference depend on the knowledge of the information bits and the knowledge of the energy matrix. On the other hand NEFAR code tracking loops by the time of writing this thesis are still an untouched research topic.

For the case of decorrelating receivers it can be easily shown that *when the delay estimation problem is solved* the MISO architecture can be downsized to SISO with no performance loss. This is demonstrated next.

4.8.1 SISO Decorrelating Detector

For the sake of simplicity let us assume that the MIMO decorrelating detector operates in a synchronous CDMA system and that all the signals are real. As was seen previously the MIMO decorrelating detector in this case can be implemented as a cascade of matched filter bank producing the vector $\mathbf{y}$ at its output and a linear combiner, with the linear combiner transforming, with the knowledge of the crosscorrelation matrix $\mathbf{R}$, the vector $\mathbf{y}$ into the decision statistic:

$$\tilde{\mathbf{x}} = \mathbf{y}\mathbf{R}^{-1} \tag{4.66}$$

The code matched filter output $\mathbf{y}$ can be obtained from the received signal $\mathbf{r}$ with the following transformation:

$$\mathbf{y} = \mathbf{r}\mathbf{C}^T \tag{4.67}$$

where $\mathbf{C}$ is the matrix,

$$\mathbf{C} = \begin{pmatrix} c_1^1 & c_2^1 & \dots & c_N^1 \\ c_1^2 & c_2^2 & \dots & c_N^2 \\ \vdots & \vdots & & \vdots \\ c_1^K & c_2^K & \dots & c_N^K \end{pmatrix} \tag{4.68}$$

We can then write that,

$$\tilde{\mathbf{x}} = \mathbf{r}\mathbf{C}^T\mathbf{R}^{-1} \tag{4.69}$$

Since the crosscorrelation matrix $\mathbf{R}$ is Toeplitz,

$$\mathbf{R}^T = \mathbf{R} \tag{4.70}$$

Consequently,

$$\tilde{\mathbf{x}} = \mathbf{r}[\mathbf{R}^{-1}\mathbf{C}]^T \tag{4.71}$$

The last equation indicates that the decorrelator can be implemented as a modified matched filter bank. Thus for the user of interest, user #1, the decorrelating detector is downsized to an FIR filter structure whose taps depend not only on the code sequence but also on the values of the 1st column of the matrix $\mathbf{R}^{-1}$.

As an example, consider the well treated 4 user system with Gold sequences of period 7. The code matched bank coefficients are computed as,

$$\begin{aligned}
[\mathbf{R}^{-1}\mathbf{C}]^T &= \left[\begin{pmatrix} 2.125 & 0.75 & -1 & -1.375 \\ 0.75 & 1.5 & -0.25 & -1 \\ -1 & -0.25 & 1.5 & 0.75 \\ -1.375 & -1 & 0.75 & 2.125 \end{pmatrix}\begin{pmatrix} 1 & -1 & -1 & 1 & 1 & 1 & -1 \\ 1 & 1 & -1 & -1 & -1 & -1 & -1 \\ -1 & 1 & -1 & 1 & 1 & 1 & -1 \\ 1 & -1 & -1 & -1 & -1 & 1 & -1 \end{pmatrix}\right]^T \\
&= \begin{pmatrix} 2.5 & -1 & -0.5 & 1.75 & 1.75 & -1 & -0.5 \\ 1.5 & 1.5 & -1 & 0 & 0 & -2 & -1 \\ -2 & 1.5 & -1 & 0 & 0 & 1.5 & -1 \\ -1 & -1 & -0.5 & -1.75 & -1.75 & 2.5 & -0.5 \end{pmatrix}^T
\end{aligned} \tag{4.72}$$

As this example indicates, the decorrelating filter coefficients deviate significantly from the optimum single-user case. This can be expected in every case where the system is heavily loaded.

The fact that the transition from the MIMO decorrelator to SISO one, *having the knowledge of the code delays and the values of the crosscorrelation matrix*, involves only architectural changes with no loss in performance is a significant step and further prompts to downsized version of MIMO MMSE receivers to be addressed in the following chapter.

4.9 CONCLUSIONS

In this chapter MMSE based detectors have been proposed as a solution to the near-far interference problem. The starting point was the theory developed for general MIMO channels. This theory was applied to CDMA channels and the analytical results indicate the following:

- The MIMO MMSE detector is not strictly near-far resistant but offers significant performance gains compared to the conventional detector.
- In both power controlled and power uncontrolled systems, the proposed detectors offer significant gains compared to the decorrelating detector. The gain increases as the system loading is increased. In that respect, the MIMO MMSE solution offers significant capacity gains compared to conventional detection and to suboptimal decorrelation based techniques.
- The MISO detector processes the vector output produced by a bank of matched filters. In that respect the MISO MMSE detector has the same requirements, as far as delay estimation is concerned, compared to the decorrelating detector
- It has been demonstrated in the case of decorrelating detectors that downsizing from the MISO architecture to SISO is not necessarily associated with performance loss. It is the subject of the next chapter to examine if this argument is true or not for MIMO MMSE detectors.

Chapter 5

ADAPTIVE SISO MMSE DETECTORS

5.1 INTRODUCTION

In the previous chapter, MMSE based algorithms able, with the knowledge of the spreading sequences of all active users, to cancel multiuser interference have been presented. The implementation of these algorithms through Multiple Input Multiple Output (MIMO) devices that equalize the multiple access interference at the output of a bank of matched filters increase the complexity of the receiver considerably compared to the conventional detector.

Thus, simpler receivers, that provide interference cancellation without explicit knowledge of the spreading sequences, seem very attractive. In this chapter we downsize the MIMO MMSE detectors to Single Input Single Output ones and we evaluate their interference rejection capability. In section 5.2 the description of the despreading operation by adaptive transversal filtering is addressed. In section 5.8 we present the linear adaptive interference canceller and we evaluate its performance in static and time-varying fading channels. In section 5.4 we present the non-linear extension of the adaptive interference canceller based on decision feedback and we evaluate its performance gain over the linear for both static and time-varying channels. In section 5.5, alternative interference cancellation methods are addressed. The later, although can provide similar performance gains to SISO MMSE, their operation is based on the knowledge of the interfering spreading sequences. Thus, the cancellation process is centralized which imposes certain restrictions in multipath channels where the delay of each path has to be determined very accurately. In section 5.6 we address the delay estimation problem under near-far interference. The implicit despreading of SISO MMSE detectors offers resistance against delay spread the benefits of which are made apparent in section 5.7 where the ability of the SISO adaptive receivers to RAKE the multipath energy in an autonomous manner is demonstrated.

5.2 ADAPTIVE DESPREADING

In this section, the despreading function will be revisited and a new receiver architecture will be presented that implements this operation by adaptive filtering. In Chapter 3, we presented two possible implementation architectures for despreading a spread spectrum signal which both are based on the concept of correlation. The code matched filter is an FIR structure whose taps are set equal to the complex conjugate time-reversed code sequence. This setting is optimum for the single-user static AWGN channel but as has been shown in Chapter 3, when multiple access interference is dominant, its optimality is lost.

The structure which is presented in this section is also FIR but with tap settings which are time-varying as they are dependent on the adaption algorithm. The settings of the FIR filter are chosen so that the Mean Square Error between the transmitted information bit and the received spread spectrum signal is minimised. The adaptive despreader is shown in Fig.5.1.

For the adaption algorithm the Least Mean Square (LMS) adaption algorithm has been chosen. The choice was based on the implementation simplicity and on the wide popularity of this algorithm. We could have used other adaption algorithms, such as, the Recursive Least Squares (RLS), the Fast Transversal Filters (FTF) algorithm etc, but our purpose is not the examination of countless adaption algorithms that exist in the open literature. Our aim is to demonstrate the adaptive correlator concept and on that respect the LMS algorithm is adequate. The employment of simple adaption algorithms like LMS can also be justified if one considers that the input signal to the adaptive correlator is at the chip rate. The number of operations that are required for the more common adaption algorithms as illustrated in Table 5.1, dictate low complexity algorithms for high rate signals. However, as the implementation of the proposed receivers is not on the scope of this thesis, it is very interesting to further investigate the effects of the various algorithms to the performance of adaptive despreaders.

The complex LMS adaption algorithm determines the vector of the new tap settings

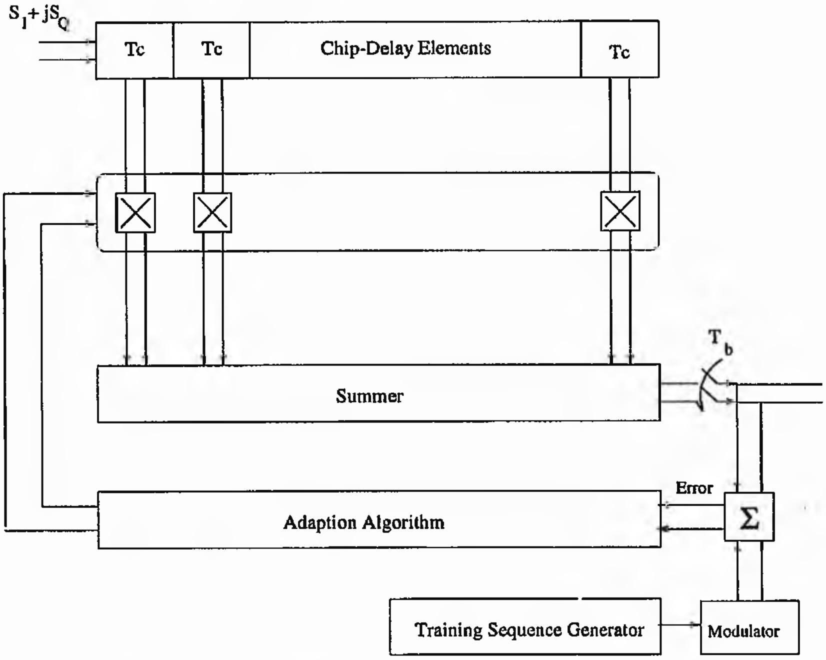

Figure 5.1: Adaptive Spread Spectrum Receiver

Algorithm	Complex Operations	Divisions
LMS DFE	$2N+1$	0
Fast RLS DFE	$20N+5$	3
Conventional RLS DFE	$2.5N^2+4.5N$	2
Square-root RLS DFE	$1.5N^2+6.5N$	N

Table 5.1: Computational Complexity of Adaptive DFE Algorithms

as,

$$\hat{\mathbf{h}}_{n+1} = \hat{\mathbf{h}}_n + \mu e_n^* \mathbf{s}_n \tag{5.1}$$

where $\hat{\mathbf{h}}_{n+1}$ is the new tap-weight vector, $\hat{\mathbf{h}}_n$, $e_n = b_n - \hat{\mathbf{h}}_n^H \hat{\mathbf{h}}_n$ and $\mathbf{s}_n$ is the tap-weight vector, error signal and input vector during the nth bit instant respectively.

Although a thorough discussion on the LMS algorithm can be found in [24], we shall also provide a limited review of the fundamentals that determine the performance of the adaptive despreader as compared to the optimal correlator receiver.

One of the most important measures of adaptive algorithms is the excess mean squared error denoted usually by J_{∞}^{ex}. Since the despreading operation is performed adaptively, the chosen tap weights are oscillating closely around the optimal Wiener solution. If we assume that the receiver knows about this optimal solution, under non-zero noise conditions, its mean squared error is the minimum possible, denoted by J_{min}. The difference between the mean squared error J_n as the number of samples n goes to infinity and the minimum mean squared error J_{min} defines the excess mean squared error J_∞^{ex}. The importance of the excess mean squared error stems from its direct relationship with the *misadjustment* which is defined as,

$$M = \frac{J_\infty^{ex}}{J_{min}} \tag{5.2}$$

The misadjustment provides a useful measure of the cost that adaptability is associated with. The misadjustment is related to the eigenvalues of the correlation matrix $\mathbf{R} = E[\mathbf{s}\mathbf{s}^H]$ of the input signal $\mathbf{s}$. When the adaption constant μ is small compared to $2/\lambda_{max}$, where λ_{max} is the maximum eigenvalue of $\mathbf{R}$, the misadjustment can be written as [47],

$$M = \frac{\mu L(P_s + P_n)}{2} \tag{5.3}$$

where P_s is the power of the input signal, $P_n = N_0$ is the noise power, and L is the length of the adaptive filter. The power of the input signal, spread by a PN sequence $\mathbf{c}$ of period N, is given by,

$$P_s = \frac{1}{N}\mathbf{c}^H\mathbf{c} \tag{5.4}$$

Thus the misadjustment for this particular application, can be written as,

$$\mathcal{M} = \frac{\mu L(\frac{1}{N}\mathbf{c}^H\mathbf{c} + N_0)}{2} \tag{5.5}$$

Increasing the length of the filter the misadjustment is increased. As can be easily be concluded from Fig.5.2, the number of filter taps must be the same as the period of the spreading sequence for proper operation.

Although Fig.5.2 refers to the Rayleigh fading case, similar conclusions can be drawn for the AWGN channel. Thus, assuming that the number of taps equals the period of the code, it is evident from (5.5) that the only control that we have over the misadjustment is through the step size or adaption constant (μ). Fig.5.3 demonstrates the relationship between the adaption constant and the misadjustment.

It is evident that the misadjustment can be minimized by having low μ. However, low values of μ will increase the training period of the LMS algorithm. Thus, there exists a tradeoff between training delay and misadjustment. For all the simulation models presented in this chapter, a training period of 500 symbols has been assumed.

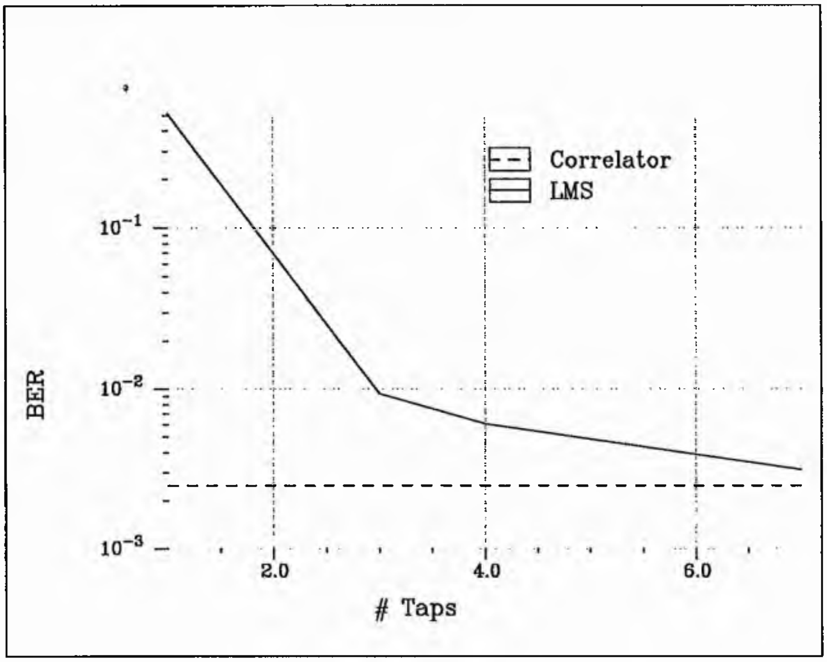

Figure 5.2: Effect of the Number of Taps on Performance, Rayleigh Fading, $E_b/N_0 = 20$ dB, $\mu = 10^{-4}$

The output of the adaptive despreader is an estimate of the transmitted bit, $\hat{\mathbf{b}}_n = \mathbf{s}_n^H \hat{\mathbf{h}}_n$. Statistics about the BER of this type of receiver have been gathered using a simulation model. The model consists of a QPSK transmitter employing one of the Gold codes of length 7, introduced in Chapter 4, and a QPSK receiver whose despreading function was implemented by an FIR adaptive filter with 7 taps. Every tap had one chip duration. The Monte-Carlo simulation of this system involved training of the LMS filter for 500 symbols after which the receiver run with detected symbols and the BER statistics were measured. The results are shown in Fig.5.4 for the AWGN channel.

The probability of bit error can also be predicted analytically. The analytical evaluation is based on treating the misadjustment as additional source of noise. Thus, for a given μ and spreading factor the new SNR/bit can be written,

$$(SNR/bit)_{LMS} = \frac{SNR/bit}{1+\mathcal{M}} \tag{5.6}$$

For the AWGN channel the BER will then be given by,

$$P_b(LMS) = \frac{1}{2} erfc\left(\sqrt{(SNR/bit)_{LMS}}\right) \tag{5.7}$$

In Fig.5.5 the latest equation has been plotted together with the optimal (for this single user example) correlator performance. For low E_b/N_0 the dominant term seems to be

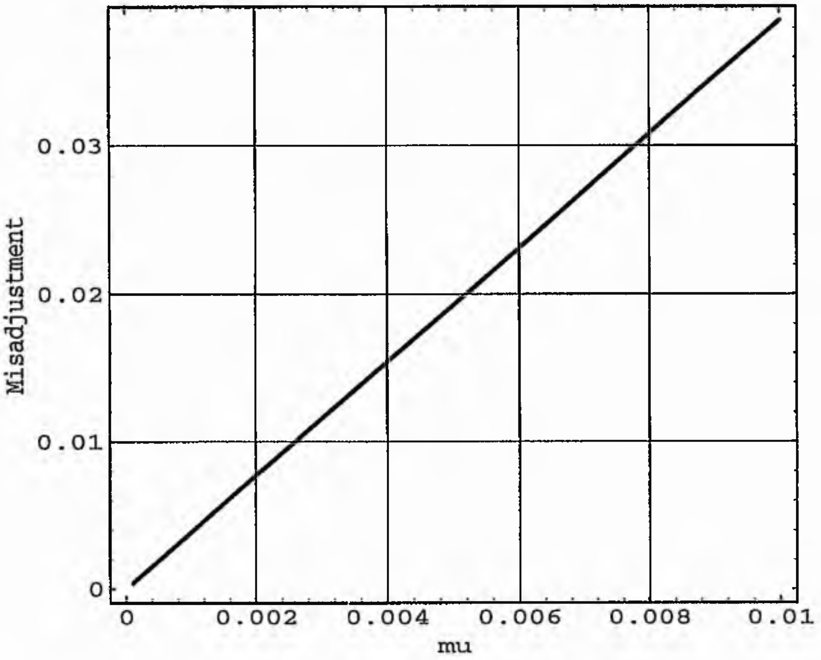

Figure 5.3: Misadjustment of LMS Detector vs LMS Adaption Constant μ

the noise induced by the channel and the performances of the correlator and the LMS filter are very similar. As the AWGN noise is reduced, the misadjustment noise becomes significant and the curves start to deviate from each other. Similar conclusions can be drawn from the Rayleigh fading case.

In Rayleigh fading channels the LMS despreader faces a time-varying environment. The LMS algorithm is adequate for slow fading channels where although the minimum MSE is time-variant, the algorithm is stable if the step size is suitably chosen. For fading channels, the total misadjustment consists of two components. The first is the misadjustment due to gradient noise which is also met in AWGN channels. The second is the misadjustment due to lag which is due to the inherent hysteresis of the LMS algorithm to track the continuously varying optimal tap weight vector. In Fig.5.6 the performance results of LMS as compared to the correlator despreader have been drawn, assuming phase coherency throughout the simulation run.

The contrasting difference between the AWGN and fading channels is the choice of the adaption constant. In Fig.5.7 the BER versus the adaption constant has been plotted for these two channels. Clearly, in the AWGN case the performance penalty paid for the adaption can be made arbitrary small provided that the algorithm is left to settle down. On the other hand in the Rayleigh fading channel there exist only one optimal value of the adaption constant.

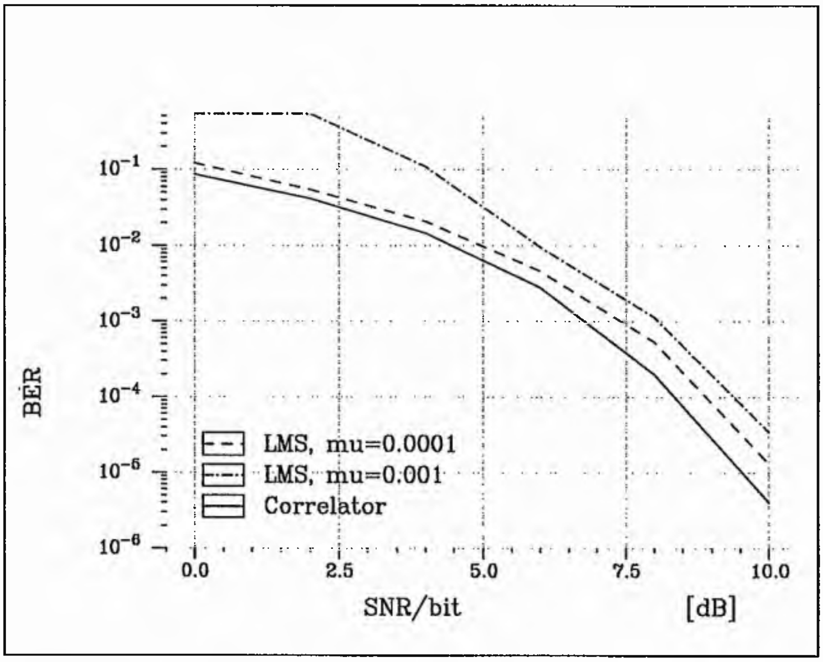

Figure 5.4: Monte-Carlo Evaluation of LMS Despreader Performance in AWGN

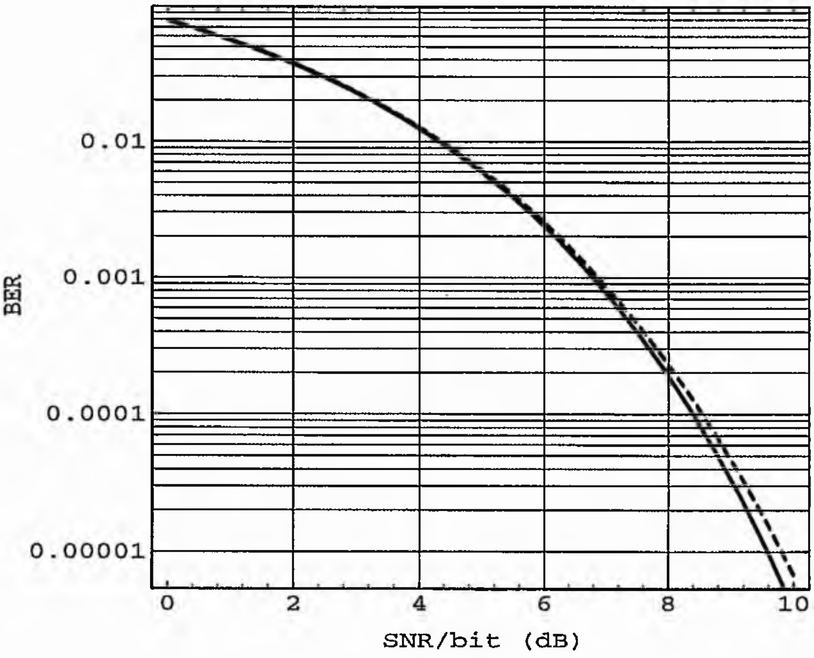

Figure 5.5: Performance of LMS Despreader Performance in AWGN Channel, $\mu = 10^{-4}$, (—) Correlator, (- -) LMS

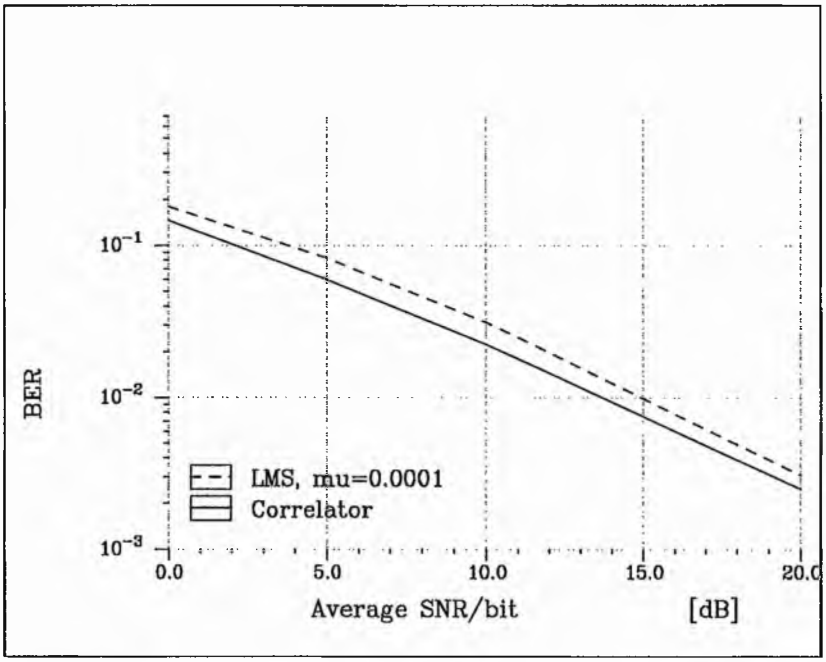

Figure 5.6: Monte-Carlo Evaluation of LMS Despreader Performance in Rayleigh Fading

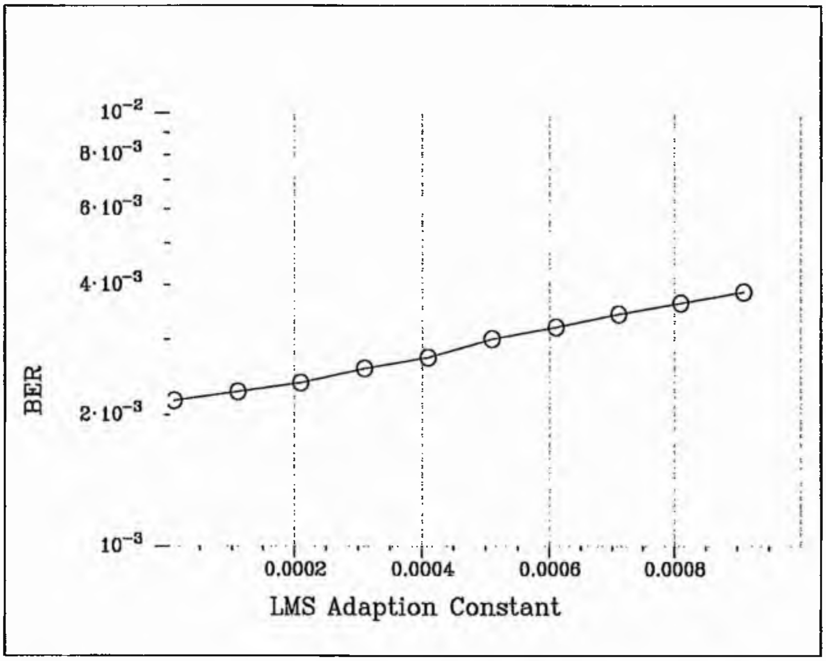

Figure 5.7: LMS Despreader Performance vs Adaption Constant in AWGN and Rayleigh Fading Channels

5.3 LINEAR FRACTIONALLY SPACED INTERFERENCE EQUALIZER

The despreading operation through minimization of the MSE, as considered in the previous section, can be performed with filters that have either chip-spaced taps or fractionally chip spaced taps. The fractionally spaced adaptive despreader has exactly the same performance as the chip-spaced one in a single user channel. However, in multiuser channels, the spacing of the taps places a fundamental role in the interference rejection ability of the receiver. Recall from Chapter 4, that the theory of MMSE detection in CDMA systems, originates from a general MIMO system model. Pioneering work in the area of cyclostationary crosstalk suppression on Digital Subscriber Loops (DSL) [44], indicates that the use of fractionally spaced filters is associated with drastic improvement in performance as compared to the symbol spaced ones. However, in [45] is supported that arguments as to whether or not the interference experienced in multiuser communication problems can be better equalised by fractionally spaced filters can only heuristically explained or proved through simulation. On support of the superiority of fractionally spaced filters comes also the formal proof of Gardner [17] who points out that linear processing of cyclostationary interfering signals can exploit spectral correlation properties, peculiar to these signals.

In this section, the first SISO MMSE detector, on the form of a Linear Fractionally Spaced Equalizer (LFSE), is evaluated. The LFSE detector as shown in Fig.5.8 resembles the adaptive despreader, however the taps in this case are separated by half the chip duration [21], [50]. The half-chip spacing has been considered a good compromise between performance and complexity since the length of the filter has to span the length of the spreading code. The shorter the spacing, the longer the filter should be and as the number of operations per detected bit is proportional to the length of the filter, there is a substantial increase in complexity.

In order to evaluate if SISO MMSE detectors are resistant to near-far interference, a Monte-Carlo simulation model, shown in Fig.5.9, has been implemented. It consists of a number of spread spectrum transmitters, each one transmits with an adjustable power level. Each signal passes through a static multipath channel whose power delay profile is distinct for each user. One of the power delay profiles used is shown in Fig.5.9. For evaluating the near-far resistance, the number of users was set to two. This two-user scenario has also been considered in Chapter 3, where the same layout, without the multipath channel, was used to examine the effects of near-far interference to the conventional detector performance. The spreading sequences were Auto Optimal Least Sidelobe Energy

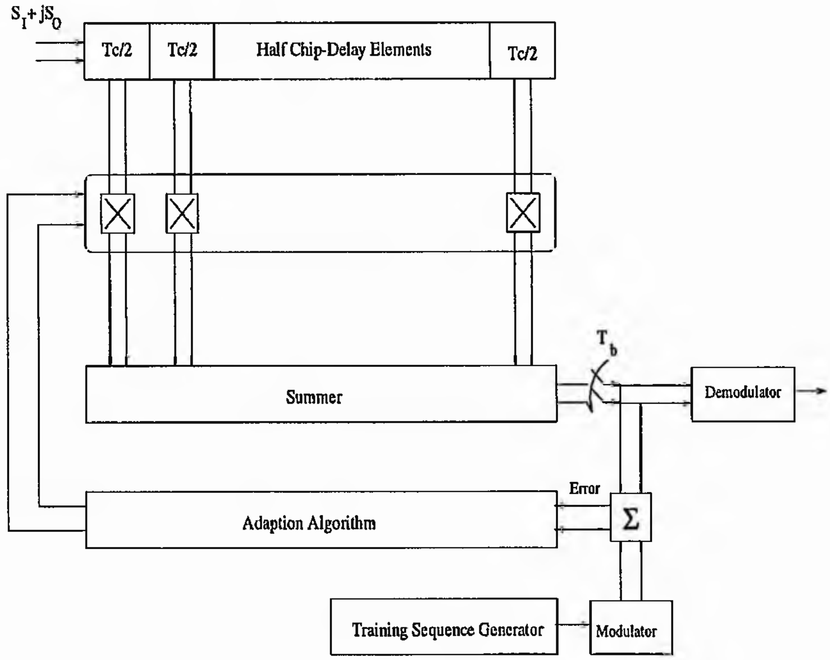

Figure 5.8: Linear Fractionally Spaced Equalizer

(AO/LSE) sequences of period 31. They were generated using the polynomials suggested in [48]. The length of the LMS adapted LFSE receiver was set to 62 taps, each having a $T_c/2$ duration. The equalizer span 1 time the length of the spreading sequence. The bit error probability for the LFSE is shown in Fig.5.10.

The SNR/bit which is required to achieve a BER of 1% with the LFSE receiver compared to the conventional receiver we studied at Chapter 3, is shown in Table 5.2 for various near-far power ratios.

Power Ratio	**Conventional**	**LFSE**
0 dB	5.5	4.35
-5 dB	7.5	4.9
-10 dB	$> 15dB$	4.9
-15 dB	-	5.0
-20 dB	∞	6.65

Table 5.2: Comparison Between the Required SNR/bit For Conventional and LFSE Receivers to Achieve 1% BER under Near-Far Interference in the AWGN Channel

These results indicate the following:

- The LFSE detector approaches the single user bound over a wide dynamic range of power ratios. The near-far resistance of LFSE remains at peak values over a

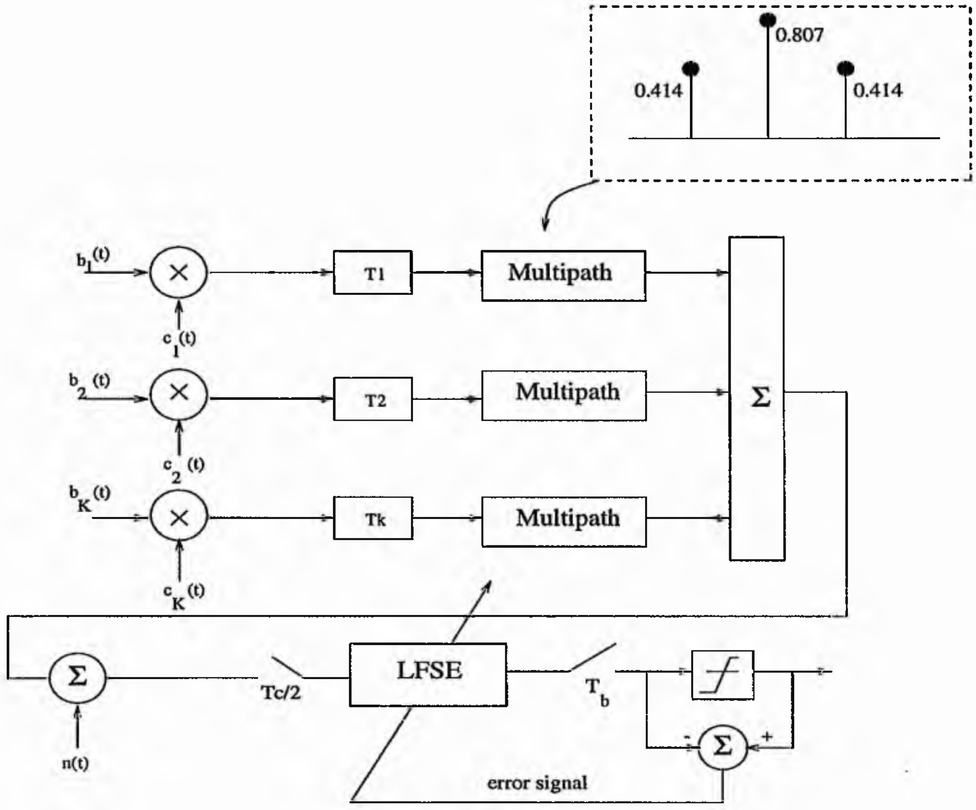

Figure 5.9: LFSE Simulation Model

dynamic range of 10 dB and starts degrading after this point. The degradation though is only a fraction of that observed in the conventional detector.

- Even when $P_1/P_2 = 0dB$ the LFSE detector performs better that the matched filter detector. This is because the MMSE criterion takes into account both the background noise and the interference.

- The performance under power controlled conditions (P_1/P_2=0dB) is of particular interest for yet another reason. As has been pointed out in [32] the MIMO linear decorrelating detector is inferior to the matched filter detector for equal power users. With our results we have demonstrated that the LFSE detector although an SISO device, is superior to the linear decorrelating detector which has an MIMO architecture.

- The E_b/N_0 degradation due to the multipath is insignificant. In fact the difference between the matched filter bound and the 2 user performance in multipath is equal to 0.5 dB which is equal to the degradation caused by the LMS adaptive filter. This means that the LFSE is also able to combine optimally the rays and act as an

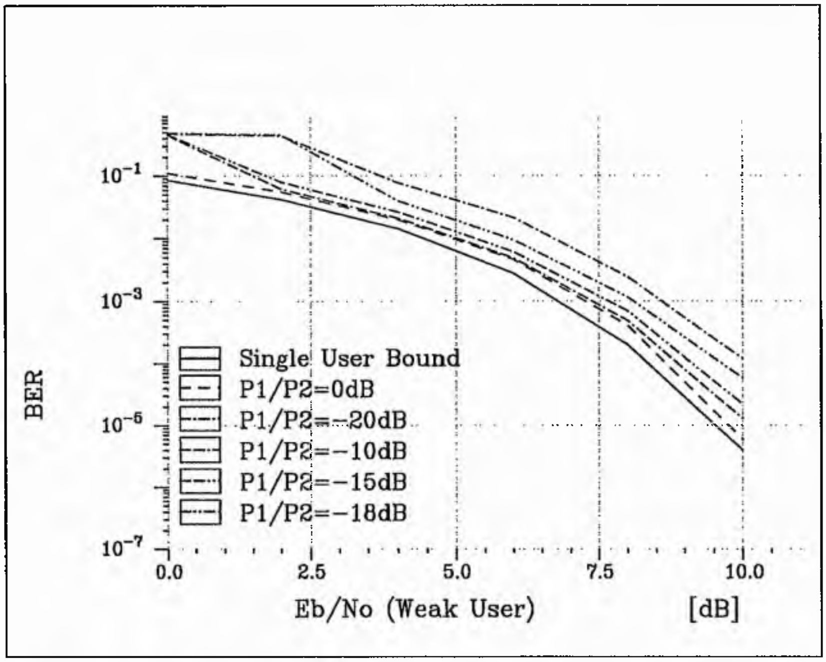

Figure 5.10: Performance of LFSE Under Unequal Power Interference.

adaptive RAKE combiner-canceller.

The question that now arises is how the performance of LFSE is compared to other interference cancellation techniques. Before answering this question we evaluate first the performance of its non-linear extension as described in the next section.

5.4 FRACTIONALLY SPACED DECISION FEEDBACK INTERFERENCE EQUALIZER

Here, we present the Fractionally Spaced Decision Feedback Equalizer (FS-DFE) and evaluate its performance for both static multipath and Rayleigh fading channels. Consider a K-user system and denote the spread signal of all the users in this system during the kth data bit interval as $\mathbf{d_k}^T = [d_k^1 d_k^2 ... d_k^i ... d_k^K]$. The (NxK) deterministic matrix of the spreading codes of period N is denoted by $\mathbf{C} = [\mathbf{c}^1, \mathbf{c}^2, ..., \mathbf{c}^K]$, where $\mathbf{c}^j = [c_1^j c_2^j ... c_N^j]^T$. If $\mathbf{b}_k = diag[b_k^1, b_k^2, ... b_k^K]$ is the vector which represents the kth data bit of the users, the transmitted signal can be written as $\mathbf{d_k} = \mathbf{C}\ \mathbf{b_k}$. The multiplicative distortion due to fading is denoted by the time-varying random matrix $\mathbf{W_k} = diag[\mathbf{w_k^1}, ..., \mathbf{w_k^K}]$, where each process $\mathbf{w_i}$ follows the Rayleigh probability density function representing the amplitude variations of each user's signal. The receiver observes the signal,

$$\mathbf{r_k} = \mathbf{W_k d_k} + \mathbf{n} \tag{5.8}$$

where $\mathbf{n}$ is an additive white noise process with covariance matrix equal to $N\ N_0/2\ \mathbf{I_N}$, with N_0 the two-sided noise power spectral density and $\mathbf{I_N}$ the (NxN) identity matrix. For the FS-DFE receiver under consideration, the task is to minimise the following expression,

$$MSE^j = E[|\tilde{b}_k^j - \hat{b}_k^j|^2] \tag{5.9}$$

where, $\hat{b}_k^j$ and $\tilde{b}_k^j$ is the decision and the output of the equalizer associated with the kth data bit of the user j, respectively. The equalizer taps are adapted using the LMS algorithm so that the mean squared error is closely oscillating around the minimum optimal value which can be determined only by solving a system of equations [24]. For adaptive MMSE detectors (like LFSE and FS-DFE) the solution of this system and the associated matrix inversion is not required. Since, the FS-DFE receiver has a fractionally spaced feedforward filter, it is equivalent to the cascade of a code matched filter (which performs the despreading operation) and of a symbol spaced DFE which implements the interference suppression. Moreover, like the LFSE detector in multipath fading channels, the feedforward filter can act as a RAKE combiner and exploit the inherent multipath diversity of spread spectrum signaling. For non-linear equalization receivers the closed form evaluation of the bit error probability involves making the significant assumption of zero error propagation. Thus, Monte Carlo simulations must be performed for a realistic evaluation of the receiver performance.

Two types of channels have been used: (1) Static multipath channel which is representative of a very slow time-varying channel and usually employed in satellite channel modelling and (2) Rayleigh fading channel representative of terrestrial mobile radio channels.

Two scenarios have been investigated. The first scenario is suitable for assessing the near-far resistance of the detector and comprises transmitters with AO/LSE m-sequences of period 31 that spread a QPSK modulated signal. At the receiver side, the feedforward filter is implemented using 62 taps, each having half a chip duration. Each of the 2 feedback taps have 1 bit duration. The second scenario is suitable for investigating the spectral efficiency and comprises transmitters with Gold sequences of period 7 and FS-DFE detector with 14 feedforward and 2 feedback taps. For both scenarios the well known least mean square (LMS) algorithm is employed for the adaption. The equalizer was run on actual decisions after a initial training period of 500 symbols.

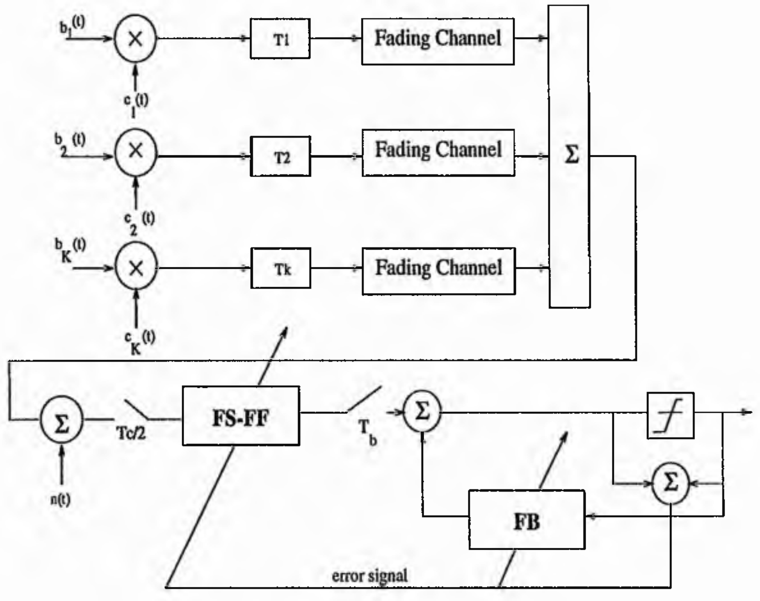

Figure 5.11: FS-DFE Simulation Model

The bit error probability for the FS-DFE for the static multipath channel model is shown in Fig. 5.12. The performance of LFSE has also been included. A comparison with the performance of the conventional matched filter detector in a AWGN channel, under the same near-far conditions, indicates that FS-DFE offers significant performance gains. As expected, the FS-DFE has better performance as compared to the LFSE detector.

The effect of system loading on the bit error probabilities of the FS-DFE and the conventional detector is shown in Fig.5.13, 5.14 and 5.15, for the Rayleigh fading case.

As can easily be concluded from the curves, the adaptive FS-DFE starts to degrade as the loading in the system increases but within the E_b/N_0 range of practical interest, it does not appear to have irreducible bit error rate. The conventional detector on the other hand, is interference limited. That is, its bit error rate is irreducible even for 28% loading.

Comparing the performance of the MIMO non-linear decorrelating detector [12], under the same loading conditions is evident that the system load affects the performance of the decorrelator very similarly to the FS-DFE. The decorrelating detector on the other hand has performance which is independent on the interfering power levels in contrast to the adaptive FS-DFE which is dependent, as shown by the results of Fig.5.12.

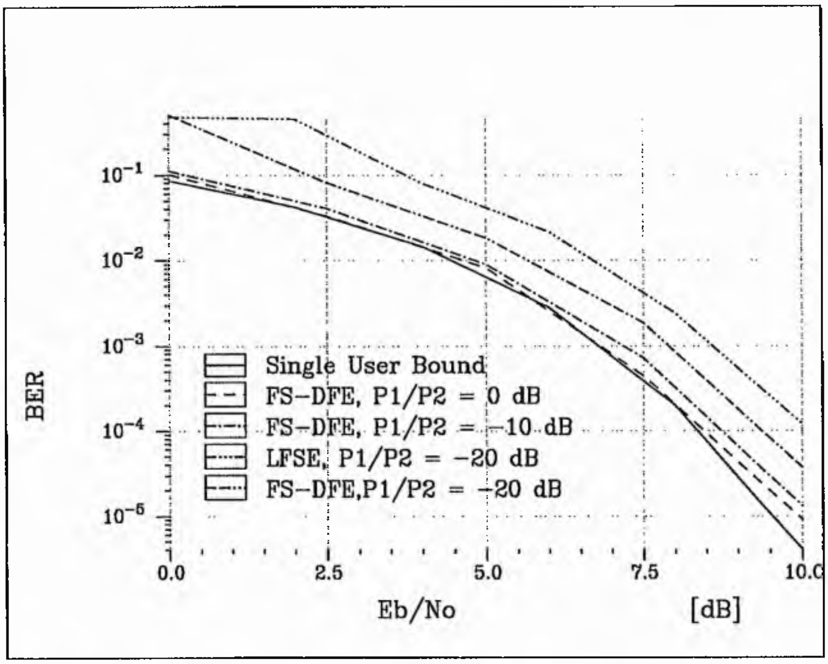

Figure 5.12: Performance of FS-DFE Under Unequal Power Interference.

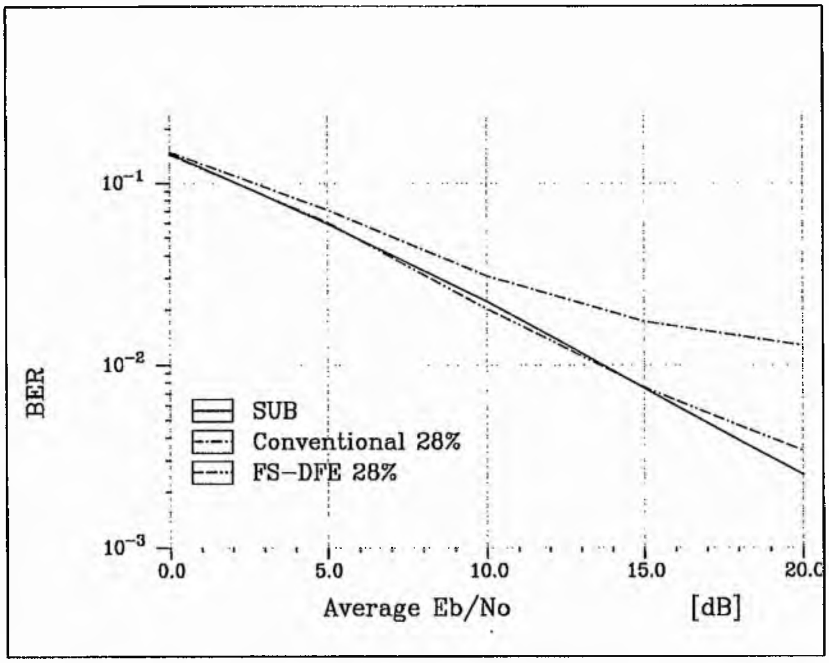

Figure 5.13: Performance of FS-DFE With 14 feedforward taps vs Conventional Detector for 28% Loading

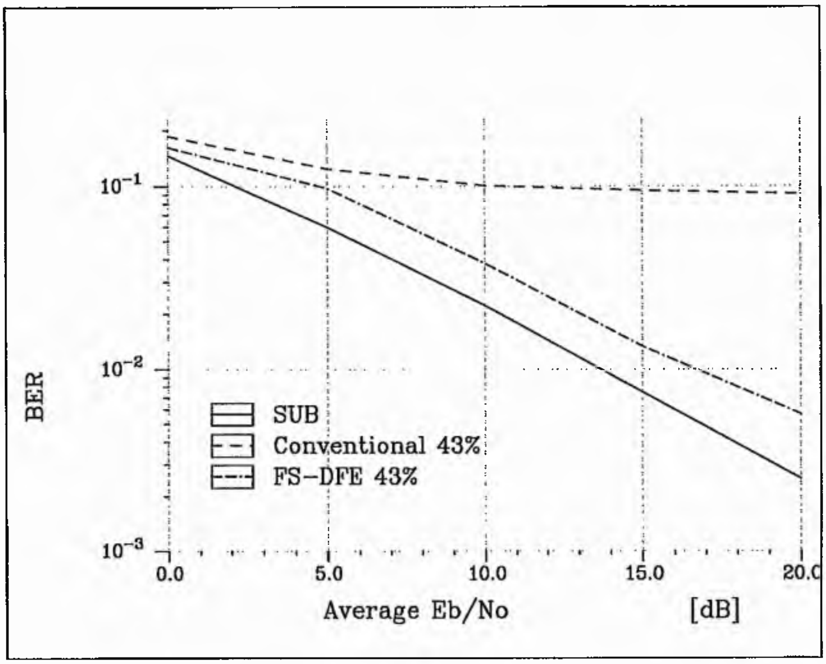

Figure 5.14: Performance of FS-DFE With 14 feedforward taps vs Conventional Detector for 43% Loading

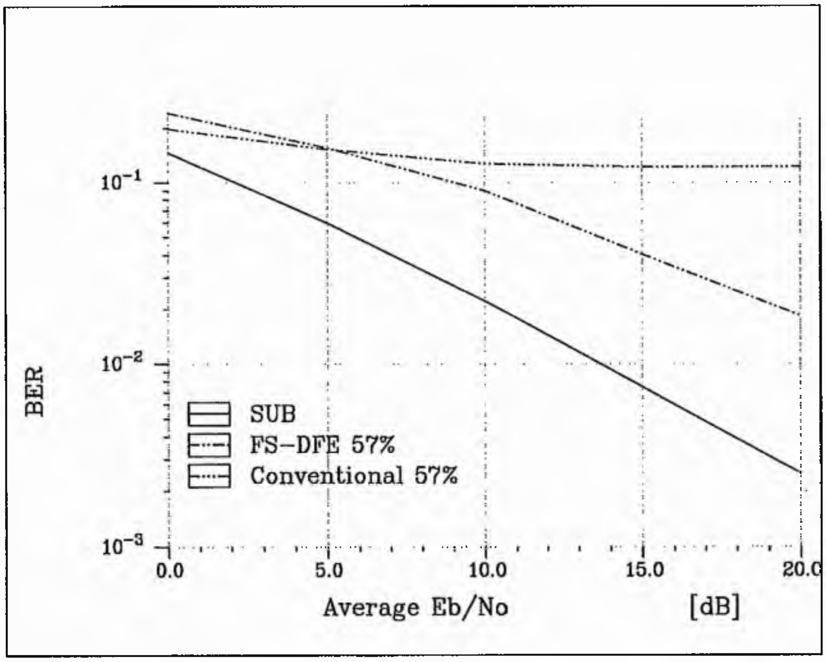

Figure 5.15: Performance of FS-DFE With 14 feedforward taps vs Conventional Detector for 57% Loading

5.5 COMPARISON AND DISCUSSION

5.5.1 Benefits of SISO MMSE Detection

Based on the results presented so far we can comment on the performance of the Conventional and SISO MMSE detectors in near-far interference environment as follows:

- FS-DFE receiver provides similar to the LFSE performance for moderate interfere conditions (up to -10 dB near-far ratio) while its effectiveness under severe interference (eg. -20 dB near-far ratio) is more pronounced. This is shown in Fig.5.16 where at SNR/bit = 10 dB for the user of interest, we compare SISO MMSE and correlation based detectors in the 2-user system with 31 chips/bit.

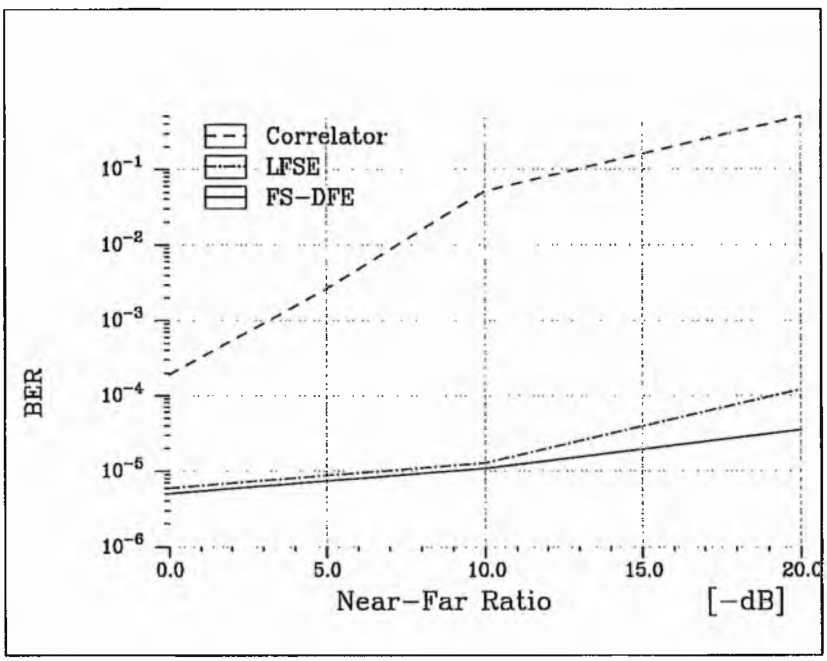

Figure 5.16: Comparison Between the SISO MMSE Detection and Correlation in Near-Far AWGN Channel

- Apart from the significant performance gain obtained in near-far conditions, SISO MMSE detector offer significant gains when the system loading is increased. This has been already predicted from Chapter 4 based on analytical results. Fig.5.17 depicts this performance improvement for a 7 chips/bit system in Rayleigh fading channel with average SNR/bit = 20 dB for the user of interest.

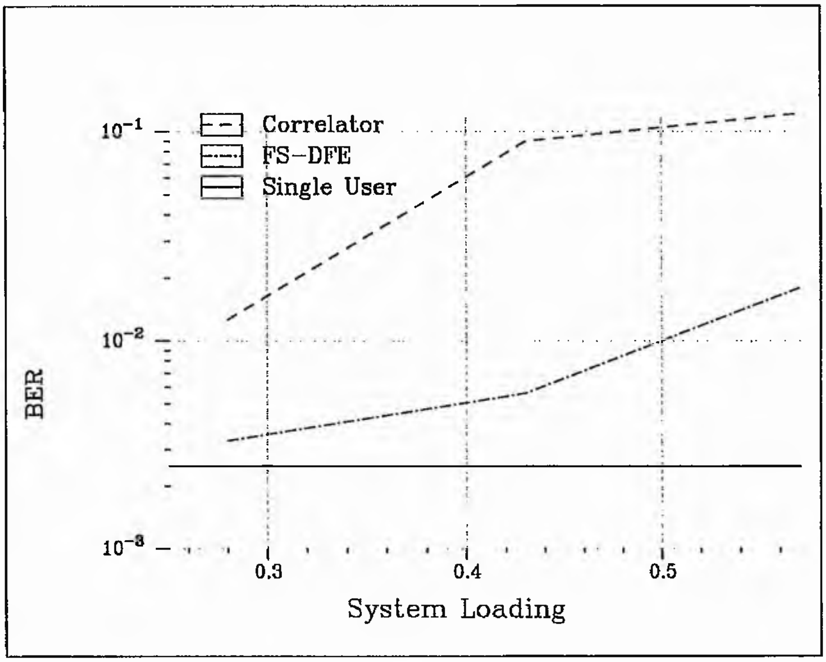

Figure 5.17: Effect of System Loading to the Performance of SISO MMSE and Correlation Detectors in Rayleigh Fading Channel, SNR/bit = 20 dB

5.5.2 Comparison With Other Interference Cancellation Methods

Although interference cancellation methods based on MMSE criterion have been shown to be effective in both near-far interference and high system loading conditions it would be of interest to compare SISO MMSE receivers with other interference cancellation techniques. The comparison will be made both in terms of performance and complexity.

Successive Interference Cancellation (SIC)

This interference rejection method first appeared in [60] and subsequently has been the subject of [40]. [10] also defined a similar technique based on Walsh Hadamard Transformations of the interfering signals. The SIC method is demonstrated in Fig.5.18.

The technique involves the cancellation of the interfering signals before the despreading operation. The cancellation process involves the regeneration of the interfering spread spectrum signals based on the knowledge of the spreading sequences and the time-varying interfering user energies. In order to evaluate the performance of SIC a simulation model has been developed. The model involved a 2-user system in single-path Rayleigh fading

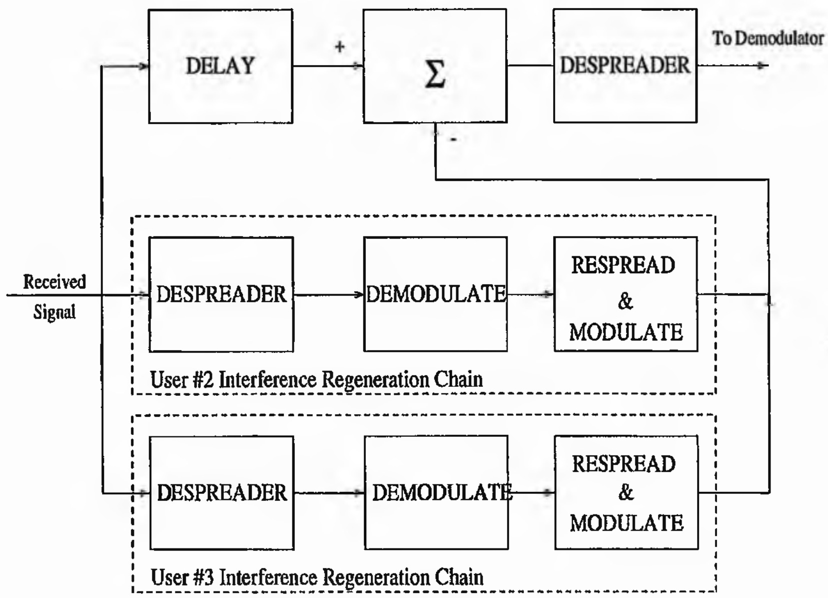

Figure 5.18: Successive Interference Cancellation For a Three User System

channel. The user signals are spread by Gold sequences of period 7. The results of the simulation can be seen in Fig.5.19 where for comparison purposes we have also included results obtained previously for the FS-DFE receiver.

Multistage Detection

The multistage detector has been invented by [56]. As shown in Fig. 5.20 its architecture resembles the architecture of the decorrelating detector.

The detector consists of a bank of code matched filters and the multistage detection algorithm. The later is a series M-stages of processing the code matched filter outputs where the mth stage ($m \geq 1$) processor acts on the statistics produced by the (m-1)st stage. The m-stage consists of (i) estimation of the unknown symbols from the (m-1)st stage statistics. When m=M the algorithm dumps the user statistics at the K outputs. If $m < M$ the algorithm proceeds with the reconstruction of the multiple access interference using the estimates obtained in step (i) and subtracts the reconstructed interference from the sufficient statistics to obtain the mth stage statistics.

From the aforementioned description of multistage detection, one can easily identify similarities with the SIC method. Both SIC and multistage receivers subtract estimates of multiple access interference from the user of interest. However, the difference between SIC and multistage detection is on the way that the multiple access interference is re-

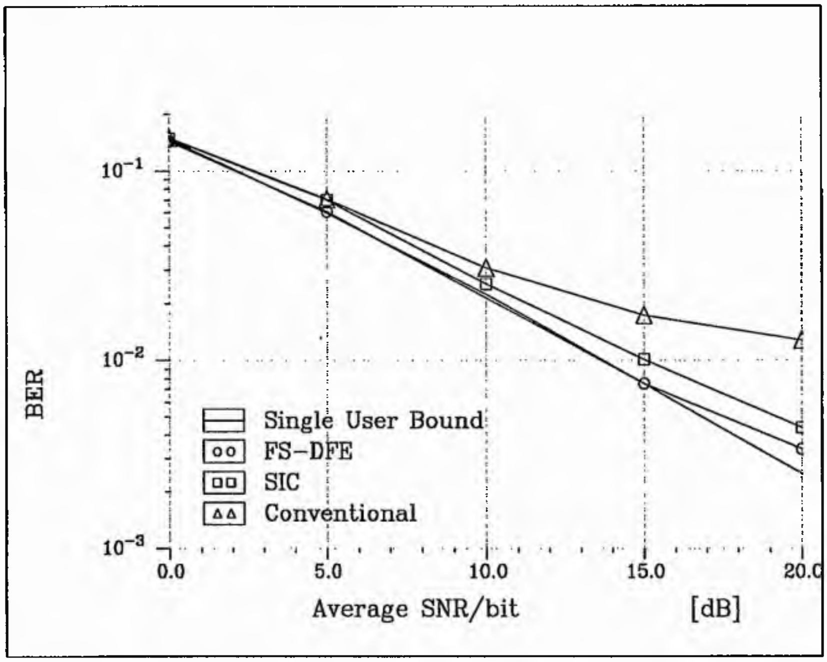

Figure 5.19: Comparison Between the FS-DFE MMSE Detector and Successive Interference Cancellation Receiver,K=2,Rayleigh Fading Channel

moved from the user of interest. In SIC this removal is clearly before the correlator (pre-correlation cancellation) while in multistage the cancellation is performed after the correlator (post-correlation cancellation).

In Fig.5.21 we have depicted the performance of multistage detector for a two user system in the AWGN channel, as reported in [56]. Every user spreads its information stream with a spreading sequence of period 3. The performance of a 62-tap FS-DFE receiver is also plotted for comparison purposes. It is clear that the multistage detector for 2-stage processing, performs better than the FS-DFE receiver while for as single stage the reverse is true.

In Fig.5.22 we present the performance of multistage and FS-DFE receivers under near-far interference. Again, a two-user system is considered where the power of the interfering user varied up to 10 dB higher than the user of interest.

The performance of FS-DFE receiver although constant over the examined near-far power ratios can not match the performance of the 2-stage detector although it is far superior to the 1-stage detector.

Having obtained some performance figures from representative interference cancellation techniques, we can now concentrate on the complexity issue and compare the afore-

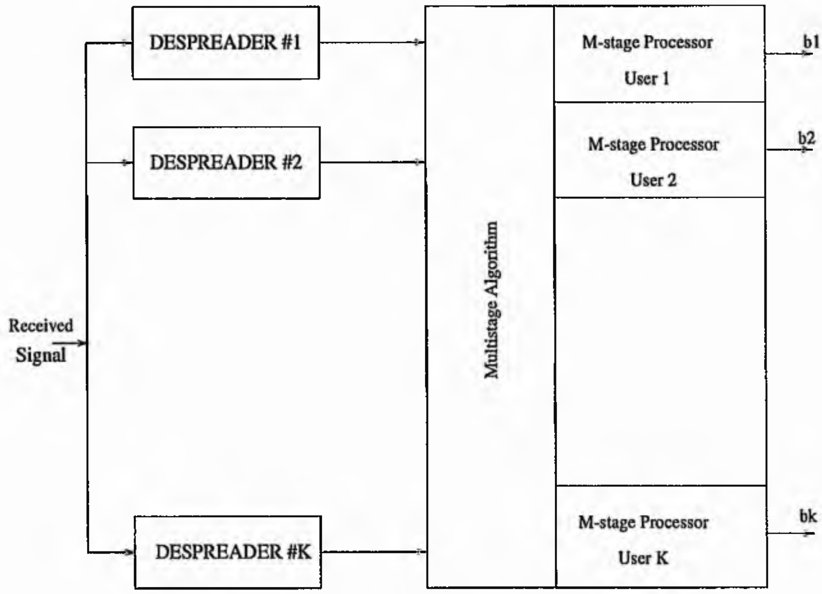

Figure 5.20: Multistage Interference Cancellation in a K-User System

mentioned techniques in terms of the required processing power. The figure of merit in this case has nothing to do with performance but with how many MFLOPS (Million Floating Point Operations Per Second) each technique requires.

Decorrelating Detector: The linear decorrelating detector complexity differs depending on whether the detector operates on a synchronous or asynchronous system. As has already been mentioned in Chapter 4, the decorrelating solution requires:

- An estimation of the cross-correlation matrix. If the same spreading codes of period L are used for every data bit the matrix estimation needs to be performed only once in the synchronous system. However, for the asynchronous case, due to the continuously changing relative delays among the users, the crosscorrelation matrix is time varying. The estimation of the (K,K) crosscorrelation matrix requires $2LK^2$ FLOPS for the synchronous case and roughly $2LK^2$ times the data rate for the asynchronous case. However it would be unfair to assume that the relative delays will change for all users within the duration of each bit. Thus, although the estimation of the crosscorrelation matrix with the bit duration would increase dramatically the computational load at the receiver, we shall assume that the relative delays among the users are very slowly varying.
- A cross-correlation matrix inversion. The matrix to be inverted is fortunately Toeplitz and this makes the inversion far simpler to implement using one of the

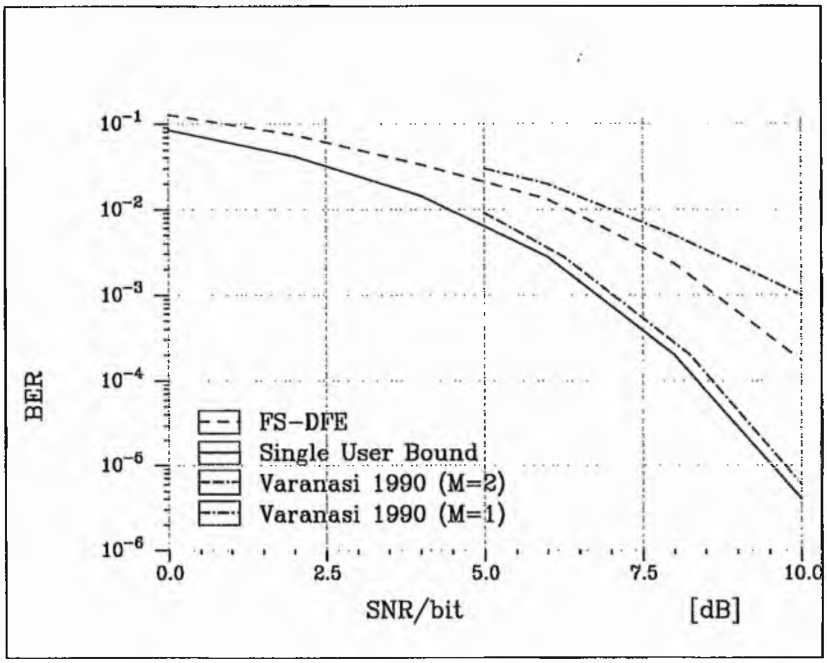

Figure 5.21: Performance of Multistage Interference Cancellation Receiver in the AWGN Channel,K=2,N=3, SNR/bit=8dB

three techniques outlined in [22]. The least expensive of these techniques based on Durbin's algorithm requires $2K^2$ FLOPS. Again, in the synchronous case the matrix inversion needs to be performed only once, while in the asynchronous case needs to be performed every data bit.

- A vector by matrix multiplication. This is the decorrelation operation ie. the multiplication of the vector at the output of the code matched filter bank with the matrix produced by the inversion procedure. This operation requires $2K^2$ FLOPS. This operation is required to be performed in every data bit for both synchronous and asynchronous case.

Table 5.3 summarises the computational complexity of performing decorrelation in a system with K=30 users each having a data rate of 9.6 kbps.

Multistage Detection: For implementing multistage detection we require the knowledge of:

- Complex amplitude and delay of every interfering user. The delay estimation is required anyway for the conventional detector due to the despreading operation (code

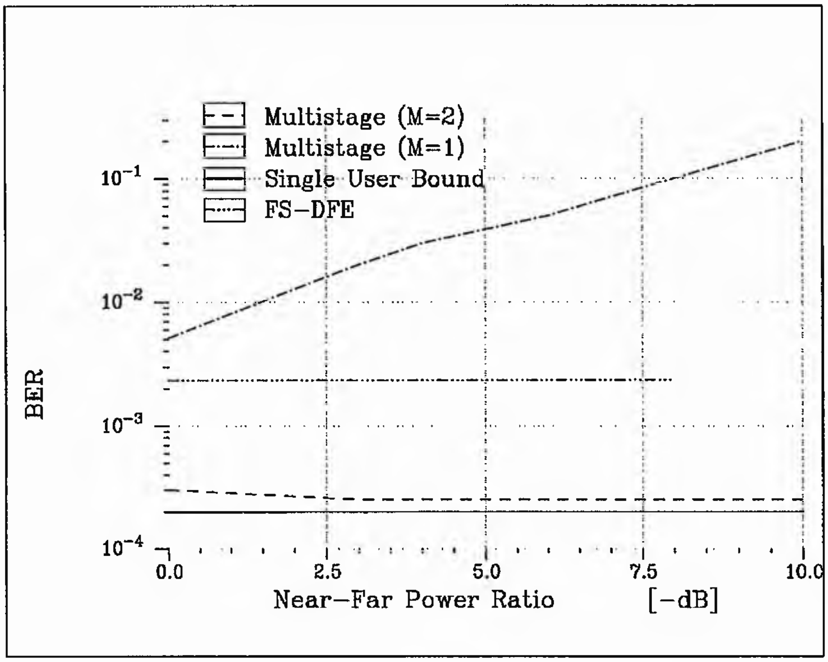

Figure 5.22: Performance of Multistage Interference Cancellation Receiver Under Near Far Interference in AWGN, K=2, N=3

Procedure	Synchronous	Asynchronous
Estimate Matrix	0.46	> 0.46
Invert Matrix (Durbin)	0.018	17.28
Decorrelate	17.28	17.28
TOTAL	17.83	> 35.0

Table 5.3: Computational Complexity in MFLOPS of the Decorrelating Detector, K=30, $R_b = 9.6$ kbps,L=256

matched filtering) which needs to be completed before the multistage algorithm starts. The complex amplitude estimation can be assumed that is also required by the conventional detector in order to perform coherent demodulation by phase-shifting the code matched filters outputs before the demodulator. Thus, we can argue that no extra complexity is required in multistage detection by the delay and amplitude requirement.

- An estimation of the cross-correlation matrix which requires the same computational complexity as that of the decorrelating detector.

- For M stages, the algorithm needs to be executed M times for every data bit. Therefore $2(M-1)(K-1)$ times the data rate FLOPS are required. The algorithm has to be executed in every data bit regardless of the synchronism or asynchronism of the interfering transmissions.

Table 5.4 summarises the computational complexity of multistage detection in a system with K=30 users each having a data rate of 9.6 kbps.

Procedure	**Synchronous**	**Asynchronous**
Estimate Matrix	0.46	> 0.46
Execute Algorithm (2 Stages)	0.55	0.55
TOTAL	1.01	> 1.01

Table 5.4: Computational Complexity in MFLOPS of the Multistage Detector, K=30, R_b = 9.6 kbps,L=256

Successive Interference Cancellation (SIC): For the implementation of SIC only the complex amplitude and delay of every interfering user are required. The interference regeneration consists of K-1 respreaders which require $(K-1)L$ times the data rate FLOPS. The synchronization or not does not affect the computational load of the regeneration module. In summary, for a 30 user system with $L = 256$ chips/bit and a data rate of 9.6 kbps, a total of 71.2 MFLOPS are required.

Fig.5.23 depicts the computational complexity for the aforementioned cancellation techniques.

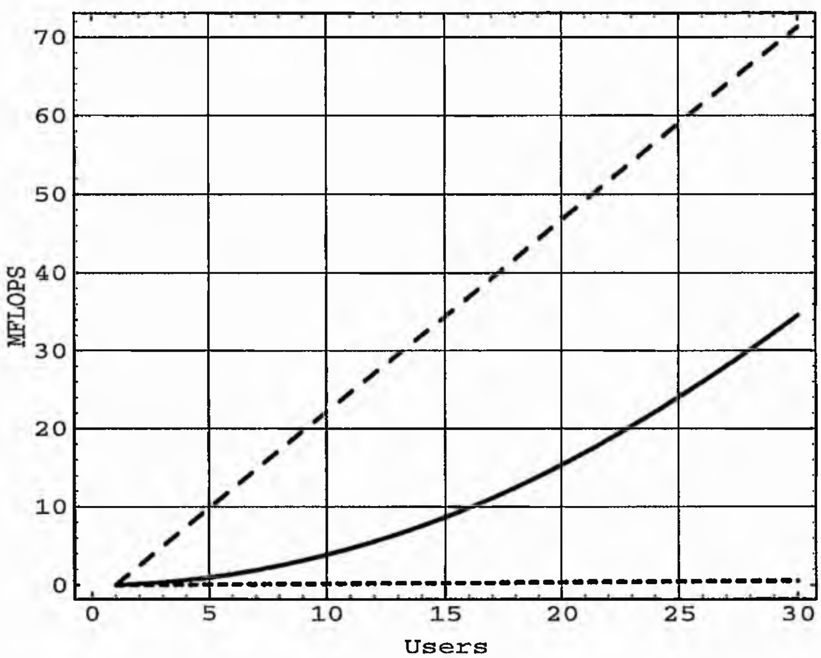

Figure 5.23: MFLOPS vs Number of Users For (—)Decorrelating Detector, (- -) Multistage Detector, (– –) Successive Interference Cancellation

5.6 ESTIMATION OF DELAY POWER SPECTRUM IN MULTIPATH CHANNELS UNDER NEAR-FAR INTERFERENCE

From the results presented in the previous sections, it is now apparent the performance gains that adaptive interference cancellation methods offer compared to the conventional detector in single path fading and static channels. The comparisons however were made under the assumption of perfect delay estimation. Over the past five years of extensive research on interference cancellation receivers, researchers were optimizing the receiver architecture with respect to the near far resistance. Since, as it has been addressed in Chapter 4, MIMO multiuser detectors process the output of code matched filters, they do not tackle the delay estimation problem. However, the assumption that the receiver has acquired synchronization under severe near-far resistance is very significant. Although, the problem of delay estimation has been widely studied for single-user channels, very little work has been done for channels where multiple access interference is the dominant performance degradation factor.

In order for the interference cancellation techniques that work with the knowledge of the interfering spreading sequences to function in multipath channels, an accurate estimation of the delay of every path is required. The multipath delay estimation procedure can be divided into two tasks. The first, is to estimate the delay of the strongest path and the second is to window the delay spectrum around the delay estimated in the first task. However, the problem of estimating the delay of the strongest path is by itself twofold. The first part, code acquisition, consists of getting an initial estimate of the delay, usually to within 1 chip resolution. The second part of the delay estimation problem, code tracking, the initial estimate is refined and continuously updated using a tracking loop.

Conventional Code Acquisition Fig.5.24 depicts the code acquisition technique usually employed in conventional receivers. The code acquisition function is implemented by a code matched filter whose coefficients are determined by an update algorithm. The input to this algorithm is the output of an energy detector device.

The behaviour of this circuit has been examined by Moon [39], which by the time of writing this thesis was the only reference that evaluated the effects of near-far interference in code acquisition. Moon evaluated the code acquisition circuitry behaviour of the weak user in a two user system and his results indicated that under near-far interference the

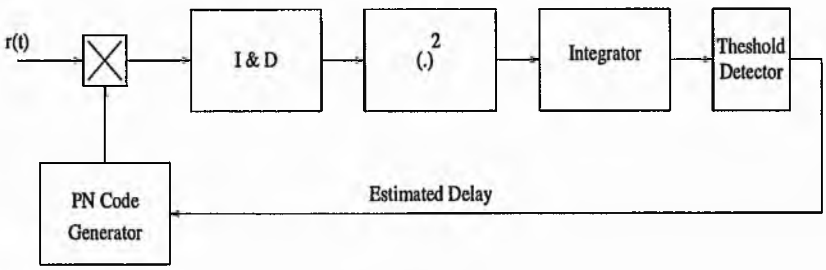

Figure 5.24: Code Acquisition Circuit

code acquisition circuit gets near-far limited ie. the time to acquire the code grows exponentially with the interfering power levels.

As the conventional detector is extremely vulnerable to incorrect delay estimation results like the ones shown in Fig.5.25 must be anticipated for a timing uncertainty of up to 1 chip duration.

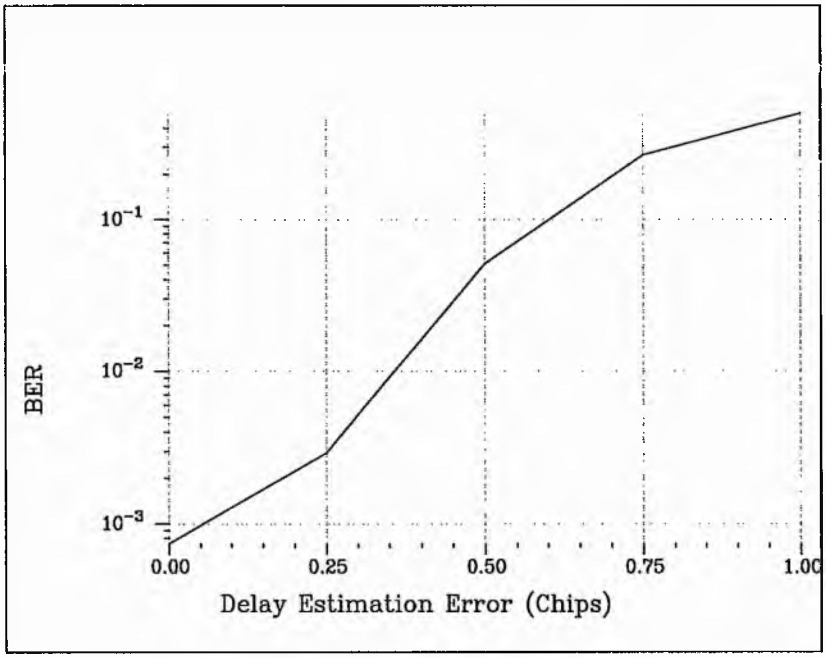

Figure 5.25: Effect of Incorrect Delay Estimation on the Performance of Conventional Receiver, AWGN Channel, $E_b/N_0 = 7$ dB

The performance of conventional RAKE receivers in multipath fading channels depends as has been highlighted in Chapter 3, by the performance of the Delay Power Spectrum (DPS) estimator. It would have been very interesting to observe how near-far interference affects the DPS estimator performance. For this demonstration we have used the DPS estimation technique employed in the RACE CODIT testbed. The CODIT DPS is based on classic code matched filter technique [7]. The results from this evaluation are shown in Fig.5.26 for 2 interfering sequences for various near-far ratios.

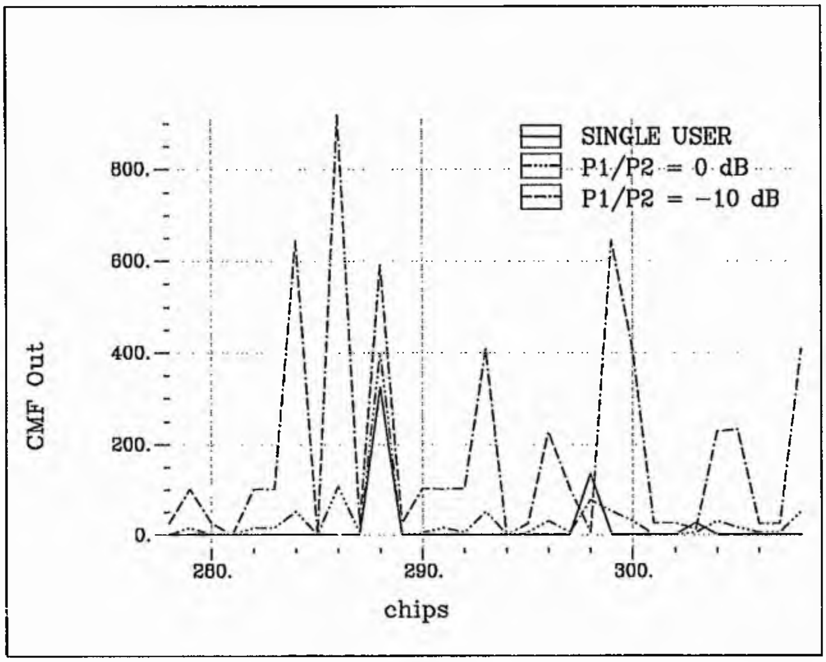

Figure 5.26: Matched Filter Delay Estimation Under Near-Far Interference

The fact that the DPS estimation quality depends on the near-far power ratio is of fundamental importance to the overall performance of interference cancellation receivers which process the despreader outputs.

However, a more critical observation of Fig.5.1 reveals that there is no explicit multiplication of the code sequence during the despreading operation, in contrast to the correlator based conventional receiver architecture. The despreading operation is implicit and is realized through minimisation of the mean square error (MSE). This could give the unique ability to provide interference cancellation and at the same time reduce the synchronization requirements imposed by the spread spectrum signalling. Verification of this argument has been made through Monte-Carlo simulation. Fig.5.27 presents the variance of the squared error of the symbol spaced LMS despreader, over 1000 samples, versus the timing error uncertainty. Fig.5.28 presents the BER performance of the LMS despreader versus the timing uncertainty.

The results indicate that with up to 2 chips uncertainty the performance remains *completely unaffected.* This is very significant to time-varying situations and extremely significant to multipath channel propagation. Our findings indicate that the accuracy requirements of the Delay Power Spectrum estimator, necessary for the operation of RAKE

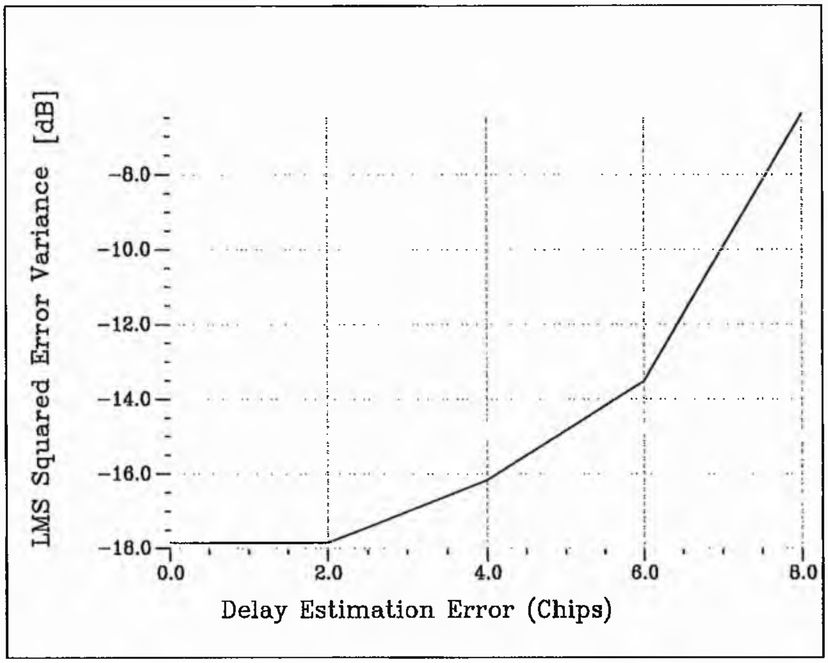

Figure 5.27: Effect of Incorrect Delay Estimation on the Error Amplitude of LMS Canceller, AWGN Channel, $E_b/N_0 = 10$ dB

receivers, can be significantly relaxed, further simplifying the signal processing overheads of NEFAR receivers.

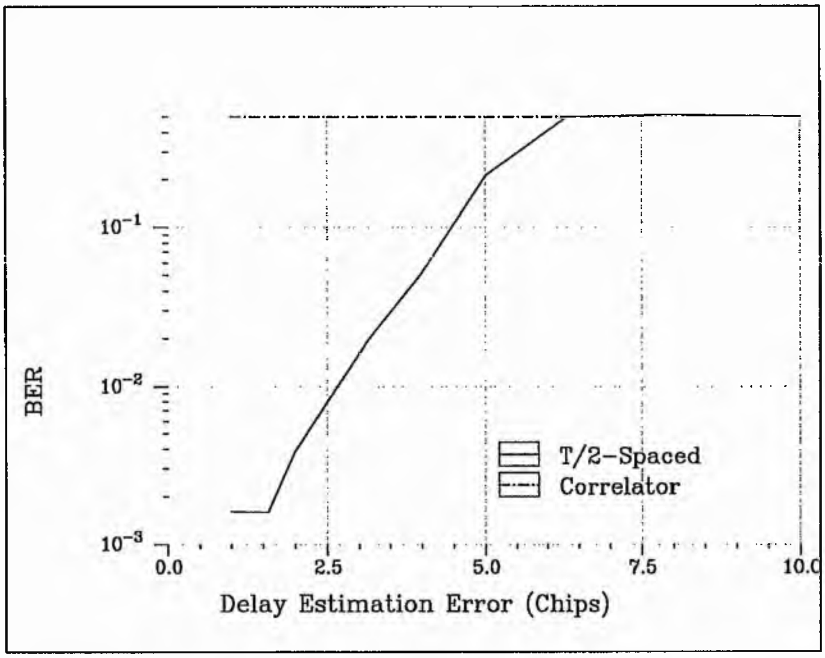

Figure 5.28: Effect of Incorrect Delay Estimation on the Performance of Linear LMS Canceller, AWGN Channel, $E_b/N_0 = 7$ dB

5.7 AUTONOMOUS MULTIPATH DIVERSITY RECEPTION

The multipath fading channel used in the simulations for the comparison between RAKE and SISO MMSE receivers is shown in Fig.5.29. The channel consists of a number of equal average power paths. This selection of this channel was made on the grounds that it offers maximum multipath diversity advantage for the RAKE receiver while it is a worst case channel for the MSE-minimizing detectors under consideration. The multipath delays are equally placed on multiples of the delay $D1$. The delay $D1$ is set to be equal to twice the chip duration T_c.

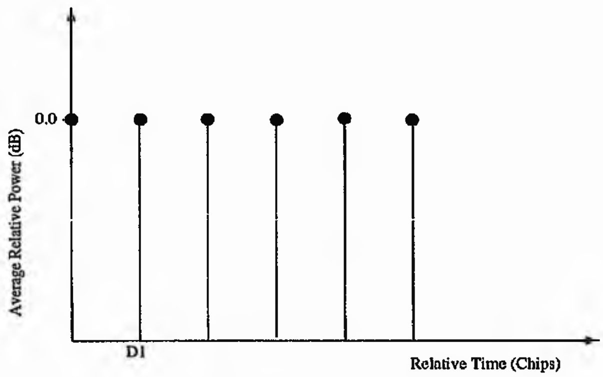

Figure 5.29: Channel Impulse Response Used In Simulations for Multipath Fading Channels

The RAKE receiver simulated in this paper has 4-fingers ($D = 4$) for the $L = 6$ path channel and 3-fingers ($D = 3$) for the $L = 3$ path channel. The latest case $L/D = 1$, represents the full RAKE condition, ie. gives the best possible performance of the RAKE receiver. Gold codes of lengths 31 and 7 have been used for this simulation. The 31 chips per bit case has been selected for the $L = 6$ path channel, while the 7 chips/bit case has been selected for the $L = 3$ path channel. As can be concluded from the curves of Fig.5.31 and Fig.5.32 the FS-DFE offers improved performance compared to the RAKE receiver and interesting enough the performance gain increases as the loading of the equivalent system, defined as the number of paths divided by the spreading factor, increases.

These results indicate that FS-DFE *without explicit estimation of the path delays* is able to combine multiple paths into a decision statistic of similar or better quality as compared to RAKE receivers.

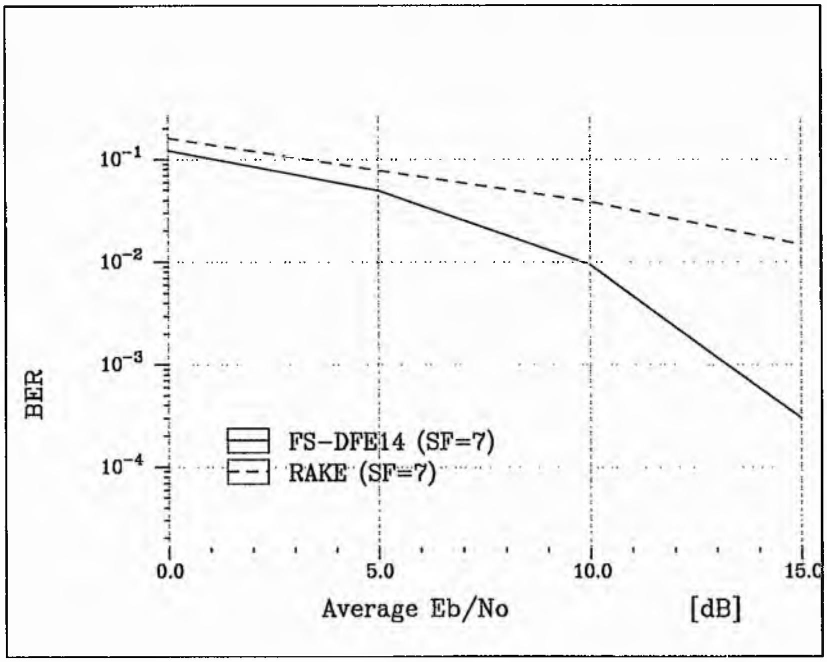

Figure 5.30: Performance Comparison Between LFSE and RAKE Receiver in L=3 Path Fading Channel, N=7

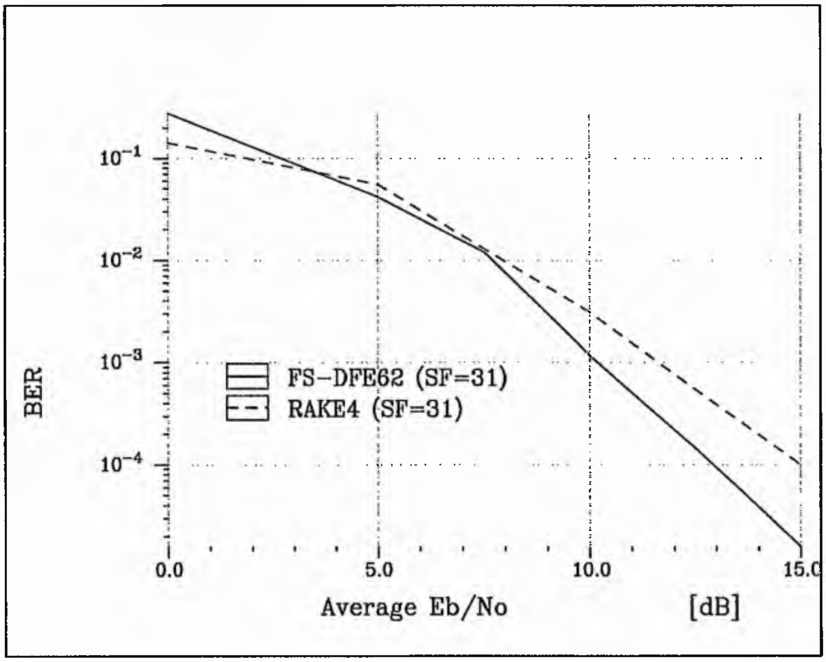

Figure 5.31: Performance Comparison Between FS-DFE and RAKE Receiver in L=6 Path Fading Channel, N=31

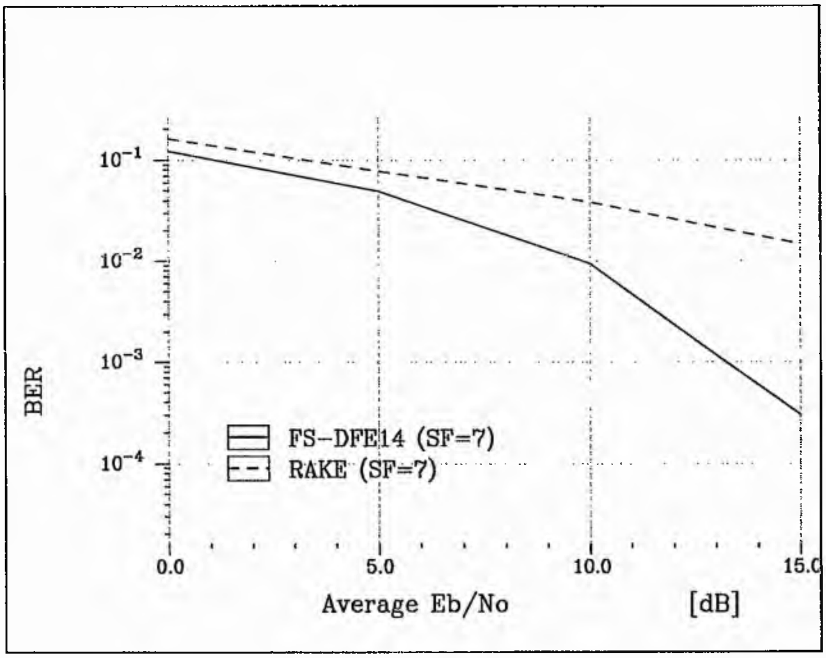

Figure 5.32: Performance Comparison Between FS-DFE and RAKE Receiver in L=3 Path Fading Channel, N=7

5.8 CONCLUSIONS

The conclusions of this work can be summarised as follows:

- We have shown by simulation that the LFSE is able, without the knowledge of interfering spreading sequences, to provide significant gains as compared to the conventional detector in a wide range of near-far scenarios. MMSE detectors that can adaptively, without using the spreading sequences of interfering users, mitigate time invariant as well as time-variant near-far interference. Even if the interference is not of near-far nature, the LFSE/FS-DFE detectors offer significant gains in spectral efficiency compared to the conventional detector.
- The MSE-minimising detectors with fractionally spaced feedforward filter is able to exploit multipath diversity acting as a RAKE combiner in multipath fading channels. The exploitation of multipath diversity is autonomous, ie. it does not depend on other signal processing blocks of the receiver as it is the case with RAKE receivers. This is particularly suitable feature for rapidly varying channels where non only the power control is troublesome but also, even under ideal power control, the performance of the delay power spectrum and channel estimation units degrade significantly, leading to severe degradation of the RAKE receiver's performance.

Chapter 6

MYTHS AND REALITIES OF CHANNEL CODING

6.1 INTRODUCTION

The end-to-end link performance is determined by the performance of devices that execute (1) signal processing tasks and (2) channel decoding tasks. A discussion on advanced CDMA receiver architectures would be incomplete if one concentrated on the merits of the former only. This is particularly true in CDMA systems where the role of channel coding has been the hot topic in much recent research correspondence. This chapter attempts to establish arguments that answer as fully as possibly the dispute about the role of channel coding in CDMA systems. Is channel coding more beneficial than pseudonoise spreading and what is the optimum channel code rate ? Is the gain from an increased Forward Error Correction (FEC) capability larger than the gain offered by the multipath diversity ?

We try to provide a unified treatment of channel coding by examining all the possible scenarios of applying channel coding technology in the CDMA radio interface. In section 6.2 we revisit the myth, which relates the channel coding with performance losses due to decrease in the effective spreading factor. In section 6.3 we start formalising one of the two conflicting arguments by evaluating both analytically and by simulation the performance of low rate convolutional coding. In section 6.4 we formalise the opposite argument by evaluating the performance of trellis coded CDMA systems. In the latter, channel coding is combined with modulation without the spectral expansion experienced by convolutionally coded signals. Section 6.5 compares all the possible coding scenarios and draws conclusions about the effectiveness of each technique. Finally, in section 6.7, we present a radio interface architecture based on channel coding. The accommodation of multiple bit rates through changing the code rate is extensively treated.

6.2 AN OLD MYTH FOR CHANNEL CODING

Although the merits of channel coding in CDMA systems have been widely published, there are different views about how channel coding must be applied in spread spectrum transmission systems. The myth can be summarised as follows: Channel coding reduces the effective processing gain, thus reduces the ability of the receiver to handle multiple access interference and exploit the multipath diversity. This myth has been one of the most arguable points among researchers. In fact even during the writing of this thesis, there is no unified treatment of the subject due to the wide variety of channel coding schemes. However, a first step to the solution of the problem is by summarising all the possible FEC implementation scenarios of a CDMA radio interface. These are depicted in Fig.6.1.

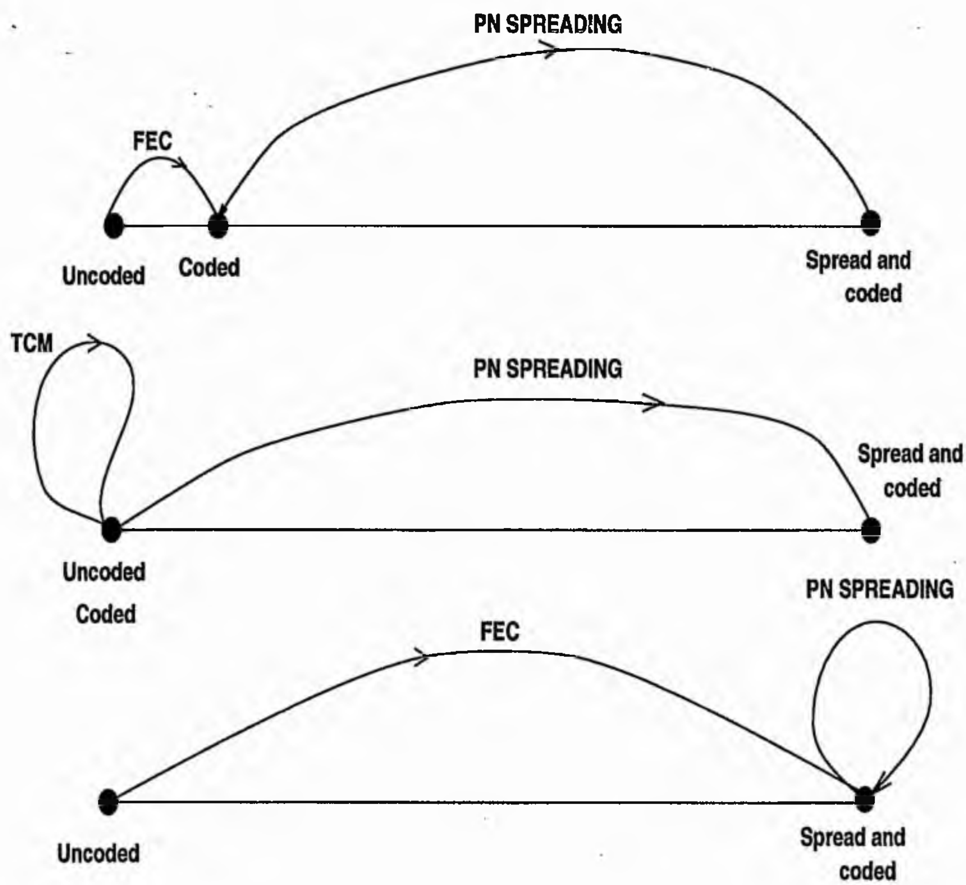

Figure 6.1: The Three Conflicting Arguments for the Role of Channel Coding

Each dot in the figure represents a different transmission rate. The first scenario uses Forward Error Correction (FEC) to transit the uncoded state to the coded state which is at a higher bit rate due to the added redundancy. With additional PN spreading a transition to the spread and coded state is achieved. This scheme is implemented in the IS-95 CDMA standard which uses 1/2 convolutional codes for FEC in the downlink direction. In the uplink, a concatenated scheme with 1/3 convolutional and orthogonal block codes based on (64,64) Hadamard matrix is employed.

The alternative scenario is to use Trellis Coded Modulation (TCM) and transit from the uncoded state to the coded state with no bandwidth expansion. Then, PN sequences are used to spread the coded signal over the whole available bandwidth. This technique has been proposed by the European Space Agency (ESA).

The third scenario follows a completely different direction. It has been proposed by [60] and uses LOw Rate Orthogonal Convolutional (LOROC) codes to spread the signal over the whole bandwidth. In this case, the PN sequences are superimposed to the LOROC coded signal without causing further spreading. They just randomise the coded signal with respect to the transmission from other users. This scheme has been expanded to a non-binary alternative by [2] while a multirate extension of this proposal has been the subject of [38]. By relaxing the requirement for orthogonal codewords, this scenario is open to the use of coding schemes other than LOROC codes.

In the next sections we investigate all three scenarios which are subsequently compared under the same channel and interference conditions. Although this investigation has been also the subject of [3], the authors confined their scope to AWGN channels. Also, [18] of ESA has evaluated the performance of a synchronous trellis coded CDMA system in the static line-of-sight channel. However static channel conditions, although used extensively in the modeling of very slow fading conditions (satellite channels), they can not be used for the performance evaluation in terrestrial systems.

6.3 LOW RATE CONVOLUTIONAL CODES

In this section we start our investigation with the treatment of low rate convolutional codes. The aim is to identify the optimum code rate of the convolutional encoder mostly for Rayleigh fading channels. For a comprehensive review of convolutional coding and decoding the reader is referred to [29],[54]. In order to be as complete as possible, all the low rate convolutional codes are treated, namely, the orthogonal, optimal free distance and spread convolutional codes.

6.3.1 Low Rate Orthogonal Convolutional Codes

Low Rate Orthogonal Convolutional codes have been proposed by [60] for implementing the function of both the channel encoder and the bandwidth spreader in CDMA systems. The produced codewords are actually rows of a Hadamard matrix ie. they are orthogonal with one another. The block diagram of an orthogonal convolutional encoder is shown in Fig.6.2.

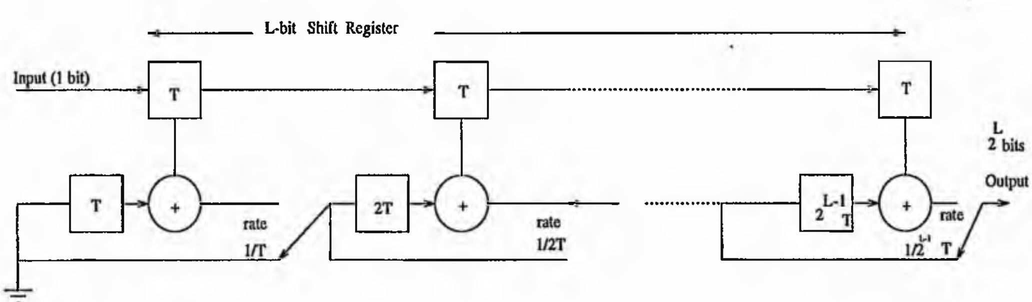

Figure 6.2: Low Rate Orthogonal Convolutional Encoder

A single bit at the input produces $n = 2^L$ output symbols, L being the constraint length, which means that the code rate is,

$$r = 2^{-L}, L \geq 3 \tag{6.1}$$

The encoding circuit consists of two shift registers. The lower shift register comprises the block orthogonal encoder, based on Hadamard matrices, producing codewords with constant weight equal to n/2 and a minimum distance of $d_{min} = n/2$. This register is shifted at the chip (coded symbol) rate. The other shift register is the convolutional register that is shifted at the bit rate. The decoding of LOROC codes is divided into two stages. The first is the Green machine [23] which computes integer symbols as described subsequently. These integer symbols are then converted to binary ones and are fed to a standard Viterbi decoder.

Green Machine Implementation The Green machine computes integer metrics that corresponds to the Hadamard matrix rows determined by the encoding operation.The Green machine, also known as serial orthogonal decoder, is a multistage structure. Each of the stages has the layout depicted in Fig.6.3.

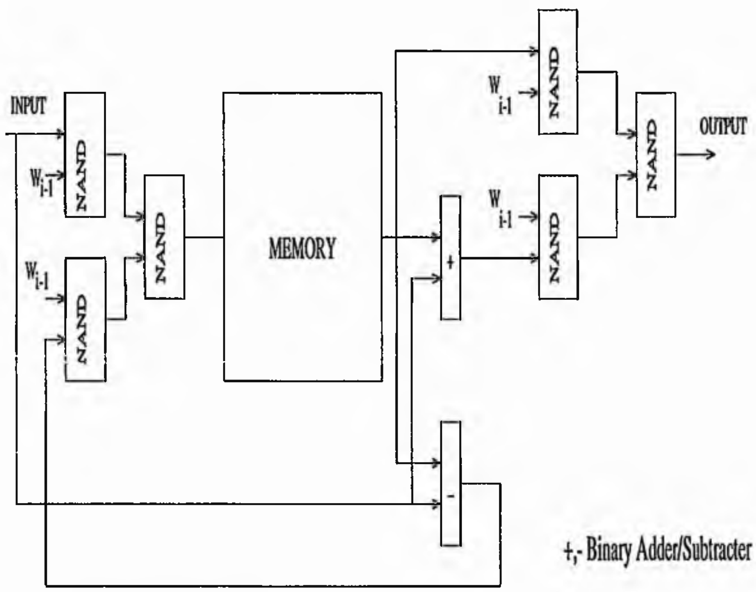

Figure 6.3: Single Stage of the Green Machine

The w_{i-1} inputs are connected to a binary counter which at the beginning of the decoding process has a start-up value of 1 and advanced by 1 as soon as a new symbol is passed to the input. The Green machine is constructed by cascading a number of these stages. The number of stages is given by the order of the Hadamard matrix whose codewords have been used during the spreading process. For example, if a LOROC coder with the code rate of 1/n has been used for spreading, then the Green decoder will consist of $log_2(n)$ stages. The memory size for the ith stage stage will be $2^{i-1}m$, where m is the symbol word length. Details on the hardware implementation of the Green machine have been provided to the author by [6]. The decoder produces the weighting matrix $\mathbf{y}$ such that,

$$\mathbf{y} = \mathbf{H}^n \mathbf{x} \tag{6.2}$$

where $\mathbf{x}$ is the sampled input matrix and $\mathbf{H}^n$ is the Hadamard matrix of order n that has been used in the encoder. The output of the Green machine will be then processed by a symbol generator which by processing the 2^n outputs will finally generate an integer metric to be processed by the Viterbi decoder.

The performance of LOROC encoded CDMA signals is dictated by the parameters of the code as given in Table 6.1.

Rate	Free Distance	Asympt. Coding Gain (ACG)
2^{-L}	$L\ 2^{L-1}$	$L/2$

Table 6.1: Parameters of LOROC Codes, $L \geq 3$

An upper bound on bit error probability is given by [62],

$$P_b < \frac{e^{-(L-1)\frac{E_b}{2N_0}}}{\left(1 - 2e^{-\frac{E_b}{2N_0}}\right)^2} \tag{6.3}$$

This upper bound has been plotted in Fig.6.4 for L=6. For the exact evaluation of bit error probability a simulation model has been developed. The model comprised a LOROC coded QPSK transmission/reception system in an AWGN channel. The results obtained from the simulation are shown in Fig.6.5.

Further bit error rate evaluations of LOROC encoded signals can not be justified at this point since other types of low rate convolutional codes may perform better. To this direction also points the fact that the input to the Viterbi decoder consists of a stream of integer symbols. Thus, the decoder can not exploit the soft-information and hard-decision decoding is performed which is associated with a 2-dB SNR/bit loss compared to the performance of hard decision decoding.

6.3.2 Low Rate Optimal Free Distance Convolutional (LOROFDC) Codes

We consider now Optimal Free Distance (OFD) convolutional codes and their performance in AWGN and Rayleigh Fading channels. Generation polynomials for low rate OFD convolutional codes are widely tabulated in many textbooks eg. [47]. Table 6.2 summarises the generator polynomials and free distance of the codes used in this thesis for rates down to 1/8.

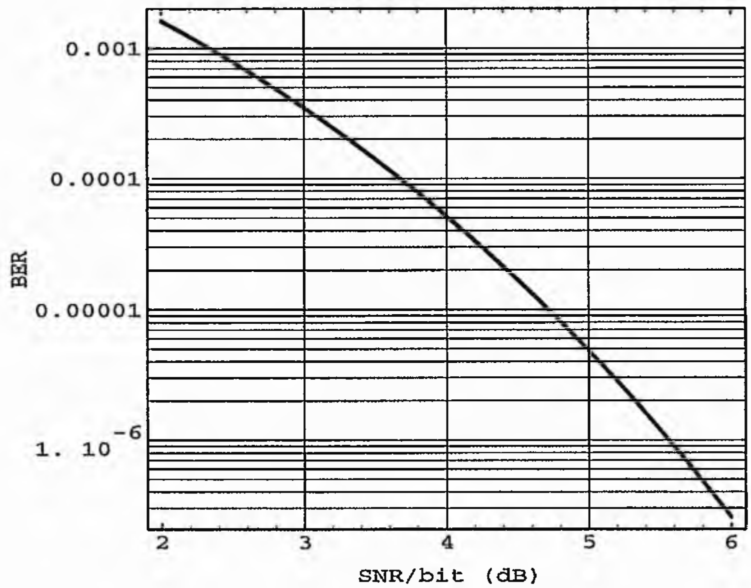

Figure 6.4: Performance Upper Bound of LOROC r=1/64 Code in AWGN

Rate	Generators	Free Distance
1/2	133o,171o	10
1/4	135o,135o,147o,163o	20
1/8	153o,111o,165o,173o 135o,135o,147o,137o	40

Table 6.2: Rate 1/n Optimal Free Distance Codes
,with the generator polynomials given in octal.

The performance of OFD low rate convolutional codes in the AWGN channel can be predicted by using the following formula mentioned in [47].

$$P_b < \frac{1}{2}\left(erfc\left(\sqrt{d_{free} r \frac{E_b}{N_0}}\right)\right) exp\left(d_{free} r \frac{E_b}{N_0}\right) \frac{\partial T(D,I)}{\partial I} | I = 1, D = e^{-r\frac{E_b}{N_0}} \qquad (6.4)$$

where $T(D,I)$ is the transfer function of the code, d_{free} denotes the free distance and r the code rate. By using the derivatives of the transfer functions of the rate 1/2,1/4 and 1/8 convolutional codes the graphs of Fig.6.6 have been produced.

The performance has also been predicted using Monte-Carlo simulation. The later is mandatory in Rayleigh fading case for which we have assumed a memoryless fading (ideal interleaving) channel. The results can be seen in Fig.6.7 for the AWGN and in Fig.6.8 for the fading case.

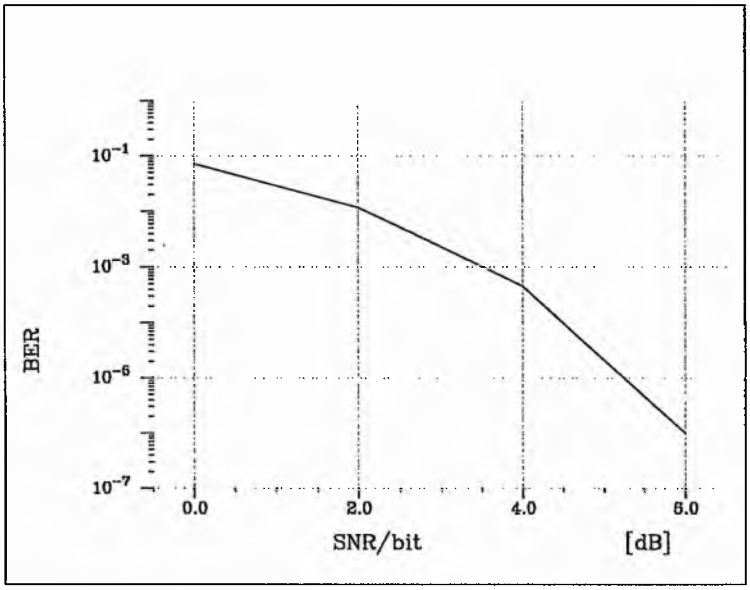

Figure 6.5: Simulated BER of LOROC r=1/64 Code in AWGN

6.3.3 Low Rate Spread Convolutional (LORSC) Codes

Research on LORSC codes has been motivated by [5]. This publication points to the direction on using low rate codes to overcome jamming in Gaussian channels. Here we first evaluate LORSC coding on spread spectrum unjammed communications for both Gaussian and fading channels and later we treat LORSC codes on multiple access "jammed" systems. The low rate spread convolutional codes can be generated and decoded as shown in Fig.6.9. The mother code has been chosen to be the optimal free distance 1/2 convolution code. The code symbols produced by the mother code are then repeated 2 times to get a rate 1/4 code or repeated 4 times to get a rate 1/8 code.

The decoding operation is a two stage process. The codewords are first "despread" with an integrate and dump filter lifting the rate back to the original 1/2. Then ordinary Viterbi decoding follows. The performance of LORSC codes has been evaluated for both AWGN and Rayleigh channels. Fig.6.10 and Fig.6.11 depict the Monte-Carlo simulation results for the two channels under consideration.

Based on the results presented so far we can now proceed with a comparison of low rate convolutional codes which will identify the best low rate convolutional code both in terms of performance and in terms of decoding complexity.

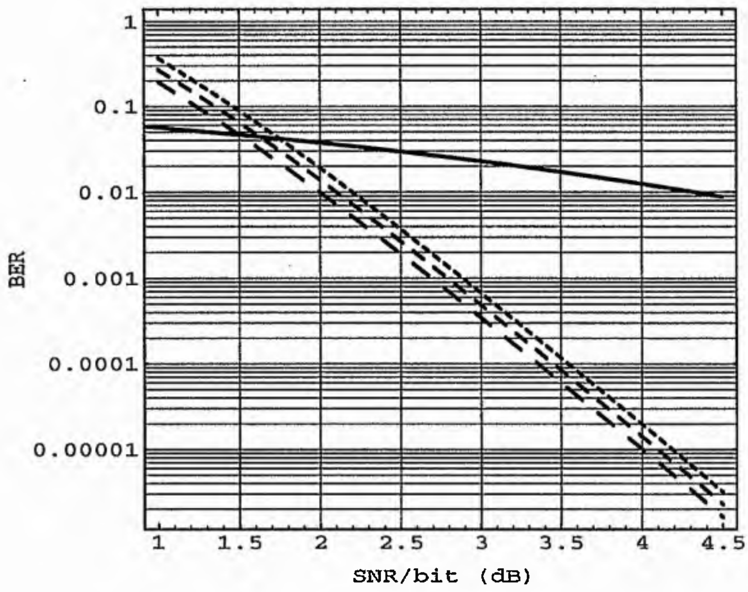

Figure 6.6: Upper Bounds on Performance of LOROFDC Codes in AWGN, (—) Uncoded, (- -) 1/2, (– –) 1/4, (— —) 1/8.

6.3.4 Best Low Rate Convolutional Codes

A comparison among the convolutional coding schemes presented so far must be made under the criterion of equal decoding complexity. This depends on the number of states for the Viterbi decoder that are given by the equation,

$$N_s = 2^{L-1} \tag{6.5}$$

where L is the constraint length. The number of states N_s corresponds to the number of add, compare and select (ACS) circuits which carry out addition of branch metrics, compare branch metrics and select one of the paths as a survivor.

In terms of decoding complexity, LOROC, LOROFDC and LORSC codes, under the assumption of equal constraint length, have the same decoding complexity. However, LORSC codes have the edge in a flexible provision of variable code rates. This is because the Viterbi decoder is the same for all rates. Thus, the widely available rate 1/2 Viterbi decoder chip can be used to implement the channel decoder for all possible code rates. This is an important feature especially in cases where channel coding is used to accommodate multiple bit rates in a CDMA radio interface.

The performance of LORSC codes in AWGN channels has been also studied, in terms of ACG, in [51] where convolutional codes like uniform, orthogonal and super-orthogonal were also treated. In [51] LORSC codes are found to offer higher ACG than LOROC

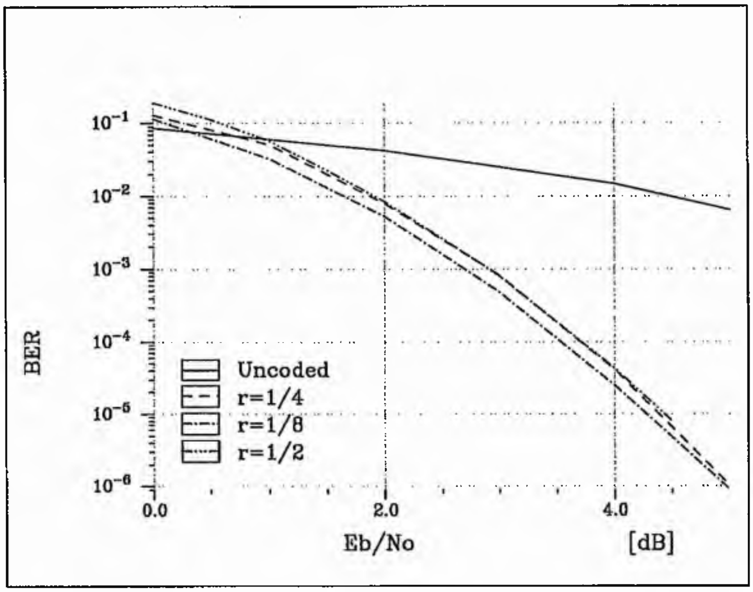

Figure 6.7: Performance of LOROFDC Codes in the AWGN Channel, Simulation

and super-orthogonal codes. In [52] the author was supplied with additional information regarding the performance of LOROC codes which agree with the simulation results of Fig.6.5. Prompted by these results we concentrate hereafter on comparing LOROFC and LORSC codes. Tables 6.3 and 6.4 summarise the coding gain for the LORSC and LOROFDC codes as has been predicted by the simulation results. The target BER for the comparison was selected to be 10^{-3}.

Code	Rate	E_b/N_0 (dB)	Gain (dB)
LOROFDC	1/2	3.0	3.8
	1/4	3.0	3.8
	1/8	2.8	4.0
LORSC	1/2	3.0	3.8
	1/4	3.0	3.8
	1/8	2.8	4.0

Table 6.3: Comparison of 64-State Low Rate Convolutional Codes in AWGN Channel

As can be clearly seen from these tables, the performance of LOROFDC and LORSC codes is identical to AWGN channel while LORSC codes perform better in Rayleigh fading channel for lower than 1/2 code rate. The net SNR/bit gain for the LORSC 1/8 code rate over the LOROFDC 1/8 code is found to be 0.5 dB at the 0.1% BER.

Up to now the simulation approach has been used extensively for the evaluation of convolutionally coded systems. However in order to validate our findings we need the

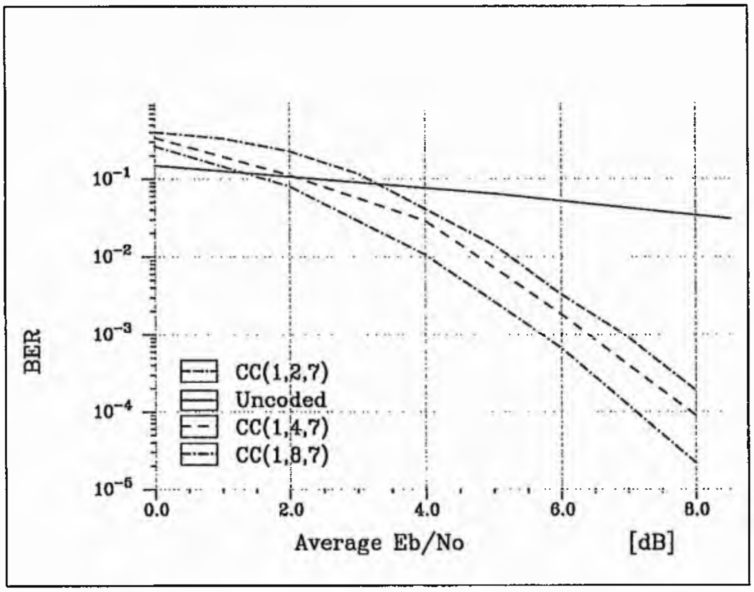

Figure 6.8: Performance of LOROFDC Codes in Rayleigh Fading Channel, Simulation

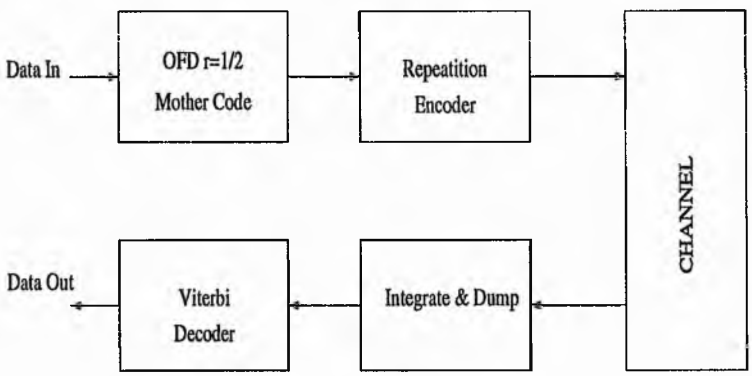

Figure 6.9: Encoding and Decoding of LORSC Codes

support of analytical tools. In the next section we establish a mathematical framework that will permit more formal means of comparisons for low rate convolutional codes.

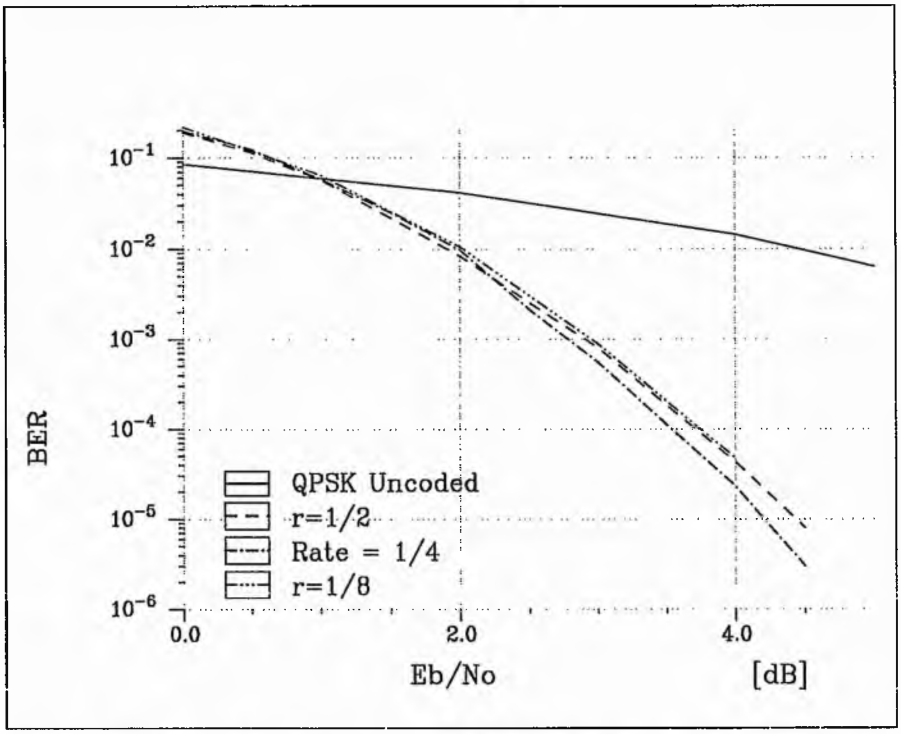

Figure 6.10: Simulated Performance of LORSC Codes in the AWGN Channel

Code	Rate	E_b/N_0 (dB)	Gain (dB)
LOROFDC	1/2	7.0	17.0
	1/4	6.5	17.5
	1/8	5.5	18.5
LORSC	1/2	7.0	17.0
	1/4	5.9	18.1
	1/8	5.0	19.0

Table 6.4: Comparison of 64-State Low Rate Convolutional Codes in Independent Rayleigh Fading Channel

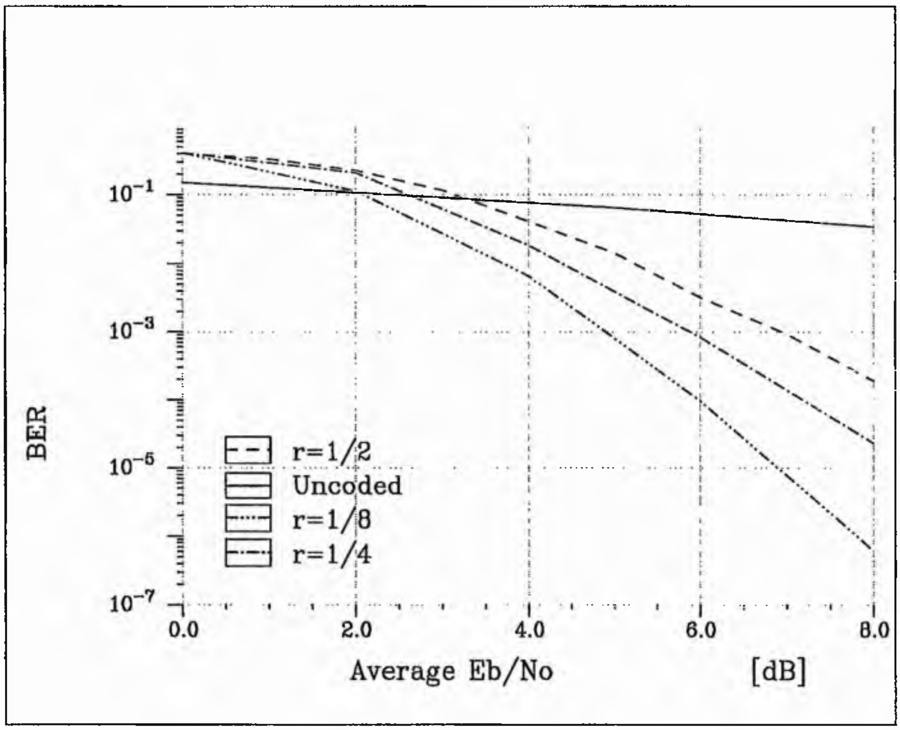

Figure 6.11: Simulated Performance of LORSC Codes in the Rayleigh Fading Channel

6.3.5 Performance Analysis of Convolutionally Encoded CDMA Systems

The performance of convolutionally encoded CDMA systems can be evaluated by employing the transfer function bound technique[3]This technique involves the calculation of the pairwise errors using the Chernoff bound and summing over all possible error patterns using the union bound. Let $\mathbf{X} = (x_1, x_2, ..., x_M)$ denote the channel input coded sequence of length M and $\mathbf{Y} = (y_1, y_2, ..., y_M)$ denote the channel output sequence. Since the channel introduces errors, $\mathbf{Y} \neq \mathbf{X}$. From the state transition diagram of the convolutional code, a transfer function can be calculated, the general form of which is,

$$T(D, I) = \sum P(\mathbf{X}) I^{d(\mathbf{X},\hat{\mathbf{X}})} P(\mathbf{X} \rightarrow \hat{\mathbf{X}}) \tag{6.6}$$

where the sum is taken over all error events. $P(\mathbf{X})$ is the probability of transmitting $\mathbf{X}$, $d(\mathbf{X}, \hat{\mathbf{X}})$ is the distortion measure ie. the number of bit errors made by choosing $\hat{\mathbf{X}}$ instead of $\mathbf{X}$.Finally, $P(\mathbf{X} \rightarrow \hat{\mathbf{X}})$ is the pairwise error event probability ie. the probability that the incorrect sequence $\hat{\mathbf{X}}$ is decoded instead of the correct sequence $\mathbf{X}$. It is well known that the bit error probability can be bounded by,

$$P_b \leq \frac{1}{n} \frac{\partial \bar{T}(D, I)}{\partial I} \Big|_{\text{I} = 1} \tag{6.7}$$

where the transfer function bound has been averaged over the multiple access interference as is indicated by the over-bar.

From the above discussion it is apparent that for the evaluation of the performance of convolutionally encoded CDMA systems, a relationship that provides the pairwise error probability is required. This pairwise error between any two events can be bounded using the Chernoff bound which is defined as,

$$P(\mathbf{X} > 0) < E[exp(\lambda \mathbf{X})] \tag{6.8}$$

where λ is the Chernoff bound parameter.

At time instant p, the channel output signal can be written as the sum of the channel input signal and two distortive terms,

$$Y_p = X_p + Z_p + n_p \tag{6.9}$$

where Z_p denotes the multiple access interference term and n_p the background noise term. The pairwise error event probability depends on the type of the channel. Two type of channels have been studied,namely the AWGN and the Rayleigh fading channel.

AWGN Channel

As has already been mentioned in Chapter 3, the output of the correlator of the user of interest (user 1) during the pth time instant, can be written as,

$$y_1^p = \sqrt{E_s} b_0^1 + \sqrt{E_s} \sum_{k=2}^{K} [b_{-1}^k R_{k,1}(t_p) + b_0^k \hat{R}_{k,1}(t_p)] cos(\phi_k - \phi_1) + n_p \tag{6.10}$$

where b_0^1 is the bit of the 1st user, n_p is a sample of Gaussian noise of variance N_0 and the functions $R_{k,m}$ and $\hat{R}_{k,m}$ have been defined as the continuous time partial crosscorrelation functions of the kth and the mth spreading codes.

The term Z_p in for the AWGN channel is equal to,

$$Z_p = \sqrt{E_s} \sum_{k=2}^{K} [b_{-1}^k R_{k,1}(t_p) + b_0^k \hat{R}_{k,1}(t_p)] cos(\phi_k - \phi_1) \tag{6.11}$$

It is evident that the transmission of the sequence $\mathbf{X}$ will be interfered by a sequence $\mathbf{Z} = (Z1, Z_2, ..., Z_M)$ denoting the multiple access interference. Assuming the optimum metric for the AWGN channel, conditioning on the sequence of multiple access interference $\mathbf{Z}$, and applying the Chernoff bound, one obtains,

$$P(\mathbf{X} \rightarrow \hat{\mathbf{X}} | \mathbf{Z}) \leq \prod_{p \epsilon \nu} E \; \{exp[\; \lambda(|Y_p - X_p|^2 - |Y_p - \hat{X}_p|^2)] \; \} \tag{6.12}$$

in which ν is a set of p such as that $X_p \neq \hat{X}_p$. The last equation can be simplified giving,

$$P(\mathbf{X} \rightarrow \hat{\mathbf{X}} | \mathbf{Z}) \leq \prod_{p \epsilon \nu} E \; \{exp[\; \lambda(|X_p|^2 - |\hat{X}_p|^2 - 2Re\{Y_p(X_p - \hat{X}_p)^*\})] \; \} \tag{6.13}$$

Substituting to the last equation the Y_p term with the equivalent (6.9) we get,

$$P(\mathbf{X} \rightarrow \hat{\mathbf{X}} | \mathbf{Z}) \leq \prod_{p \epsilon \nu} E \; \{exp[\; \lambda(|X_p|^2 - |\hat{X}_p|^2 - 2Re\{(X_p + Z_p + n_p)(X_p - \hat{X}_p)^*\})] \; \} \tag{6.14}$$

Finally after some mathematical manipulations,

$$\begin{aligned} & P(\mathbf{X} \rightarrow \hat{\mathbf{X}} | \mathbf{Z}) \leq \\ & \quad \Pi_{p \epsilon \nu} \; exp[\; (-\lambda E_s |x_p - \hat{x}_p|^2) \; E\{exp[-2\lambda \sqrt{E_s} Re\{n_p(x_p - \hat{x}_p)^*\})] \; \} \\ & \qquad\qquad E\{exp[-2\lambda E_s Re\{z_p(x_p - \hat{x}_p)^*\})] \; \} \end{aligned}$$

Assuming the Gaussianity of multiple access interference we can evaluate the expectation with respect to z in the last equation as follows,

$$E\{exp[-2\lambda E_s Re\{z_p(x_p - \hat{x}_p)^*\}]\} \approx exp(2\lambda^2 E_s^2 \sigma_z^2 |x_p - \hat{x}_p|^2) \tag{6.15}$$

where σ_z^2 is the variance of multiple access interference in the I or Q channels. By replacing the last equation into (6.15), we finally have the expression of the pairwise error probability expressed in terms of λ, noise variance and the variance of z,

$$P(\mathbf{X} \to \hat{\mathbf{X}}|\mathbf{Z}) \leq \prod_{p \epsilon \nu} exp\{-\lambda(1 - 2\lambda(N_0/2 + \sigma_z^2 E_s))E_s|x_p - \hat{x}_p|^2\} \tag{6.16}$$

Optimizing the last equation with respect to the Chernoff parameter λ gives,

$$\lambda_{opt} = \frac{1}{4(N_0/2 + \sigma_z^2)} \tag{6.17}$$

We can then write down the pairwise error event probability as,

$$P(\mathbf{X} \to \hat{\mathbf{X}}|\mathbf{Z}) \leq \prod_{p \epsilon \nu} exp\{-\frac{|x_p - \hat{x}_p|^2 \frac{E_s}{N_0}}{4(1 + \frac{2(K-1)}{3N}\frac{E_s}{N_0})}\} \tag{6.18}$$

Expressed in terms of E_b/N_0 the last equations can be written,

$$P(\mathbf{X} \to \hat{\mathbf{X}}|\mathbf{Z}) \leq \prod_{p \epsilon \nu} exp\{-\frac{|x_p - \hat{x}_p|^2 \frac{rE_b}{N_0}}{4(1 + \frac{2r(K-1)}{3N}\frac{E_b}{N_0})}\} \tag{6.19}$$

where r is the convolutional code rate.

Rayleigh Fading Channel

The output of the correlator of the user of interest (user 1) during the pth time instant, can be written as,

$$y_1^p = A_p^1 \sqrt{E_s} b_0^1 + \sum_{k=2}^{K} A_p^k cos(\phi_p^k - \phi_p^1)[b_{-1}^k R_{k,1}(t_p) + b_0^k \hat{R}_{k,1}(t_p)] + n_p \tag{6.20}$$

The decision statistic consists of the faded symbol of interest interfered by the multiple access term which is given by,

$$Z_p = \sum_{k=2}^{K} A_p^k cos(\phi_p^k - \phi_p^1)[b_{-1}^k R_{k,1}(t_p) + b_0^k \hat{R}_{k,1}(t_p)] \tag{6.21}$$

Considering a perfect knowledge about the channel state information (CSI),

$$P(\mathbf{X} \rightarrow \hat{\mathbf{X}}|A) \leq \prod_{p\epsilon\nu} exp\{(-\lambda A_p^2 E_s(x_p - \hat{x}_p)^2(1 - 2\lambda(N_0/2 + \sigma_z^2))\} \tag{6.22}$$

Optimizing the last equation over the Chernoff parameter yields,

$$\lambda_{opt} = \frac{1}{4(N_0/2 + \sigma_z^2)} \tag{6.23}$$

By substitution of this optimal λ gives the conditional pairwise error probability,

$$P(\mathbf{X} \rightarrow \hat{\mathbf{X}}|A) \leq exp\{-\frac{1}{8(N_0/2 + \sigma_z^2)} \sum_{p\epsilon\nu} A_p^2 |x_p - \hat{x}_p|^2\} \tag{6.24}$$

Averaging over the probability density function of A_p (Rayleigh distribution), results to the unconditional pairwise error event probability,

$$P(\mathbf{X} \rightarrow \hat{\mathbf{X}}) \leq exp\{-a \sum_{p\epsilon\nu} a^{-1} ln(1 + a|x_p - \hat{x}_p|^2) \tag{6.25}$$

with,

$$a = \frac{\frac{rE_b}{N_0}}{4\left(1 + \frac{2r(K-1)}{3N}\frac{E_b}{N_0}\right)} \tag{6.26}$$

Further simplification leads to the final expression for the single path Rayleigh fading channel,

$$P(\mathbf{X} \rightarrow \hat{\mathbf{X}}) \leq \prod_{p\epsilon\nu} \left[1 + \frac{|x_p - \hat{x}_p|^2 \frac{rE_b}{N_0}}{4\left(1 + \frac{2r(K-1)}{3N}\frac{E_b}{N_0}\right)}\right] \tag{6.27}$$

With the knowledge of the pairwise error probability for the AWGN and Rayleigh fading channels, we can now: (1) justify the simulation results presented so far and (2) identify the trade-off between the channel coding and PN spreading.

6.3.6 Tradeoff Between Channel Coding and PN Spreading

Let's have a more critical view at the pairwise error probability of convolutional encoded CDMA systems. For the AWGN channel, the *asymptotic* pairwise probability can be easily derived from equation (6.19) as,

$$P(\mathbf{X} \rightarrow \hat{\mathbf{X}}|\mathbf{Z}) \leq \prod_{p\epsilon\nu} exp\{-\frac{d_f(1/n)\frac{(1/n)E_b}{N_0}}{4(1 + \frac{2(1/n)(K-1)}{3N}\frac{E_b}{N_0}}\} \tag{6.28}$$

Similarly, for the Rayleigh fading channel, the asymptotic pairwise probability can be derived from equation (6.27) as,

$$P(\mathbf{X} \rightarrow \hat{\mathbf{X}}) \leq \left[1 + \frac{\frac{rE_b}{N_0}}{\left(1 + \frac{2r(K-1)}{3N}\frac{E_b}{N_0}\right)} \right]^{-d_{free}} \tag{6.29}$$

For a given decoding complexity (given L), the d_{free} of a 1/2n convolutional encoder is approximately twice the d_{free} is the 1/n code.

$$d_{free}(1/n) \cong \frac{1}{2} d_{free}(1/2n) \quad , n \geqslant 2 \tag{6.30}$$

If N_T is the total available spreading factor, then the spreading which is dedicated to PN sequences in a system employing $1/n$ convolutional codes is,

$$N = \frac{N_T}{n} \tag{6.31}$$

According to (6.31), every time the code rate is decreased the length of the code sequence has also to be decreased accordingly in order to keep the chip rate (bandwidth) constant. Equations (6.28) and (6.29) have been plotted in Fig.6.12 and Fig.6.13 respectively. From these figures we can make the following observations:

- By lowering the code rate the performance is relatively unaffected in AWGN channels while in Rayleigh fading channels we experience significant performance gains.
- The asymptotic behaviour of the pairwise error probability validates the bit error probability we have presented using Monte-Carlo simulation techniques.

For evaluating the performance advantages of low rate convolution codes in multiuser Rayleigh fading channels, a simulation model has been developed. The model uses LORSC codes with a rate 1/2 Optimal Free Distance convolutional code. The portions of the bandwidth which is dedicated to channel coding and to PN spreading are shown in Table 6.5. The total spreading factor is very close to 255.

Notice that channel coding and PN spreading act in a complementary fashion shifting the SNR/chip to the SNR/bit as indicated in Fig.6.14. However, as the coding rate decreases the despreader delivers increasingly noisy symbols to the decoder. It was shown analytically that not only the decoder can handle this increased input symbol error rate but also deliver a significant gain in Rayleigh fading channels. The simulation results

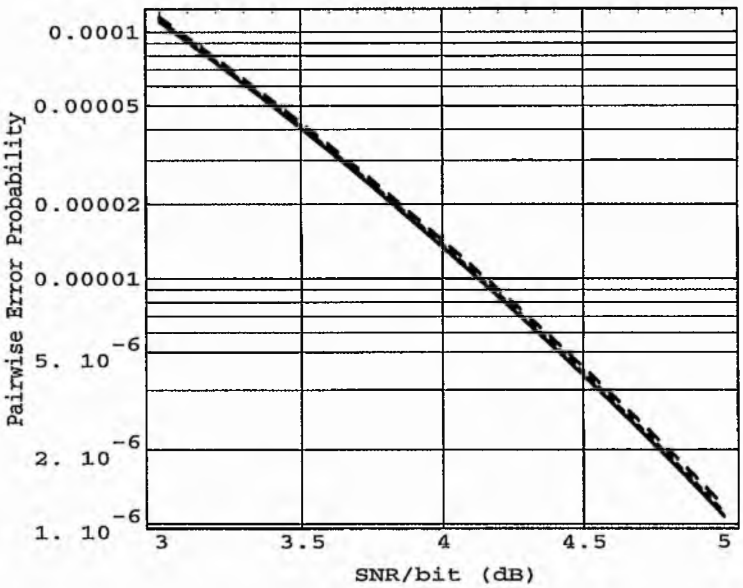

Figure 6.12: Trade-off Between PN Spreading Factor N and Channel Coding in AWGN, (—) r=1/2 N=63, (- -) r=1/4 N=31, (– –) 1/8 N=15

Code Rate	**PN Spreading Factor**
Uncoded	256
r=1/2	128
r=1/4	64
r=1/8	32
r=1/256	1

Table 6.5: Adjustment of PN Spreading Factor With Respect to Code Rate

of Fig.6.15 further enhance this view. Notice that the $r = 1/256$ case corresponds to the third implementation scenario (as outlined in section 6.2) where the total spreading factor is dedicated to channel coding.

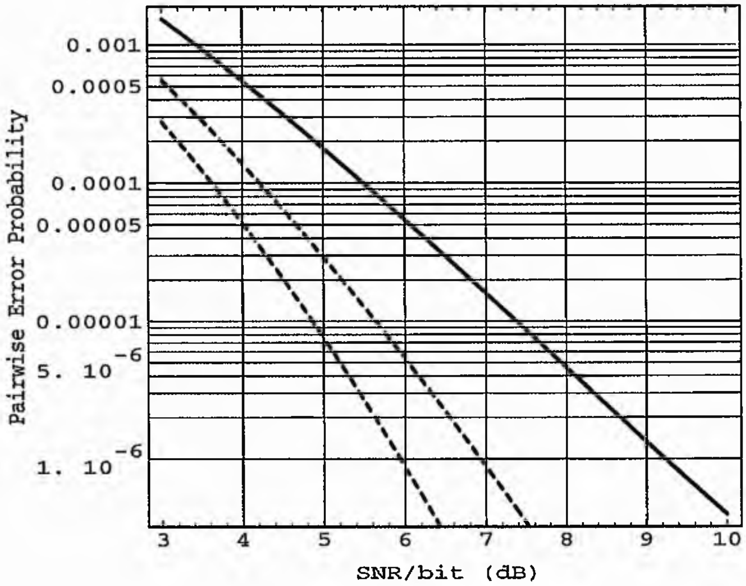

Figure 6.13: Trade-off Between PN Spreading Factor N and Channel Coding in Rayleigh Fading, (—) r=1/2 N=63, (- -) r=1/4 N=31, (– –) 1/8 N=15

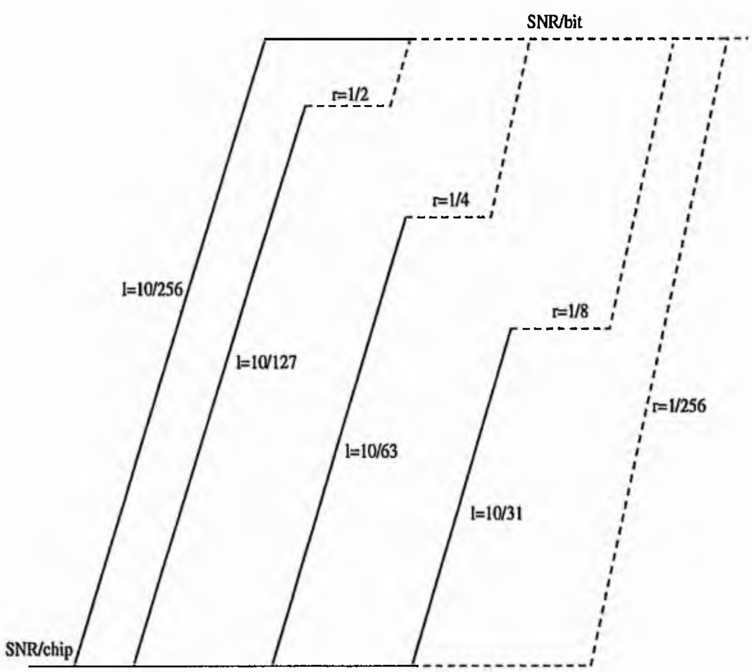

Figure 6.14: Increase of Effective System Loading l as Coding Rate r Decreases

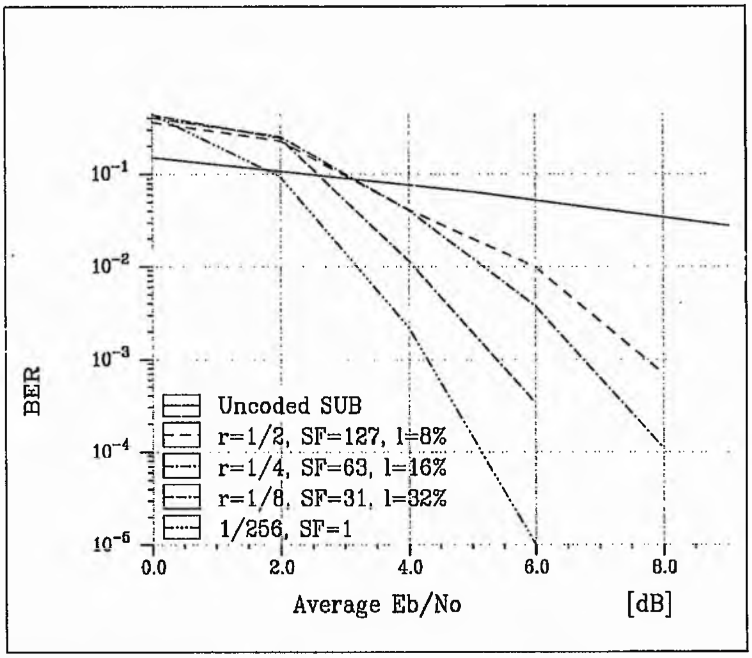

Figure 6.15: Performance of LORSC Codes in the Rayleigh Fading Channel, N=255, K=10, Coherent Demodulation

6.3.7 The Role of Channel Estimation

Up to now both by analysis and by simulation we have shown that it is beneficial to spread the signal by channel coding. However an important point was not taken into account in the analysis or in the Monte-Carlo simulations. This point is related the phase coherency assumption ie. the perfect knowledge of the channel variations. The phase coherency is related to the quality of the channel estimator. Since channel estimation is apparently performed before decoding, the performance of the estimator will be dictated by the input SNR/symbol which is related with the SNR/bit via the equation:

$$\frac{E_s}{N_0} = r\frac{E_b}{N_0} \tag{6.32}$$

The lower the code rate is, the lower the SNR at the input of the channel estimator. The effects of this SNR reduction for mobile radio systems has to be considered separately for the uplink and the downlink direction as follows:

- **Optimal Channel Code Rate in the Downlink:** In the downlink channel information is extracted from the pilot signal. Since the pilot channel is orthogonal to the traffic channels, the use of low rate codes will not influence the ability of the channel estimator to track the phase variations. Consequently, our conclusion that the optimal channel code rate will be significant smaller than the r=1/2 optimal free distance code rate found in the IS-95 digital cellular system should be adopted without much criticism.

- **Optimal Channel Code Rate in the Uplink:** In the uplink direction, as described in Chapter 3, we have to take into consideration the type of demodulation that is to be performed. Thus we can distinguish two cases, (1) Differential demodulation and (2) Coherent demodulation.

  1. In uncoded DPSK demodulation phase information is received from the state of the previous data bit. For coded transmissions, the lower the code rate is, the lower the E_s/N_0 ratio at the input of the differential decoder. Thus, for very low rates it is expected that the performance gain due to extensive channel coding will present a limit. We have investigated this issue by simulating the performance of a LORSC encoded Differential Balanced QPSK (DBQPSK) transmission system. The results are shown in Fig.6.16.

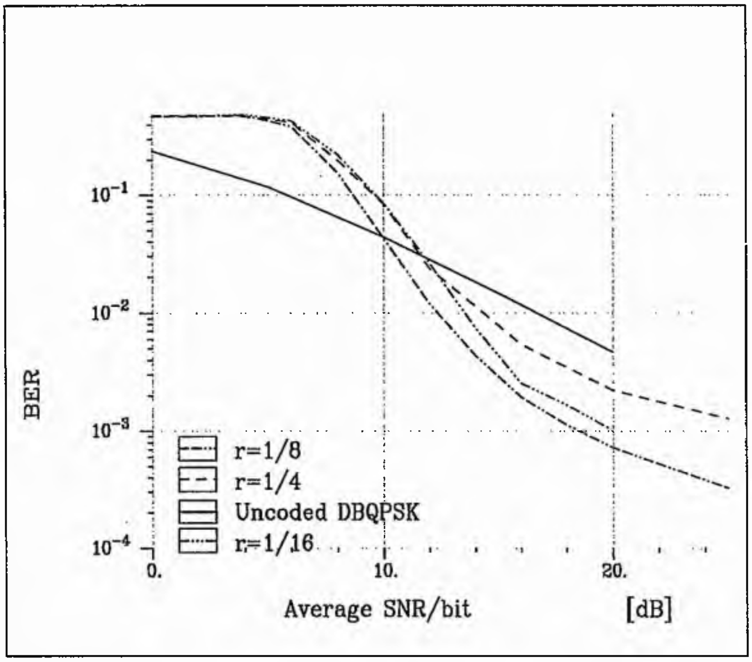

Figure 6.16: Performance of LORSC Codes in the Rayleigh Fading Channel, N=256, K=10, DBQPSK Demodulation

Code	Rate	E_b/N_0 (dB)	Coherency Loss (dB)
LORSC	1/2	-	-
	1/4	26.0	18.25
	1/8	18.0	12.5
	1/16	20.0	-

Table 6.6: Comparison of 64-State Low Rate Convolutional Codes in Multiuser Independent Rayleigh Fading Channel,K=10,N=256,Non-Coherent Demodulation

2. The possibility of coherent demodulation in the uplink based on information received from the control channel was extensively discussed in Chapter 3. In this case, the channel estimator will be completely independent of the relation of the E_b/N_0 and E_s/N_0 in the traffic channel. The performance in this case will be limited, as has been demonstrated in Chapter 3, from the post-decoder error rate of the control channel ie. the ability of the decoder to provide a training sequence which the channel estimator will base its estimates upon. It was shown that if the post-decoder error rate is $< 10^{-2}$ the degradation will be insignificant.

Up to now, we have extensively discussed the merits of using FEC spreading in CDMA systems. In the rest of this chapter we shall examine a different scenario by

Code	Rate	E_b/N_0 (dB)	Interference Loss (dB)
LORSC	1/2	7.75	0.75
	1/4	6.75	0.25
	1/8	5.5	0.0

Table 6.7: Comparison of 64-State Low Rate Convolutional Codes in Multiuser Independent Rayleigh Fading Channel,K=10,N=256, Coherent Demodulation

employing a well known concept which does not associate channel coding with bandwidth expansion.

6.4 TRELLIS CODED CDMA SYSTEMS

As we have seen in Chapter 3, the performance of the conventional detector even when it employs multipath diversity degrades significantly when the receiver suffers interference by other users. Under the assumption that the system loading is kept low enough so that there is no irreducible bit error rate, we can increase the transmission power (in effect the E_b/N_0 ratio) in order to achieve the target BER. However, the increase in the transmission power creates an increase in the interference experienced by the other users. Furthermore, the power controller may not allow this power increase for the sake of the rest of the users.

One solution to the problem is to employ channel coding which, as was made evident from the first part of this chapter, can reduce the required E_b/N_0 significantly compared to the uncoded case. The bandwidth is however increased by an amount equal to the reciprocal of the code rate. For a given available bandwidth, this increase should be accompanied by a decrease of the spreading caused by the PN coding. The only way to avoid this bandwidth expansion is to increase the number of points in the constellation.

For example, consider a rate 2/3 convolutionally coded QPSK. Compared to the uncoded QPSK the required bandwidth of the coded system is 3/2 times greater than the uncoded. This bandwidth expansion can be cancelled if one increases the signal points to 8-PSK. However this increase requires 4 dB greater E_b/N_0 to maintain the same error rate. This E_b/N_0 penalty must be overcome by employing coding with coding gain in excess of 4 dB. Simply cascading the encoder and the modulator this coding gain can not be achieved with moderate decoding complexity. Massey showed that rather than treating the coding and modulation as quite separate processes, they should be integrated by matching the code to the modulation scheme. This led directly to the Ungerboeck's proposal [15] of Trellis Coded Modulation from which the whole concept stems.

6.4.1 TCM Concept

The fundamental observation behind TCM was that the error performance of an uncoded M-ary modulation depends on the distance between the pair of coded signals. The objective of Trellis Coded Modulation is to increase this distance. To overcome the problem of power due to the larger constellation set, the TCM encoder combines encoding and modulation in the same step. The general structure of a TCM encoder is shown in Fig. 6.17. The m information bits are separated into two subsets of k_1 and k_2 bits. The group of k_1 bits are encoded by a convolutional encoder into n bits ($n > k_1$) and the group of k_2 are left uncoded. The n bits are used to select one of the 2^n subsets and the k_2 are used to select one of the 2^{k2} points in this subset. If $k_2 = 0$ then all the information bits are encoded.

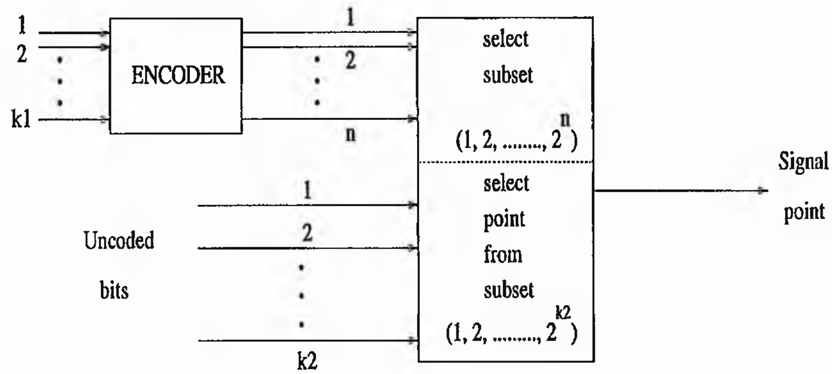

Figure 6.17: General Structure of Combined Encoding/Modulation

The second element of the TCM encoder is the mapper. The mapper relates the encoder output with the transmitted complex symbol. If we assume that the receiver makes maximum-likelihood soft decision decoding, which guarantees the best performance, then the codes should be designed to maximize free *Euclidean* distance rather than Hamming distance as is the case with conventional coding schemes. Such method was developed by [15], based on the principle of mapping by set partitioning. The concept of set partitioning is shown in Fig. 6.18.

The eight-phase signal constellation will be partitioned such that the minimum distance is increased. At the beginning, the distance between the eight signal points on a circle of radius unity is $d_0 = 2 \sin(\pi/8)$. We then subdivide these points into two subsets of 4 points, such that the minimum distance increases to $d_1 = \sqrt{2}$. In the second level of partitioning, we have 4 subsets of 2 points where the distance between them is d_2=2. Finally, the last step leads to 8 subsets of a single point each. The following example explains how this set partitioning is performed.

Set Partitioning Example: We consider a coded 8-PSK modulation with a rate of 1/2, L = 2 (constraint length). The mapping and the encoder are showed in Fig. 6.19. The bits y_2 and y_1 select one of the 4 subsets C0, C1, C2, C3, shown in Fig.6.18, where C0 contains the two signal points corresponding to the bits (000,100) or (0,4) in octal.

The trellis diagram of this encoder is described in the Fig.6.20(b). From each state,

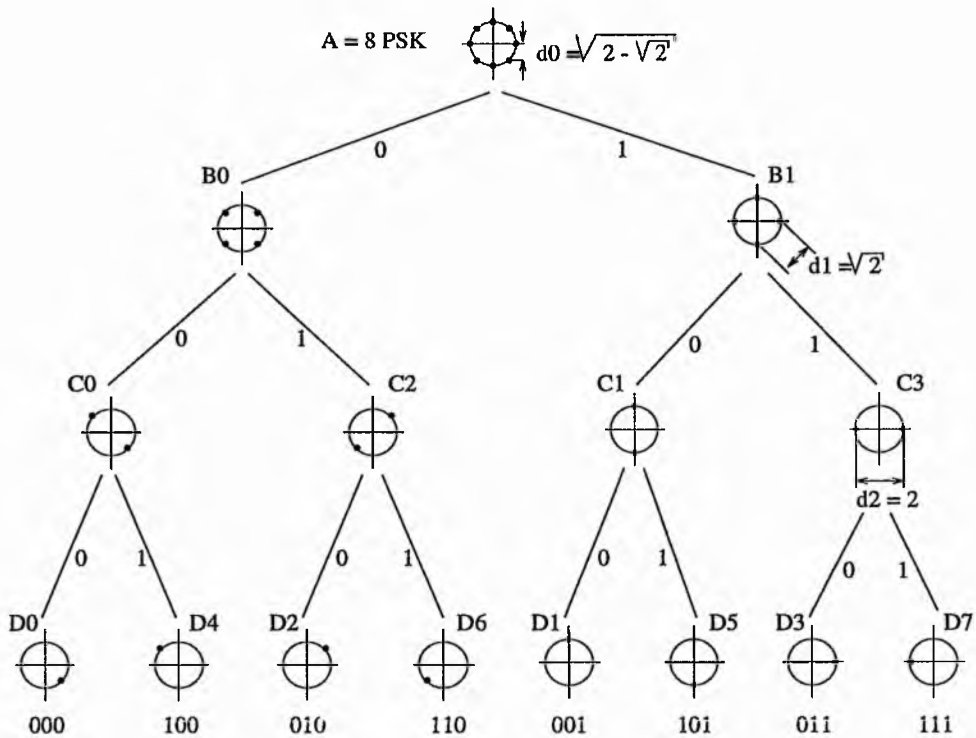

Figure 6.18: Set Partitioning of an 8-PSK Signal Set

there are two paths to another state due to the uncoded bit. Now, we must determine the minimum distance in the trellis. The distance between two signal paths which diverge from one state and merge at the same state after more than one transition have a squared Euclidean distance of $d_0^2 + 2d_1^2 = 4.585$. On the other hand, the squared Euclidean distance between two parallel transitions is $d_2^2 = 4$. So, the free Euclidean distance is 2 and compared with the Euclidean distance $d_0 = \sqrt{2}$ of the uncoded 4-PSK whose trellis diagram is shown its in Fig.6.20(a), we obtain a coding gain of 3 dB.

For a four-state trellis code the largest free Euclidean distance that we can achieve is

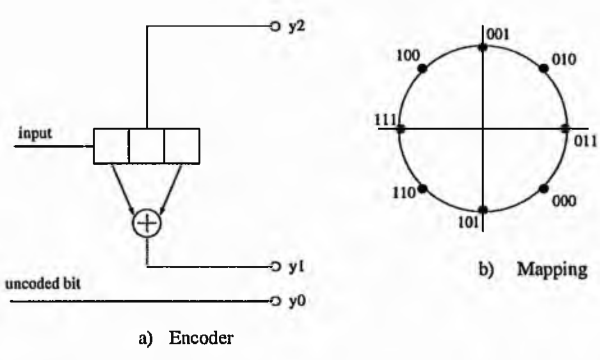

Figure 6.19: 4-state Trellis Coded 8-PSK Modulation

2, so this trellis code is optimum. However, it's possible to obtain larger coding gains with trellis code with more than 4 states. For example, Fig.6.20(c) illustrates an Ungerboeck 8-state trellis code [15] for the 8-PSK signal constellation. In that case, the squared free Euclidean distance is $d_{free}^2 = 4.585$ which represents a gain of 3.6 dB on the uncoded QPSK. For the construction of these codes, Ungerboeck applied the following rules:

1. The signal points should occur with equal frequency.
2. Transitions originating from the same state receive signals from subset B0 or B1.
3. Transitions joining in the same state receive signals either from subset B0 or B1.
4. Parallel transitions receive signals either from subset C0 or C1 or C2 or C3.

The first rule guarantees that the trellis codes have regular structure while the rest guarantee that d_{free}, associated with all the single and multiple paths that diverge from any state and merge in this state, exceeds the d_{free} of uncoded 4-PSK by at least 3 dB.

6.4.2 Phase Offset Considerations

As TCM is applied to CDMA personal communication systems, its would be of interest to examine their performance with respect to imperfect channel estimation ie. their susceptibility to phase offset. This problem has been the subject of [16] who evaluated the performance of 4 and 8-state coded 8-PSK on the presence of phase offset as illustrated in Fig.6.21. The required signal to noise ratio increases with increasing phase offset. Both 4-state and 8-state TCM schemes appear to have an irreducible BER for phase offsets ≥ 22.5 degrees.

This demonstrates that the performance degradation due to phase offsets is significant. This degradation can be explained as follows. In the trellis diagram, there are distinct paths with only the smallest distance d_0 between them. However, if phase offset rotates the received signal, the difference between received signal and the signal on distinct transitions that are d_0 may be reduced to zero. There may then be no difference in distance between a long segment of received signals and 2 distinct trellis paths ie. a condition of catastrophic error propagation is created.

The effect of the imperfect phase recovery and quantization of the signal at the input of the Viterbi decoder on the performance has been simulated for both Gaussian and fading channels.

Fig. 6.22 represents the effect of an incorrect phase recovery at the receiver for an 8-state TCM over Gaussian channel and Rayleigh channel. The E_b/N_0 ratios have been adjusted so that both channel cases have the same BER for null phase offset.

The inability of TCM decoders to handle phase offsets lead to the introduction of Rotationally Invariant Codes (RIC). RIC is a code that allows decoding which is invariant to offsets of the phase in symmetry angles of the modulation symbols. In many applications this often makes the task of correct phase synchronization much easier and shortens the acquisition of the receiver. For the scope of this thesis we assume that the phase offset introduced by the channel can be perfectly estimated. This is not very realistic in practice as it was shown in Chapter 3 for QPSK modulated spread spectrum signals, but our aim is to push TCM to the best performance limit ie. to provide TCM with the best working environment and then to compare its performance with that of low rate convolutional coding.

In the following sections we evaluate the performance of TCM coded CDMA systems in AWGN and Rayleigh single-path as well as multipath fading channels. In all evaluations an 8-PSK signal set has been employed (coded by a rate 2/3 convolutional code) since Ungerboeck [15] has shown that by doubling the number of channel signals, ie. from QPSK to 8-PSK, almost all is gained in terms of channel capacity.

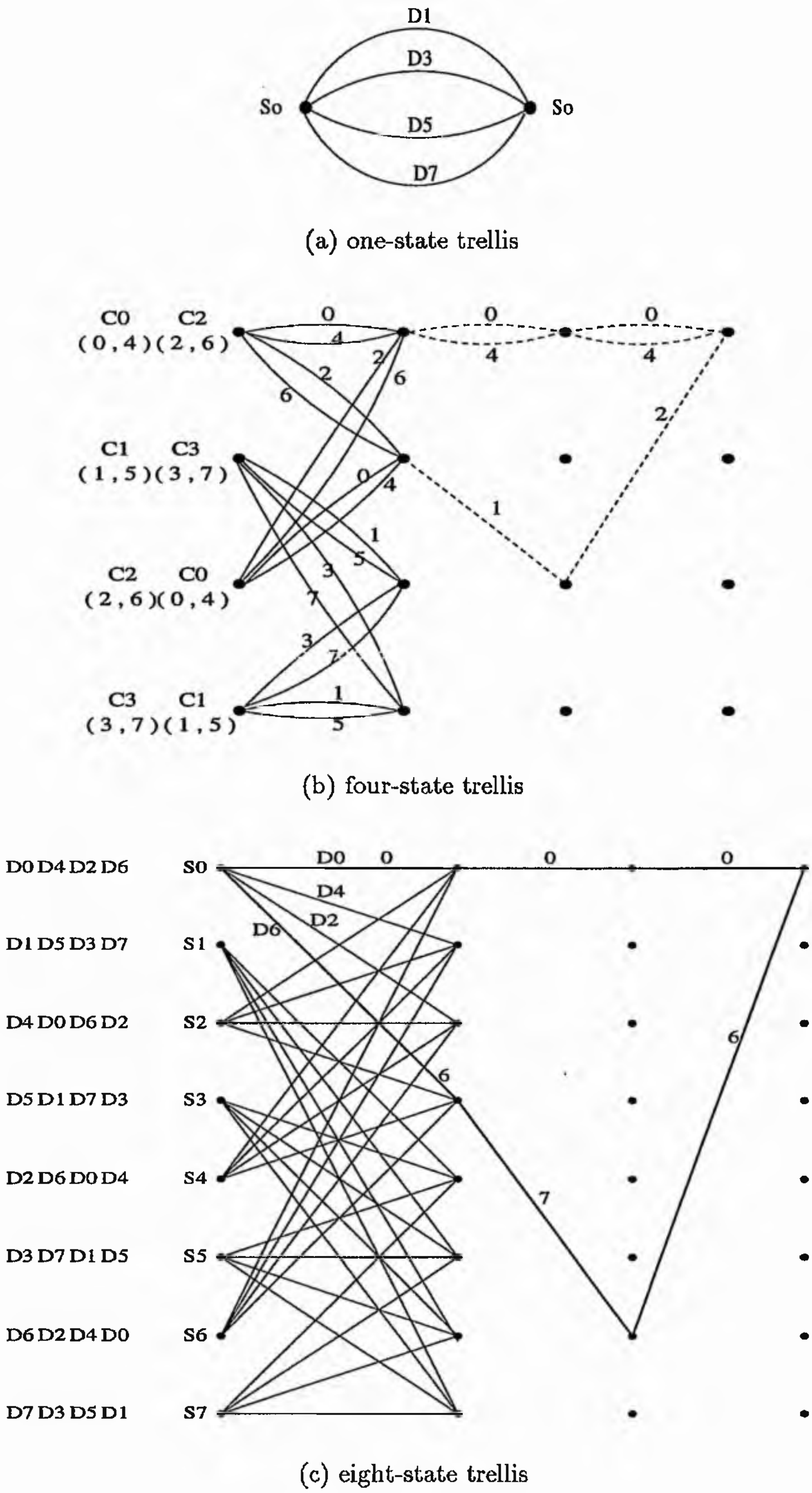

Figure 6.20: Trellis representation for 1, 4 and 8 states

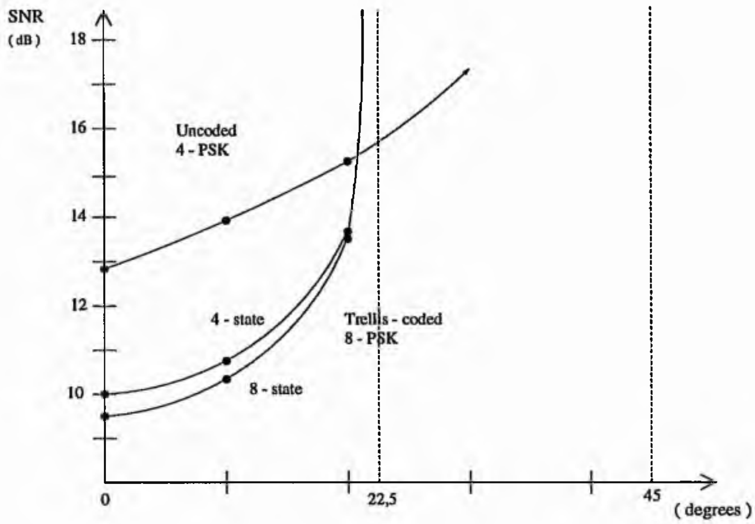

Figure 6.21: Required SNR For Coded 8-PSK and Uncoded 4-PSK vs Phase Offset

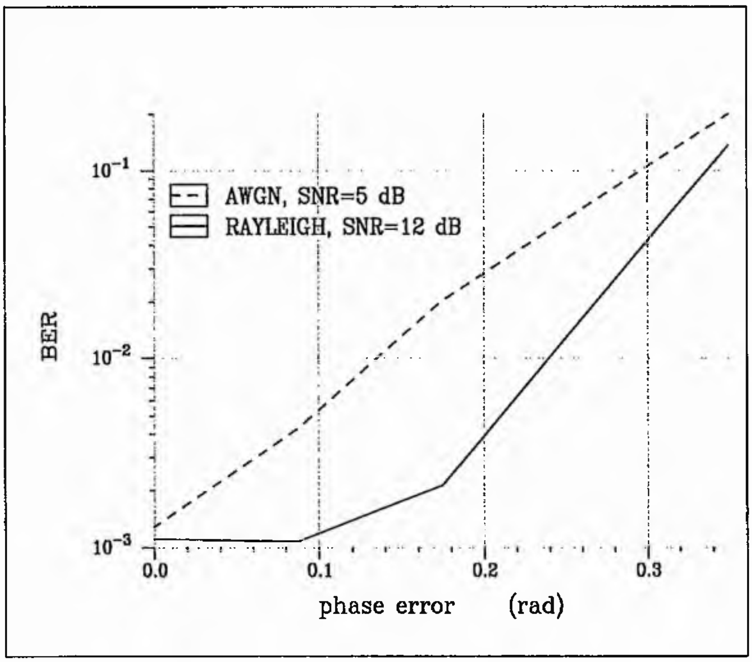

Figure 6.22: Effect of the phase offset on the bit error rate

6.4.3 Performance in the AWGN Channel

In this section we present performance results for TCM CDMA systems in the AWGN channel. The performance of TCM CDMA in AWGN can be derived similarly to performance of convolutionally coded CDMA signals. Given two signal sequences $\mathbf{x} = (..., x_1, x_2, ..., x_l, ...)$ and $\hat{\mathbf{x}} = (..., \hat{x}_1, \hat{x}_2, ..., \hat{x}_l, ...)$ which are members of the 8-PSK signal set, the distance between the two codewords determines the likelihood of decoding one codeword when the other one was sent. For the AWGN channel, the squared Euclidean distance between the two signal sequences $\mathbf{x}$ and $\hat{\mathbf{x}}$ determines the likelihood of receiving $\hat{\mathbf{x}}$ given that $\mathbf{x}$ was sent. The performance of a trellis code depends on the distribution of distances between encoder output sequences and corresponding encoder input sequences.

A union bound on the first event error probability P_e of trellis codes is obtained by summing the error probability over all possible incorrect paths which re-merge with the all possible correct paths. At any time unit, P_e is bounded by,

$$P_e \leq \sum_{d=d_{free}}^{\infty} A_d Q(\sqrt{\frac{d}{2No}}) \tag{6.33}$$

where d is the squared Euclidean distance between signal sequences. A_d is the average number (multiplicity) of codewords at distance d from the specific codeword, where the average is taken over all codewords in the code and d_{free} is the minimum free squared Euclidean distance of the code. Q() denotes the Q-function [1].

The last equation can also be written as,

$$P_e \leq \sum_{d=d_{free}}^{\infty} A_d P_d \tag{6.34}$$

where $P_d = Q(\sqrt{\frac{d}{2No}})$ is the two codeword error probability for distance d. The bit error probability is the average number of bit errors per decoded information bit. By weighting each term P_d by the average number B_d of information bits on all paths at distance d from the correct path we obtain the following bound on P_b:

[1]The Q-function is defined as:

$$Q(x) = \frac{1}{\sqrt{2\pi}} \int^{\infty} exp(\frac{-y^2}{2}) dy$$

$$P_b \leq \sum_{d=d_{free}}^{\infty} B_d Q(\sqrt{\frac{d}{2No}}) \qquad (6.35)$$

A spectral line is defined by the distance d and its average multiplicity A_d. The set of all spectral lines is called the distance spectrum of the code. Thus the knowledge of the distance spectrum of the code is compulsory information in order to compute the aforementioned performance bound. We have used a computer program developed by A. Rioual [2] according to the instructions given in [33].

The parity check coefficients of the best TCM 8-PSK codes that have been used in the performance evaluation in AWGN channels are tabulated in Table 6.8. The table also presents the asymptotic coding gain over uncoded QPSK [16].

# States	Bits Encoded	Parity Check Coefs. (h_0, h_1, h_2)	Gain (dB)	B_d
4	1	(-,2,5)	3	1
8	2	(4,2,11)	3.60	2
16	2	(16,04,23)	4.13	2.3
32	2	(34,16,45)	4.59	4
64	2	(66,30,103)	5.01	5.3
128	2	(122,54,277)	5.17	0.5
256	2	(130,72,435)	5.75	1.5

Table 6.8: Performance Gain of TCM 8-PSK Over Uncoded QPSK

With the knowledge of the distance spectrum, we can predict analytically the performance of TCM in single user CDMA systems and evaluate the effect of the number of states upon the BER. A good approximation in performance can easily be obtained if one considers the first 10 terms of the distance spectrum. This guideline was followed throughout this thesis. The upper bound on performance for various number of states can be seen in Fig.6.23.

A Monte-Carlo simulation model was also developed. We have limited the maximum number of states to 64 due to computer processing power limitation. For the Viterbi decoding, a survivor path equal to 7 times the constraint length was assumed. From Fig.6.25 and Fig.6.24, it can be clearly observed that the simulated performance agrees well with the analytical bound.

[2] The author wishes to express his gratitude to Allain Rioual for this software contribution.

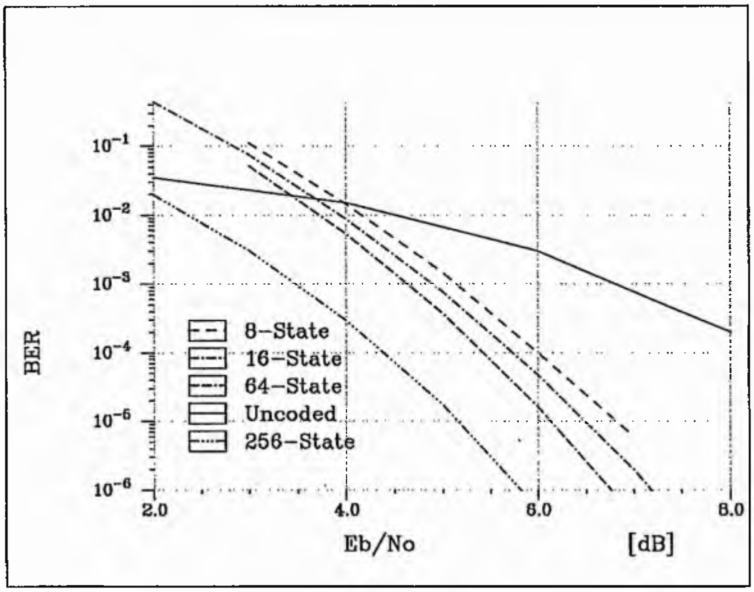

Figure 6.23: Effect of the Number of States on Performance, Single User AWGN Channel

Remark: Assuming that the receiver receives the same average power from all transmitters, we can evaluate the performance of a TCM CDMA system by adopting the Gaussian approximation. The SNR/bit in a multiuser asynchronous trellis coded CDMA system is reduced by a factor which compared to the uncoded transmission systems studied in Chapter3, has as additional variables, the number of signal points in the constellation M and the code rate r. This factor is,

$$F = \frac{2}{3}\frac{(K-1)}{N\ r\ log_2 M}\ SNR/bit \tag{6.36}$$

where K is the number of users and N is the total spreading factor. Notice that the length of the sequence to be used for spreading the trellis coded signal is $N\ r\ log_2 M$. If the system uses a rate p/m encoder and an M-PSK modulator where m=log_2M then the length of the spreading sequence should be,

$$L = N\ p \tag{6.37}$$

This is an important remark when we compare TCM CDMA with convolutionally coded CDMA which uses BPSK or BQPSK modulation. In the latter, it is the bits that are spread since there is no reduction in the output rate of the modulator compared to its input. For multiuser simulation models where the Gaussian approximation is used to model multiple access interference the choice of the spreading sequence does not influence

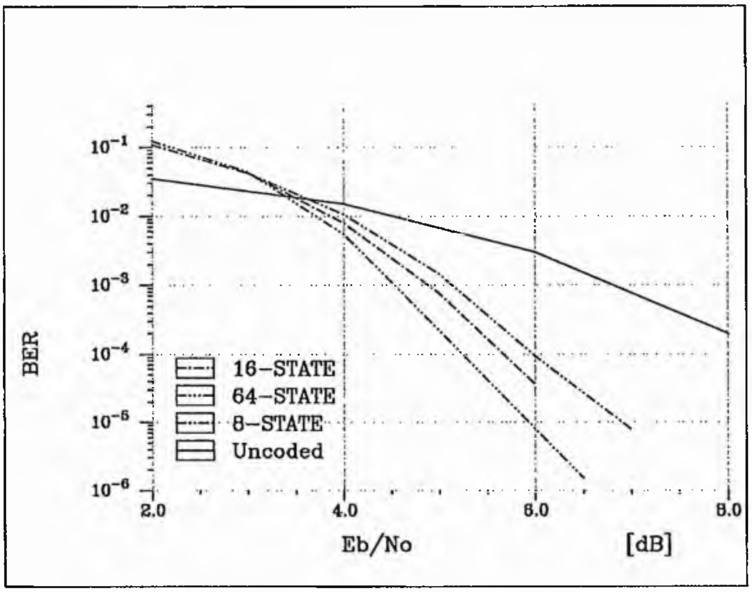

Figure 6.24: Simulated Performance in a Single User AWGN Channel

the performance.[3] Without loss of generality an AO/LSE Gold sequence of length 127 was used in this model.

[3]However, in multipath fading channels the spreading sequence must be chosen such that the self-noise is minimised.

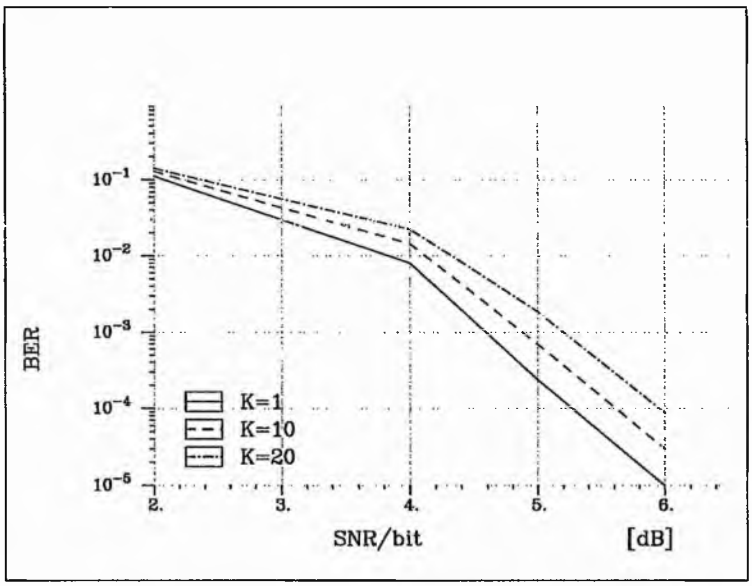

Figure 6.25: Simulated Performance for 64-state TCM CDMA System in the AWGN Channel,L=127

6.4.4 Performance in Rayleigh Fading Channels

In this section we consider the performance of TCM CDMA over the Rayleigh fading channel, assuming perfect phase coherency at the receiving end. We consider two channel cases: (1) Correlated Rayleigh fading channel and (2) Uncorrelated (independent) Rayleigh fading channel.

The correlated fading channel is a channel with memory. In this case, errors occur in bursts. By interleaving the coded bits before modulation and deinterleaving after reception causes, the bursts of channel errors are spread out in time and handled by the decoder as if they were random errors. The interleaving depth required is determined by the burst duration but the real constraint comes from the delay especially for real time services like voice and video. The most common interleaver is the block interleaver which is simply a matrix which is filled by columns and read by rows. At the receiver, the deinterleaver performs the inverse operation. So, two consecutive symbols (at the input of the interleaver) are separated by the number of columns minus 1 in the channel. The number of columns must be greater than the burst lengths and the number of rows must be chosen in the order of the constraint length. In our simulations with correlated fading channels we have used block interleavers with various depths. As it will be made evident, there is a tradeoff between interleaving depth (delay) and achievable performance.

In the uncorrelated Rayleigh fading channel, the error occurrence is memoryless. This type of channel is usually employed in analytical derivations of performance. In this thesis we shall refer to this channel case as either uncorrelated (independent) fading channel or fading channel with ideal interleaving.

In our treatment we consider the decoding of trellis codes in both correlated and independent fading channels using the Viterbi decoding algorithm. We shall also study the effects of providing Channel State Information to the Viterbi decoder. CSI is an estimate of the instantaneous SNR/symbol which when taken into account in the decoding process improves the post-decoder error rate performance. If x_n and $\hat{x}_n$ are the nth elements of the transmitted sequence $\mathbf{x}$ and the (incorrectly) chosen sequence $\hat{\mathbf{x}}$, and ρ denotes the normalized random fading amplitude (CSI) then the metric used inside the Viterbi decoder is:

- *Without CSI:* Viterbi Decoder Metric $= \sum_n (\mid x_n - \hat{x}_n \mid)^2$
- *With CSI:* Viterbi Decoder Metric $= \sum_n (\mid x_n - \rho\hat{x}_n \mid)^2$.

Using these metrics [13] calculated simple upper bounds on the asymptotic performance of TCM over fading channels. We summarise his findings by distinguishing two cases:

Case 1: Ideal Interleaving Fading Channel In this case the bit error probability is given by,

- *Coherent Detection with Ideal CSI*

$$P_b \leq \frac{1}{k} \sum_{(x_n,\hat{x}_n)} \frac{4^L[\sum_n(\mid x_n - \hat{x}_n \mid)^2]^{-1}}{(E_s/N_o)^L} \tag{6.38}$$

- *Coherent Detection without CSI*

$$P_b \leq \frac{1}{k} \sum_{(x_n,\hat{x}_n)} \frac{(\frac{2e}{L})^L(\prod_n \frac{(|x_n-\hat{x}_n|)^2}{(\sum_n |x_n-\hat{x}_n|^2)^{1/2}})^{-2}}{(E_s/N_o)^L} \tag{6.39}$$

- *Differentially Coherent Detection without CSI*

$$P_b \leq \frac{1}{k} \sum_{(x_n,\hat{x}_n)} \frac{8^L[\sum_n(\mid x_n - \hat{x}_n \mid)^2]^{-1}}{(E_s/N_o)^L} \tag{6.40}$$

Case 2: Correlated Fading Channel With No Interleaving In this case the bit error probability is given by,

- *Coherent Detection with Ideal CSI*

$$P_b \cong \frac{4^L[\sum_n(\mid x_n - \hat{x}_n \mid)^2]^{-1}}{d_{free}^2(\frac{E_s}{N_0})} \tag{6.41}$$

- *Coherent Detection without CSI*

$$P_b \cong \frac{(\frac{2e}{L})^L(\prod_n \frac{(|x_n-\hat{x}_n|)^2}{(\sum_n |x_n-\hat{x}_n|^2)^{1/2}})^{-2}}{d_{free}^2(\frac{E_s}{N_0})} \tag{6.42}$$

- *Differentially Coherent Detection without CSI*

$$P_b \cong \frac{8^L[\sum_n(\mid x_n - \hat{x}_n \mid)^2]^{-1}}{d_{free}^2(\frac{E_s}{N_0})} \tag{6.43}$$

The important point to observe in the case with ideal interleaving is that the probability of error varies inversely with the average SNR/bit which is raised to the power of L. This means that L has a notion of diversity. This fact should always be considered when trellis codes for fading channels are designed. Maximising L we get the best possible performance in fading channels. Apart from the length of the shortest error event path, another primary design criterion is the product of branch distances along that path. The larger the product of the branch distances along that path is, the better the code will perform even though d_{free} does not achieve its optimum value over the AWGN. In AWGN channels the primary design criterion is the maximization of d_{free}. So codes that have been specified for the AWGN channel are no longer optimal for fading channels.

These optimality considerations lead to research towards new trellis codes specially designed for fading channels. One of the most significant outcomes of this research is that of Schlegel and Costello [4] who specified new codes for fading channels. Table 6.9 summarises the specifications of these new codes. In this table, we present the comparison of the minimal effective length and the squared product distance between trellis codes designed for AWGN (numbers in the parenthesis) and trellis codes designed for fading channels.

# States	Parity Check Coefs. (h_0, h_1, h_2)	Effective Length	Min. Squared Product Distance
8	(4,2,11)	2(2)	8(8)
16	(16,04,23)	3(3)	4.68(4.68)
32	(34,14,43)	3(2)	16(8)
64	(154,36,103)	4(3)	8(16)
128	(314,76,223)	4(4)	8(2.75)
256	(164,336,673)	5(3)	5.49(16)
512	(244,756,1413)	5(3)	18.75(16)

Table 6.9: Fading Channel Optimized Specifications of Trellis Codes

From the third and fourth column of the previous table we can easily conclude that the new codes will perform significantly better compared to the AWGN channel optimized ones. To verify this argument, we have calculated the upper bounded bit error probability of these codes in Rayleigh fading channels. Fig. 6.26 and 6.27 depict their performance for Rayleigh fading channel with and without CSI respectively. The codes designed by Ungerboeck for the AWGN channel is also shown for comparison. The performance upper bounds have once again been calculated using the program developed for the computation of the distance spectrum of TCM codes over AWGN, which has been adapted for Rayleigh fading channels with some modifications as suggested in [4].

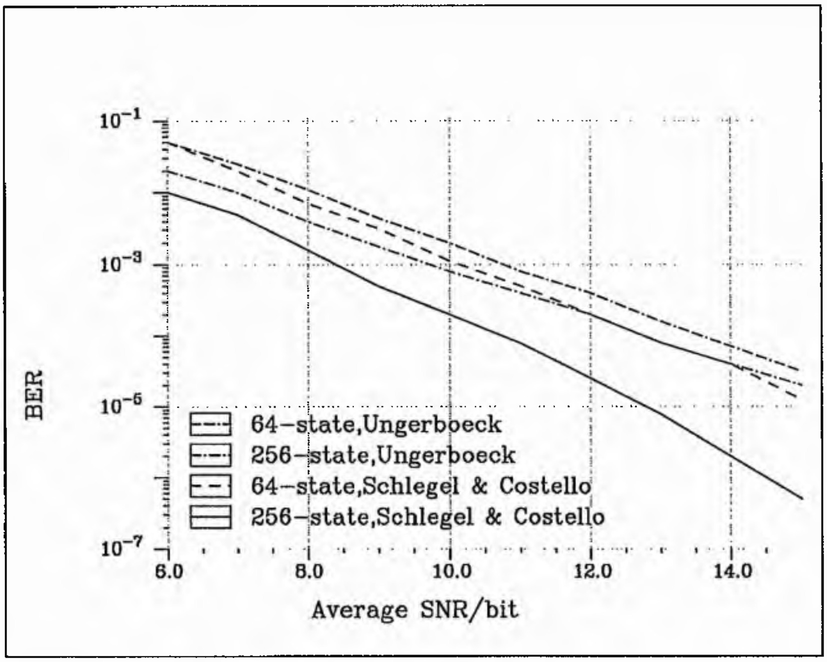

Figure 6.26: Comparison Between the Upper Bounds of TCM Designed by Ungerboeck for AWGN and by Schlegel and Costello for Fading Channels, Ind. Rayleigh Fading with Perfect CSI

Up to very recently (1992) the only analytical guide to the error performance of TCM on fading channel has been the upper bound on the pairwise error event probability. The asymptotic results p loted previously are based on this upper bound. In 1992, Cavers and Ho [27] provided a very significant contribution. They have managed to find the *exact* expression for the pairwise error event of TCM transmitted over Rayleigh fading channels. They have also shown that the upper bound on bit error probability can deviate significantly from the actual performance of TCM systems. In [27] it is shown that in the case of an 8-state TCM with perfect CSI and ideal interleaving, there is a difference of 3.6 dB between this upper bound and the exact bound. In order to justify the claims of [27], a Monte-Carlo simulation model shown was developed. It is assumed that the fading is roughly constant over the duration of a symbol. While the Viterbi decoder does not make use of CSI a comparison with the theoretical result of [27] can be justified. The results are shown in Fig. 6.28 and Fig. 6.29 for the 8-state and 64-state codes respectively.

The effect of interleaving depth can only be observed through simulation since in the analysis the assumption of memoryless channels is made. The Jake's type of Doppler spectrum specified in GSM recommendation 5.05 has been used in the fading channel. The performance degradation, as can be seen from Fig.6.30 and Fig.6.31, is very significant for no interleaving. In fact in this case the uncoded QPSK system performs better than

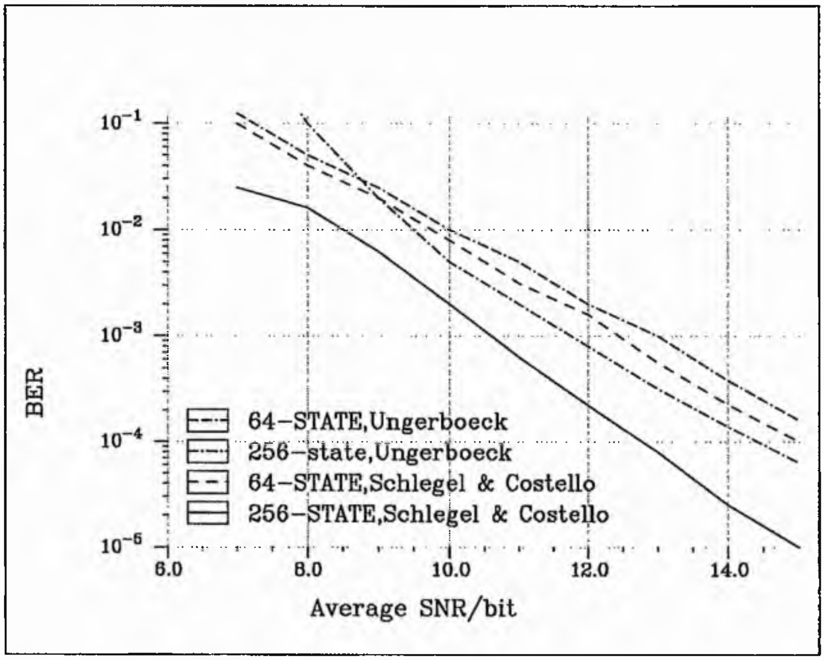

Figure 6.27: Comparison Between the Upper Bounds of TCM Designed for AWGN and Fading Channels, Ind. Rayleigh Fading without CSI

the coded 8-PSK.

The effect of multiple access interference is shown in Fig.6.32. AO/LSE Gold sequences of period 127 were employed. As the results indicate TCM is more sensitive to multiple access interference with Rayleigh fading as compared to the AWGN channel.

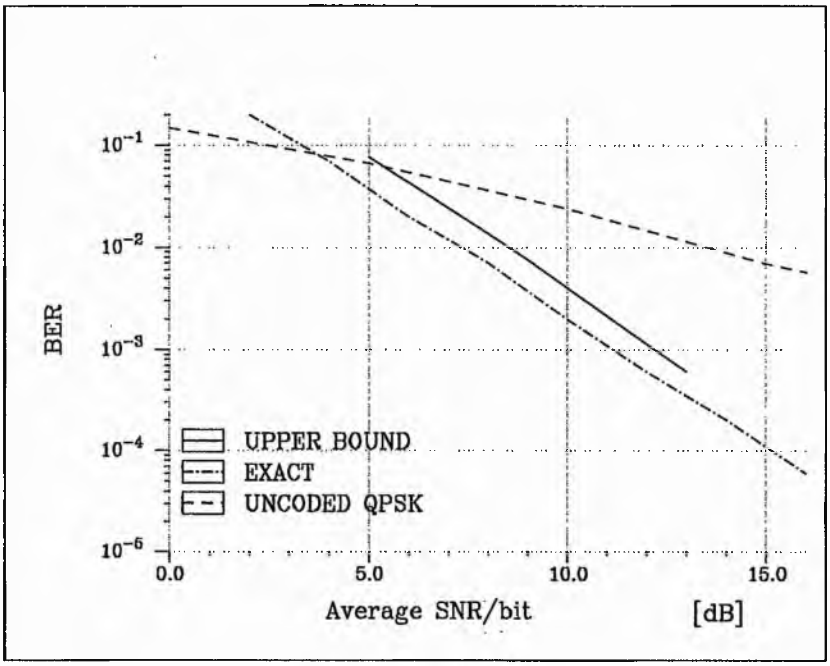

Figure 6.28: Comparison Between Exact and Bounded Performance over Independent Rayleigh Fading channel with CSI, 8-states

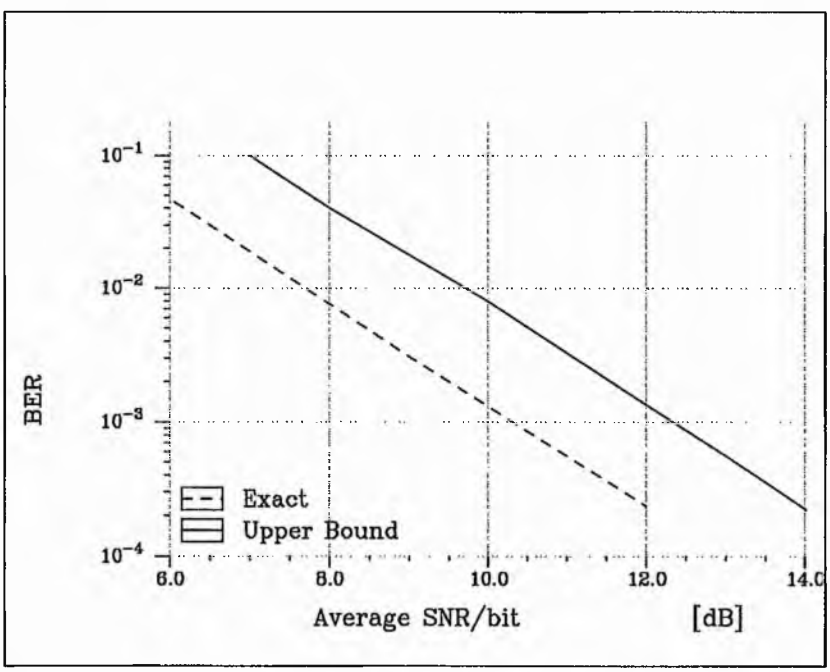

Figure 6.29: Comparison Between Exact and Bounded Performance over Rayleigh Fading channel, 64-states

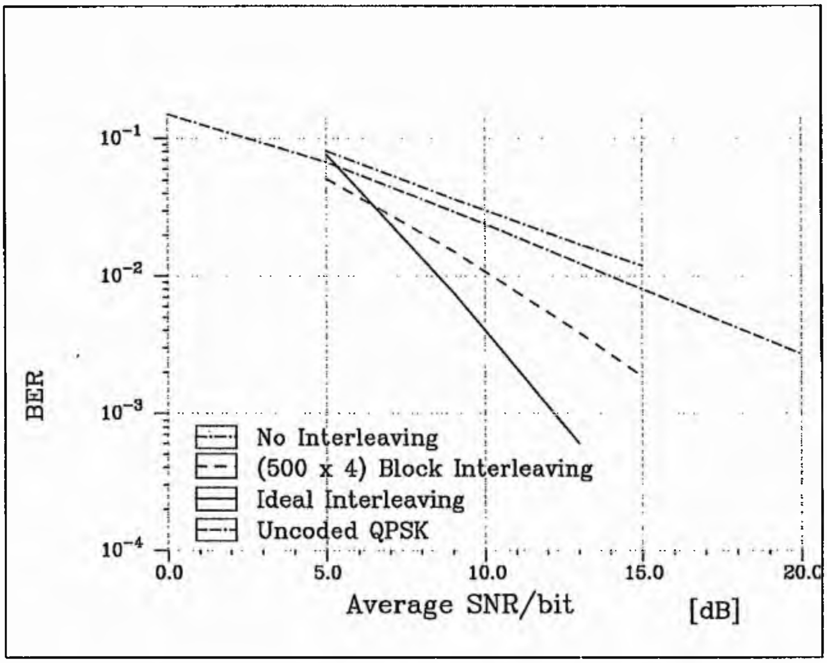

Figure 6.30: Effect of Interleaving Depth on Exact Performance over Rayleigh Fading channel, 8-states

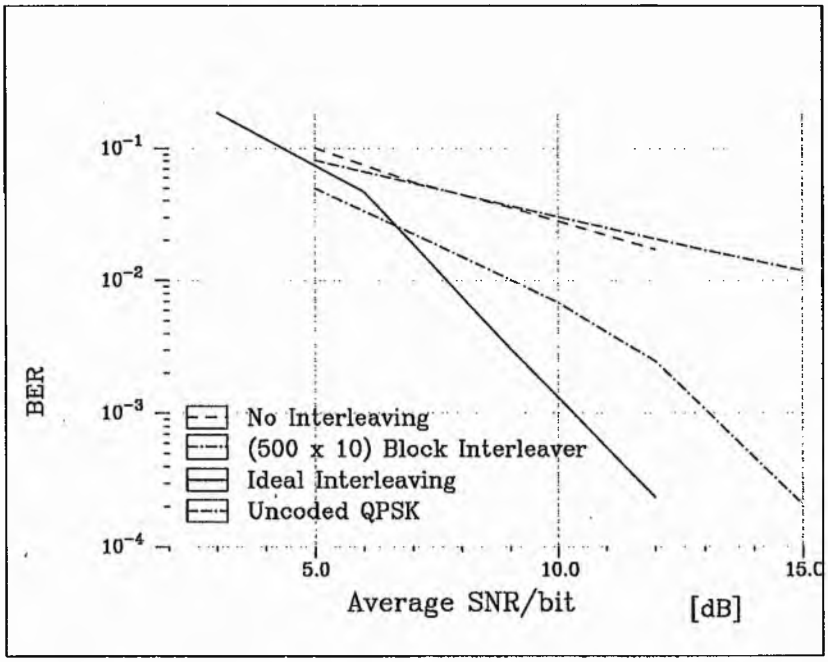

Figure 6.31: Effect of Interleaving Depth on Exact Performance over Rayleigh Fading channel, 64-states

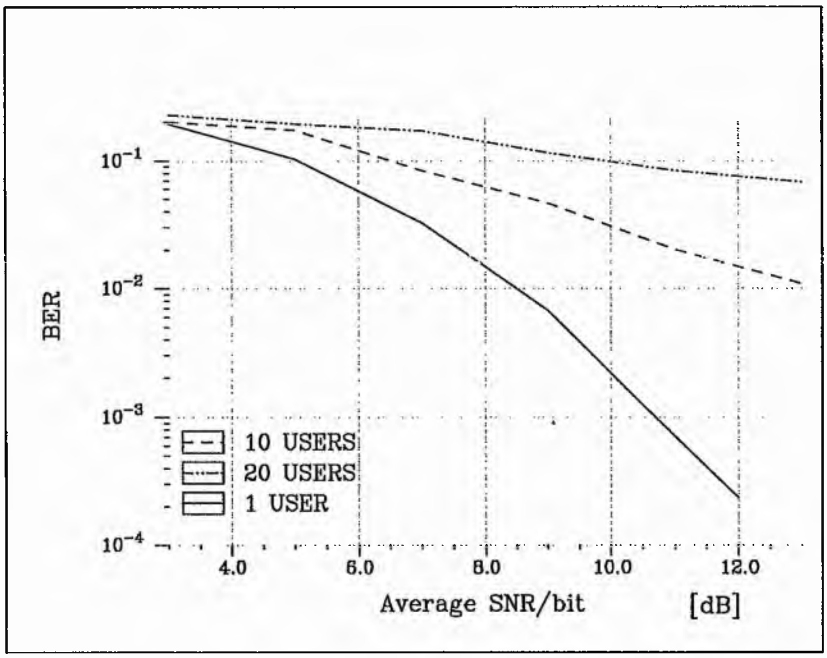

Figure 6.32: Simulated Performance of 64-state 8-PSK TCM CDMA over Independent Rayleigh Channel without CSI, N=127

6.5 COMPARISON AND CRITIQUE

In this section we compare the convolutional and trellis coded CDMA systems. For the comparison to be fair, we have to take into consideration the following factors:

- **Throughput:** The two systems should have the same throughput ie. the number of bits/coded symbol transmitted with TCM should equal the number of bits transmitted by convolutionally coded BPSK.
- **Decoding Complexity:**The number of states which determines the decoding must be the same for both systems. A good compromise between decoding complexity and performance is 64 states.
- **Interference:** Both transmission systems should be interfered by the same number of users. For the purposes of this thesis we have chosen 10 interfering users.
- **Chip rate:** Both systems should have a common chip rate.

A common misconception regarding the comparison of convolutional and trellis coded systems is that of the equal throughput. This is demonstrated in Fig.6.33 where a 2/3 8-PSK trellis coded system which uses a spreading sequence of N_1 chips is compared against low rate convolutional coded systems. Two bits/coded symbol are transmitted in the 2/3 8-PSK TCM system, while 0.5 bits/coded symbol are transmitted in the rate 1/2 convolutional coded BQPSK system. Thus for equal throughput, the length N_2 of the spreading sequence of the 1/2 BQPSK system should be 4 times less than N_1.

Table 6.10 illustrates the spreading factors to be used for a fair comparison of trellis and convolutional coded systems.

As it is evident from the table, the final chip rate of the convolutional coded systems does not exactly match the chip rate of the trellis coded system. In fact, the final chip rate slightly favours the trellis codes but this does not influence significantly the fairness of the comparison.

Based on the aforementioned simulation results we can make the following conclusive remarks:

- The superiority of low rate convolutionally coded as compared to equivalent trellis coded CDMA systems is total.

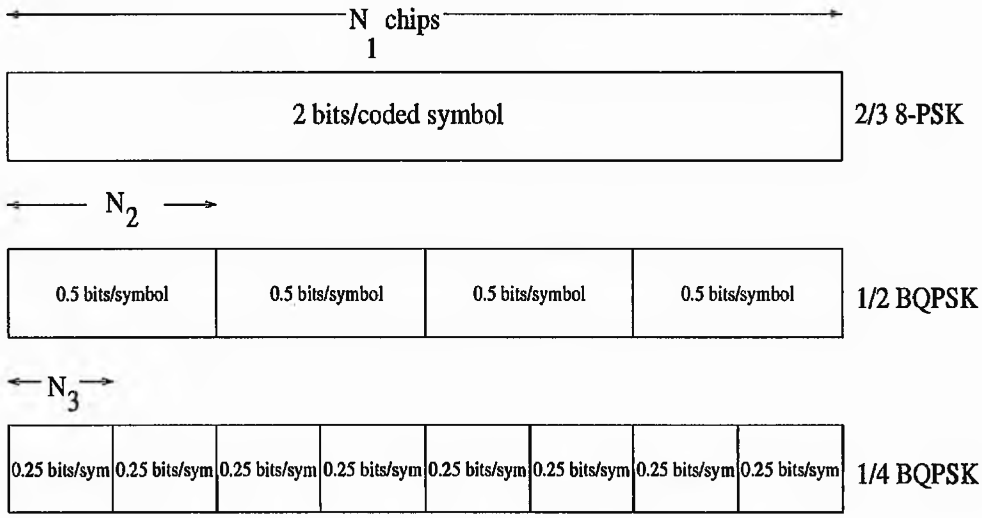

Figure 6.33: Equal Throughput Between Convolutional and Trellis Codes CDMA Systems

- Trellis codes degrade substantially in Rayleigh fading channel and the effects of interference are more pronounced for trellis compared to convolutional codes. This is in accordance to Viterbi conclusions who suggested that in very noisy channels bandwidth has to be spend in order to achieve our performance goals. Bandwidth for channel coding in CDMA is widely available, however as has been also mentioned in section 6.3.7 it is the availability of phase coherency who determines the coding gain of low rate convolutional codes.

- Our treatment for trellis coding is not complete. We have addressed neither multidimensional trellis codes nor multiple TCM or rotationally invariant trellis codes. We believe that a complete treatment of trellis codes in CDMA mobile radio channels is a subject by itself. However, the results for the trellis codes investigated in this chapter are conclusive as far as the severe degradation in performance of trellis codes in fading channels is concerned. Although we used fading channel optimized trellis codes, these appeared to be easily superpassed by convolutional codes in fading channels.

The fact that the performance of trellis coding degrades significantly with Rayleigh fading statistics lead to examine the possibility of improvement of the fading statistics at the input of the Viterbi decoder. If we exclude the possibility that the fading statistics can be improved if the CDMA system operates in microcells where Rician fading instead of Rayleigh is present, it seems that the only means to improve the fading statistics is to employ multipath diversity. It is very interesting to quantify the multipath diversity gain

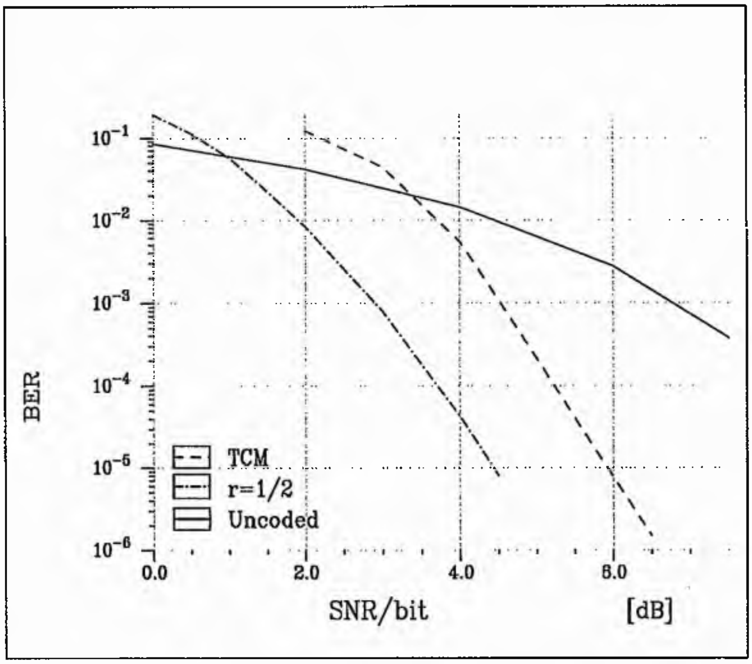

Figure 6.34: Performance Comparison of Trellis and Convolutionally Coded CDMA Systems in the AWGN Channel,K=1

in trellis coded systems and examine if RAKEing the multipath Rayleigh fading signal can drastically improve the performance of trellis codes.

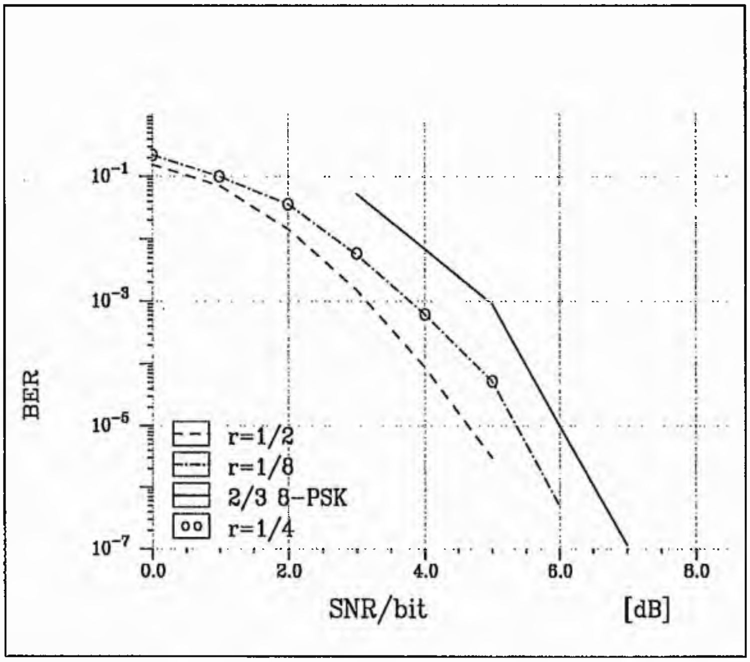

Figure 6.35: Performance Comparison of Trellis and Convolutionally Coded CDMA Systems in the AWGN Channel,K=10

Coding	Modulation	N	Bit Rate (kbps)	Coded Symbol Rate (ksps)	Chip Rate (kcps)
2/3	8-PSK TCM	127	9.6	4.8	609.6
1/2	BQPSK	31	9.6	19.2	595.2
1/4	BQPSK	15	9.6	38.4	576.0
1/8	BQPSK	7	9.6	76.8	537.6

Table 6.10: Spreading Factors For Fair Comparison of Convolutional and Trellis Coded Systems

# Users	1/2	1/4	1/8	2/3 TC 8-PSK
1	3.0	3.0	2.8	4.5
10	3.1	3.7	3.7	5.0

Table 6.11: Comparison Between the Required E_b/N_0 for Convolutional and Trellis Codes in the AWGN Channel

# Users	1/2	1/4	1/8	2/3 8-PSK TCM
1	7.0	5.9	5.0	11.0
10	9.0	8.5	6.5	> 12

Table 6.12: Comparison Between the Required E_b/N_0 for Convolutional and Trellis Codes in the Independent Rayleigh Fading Channel

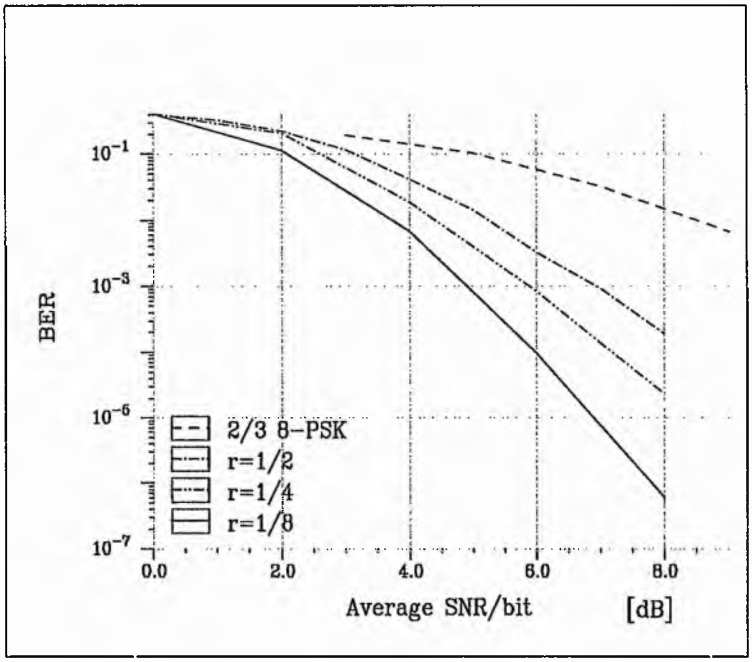

Figure 6.36: Performance Comparison of Trellis and Convolutionally Coded CDMA Systems in Independent Rayleigh Fading Channel,K=1

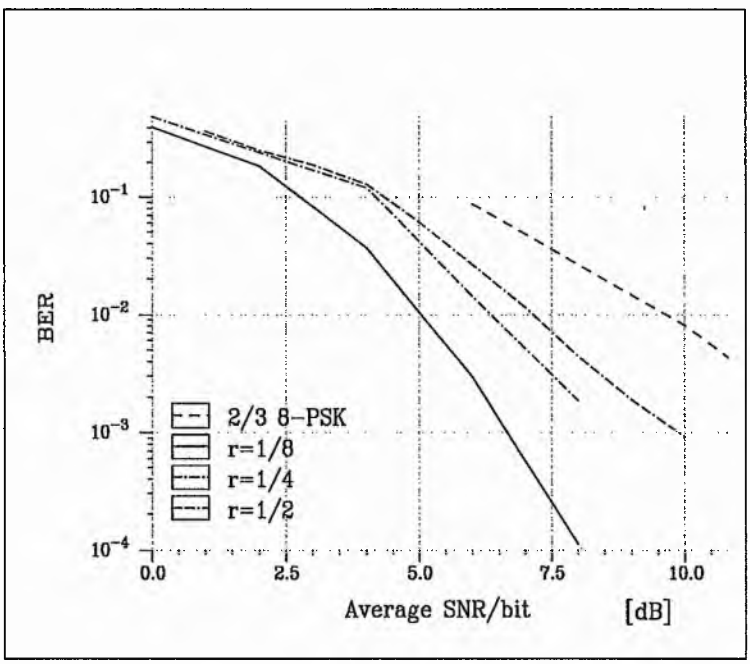

Figure 6.37: Performance Comparison of Trellis and Convolutionally Coded CDMA Systems in Independent Rayleigh Channel,K=10

6.6 COMBINING TCM WITH MULTIPATH DIVERSITY

In this section, the performance of TCM over multipath Rayleigh fading channels will be addressed. The ability of RAKE reception can be easily realised if several replicas of the information signal can be supplied to the Viterbi decoder. The model that realises the combined multipath diversity receiver and TCM is shown in Fig.6.38.

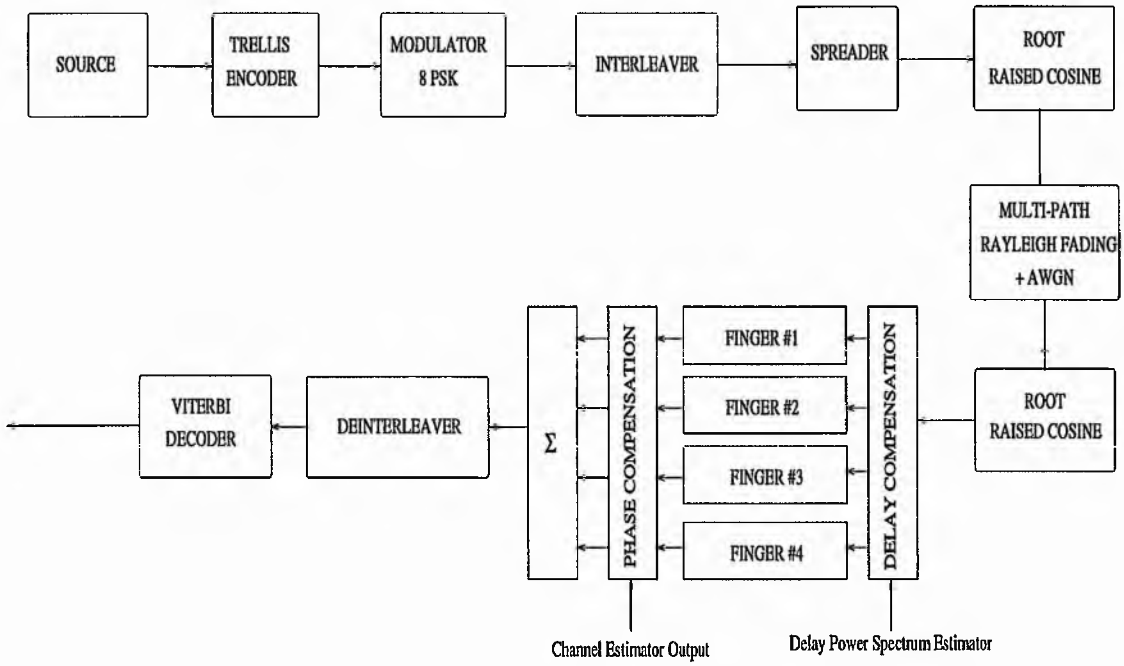

Figure 6.38: Model for Multipath Diversity Reception of Trellis Coded CDMA Signals

The channel model that has been employed consists of 6 paths. The values of the path delays and average path power follow the Typical Urban channel model described in the GSM recommendation 5.05. The following table summarises the channel parameters.

Path	Delay (ms)	Power (dB)
1	0	-3
2	5.8E-3	0
3	9.7E-3	-2
4	1.4E-2	-6
5	1.9E-2	-8
6	2.4E-2	-10

Table 6.13: Typical Urban Multipath Channel Model Parameters

Apart from the multipath fading channel case, a static multipath channel has also been employed in order to model quasi-static channels like the land mobile satellite channel. For the static multipath channel, the non-fading path attenuation follows the Typical Urban path attenuation of Table 6.13.

The RAKE receiver combines the 4 stronger paths while two cases have been examined. The first uses Gold sequences of length 1023 aiming to minimise the self-noise and to provide an unbiased measure of the multipath diversity gain. The second uses Gold sequences of length 127 and has been used for studying the effects of system loading on the performance. Fig.6.39 shows the results for static multipath and for the multipath Rayleigh fading with ideal interleaving for the $L = 1023$ case. Fig. 6.40 examines the effects of finite interleaver depth for the 6-path correlated fading channel having a Jake's type of Doppler spectrum. Finally, Fig.6.41 shows the effect of system loading for the $L = 127$ case. For the latter an interleaver depth of 500 has been used.

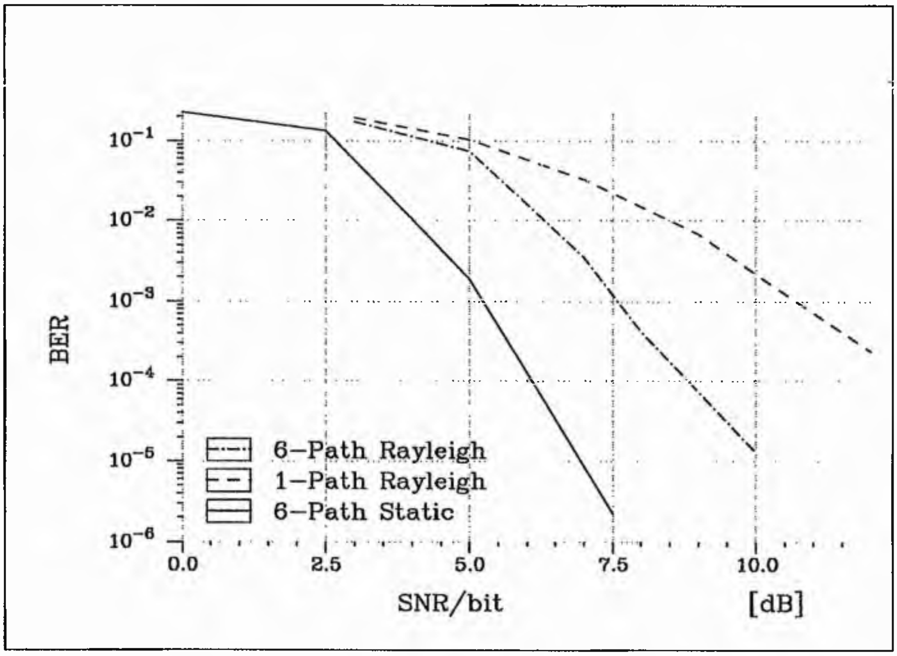

Figure 6.39: Performance of RAKE Reception of a 64-state TCM-CDMA System, L=1023

We can summarise our findings as shown in Table6.14:

There is indeed a significant reduction of the required SNR/bit to achieve the target BER of 0.1%. With 1023 chips/bit in a single user system, the required SNR falls from 10.5 dB to 7.5 dB, a net gain of 3.0 dB. For spreading factor of 127 chips/bit the required SNR/bit is 8.5 dB. This 1 dB increase from the 1023 chips/bit case is due to the self-noise which starts affecting the performance as the length of the spreading sequences decrease.

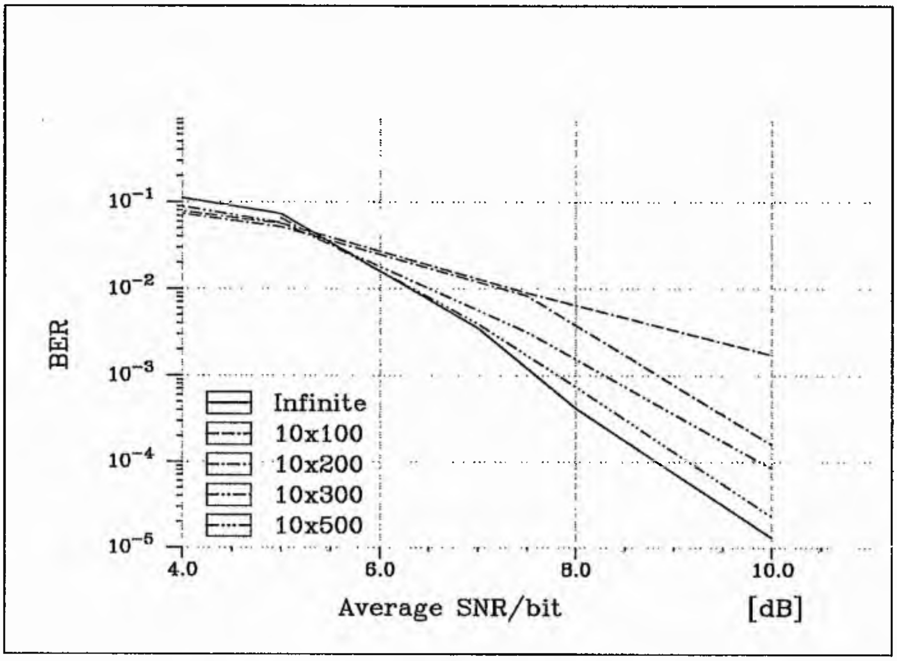

Figure 6.40: Performance of RAKE Reception of a 64-state TCM-CDMA in Multipath Jake's-Type Rayleigh Fading Channel For Various Interleaving Depth,L=1023

L	Without RAKE	With RAKE	Gain (dB)
127	10.75	8.50	2.25
1023	10.75	7.50	3.25

Table 6.14: Required SNR/bit to Achieve a 0.1% BER in a Single User TCM CDMA System

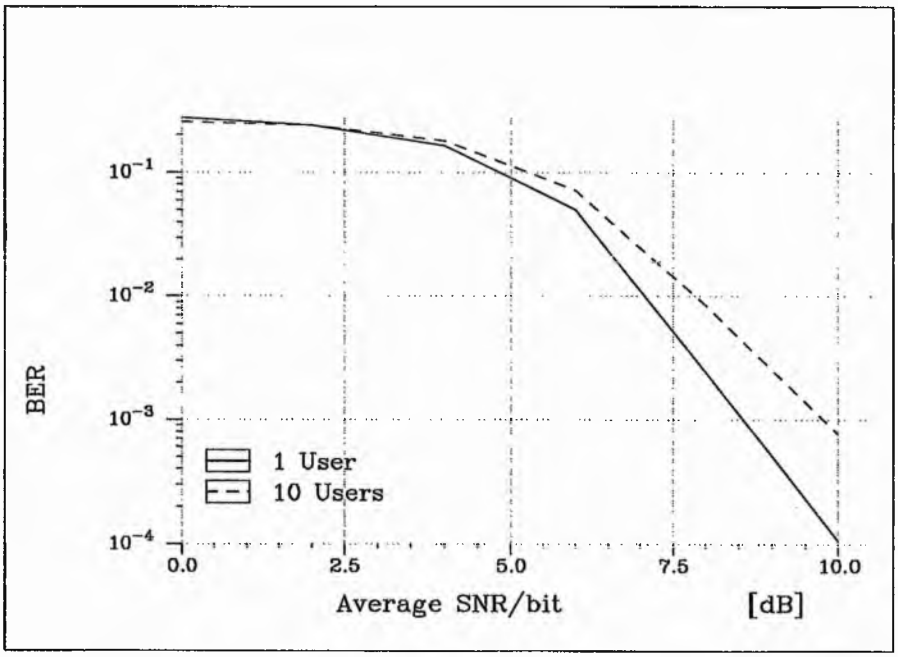

Figure 6.41: Effect of System Loading on the Performance of TCM-CDMA in Multipath Jake's-Type Rayleigh Fading Channel,L=127

6.7 MULTIPLE BIT RATE RADIO INTERFACE BASED ON CHANNEL CODING

A first discussion in Chapter 2 regarding the provision of multiple bit rates in the CDMA radio interface lead to distinguish two scenarios. The first is the conventional approach which involved dividing the frequency spectrum into multiple unequal frequency bands and dedicate each band for each service. This conventional multicarrier CDMA system has some inherent disadvantages:

- As already mentioned briefly in Chapter 2, in the handover mode the terminal can not receive at the same time the carrier frequencies of two adjacent Base Stations unless they are the same. Thus, the great performance gains during soft handover are lost. In CODIT this problem has received extensive research. The technique that has been found to offer quasi-soft handover is called seamless handover during which the mobile terminal enters what is called compressed mode. In this operational status the processing gain is halved since the frame duration is shared between the originating and the target Base Stations. Quantification of the inevitable performance losses during seamless handover is outside the scope of this thesis and to the knowledge of the author has not received the attention it deserves.

- The ability to enter macro diversity mode again depends on the frequency planning of surrounding sites. The capacity gains due to macrodiversity are significant. In fact macrodiversity increases the effective order of diversity employed at the transmitter. If a RAKE receiver exploits a 4-order multipath diversity then the combining of three downlink signals effectively increases the order of diversity to 12. However, macrodiversity comes at an expense of complexity since one RAKE is required for each additional downlink signal.

The second scenario that employs channel coding to provide multiple bit rates, as has been briefly outlined in Chapter 2, has the following characteristics:

- All services have a common chip rate.

- A single carrier occupies the totality of the available spectrum.

- Channel coding is used to spread the multiple bit rate signals.

- PN sequences are used only if the spreading caused by channel coding is not adequate to reach the common spreading factor.

For example, Table 6.15 summarises a multirate radio interface with voice, 128 kbps and 2048 kbps data services.

Data Rate	Total Spreading Factor	Chip Rate	Cell Type
9.6 kbps	2048	20.48 Mcps	macro/micro
128 kbps	160	20.48 Mcps	macro/micro
2048 kbps	10	20.48 Mcps	pico

Table 6.15: A Multirate Scenario

For an available bandwidth of 20 MHz the total spreading factor reduces from 2048 to 10 as the data rate increases from 9.6kbps to 2048 kbps. This reduction is however inevitable for both scenarios. Assuming that the techniques presented in Chapter 4 and Chapter 5 are not implemented then the reduced processing gain for this case dictates the provision of such high bit rate services only indoors.

Fig. 6.42 depicts the mapping of multiple bit rates to the common chip rate.

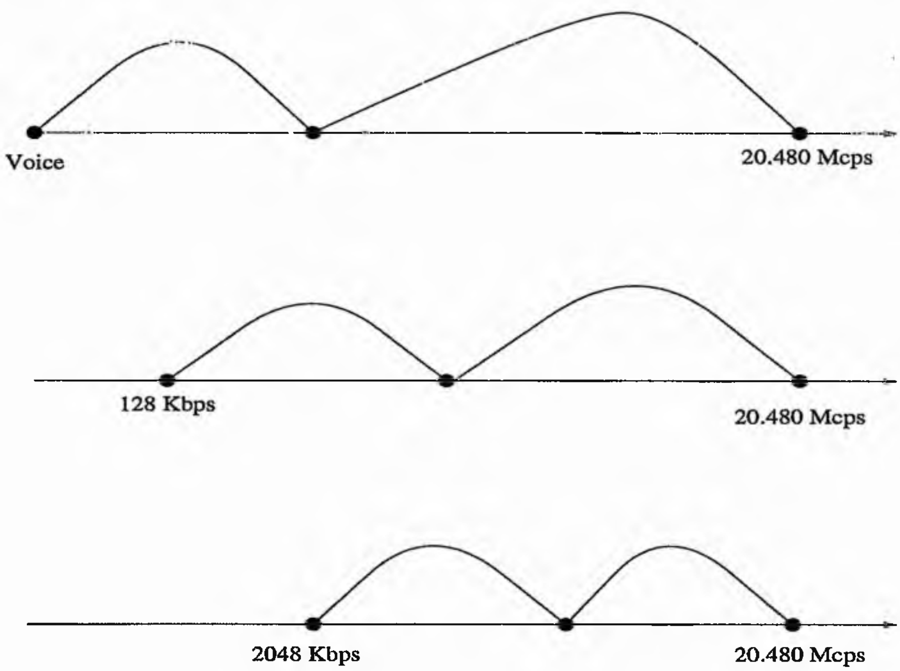

Figure 6.42: Mapping of Multiple Bit Rates to Chip Rate

For every service the final chip rate is achieved in two steps. The intermediate coded state can vary according to the service type and to the channel conditions. In fact for every service the designer should optimise the channel coding parameters. This optimisation will be in accordance to other variables such as delay and transmission type. The optimization of the coding parameters is outside the scope of this thesis. What this thesis addresses is the feasibility of achieving multiple access capability with channel coding as the prime spreading device. Thus, assuming that LOROC encoded spread spectrum signals are used to spread the bandwidth, it would be of high interest to evaluate their aperiodic and periodic crosscorrelation values. Core element for the evaluation of the MAI are the following definitions:

Relative Code Rate $\rho_{x,y}$: We define the Relative Code Rate (RCR) between two LOROC encoded signals as the difference in their coding rates. For example, with 5 MHz of bandwidth available and 4-PSK modulation, the voice and the 144 kbps user are transmitting at 10 Mcps. The chip rate is identical but the underlying coding rate differs. RCR shows how much different are the coded information bit streams. Thus, after 1 sec the voice user proceeds 1 codeword while the 144 kbps user proceeds 15 codewords.

Multirate Aperiodic Crosscorrelation: The aperiodic crosscorrelation function is a modified version of [53]. Let $\mathbf{y}$ be the reference codeword of the low rate (eg. voice) user having length N_y and $\mathbf{x}$ the interfering codeword of the high rate user having length N_x. If the system was synchronous then in a single codeword of the low rate user there would be ρ codewords of a high rate user. In order to obtain the correlation interference over a single codeword of a low rate user we construct a sequence $\mathbf{z}$ of ρ high rate codewords such that:

$$\mathbf{z}^{\rho} = (\mathbf{x_1}, \mathbf{x_2}, ..., \mathbf{x}_{\rho}) \tag{6.44}$$

With this way we are now correlating two equal length codewords, defining their Multirate Aperiodic Correlation (MAC) function as follows:

$$C_{\mathbf{x},\mathbf{y}}(l,\rho) = \frac{1}{N}\sum_{n=0}^{N-1} x_n z^{\rho}_{n+l} \tag{6.45}$$

where $N = N_x = N_z$.

There is no doubt that because of the finite alphabet of LOROC spread signals (every output codewords is one of the 2^L Hadamard rows) the phenomenon where two users of the same data rate need to transmit the same Hadamard row could be frequent. These users will then have for the duration of this row, crosscorrelation of unity. As Viterbi suggested in [60] the superposition of a randomising PN sequence will solve this problem. This is represented in Fig. 6.43.

With the definition of the multirate crosscorrelation functions, we are able to evaluate the multiple access interference by computer simulation. Results from the asynchronous uplink is shown in Fig.6.44.

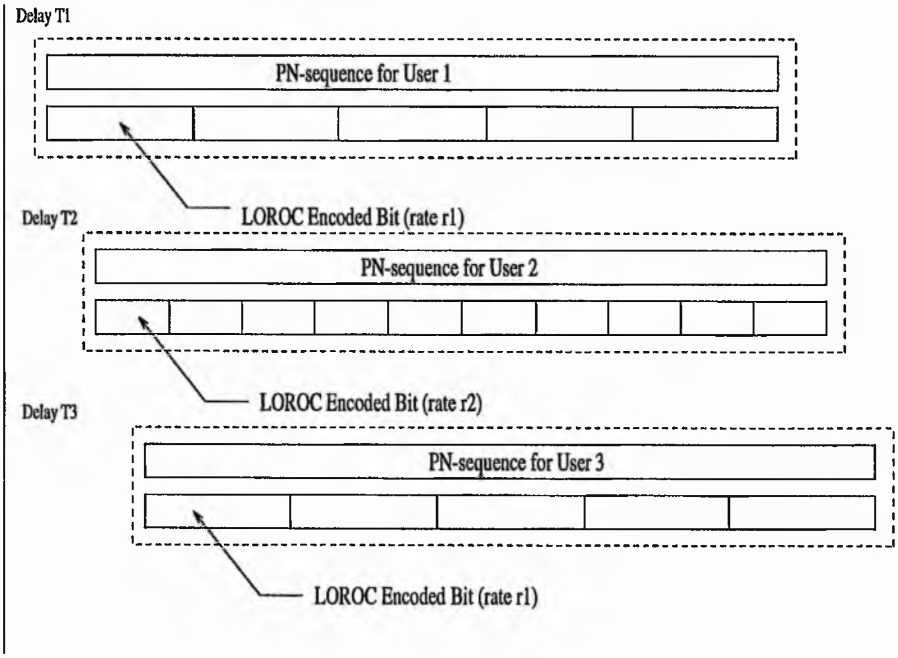

Figure 6.43: Representation of LOROC Encoded Signals in the Uplink

The simulation results indicate that LOROC codes have low values of multiple access interference. This is due to the superposition of a very long PN sequence, that although causes no spreading it randomizes the LOROC encoded signals. One of the advantages of using channel coding to spread the signal over the entire available bandwidth is that there are no optimum or sub-optimum codes to choose from. This is in contrast to conventional spreading methods where the choice of periodic spreading sequences affects to a great extend the performance of the system.

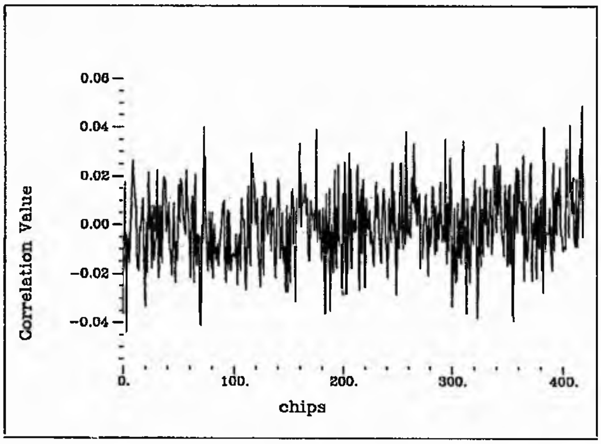

(a) Voice and a 144 kbps user

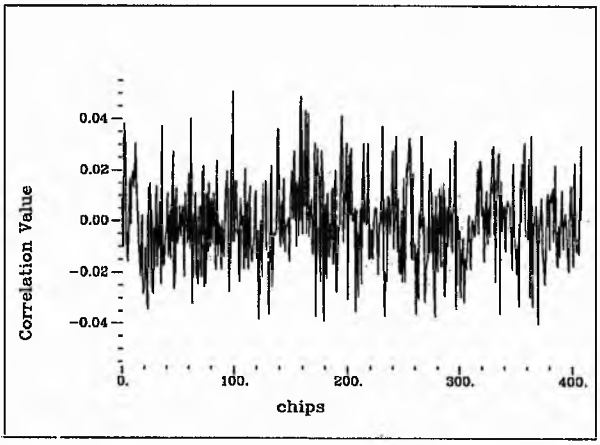

(b) Voice and a 2 Mbps user

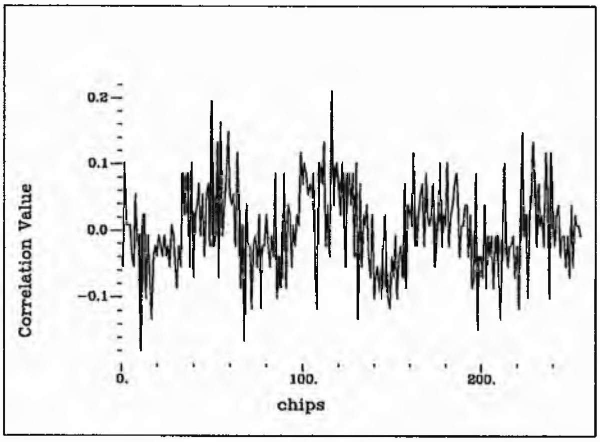

(c) A 144 kbps and a 2 Mbps User

Figure 6.44: Multirate Crosscorrelograms

6.8 CONCLUSIONS

The conclusive remarks from our investigations on the role of channel coding in CDMA systems can be put together as follows:

- The myth that FEC prevents the CDMA receiver from its valuable processing gain has been shown to be invalid. Bandwidth hungry FEC techniques (convolutional coding) have been found to offer significant performance gains compared to bandwidth efficient coding (trellis codes).
- We have shown that a multifunctional approach (co-designed coding and modulation) when applied to CDMA is inferior to a non-multifunctional approach (convolutional coding). However we can not generalise this conclusion since the benefits of multifunctional design have been demonstrated in other systems.
- The optimum implementation of a CDMA radio interface is to divide the available bandwidth into two parts. The part to be dedicated to channel coding should be larger or smaller than the part dedicated to PN spreading depending on the demodulation type. In fact, if phase coherency is achieved with the practical channel estimation techniques described in Chapter 3, the optimal solution is to dedicate all the bandwidth to channel coding. If phase coherency can not be achieved then the optimal channel code is the rate 1/8 convolutional code
- Channel coding can play an important role to the provision of multiple bit rates in the CDMA radio interface.

Chapter 7

CONCLUSIONS

7.1 A VIEWPOINT

It is not a surprise that research towards third generation Personal Communication Systems (PCS) has engaged the totality of the European telecommunication industry into a 'RACE'. With the current schedule, by the end of 1994, the first demonstrator of multimedia wireless communications based on CDMA technology should be a reality. By the end of 1995, a competing multimedia wireless demonstrator based on TDMA technology will also be put on trial.

Our part in this 'RACE' was on advanced CDMA research which, happily, is more motivating than research for advanced TDMA systems. Although the understanding of the CDMA concept is more difficult than TDMA, the former substantially rewards any attempt to exploit its horizons. The aim from the beginning of this project was to free CDMA from the restrictions imposed by the use of the simplistic RAKE receiver technology. Considering that the origins of RAKE receivers were founded in the early 50s, any attempt in this area is timely.

Despite sincere efforts to implement the new receiver technology in the CODIT testbed, a lower risk solution was eventually selected. This should not come as a surprise as European conservatism has rejected many examples of sincere technological innovation. [1] When one considers the hardware development of RAKE receivers, there appears little scope for innovation. Looking at the more problematic up-link, CODIT has used control channel information in order to achieve the ultimate performance of RAKE receivers,

[1] The CD-900 system, a combination of TDMA and CDMA was largely rejected in favor of a low risk TDMA/SFH solution during the standardisation of GSM.

through coherently demodulating the received signal. Although this is a more advanced step compared to the technique used in the IS-95 standard, it is questionable if it can provide the performance edge that CDMA needs over the competing advanced TDMA systems. This is particularly evident when one considers that if CDMA is ever to be employed in a UMTS system, its radio interface has to provide ISDN services. It is true that CODIT will be the first wireless cellular system to demonstrate simultaneous voice and 128 kbps data, but is the processing gain of 16 dB enough to provide a capacity equal to the ATDMA ?

It is also true that CDMA radio engineers can invest heavily on channel coding to provide the bit error rates needed for voice as well as data services. It comes as no surprise that a very powerful concatenated scheme using Reed-Solomon/convolutional coding, very similar to that one used for deep space communications, was chosen for the CODIT 128 kbps traffic channel [37]. Is it wise however to invest in channel coding when the signal processor, in the presence of just a handful of interfering users of similar data rates, struggles to achieve a decent channel error rate ? The favourable voice activity detection technique unfortunately can not be used in real-time data services. The only solution for non delay sensitive services, is the Automatic Repeat reQuest (ARQ) scheme. However, the throughput penalty could also be severe under interference limited conditions.

Research towards advanced CDMA receiver designs which do not inherit the limitations of the conventional technology has been recently intensified. However, the proposed CDMA receivers require very complicated signal processing, they are centralised, massively parallel and consequently very expensive to implement. The complexity of the proposed receivers can increase linearly with the number of interfering users, but this is of little engineering value when hundreds of millions of operations per second are needed at the receiving end, for cancelling a handful of interfering users. By recalling the results regarding MIMO detection strategies, it seems that the community have oscillated between extremes; from a receiver architecture that is simple to implement but has no near-far resistance, to receiver architectures that are near-far resistant but unrealistic to implement.

CDMA research for interference cancellation receivers should be positioned somewhere between these two extremes. SISO MMSE detectors may not have the near-far resistance of the MIMO receiver architectures but they do have an engineering future as they are implementable at a reasonable cost with current technology.

We can now summarise some of the conclusions and implications of the work outlined in this thesis:

- The conventional CDMA receiver demands the support of power control to overcome the time-varying near-far effects. As the standard deviation of the power control error increases, the receiver becomes near-far interference limited and even under lightly loaded conditions presents an irreducible BER.

- In well power controlled situations, the effectiveness of RAKEing depends on the combining technique. The non-coherent combining (DRAKE) is associated with significant SNR/bit losses which increase with the number of combined multipath components. Coherent combining can be achieved through effective channel estimation methods. Given that the delay power spectrum estimator is perfect, with coherent combining, RAKE receivers can approach their performance limits in the uplink. In this thesis, a particular channel estimation method has been addressed based on control channel side-information. This method is well suited for systems with multiple frame structures that are needed to support other than voice services in CDMA systems with multiple chip rates.

- Joint interference cancellation technology can significantly enhance the capacity of CDMA but at the expense of receiver complexity. Zero-forcing joint detection receivers are near-far resistant but their performance degrades significantly with the system loading. On the other hand, MMSE based receivers have been shown to tolerate the interfering traffic better, but they demand additional information such as accurate estimation of the interfering complex envelopes (energy matrix).

- Adaptive single input MMSE receivers offer adequate near-far resistance without making any use of the interfering code sequences. Their operation is autonomous and they have RAKE abilities in multipath fading channels. Furthermore they present an implementable migration path from RAKE to more advanced receiver architectures.

- Proper definition of the radio interface for CDMA systems that support multiple bit rates is strongly related to the implementation of the channel coding functions. The three different implementation scenarios for the sharing of the bandwidth between channel coding and dumb spreading have been evaluated. It has been shown that low rate spread convolutional codes not only outperform trellis coding in mobile radio channels with Rayleigh statistics but they can also be easily implemented using standard Viterbi decoders. The degree that FEC should be biased against PN spreading depends on the availability of phase coherency. Should phase coherency be achieved, the myth that associates channel coding with losses in the interference margin of the system has been proved to be invalid.

7.2 FURTHER WORK

The achievements of this thesis, prompt several thoughts on developments in this area. In the following, some areas where the research effort should be directed have been identified:

1. The strategy that we have followed in demonstrating that the near-far problem is an inherent feature of the correlation based receivers, rather than an inherent feature of CDMA, has been exclusively concentrated on enhancing signal processing tasks. A point as which our strategy in providing the solution for near-far problems, could be challenged, is on treating the signal processing task and the channel decoding task as separate entities. Channel coding and signal processing contribute in a complementary manner to the receiver performance, and as such, they should be co-designed. Our argument that channel coding, under the conditions reported in Chapter 6, is much more helpful in Rayleigh fading channels than the "dumb" PN spreading, would prompt an investigation towards Integrated Cancellation and Coding (ICC) schemes. Non-linear signal processing such as the FS-DFE receiver, can act as the platform in which the ICC concept could be demonstrated. In one possible ICC arrangement, a noise-predictive FS-DFE and a Soft-Output Viterbi Algorithm (SOVA) could be linked together. In this arrangement, it is the feedback of the post-Viterbi decoder soft symbols, having much higher reliability compared to the pre-Viterbi decoder symbols, which would account for a significant performance improvement.

2. The complexity of MIMO detection strategies could be reduced if they are implemented according to the guidelines of systolic array processors. Systolic arrays have been used in the past for adaptive antenna arrays which constitutes another MIMO detection problem. The conditions under which systolic array processors can be used in CDMA interference cancellation and for what cost, could be a useful extension of the work carried out here.

3. The replacement of the transversal filter architecture of SISO MMSE detectors with a lattice architecture and the evaluation of the possible performance gains is another area worth pursuing. It would be of interest to make a true comparative evaluation of

the transversal LMS, transversal RLS, Gradient Adaptive Lattice (GAL) and Least Squares Lattice (LSL) algorithms in CDMA interference equalization problems.

4. The evaluation of the Trellis Coded Modulation in channels where Rician statistics are mostly present. This evaluation might lead to new conclusions regarding the approach that European Space Agency has followed on merging TCM and CDMA.

Some advice for people who will take on these suggestions to further exploit the horizons of CDMA: "All possible evolutionary steps in advanced signal processing and coding techniques should be designed with the complexity issue always in mind." After all, we all want CDMA to be a winning *technology*, don't we ?

APPENDICES

Appendix A

LIST OF PUBLICATIONS

A.1 Patent

1. **Title:** DS-CDMA Receiver,**Applicant:**Philips Electronics, UK Limited,**Inventors:**P. Monogioudis (Surrey University), M. Edmonds (Philips Research Laboratories), **Filing Details:** UK Patent Office (Filing Date 24/8/93, Patent # 9317604.8).

A.2 Journals-Conferences

1. "**Near-Far Resistant Multiuser Detectors**", IEE Colloquium on Spread Spectrum Techniques for Mobile Radio Applications", London 1992.
2. "**On the Radio Interface of Future ACDMA Systems**", IEE Colloquium on Advanced Modulation and Coding For Digital Cellular Systems, London 1992.
3. "**Multimedia Advanced CDMA Systems**", IEE International Conference of Telecommunications, Manchester 1993.
4. "**Multirate 3rd Generation CDMA Systems**", IEEE International Conference on Communications (ICC), Geneva 1993.
5. "**Multirate CDMA Systems**", International Union of Radio Science (URSI), Kyoto, Japan 1993
6. "**LFSE Interference Cancellation in CDMA Systems**", IEEE International Conference on Communications (ICC), N. Orleans 1994.

7. **"An Autonomous CDMA Receiver Architecture"**, International Symposium of Spread Spectrum Techniques and Applications, Finland June 1994.

8. **"Linear Adaptive Fractionally Spaced Equalization of CDMA Multiple Access Interference"**, *IEE Electronics Letters*, Oct. 1993

9. **"Performance of an Adaptive non-linear NEFAR CDMA Receiver Architecture"**, *IEE Electronics Letters*, Feb. 1994

10. **"NEFAR Receiver Architectures for CDMA Personal Communication Systems"**, *European Transactions on Telecommunications*, Invited for the Special Issue on Spread Spectrum Techniques, January-February 1995

11. **"The Role of Channel Coding on Multirate Radio Interface Design of CDMA Personal Communication Systems"**, *IEEE Transactions on Vehicular Technology*, Submitted May 1994

A.3 CODIT Internal

1. CODIT/PRL/RI-001/1.0: **Radio Signal Characteristics for the CODIT testbed.**

2. CODIT/PRL/RI-002/1.0: **Normalized PSD for OQPSK/QPSK.**

3. CODIT/PRL/RT-002/1.0: **Performance of Low Rate Orthogonal Convolutional Codes in AWGN and CDMA Channels.**

4. CODIT/PRL/RT-005/1.0: **A Simulation Framework for the Assessment of NEFAR Multiuser Detection Techniques.**

5. CODIT/PRL/RT-007/1.0: **Near-Far Effect Resistant Multiuser Detectors.**

6. CODIT/PRL/RT-008/1.2: **Technological Implications of CDMA.**

7. CODIT/PRL/RT-009/1.0: **A Proposal for the CODIT Multirate Radio Interface.**

8. CODIT/PRL/RT-010/1.0: **Combined LOROC-NEFAR Multiuser Detection.**

9. CODIT/PRL/RT-019/1.0: E_b/N_0 **and** E_b/I_0 **Measurements for the Testbed.**

10. CODIT/PRL/RT-020/1.0: E_b/N_0 **Measurement Algoritms.**

11. CODIT/PRL/RT-022/1.0: **Simulation of Bit and Symbol Error Rates for the TCH/D128 channel.**

12. CODIT/PRL/RT-018/2.0: **Preliminary Specifications of the MS/BS Signal Processing for Testbed**

References

[1] M. Abdulrahman and D. Falconer. Cyclostationary crosstalk suppression by decission feedback equalization on digital subscriber loops. *IEEE Journal on Selected Areas on Communication*, April 1992.

[2] Q. Bi. On performance improvement of asynchronous cdma systems through the use of orthogonal sequence spreading. *IEEE International Conference on Communications*, May 1993.

[3] G. Boudreau, D. Falconer, and S. Mahmoud. A comparison of trellis coded versus convolutionally coded spread-spectrum multiple-access systems. *IEEE Journal on Selected Areas on Communication*, 8(4):628–640, May 1990.

[4] Schlegel C. and Costello D. J. Bandwith efficient coding for fading channels code construction and performance analysis. *Journal on Selected Areas on Communication*, 7(9):1356–1368, December 1989.

[5] D. Chase. Code combining-a maximum-likelihood decoding approach for combining an arbitrary number of noisy packets. *IEEE Transactions on Communications*, 33(5):385–393, May 1985.

[6] A. Cloke. Green machine implementation. *Private Communication, Philips Research Laboratories,Redhill*, July 1992.

[7] A. Cloke, A. Prentice, and A. Thomas. The implementation of a channel estimation scheme for the codit testbed. *RACE Mobile Telecommunications Workshop, Amsterdam*, May 1994.

[8] CODIT/ERA/LC-034/1.0. The execution of soft-handover. August 1993.

[9] CODIT/PKI/RI/DS/I/005/b1. Study report on cdma for umts. December 1993.

[10] P. Dent, B. Gudmundson, and M. Ewerbring. Cdma-ic:a novel code division multiple access scheme based on interference cancellation. *The Third IEEE International Symposium on Personal, Indoor and Mobile Radio Communications*, October 1992.

[11] A. Duel-Hallen. Equalizers for multiple input/multiple output channels and pam systems with cyclostationary input sequences. *IEEE Journal on Selected Areas on Communication*, 10(3):630–639, April 1992.

[12] A. Duel-Hallen. Decorrelating decision feedback multiuser detector for synchronous code division multiple access channel. *IEEE Transactions on Communications*, 41(2):285–290, February 1993.

[13] Biglieri E., Divsalar D., Mc Lane P., and Simon M. *Introduction to Trellis-Coded Modulation with Applications.* Macmillan Publishing Company, 1991.

[14] K. Gilhousen et al. On the capacity of a cellular cdma system. *IEEE Transactions on Vehicular Technology*, 40(2):303–312, May 1991.

[15] Ungerboeck G. Channel coding with multilevel/phase signals. *IEEE Transactions on Information Theory*, 28(1):55–56, January 1982.

[16] Ungerboeck G. Trellis coded modulation with redundant signal sets - part i: introduction - part ii: state of art. *IEEE Communications Magazine*, 25(2):12–21, February 1987.

[17] W. A. Gardner and W. A. Brown. Frequency shift filtering theory for adaptive cochannel interference removal. *Proc. 23rd Asilomar Conf. Signals, Syst. Comput., Pacific Grove, CA*, November 1989.

[18] R. De Gaudenzi and F. Giannetti. Synchnonous trellis coded cdma: Analysis and system performance. *IEEE International Conference on Communications*, May 1993.

[19] E.A. Geraniotis and M.B.Pursley. Error probability for direct sequence spread-spectrum multiple-access communications -part ii: Approximations. *IEEE Transactions on Communications*, 30(5):985–995, May 1982.

[20] E.A. Geraniotis and M.B.Pursley. Performance of coherent direct sequence spread-spectrum communications over specular multipath fading channels. *IEEE Transactions on Communications*, 33(5), June 1985.

[21] R. Gitlin and S. Weinstein. Fractionally spaced equalization:an improved digital transversal equalizer. *The Bell System Technical Journal*, February 1981.

[22] G. Golub and C. Van Loan. *Matrix Computations.* The John Hopkins University Press, second edition, 1989.

[23] R. Green. A serial orthogonal decoder. *JPL Space Programs Summary, Vo. 37-39-IV*, 1966.

[24] S. Haykin. *Adaptive Filter Theory.* Prentice Hall International, second edition, 1991.

[25] J. Holmes and C. Chen. Acquisition time performance of pn spread spectrum systems. *IEEE Transactions on Communications*, 25(8):779–784, August 1977.

[26] Qualcomm Inc. *An Overview of the Application of Code Division Multiple Access (CDMA) to Digitral Cellular Systems and Personal Cellular Networks.* Submitted to TIA TR45.5 Subcommittee, 1992.

[27] Cavers J. K. and Ho P. Analysis of the error performance of trellis coded modulations in rayleigh fading channels. *IEEE Transactions on Communications*, 40(1):74–83, January 1992.

[28] W. Lam and R. Steele. Performance of direct sequence spread-spectrum mutliple access systems in mobile radio. *IEE Proceedings-I*, 138(1):1–14, February 1991.

[29] S. Lin and Jr. D. Costello. *Error Control Coding:Fundamentals and Applications.* Prentice Hall, 1983.

[30] F. Ling. Coherent detection with reference based channel estimation for direct sequence cdma uplink communications. *IEEE Vehicular Technology Conference*, May 1993.

[31] R. Lupas and S. Verdu. Linear multiuser detectors for synchronous code division multiple access channels. *IEEE Transactions on Information Theory*, 34(5), May 1988.

[32] R. Lupas and S. Verdu. Near-far resistance of multiuser detectors in asynchronous channels. *IEEE Transactions on Communications*, 38(4):496–508, April 1990.

[33] Rouanne M. An algorithm for computing the distance spectrum of trellis codes. *Journal on Selected Areas on Communication*, 7(6):929–939, August 1989.

[34] F. Matas. *Capacity Increase of TDMA Systems Through Multidimensional Equalization.* MSc Thesis, University of Surrey, 1993.

[35] P. Monogioudis and M. Edmonds. e_b/n_0 and e_b/i_0 measurements for the testbed. *CODIT/PRL/RT-019/1.0*, May 1993.

[36] P. Monogioudis and M. Edmonds. e_b/n_0 measurement algoritms. *CODIT/PRL/RT-020/1.0*, June 1993.

[37] P. Monogioudis and M. Edmonds. Simulation of bit and symbol error rates for the tch/d128 channel. *CODIT/PRL/RT-022/1.0*, August 1993.

[38] P. Monogioudis, R. Tafazolli, and B. G. Evans. Multirate 3rd generation CDMA systems. *IEEE International Conference on Communications*, May 1993.

[39] T. Moon. *Parameter Estimation in SSMA Systems.* PhD thesis, University of Utah, 1991.

[40] R. Mowbray, R. Pringle, and P. Grant. Increased cdma system capacity through adaptive cochannel interference regeneration and cancellation. *IEE Proceedings-I*, 139(5):515–524, October 1992.

[41] M. Neppleton. Spread spectrum for mobile radio communications. *IEEE Transactions on Vehicular Technology*, 27(11):264–275, November 1978.

[42] K. Pahlavan and J. Matthews. Performance of adaptive matched filter receivers over fading multipath channels. *IEEE Transactions on Communications*, 38(12):2106–2113, December 1990.

[43] J. Parsons. *The Mobile Radio Propagation Channel.* Pentech Press, first edition, 1992.

[44] B. Petersen and D. Falconer. Minimum mean square equalization in cyclostationary and stationary interference-analysis and subsriber line calculations. *IEEE Journal on Selected Areas on Communication*, 9(6):931–940, August 1991.

[45] B. R. Petersen. Suppression of adjacent channel interference in digital radio by equalization. *Proc. International Conference on Communications*, June 1992.

[46] H.V. Poor. Statistical signal processing for wideband communications. *3rd International Workshop on Digital Signal Processing Techniques Applied to Space Communications, ESTEC, ESA*, September 1992.

[47] J. Proakis. *Digital Communications.* McGraw-Hill, second edition, 1989.

[48] M. Pursley and H. Roefs. Numerical evaluation of correlation parameters for optimal phases of binary shift-registers sequences. *IEEE Transactions on Communications*, 27(10):1597–1604, October 1979.

[49] M.B. Pursley. Performance evaluation of phase coded spread-spectrum multiple-access communications - part i : System analysis. *IEEE Transactions on Communications*, 25(8):795–799, August 1977.

[50] S. Qureshi. Adaptive equalization. *IEEE Proceedings*, September 1985.

[51] M. Rupf. On low rate convolutional codes. *IEEE International Symposium on Information Theory*, 1991.

[52] M. Rupf. *Private Communication*, June 1992.

[53] D. Sarwate and M. Pursley. Crosscorrelation properties of pseudorandom and related sequences. *Proceedings of the IEEE*, May 1980.

[54] P. Sweeney. *Error Control Coding-An Introduction*. Prentice Hall, first edition, 1991.

[55] C. Therien. *Discrete Random Signals and Statistical Signal Processing*. Prentice Hall International, 1992.

[56] M.k. Varanasi and B. Aazhang. Multistage detection in asynchronous code division multiple access communications. *IEEE Transactions on Communications*, 38(4):509–519, April 1990.

[57] M.k. Varanasi and B. Aazhang. Near-optimum detection in synchronous code-division multiple-access system. *IEEE Transactions on Communications*, 39(5):725–736, May 1991.

[58] S. Verdu. *Optimum Multiuser Signal Detection*. PhD thesis, University of Illinois, Urbana, 1984.

[59] S. Verdu. Minmum probability of error for asynchronous gaussian multiple-access channels. *IEEE Transactions on Information Theory*, 32(1):85–96, January 1986.

[60] A. Viterbi. Very low rate convolutional codes for maximum theoretical performance of spread spectrum multiple access channels. *IEEE Journal on Selected Areas on Communication*, 8(4):641–649, May 1990.

[61] A. Viterbi. Wireless digital communication: A view based on three lessons learned. *IEEE Communications Magazine*, 29(9):33–36, September 1991.

[62] A. Viterbi and J. Omura. *Principles of Digital Communication and Coding.* McGraw-Hill, first edition, 1979.

[63] A. M. Viterbi and A. J. Viterbi. Erlang capacity of a power controlled cdma system. *IEEE Journal on Selected Areas on Communication*, 41(6):892–899, August 1993.